Phenotypic Heterogeneity and its influence on visual and morphological outcomes in age-related macular degeneration

Shruti Chandra

Institute of Ophthalmology, University College London

A Thesis submitted for the degree of

Doctor of Philosophy

December 2023

Supervisors: Prof. Sobha Sivaprasad, Prof. Glen Jeffery

To my Dadi

Thank you. You would have been so proud of what I've accomplished, and I dedicate this thesis to you.

Declaration

I, Shruti Chandra, confirm that the work presented in this thesis is my own. Where information has been derived from other sources, I confirm that this has been indicated in the thesis.

Shruti Chandra

15th December 2023

Abstract

Age related macular degeneration (AMD) is a complex condition with significant heterogeneity in presentation, rate of progression and outcomes. The overarching aim of the studies in this thesis was to characterize the heterogeneity by conducting in-depth imaging and visual function tests to inform future clinical trial design in non-neovascular AMD, neovascular AMD (nAMD) and geographic atrophy (GA).

In a prospective structure-function correlation study on 254 participants with normal fundus and varying severity of non-neovascular AMD, subretinal drusenoid deposits (SDD), hyperreflective foci and nascent GA were found to be imaging characteristics that are associated with visual function losses. In addition, quantitative fundus autofluorescence decreased with increasing AMD severity suggesting that decreasing lipofuscin load is of questionable therapeutic benefit in AMD.

In a cohort study on 2,128 patients with new-onset nAMD that completed the loading phase of aflibercept injections, structure-function correlation identified non-white ethnicity, male and eyes with increased CST or those presenting with SRF only as determinants of residual fluid post-loading. Restricting early-phase interventional clinical trials to patients with these characteristics is more likely to provide an indication of benefit over aflibercept, the current comparator of clinical trials in nAMD.

In a study on 50 patients with GA, multifocality, SDD, and junctional hyperautofluorescence were identified as features of fast progression and so targeting interventional trials to this GA group would likely yield more reliable results in a shorter period. Using a computer-aided tool on OCT scans on 13 GA patients also revealed that photoreceptor loss precedes GA growth and could be used as an early clinical endpoint for GA trials.

In conclusion, various phenotypes were identified within each AMD stage that largely explains differences in visual function, treatment responses and disease progression. These findings could be used to design more efficient and effective clinical trials in AMD.

Impact Statement

The findings in this thesis advance our understanding of phenotypic heterogeneity in each stage of age-related macular degeneration (AMD) and how it impacts the visual and anatomical outcomes. Current staging of AMD is based on features seen only on colour photographs and the work in this thesis highlight several biomarkers and phenotypes on multimodal imaging that better explain disease stratification and progression. These findings will likely contribute to a new classification system of AMD. Furthermore, the new knowledge can be utilised for future drug development strategies and improved clinical trial designs.

The prospectively collected comprehensive datasets on several imaging and visual function tests done on 254 patients with non-neovascular AMD and the nationally collected data and graded images of 2,128 patients with neovascular AMD are unique legacies of this thesis that can be used for future studies to test new hypotheses or for artificial intelligence algorithm development and validation studies. The work on geographic atrophy has already resulted in current and future international collaborations with Wisconsin Reading Centre, Madison, USA and Institute of Molecular and Clinical Ophthalmology, Basel, Switzerland and with industry partner IBM, Australia.

The work conducted in the thesis has expanded the knowledge on response to anti vascular endothelial growth factor (anti VEGF) therapy describing good and poor responders. This information was employed while drafting the AMD Clinical Commissioning Guidance (CCG) for the Royal College of ophthalmologists (Role: Trainee representative on CCG committee) to improve current patient pathways for anti VEGF therapy.

The work presented in this thesis has led to eight publications in peer reviewed journals (excluding one manuscript on dark adaptation and another on deep learning for GA measurement currently under preparation). The findings have been presented at both national and international scientific meetings as paper presentations and posters. Importantly, the work from this PhD has generated pilot data that was used for a successful grant application. Funding was received from Boehringer Ingelheim International GmBH, Germany, with a project “A

Prospective, Observational study for identification of biomarkers of disease progression in Intermediate Age-related Macular Degeneration and Geographic Atrophy (PROBE-IGA)" (£605,000, March 2023. Role: Main applicant).

Perhaps the most significant impact of this thesis was the patient public involvement and engagement (PPIE) activities. Interested patients from the Fight for Sight funded PEONY study on non-neovascular AMD formed the PPIE representative group to help design the study protocol for PROBE IGA study. Moreover, two patients from this cohort displayed art exhibits "PRISMS: AMD in Art" at the SoCo Artists (THREE: through time and space) exhibition in February 2023 acknowledging the PEONY study and their participation as the inspiration behind it. The results of this thesis were also presented to the patients and public at the National Institute of Health and Research Biomedical Research Centre (NIHR-BRC) Open day and won the "Best PhD Talk" award.

Research Paper Declaration Forms

UCL Research Paper Declaration Form No. 1

Referencing the doctoral candidate's own published work(s)

Referenced in Chapter 3

1. For a research manuscript that has already been published (if not yet published, please skip to section 2)

a) What is the title of the manuscript?

Quantitative Autofluorescence in Non-Neovascular Age Related Macular Degeneration.

b) Please include a link to or doi for the work

doi:10.3390/biomedicines11020560

c) Where was the work published?

Biomedicines Journal, Volume 11, Issue 2. Special Issue Advanced Research in Age-Related Macular Degeneration (AMD)

d) Who published the work? (e.g. OUP)

Multidisciplinary Digital Publishing Institute (MDPI)

e) When was the work published?

February 15, 2023

f) List the manuscript's authors in the order they appear on the publication

Shruti Chandra, Manjot K Grewal, Sarega Gurudas, Rajan Sondh, Alan Bird, Glen Jeffery, Victor Chong, Sobha Sivaprasad.

g) Was the work peer reviewed?

Yes

h) Have you retained the copyright?

Yes

i) Was an earlier form of the manuscript uploaded to a preprint server? (e.g. medRxiv). If 'Yes', please give a link or doi)

No

If 'No', please seek permission from the relevant publisher and check the box next to the below statement:

☒

I acknowledge permission of the publisher named under **1d** to include in this thesis portions of the publication named as included in **1c**.

2. For a research manuscript prepared for publication but that has not yet been published (if already published, please skip to section 3)

a) What is the current title of the manuscript?

N/A

b) Has the manuscript been uploaded to a preprint server? (e.g. medRxiv; if 'Yes', please give a link or doi)

N/A

c) Where is the work intended to be published? (e.g. journal names)

N/A

d) List the manuscript's authors in the intended authorship order

N/A

e) Stage of publication (e.g. in submission)

N/A

3. For multi-authored work, please give a statement of contribution covering all authors (if single-author, please skip to section 4)

Conceptualisation, S.C.(Shruti Chandra) and S.S.; methodology, S.C. and S.S.; formal analysis, S.G. and S.C.; investigation, S.C., M.K.G. and R.S.; data curation, S.C. and R.S.; writing—original draft preparation, S.C., S.G. and S.S.; writing—review and editing, G.J., V.C., S.S. and A.B.; supervision, S.S., V.C., G.J. and A.B.; funding acquisition, S.S. All authors have read and agreed to the published version of the manuscript.

4. In which chapter(s) of your thesis can this material be found?

Chapter 3, Section 3.4

5. **e-Signatures confirming that the information above is accurate** (this form should be co-signed by the supervisor/ senior author unless this is not appropriate, e.g. if the paper was a single-author work)

Candidate

Shruti Chandra

*Date:*01 December 2023

Supervisor and Senior Author

Sobha Sivaprasad

Date: 01 December 2023

UCL Research Paper Declaration Form No. 2

referencing the doctoral candidate's own published work(s)

Referenced in Chapter 4

1. For a research manuscript that has already been published (if not yet published, please skip to section 2)

a) What is the title of the manuscript?

Associations of presenting visual acuity with morphological changes on OCT in neovascular age-related macular degeneration: PRECISE Study Report 2.

b) Please include a link to or doi for the work

doi:10.1038/s41433-023-02769-5

c) Where was the work published?

Eye (London)

d) Who published the work? (e.g. OUP)

Springer Nature

e) When was the work published?

October 18, 2023

f) List the manuscript's authors in the order they appear on the publication

Shruti Chandra, Sarega Gurudas, Benjamin J. L. Burton, Geeta Menon, Ian Pearce, Martin Mckibbin, Ajay Kotagiri, James Talks, Anna Grabowska, Faruque Ghanchi, Richard Gale, Andrea Giani, Victor Chong, Taffeta Ching Ning Yamaguchi, Bishwanath Pal, Sridevi Thottarath, Raheeba Muhamed Pakeer, Swati Chandak, Andrea Montesel & Sobha Sivaprasad.

g) Was the work peer reviewed?

Yes

h) Have you retained the copyright?

Yes

i) Was an earlier form of the manuscript uploaded to a preprint server? (e.g. medRxiv). If 'Yes', please give a link or doi)

No

If 'No', please seek permission from the relevant publisher and check the box next to the below statement:

☒

I acknowledge permission of the publisher named under **1d** to include in this thesis portions of the publication named as included in **1c**.

2. For a research manuscript prepared for publication but that has not yet been published (if already published, please skip to section 3)

a)What is the current title of the manuscript?

N/A

b) Has the manuscript been uploaded to a preprint server? (e.g. medRxiv; if 'Yes', please give a link or doi)

N/A

c) Where is the work intended to be published? (e.g. journal names)

N/A

d) List the manuscript's authors in the intended authorship order

N/A

e) Stage of publication (e.g. in submission)

N/A

3. For multi-authored work, please give a statement of contribution covering all authors (if single-author, please skip to section 4)

Conceptualization: ShC (Shruti Chandra) and SS; Data curation: ShC, ST, RMP, SC, and AM; Formal analysis: SG and SS; Funding acquisition: AGi, VC and SS; Investigation: ShC, SG and SS; Methodology: ShC, SG, and SS; Project administration: AGi. and SS; Resources: ShC, GM, BJB, IP, MM, ST, SC, RPM, AM, AK, JT, AGr, FG, RG, BP and SS; Supervision: AGi, VC and SS; Visualisation: SG and ShC; Writing – original draft: ShC, SG and SS; Writing - review & editing: AGi, VC and SS Review and approval of final manuscript: ShC, SG., AGi, VC, SS, GM, BJB, IP, MM, ST, RPM, SC, AM, AK, JT, AGr, CC, FG, RG, and BP. All authors have read and agreed to the published version of the manuscript.

4. In which chapter(s) of your thesis can this material be found?

Chapter 4, Section 4.2

5. **e-Signatures confirming that the information above is accurate** (this form should be co-signed by the supervisor/ senior author unless this is not appropriate, e.g. if the paper was a single-author work)

Candidate

Shruti Chandra

Date: 01 December 2023

Supervisor and Senior Author

Sobha Sivaprasad

Date: 01 December 2023

UCL Research Paper Declaration Form No. 3

referencing the doctoral candidate's own published work(s)

Referenced in Chapter 4

1. For a research manuscript that has already been published (if not yet published, please skip to section 2)

a) What is the title of the manuscript?

Baseline characteristics of eyes with early residual fluid post loading phase of aflibercept therapy in neovascular AMD: PRECISE Study Report 3

b) Please include a link to or doi for the work

doi: 10.1038/s41433-023-02886-1

c) Where was the work published?

Eye (London)

d) Who published the work? (e.g. OUP)

Springer Nature

e) When was the work published?

December 01, 2023

f) List the manuscript's authors in the order they appear on the publication

Shruti Chandra, Sarega Gurudas, Ian Pearce, Martin Mckibbin, Ajay Kotagiri, Geeta Menon, Benjamin JL Burton, James Talks, Anna Grabowska, Faruque Ghanchi, Richard Gale, Andrea Giani, Victor Chong, Ching Ning Taffeta Chen, Luke Nicholson, Sridevi Thottarath, Swati Chandak, Sobha Sivaprasad.

g) Was the work peer reviewed?

Yes

h) Have you retained the copyright?

Yes

i) Was an earlier form of the manuscript uploaded to a preprint server? (e.g. medRxiv). If 'Yes', please give a link or doi)

No

If 'No', please seek permission from the relevant publisher and check the box next to the below statement:

☒

I acknowledge permission of the publisher named under **1d** to include in this thesis portions of the publication named as included in **1c**.

2. For a research manuscript prepared for publication but that has not yet been published (if already published, please skip to section 3)

a) What is the current title of the manuscript?

Click or tap here to enter text.

b) Has the manuscript been uploaded to a preprint server? (e.g. medRxiv; if 'Yes', please give a link or doi)

Click or tap here to enter text.

c) Where is the work intended to be published? (e.g. journal names)

Click or tap here to enter text.

d) List the manuscript's authors in the intended authorship order

Click or tap here to enter text.

e) Stage of publication (e.g. in submission)

Click or tap here to enter text.

3. For multi-authored work, please give a statement of contribution covering all authors (if single-author, please skip to section 4)

Conceptualization: Sh.C. (Shruti Chandra) and S.S.; Data curation: Sh.C., S.T. and S.C.; Formal analysis: Sh.C. , S.G. and S.S.; Funding acquisition: An.G., V.C. and S.S.; Investigation: Sh.C., S.G. and S.S.; Methodology: Sh.C., S.G. and S.S Project administration: An.G. and S.S.; Resources: Sh.C., G.M., B.J.B., I.P., M.M., S.T., S.C., A.K., J.T., A.G., F.G., R.G., L.K. and S.S.; Supervision: An.G., V.C. and S.S.; Visualization: S.G. and Sh.C.; Writing – original draft: Sh.C, S.G. and S.S.; Writing - review & editing: An.G., V.C. and S.S. Review and approval of final manuscript: Sh.C., S.G., An.G., V.C. S.S, G.M., B.J.B., I.P., M.M., S.T.,S.C., A.K., J.T., A.G., C.C., F.G., R.G. and L.N. All authors have read and agreed to the published version of the manuscript.

4. In which chapter(s) of your thesis can this material be found?

Chapter 4, Section 4.3

5. **e-Signatures confirming that the information above is accurate** (this form should be co-signed by the supervisor/ senior author unless this is not appropriate, e.g. if the paper was a single-author work)

Candidate

Shruti Chandra
Date: 01 December 2023
Supervisor and Senior Author

Sobha Sivaprasad
Date: 01 December 2023

UCL Research Paper Declaration Form No. 4

referencing the doctoral candidate's own published work(s)

Referenced in Chapter 4

1. For a research manuscript that has already been published (if not yet published, please skip to section 2)

a) What is the title of the manuscript?

A Multi-Modal AI-Driven Cohort Selection Tool to Predict Suboptimal Non-Responders to Aflibercept Loading-Phase for Neovascular Age-Related Macular Degeneration: PRECISE Study Report 1

b) Please include a link to or doi for the work

doi:10.3390/jcm12083013

c) Where was the work published?

Journal of Clinical Medicine, Volume 12, Issue 8.

d) Who published the work? (e.g. OUP)

Multidisciplinary Digital Publishing Institute (MDPI)

e) When was the work published?

April 20, 2023

f) List the manuscript's authors in the order they appear on the publication

Michal Chorev*, Jonas Haderlein*, **Shruti Chandra*,** Geeta Menon, Benjamin J L Burton, Ian Pearce, Martin McKibbin, Sridevi Thottarath, Eleni Karatsai, Swati Chandak, Ajay Kotagiri, James Talks, Anna Grabowska, Faruque Ghanchi, Richard Gale, Robin Hamilton, Bhavna Antony, Rahil Garnavi, Iven Mareels, Andrea Giani, Victor Chong, Sobha Sivaprasad.

***Joint first authors**

g) Was the work peer reviewed?

Yes

h) Have you retained the copyright?

Yes

i) Was an earlier form of the manuscript uploaded to a preprint server? (e.g. medRxiv). If 'Yes', please give a link or doi)

Yes, 10.21203/rs.3.rs-2114436/v1

If 'No', please seek permission from the relevant publisher and check the box next to the below statement:

☐

I acknowledge permission of the publisher named under **1d** to include in this thesis portions of the publication named as included in **1c**.

2. For a research manuscript prepared for publication but that has not yet been published (if already published, please skip to section 3)

a) What is the current title of the manuscript?

Click or tap here to enter text.

b) Has the manuscript been uploaded to a preprint server? (e.g. medRxiv; if 'Yes', please give a link or doi)

Click or tap here to enter text.

c) Where is the work intended to be published? (e.g. journal names)

Click or tap here to enter text.

d) List the manuscript's authors in the intended authorship order

Click or tap here to enter text.

e) Stage of publication (e.g. in submission)

Click or tap here to enter text.

3. For multi-authored work, please give a statement of contribution covering all authors (if single-author, please skip to section 4)

Conceptualisation: M.C., S.C. (Shruti Chandra), B.A., R.G. (Rahil Garnavi), I.M., A.G. (Andrea Giani), V.C. and S.S.; Data curation: S.C. (Shruti Chandra), G.M., B.J.L.B., I.P., M.M., S.T., E.K., S.C. (Swati Chandak), A.K., J.T., A.G. (Anna Grabowska), F.G., R.G. (Richard Gale), and R.H.; Formal analysis: M.C. and J.H.; Funding acquisition: R.G. (Rahil Garnavi), I.M., A.G. (Andrea Giani), V.C. and S.S.; Investigation: M.C., J.H., S.C. (Shruti Chandra), and S.S.; Methodology: M.C. and J.H.; Project administration: R.G. (Rahil Garnavi), I.M., A.G. (Andrea Giani), and S.S.; Resources: S.C. (Shruti Chandra), G.M., B.J.L.B., I.P., M.M., S.T., E.K., S.C. (Swati Chandak), A.K., J.T., A.G. (Anna Grabowska), F.G., R.G. (Richard Gale), R.H. and S.S.; Software: M.C. and J.H.; Supervision: R.G. (Rahil Garnavi), I.M., A.G. (Andrea Giani), V.C. and S.S.; Validation: M.C. and J.H.; Visualisation: M.C. and J.H.; Writing—original draft: M.C., J.H. and S.C. (Shruti Chandra); Writing—review and editing: I.M., A.G. (Andrea Giani), V.C. and S.S.; Review and approval of final manuscript: M.C., S.C. (Shruti Chandra), J.H., B.A., R.G. (Rahil Garnavi), I.M., A.G. (Andrea Giani), V.C., S.S., G.M., B.J.L.B., I.P., M.M., S.T., E.K., S.C. (Swati Chandak), A.K., J.T., A.G. (Anna Grabowska), F.G., R.G. (Richard Gale), and R.H. All authors have read and agreed to the published version of the manuscript.

4. In which chapter(s) of your thesis can this material be found?

Chapter 4, Section 4.4

5. **e-Signatures confirming that the information above is accurate** (this form should be co-signed by the supervisor/ senior author unless this is not appropriate, e.g. if the paper was a single-author work)

Candidate

Shruti Chandra

Date: 01 December 2023

Supervisor and Senior Author

Sobha Sivaprasad

Date 01 December 2023

UCL Research Paper Declaration Form No. 5

referencing the doctoral candidate's own published work(s)

Referenced in Chapter 4

1. For a research manuscript that has already been published (if not yet published, please skip to section 2)

a) What is the title of the manuscript?

Ten-year outcomes of anti-vascular endothelial growth factor therapy in neovascular age-related macular degeneration

b) Please include a link to or doi for the work

doi:10.1038/s41433-020-0764-9

c) Where was the work published?

Eye (London), Volume 34, Issue 10.

d) Who published the work? (e.g. OUP)

Springer Nature

e) When was the work published?

January 24, 2020

f) List the manuscript's authors in the order they appear on the publication

Shruti Chandra (SC), Cristina Arpa (CA), Deepthy Menon (DM), Hagar Khalid (HK), Robin Hamilton (RH), Luke Nicholson (LK), Bishwanath Pal (BP), Sandro Fasolo (SF), Philip Hykin (PH), Pearse A. Keane (PAK), and Sobha Sivaprasad (SS).

g) Was the work peer reviewed?

Yes

h) Have you retained the copyright?

Yes

i) Was an earlier form of the manuscript uploaded to a preprint server? (e.g. medRxiv). If 'Yes', please give a link or doi)

No

If 'No', please seek permission from the relevant publisher and check the box next to the below statement:

☒

I acknowledge permission of the publisher named under **1d** to include in this thesis portions of the publication named as included in **1c**.

2. For a research manuscript prepared for publication but that has not yet been published (if already published, please skip to section 3)

a) What is the current title of the manuscript?

Click or tap here to enter text.

b) Has the manuscript been uploaded to a preprint server? (e.g. medRxiv; if 'Yes', please give a link or doi)

Click or tap here to enter text.

c) Where is the work intended to be published? (e.g. journal names)

Click or tap here to enter text.

d) List the manuscript's authors in the intended authorship order

Click or tap here to enter text.

e) Stage of publication (e.g. in submission)

Click or tap here to enter text.

3. For multi-authored work, please give a statement of contribution covering all authors (if single-author, please skip to section 4)

Conceptualisation: SC; Data curation: SC, DM, CA, HK; Formal analysis: SC; Funding acquisition: N/A; Investigation: SC; Methodology: S.C and S.S; Project administration: S.S.; Resources: S.C and SF; Software: N/A ; Supervision: RH, LK, BP, PH, PAK, and SS; Writing—original draft: SC; Writing—review and editing: SC and SS; Review and approval of final manuscript: All authors. All authors have read and agreed to the published version of the manuscript.

4. In which chapter(s) of your thesis can this material be found?

Chapter 4, Section 4.5

5. **e-Signatures confirming that the information above is accurate** (this form should be co-signed by the supervisor/ senior author unless this is not appropriate, e.g. if the paper was a single-author work)

Candidate

Shruti Chandra

Date: 01 December 2023

Supervisor and Senior Author

Sobha Sivaprasad

*Date*01 December 2023

UCL Research Paper Declaration Form No. 6

referencing the doctoral candidate's own published work(s)

Referenced in Chapter 4

1. For a research manuscript that has already been published (if not yet published, please skip to section 2)

a) What is the title of the manuscript?

Impact of injection frequency on 5-year real-world visual acuity outcomes of aflibercept therapy for neovascular age-related macular degeneration.

b) Please include a link to or doi for the work

doi:10.1038/s41433-020-0851-y

c) Where was the work published?

Eye (London), Volume 35, Issue 2.

d) Who published the work? (e.g. OUP)

Springer Nature

e) When was the work published?

February 2021

f) List the manuscript's authors in the order they appear on the publication

Shruti Chandra, Rajna Rasheed, Deepthy Menon, Namritha Patrao, Ali Lamin, Sarega Gurudas, Konstantinos Balaskas, Praveen J. Patel, Naser Ali, and Sobha Sivaprasad.

g) Was the work peer reviewed?

Yes

h) Have you retained the copyright?

Yes

i) Was an earlier form of the manuscript uploaded to a preprint server? (e.g. medRxiv). If 'Yes', please give a link or doi)

No

If 'No', please seek permission from the relevant publisher and check the box next to the below statement:

☒

I acknowledge permission of the publisher named under **1d** to include in this thesis portions of the publication named as included in **1c**.

2. For a research manuscript prepared for publication but that has not yet been published (if already published, please skip to section 3)

a) What is the current title of the manuscript?

Click or tap here to enter text.

b) Has the manuscript been uploaded to a preprint server? (e.g. medRxiv; if 'Yes', please give a link or doi)

Click or tap here to enter text.

c) Where is the work intended to be published? (e.g. journal names)

Click or tap here to enter text.

d) List the manuscript's authors in the intended authorship order

Click or tap here to enter text.

e) Stage of publication (e.g. in submission)

Click or tap here to enter text.

3. For multi-authored work, please give a statement of contribution covering all authors (if single-author, please skip to section 4)

Conceptualisation: SC; Data curation: SC, DM, RR, NP, AL; Formal analysis: SC and SG; Funding acquisition: N/A; Investigation: SC; Methodology: S.C, SG and S.S; Project administration: S.S.; Resources: S.C; Software: N/A ; Supervision: KB, PJP, NA, and SS; Writing—original draft: SC; Writing—review and editing: SC and SS; Review and approval of final manuscript: All authors. All authors have read and agreed to the published version of the manuscript.

4. In which chapter(s) of your thesis can this material be found?

Chapter 4, Section 4.6

5. **e-Signatures confirming that the information above is accurate** (this form should be co-signed by the supervisor/ senior author unless this is not appropriate, e.g. if the paper was a single-author work)

Candidate

Shruti Chandra

Date: 01 December 2023

Supervisor and Senior Author

Sobha Sivaprasad

Date 01 December 2023

UCL Research Paper Declaration Form No. 7

referencing the doctoral candidate's own published work(s)

Referenced in Chapter 5

1. For a research manuscript that has already been published (if not yet published, please skip to section 2)

a) What is the title of the manuscript?

Perspectives from clinical trials: is geographic atrophy one disease?

b) Please include a link to or doi for the work

doi:10.1038/s41433-022-02115-1

c) Where was the work published?

Eye (London), Volume 37, Issue 3.

d) Who published the work? (e.g. OUP)

Springer Nature

e) When was the work published?

May 31, 2022

f) List the manuscript's authors in the order they appear on the publication

Sobha Sivaprasad, **Shruti Chandra**, Jeha Kwon, Noorulain Khalid & Victor Chong.

g) Was the work peer reviewed?

Yes

h) Have you retained the copyright?

Yes

i) Was an earlier form of the manuscript uploaded to a preprint server? (e.g. medRxiv). If 'Yes', please give a link or doi)

No

If 'No', please seek permission from the relevant publisher and check the box next to the below statement:

☒

I acknowledge permission of the publisher named under **1d** to include in this thesis portions of the publication named as included in **1c**.

2. For a research manuscript prepared for publication but that has not yet been published (if already published, please skip to section 3)

a) What is the current title of the manuscript?

Click or tap here to enter text.

b) Has the manuscript been uploaded to a preprint server? (e.g. medRxiv; if 'Yes', please give a link or doi)

Click or tap here to enter text.

c) Where is the work intended to be published? (e.g. journal names)

Click or tap here to enter text.

d) List the manuscript's authors in the intended authorship order

Click or tap here to enter text.

e) Stage of publication (e.g. in submission)

Click or tap here to enter text.

3. For multi-authored work, please give a statement of contribution covering all authors (if single-author, please skip to section 4)

SS and VC- conceptualization; SC, JK and NK – methodology and literature review; SS and SC – writing (original draft preparation); SC, SS and VC – writing (review and editing). All authors have read and agreed to the published version of the manuscript.

4. In which chapter(s) of your thesis can this material be found?

Chapter 1, Section 1.5

Chapter 5, Section 5.1

5. **e-Signatures confirming that the information above is accurate** (this form should be co-signed by the supervisor/ senior author unless this is not appropriate, e.g. if the paper was a single-author work)

Candidate

Shruti Chandra

Date: 01 December 2023

Supervisor

Sobha Sivaprasad

Date 01 December 2023

UCL Research Paper Declaration Form No. 8

referencing the doctoral candidate's own published work(s)

Referenced in Chapter 5

1. For a research manuscript that has already been published (if not yet published, please skip to section 2)

a) What is the title of the manuscript?

Inter-rater reliability for diagnosis of geographic atrophy using spectral domain OCT in age-related macular degeneration.

b) Please include a link to or doi for the work

doi: 10.1038/s41433-021-01490-5

c) Where was the work published?

Eye (London), Volume 35, Issue 2.

d) Who published the work? (e.g. OUP)

Springer Nature

e) When was the work published?

February 2021

f) List the manuscript's authors in the order they appear on the publication

Shruti Chandra, Rajna Rasheed, Piyali Sen, Deepthy Menon, and Sobha Sivaprasad.

g) Was the work peer reviewed?

Yes

h) Have you retained the copyright?

Yes

i) Was an earlier form of the manuscript uploaded to a preprint server? (e.g. medRxiv). If 'Yes', please give a link or doi)

No

If 'No', please seek permission from the relevant publisher and check the box next to the below statement:

☒

I acknowledge permission of the publisher named under **1d** to include in this thesis portions of the publication named as included in **1c**.

2. For a research manuscript prepared for publication but that has not yet been published (if already published, please skip to section 3)

a) What is the current title of the manuscript?

Click or tap here to enter text.

b) Has the manuscript been uploaded to a preprint server? (e.g. medRxiv; if 'Yes', please give a link or doi)

Click or tap here to enter text.

c) Where is the work intended to be published? (e.g. journal names)

Click or tap here to enter text.

d) List the manuscript's authors in the intended authorship order

Click or tap here to enter text.

e) Stage of publication (e.g. in submission)

Click or tap here to enter text.

3. For multi-authored work, please give a statement of contribution covering all authors (if single-author, please skip to section 4)

Conceptualisation: SC and SS; Data curation: SC, DM, RR, PS; Formal analysis: SC; Funding acquisition: N/A; Investigation: SC; Methodology: S.C and SS; Project administration: S.S.; Resources: S.C; Software: N/A ; Supervision: SS; Writing—original draft: SC; Writing—review and editing: SC and SS; Review and approval of final manuscript: All authors. All authors have read and agreed to the published version of the manuscript.

4. In which chapter(s) of your thesis can this material be found?

Chapter 5, Section 5.3

5. **e-Signatures confirming that the information above is accurate** (this form should be co-signed by the supervisor/ senior author unless this is not appropriate, e.g. if the paper was a single-author work)

Candidate

Shruti Chandra

Date: 01 December 2023

Supervisor and Senior Author

Sobha Sivaprasad

Date 01 December 2023

Contents

Acknowledgement

I am indebted to my supervisors, Prof. Sobha Sivaprasad and Prof. Glen Jeffery who have generously provided support and advice over the past 4 years. I am extremely grateful for their kindness, wisdom, and persistence.

Sincere thanks to Prof. Sivaprasad for her inexhaustible belief in me and for being my role model.

I am thankful to my funders, Fight for Sight, UK and Boehringer Ingelheim International GmBH, Germany for their sponsorship.

The work done in this thesis would not have been possible without the support and resources provided by the National Institute of Health and Research (NIHR) Moorfields Biomedical Research Centre and Clinical Research Facility.

In addition, work presented in this thesis has been highly collaborative. I would like to thank the principal investigators and research teams across all the sites for PRECISE study, who have kindly contributed their data. Above all, I would like to extend my gratitude to all the participants who agreed to participate in my studies.

To my friend and biostatistician Ms. Sarega Gurudas for enhancing the quality of the work in this thesis with her analysis, thank you.

Finally, I would like to express my love and appreciation to my family for their enduring support and encouragement. You have always believed in me, for which I will forever be grateful. To my husband Ankit and my son Veydant, thank you for being my strength always.

Abbreviations

A2E	Apolipoprotein E
AAV2	Adeno-associated Virus type 2
AI	Artificial Intelligence
AMD	Age related Macular Degeneration
AREDS	Age related Eye Disease Study
ARMS2	Age Related Maculopathy Susceptibility 2 gene
ART	Averaging Retinal Frames
AUC	Area under the curve
BAF	Blue Autofluorescence
BCVA	Best Corrected Visual Acuity
b-FGF	Basic-Fibroblast Growth Factor
BLamD	Basal laminar deposits
BMI	Body Mass Index
BrM	Bruch's Membrane
BrM-CC	Bruch's Membrane-Choriocapillaris
CAM	Classification of Atrophy Meeting
CC	Choriocapillaris
CCR3	C-C chemokine receptor 3
CFH	Complement Factor H
CFP	Colour Fundus Photography
CI	Confidence Interval
CNV	Choroidal Neovascular Membrane
CONAN	Consensus Nomenclature for Reporting Neovascular AMD
cRORA	Complete retinal pigment epithelium and outer retinal atrophy
CRT	Central Retinal Thickness
CSFT/CST	Central Subfield Thickness
cSLO	Confocal Scanning Laser Ophthalmoscopy
DA	Dark Adaptation
DLS	Double Layer Sign
ECM	Extracellular Matrix
EDI	Enhanced Depth Imaging
ELM	External Limiting Membrane
ERF	Early Residual Fluid
ERM	Epiretinal Membrane
ETDRS	Early Treatment Diabetic Retinopathy Study
EZ	Ellipsoid Zone
FAF	Fundus Autofluorescence
FAM	Fundus Autofluorescence in Age-Related Macular Degeneration
FAZ	Foveal Avascular Zone
FCPT	Foveal Centre Point Thickness
FFA	Fundus Fluorescein Angiography
fPED	Fibrovascular Pigment Epithelial Detachment
GA	Geographic atrophy

GCL	Ganglion Cell Layer
GEE	Generalized Estimating Equations
GPS	Granular with peripheral punctate spots
hDc/HDL	Hyporeflective drusenoid cores/hyporeflective drusenoid lesions
hESC	Human embryonic stem cells
HFL	Henle Fiber Layer
hPED	Hemorrhagic Pigment Epithelial Detachment
HRF	Hyperreflective foci
HS	High Speed
HTRA1	High-Temperature Requirement protein A1
hUTC	Human umbilical tissue-derived cells
iAMD	Intermediate Age related Macular Degeneration
ICGA	Indocyanine Green Angiography
ILM	Internal Limiting Membrane
INL	Inner Nuclear Layer
IPL	Inner Plexiform Layer
iPSC	Induced pluripotent stem cells
IQR	Interquartile Range
IRF	Intraretinal Fluid
iRORA	Incomplete retinal pigment epithelium and outer retinal atrophy
IS	Inner segments
IZ	Interdigitation Zone
LLD	Low Luminance Deficit
LLVA	Low Luminance Visual Acuity
MAC	Membrane Attack Complex
MNV	Macular Neovascularization
nAMD	Neovascular Age related Macular Degeneration
neMNV	Non-exudative Macular Neovascularization
NICE	National Institute for Health and Care Excellence
NIR	Near Infrared Reflectance
OCT-A	Optical Coherence Tomography Angiography
ONL	Outer Nuclear Layer
OPL	Outer Plexiform Layer
OR	Odd Ratio
ORT	Outer retinal tubulation
OS	Outer segments
PCV	Polypoidal Choroidal Vasculopathy
PDGF	Platelet-Derived Growth Factor
PED	Pigment Epithelial Detachment
PGF	Placental Growth factor
PIS	Patient Information Sheet
PLGA	poly(d,l-lactide-co-glycolide)
PRL	Photoreceptor Layer
qAF/qAF8	Quantitative Autofluorescence/qAF mean of middle 8 segments of Delori Ring
RAP	Retinal Angiomatous Proliferation

RIT	Rod Intercept Time
RNFL	Retinal Nerve Fiber Layer
ROC	Receiver operating characteristic
ROS	Reactive Oxygen Species
RPD	Reticular Pseudodrusen
RPE	Retinal Pigment Epithelium
RPE-BrM/RPE-BM	Retinal pigment epithelium- Bruch's Membrane
SD	Standard Deviation
SDD	Subretinal Drusenoid Deposits
SD-OCT	Spectral Domain Optical Coherence Tomography
SFCT	Subfoveal Choroidal Thickness
sFlt-1	soluble fms-like tyrosine kinase-1
SHRM	Subretinal Hyper Reflective Material
SIRE	Shallow Irregular Retinal pigment epithelium elevation
SRF	Subretinal Fluid
sPED/svPED	Serous pigment epithelial detachment/serous vascularized PED
SS-OCT	Swept source optical coherence tomography
TF	Tissue Factor
TRV	Total Retinal volume
UWF	Ultrawide Field
VEGF	Vascular Endothelial Growth Factor
VE-PTP	Vascular endothelial tyrosine phosphatase
VEGFR	Vascular Endothelial Growth Factor Receptor
VMT	Vitreomacular Traction
WCR	Within Cluster Resampling

List of Figures

List of Tables

1 Chapter 1 Introduction

1.1 General Introduction

Age related macular degeneration (AMD) is the leading cause of irreversible blindness in the developed countries. It predominantly affects the central region of retina, namely the macula, and results from age related pathological changes in the retinal pigment epithelium (RPE), choroid and neural retina (Khandhadia, Cherry et al. 2012). Broadly AMD has 2 phenotypes, the more common being 'dry' or non-neovascular AMD characterised by extracellular sub-RPE deposits of varying size and number called drusen and/or pigmentary irregularities of the RPE that may progress to an advanced form termed geographic atrophy (GA) characterised by atrophy of RPE and outer retina. The other advanced phenotype called 'wet' or neovascular AMD (nAMD) presents with macular neovascularization (MNV) and may occur at any point in the course of dry AMD. Both advanced phenotypes cause severe vision loss (Fleckenstein, Keenan et al. 2021).

The pathogenesis of AMD is complex and although aging is the strongest risk factor for AMD, environmental factors such as smoking that increases oxidative stress and other pathological pathways may contribute to its occurrence and/or progression (Merle, Silver et al. 2015, Garcia-Garcia, Usategui-Martin et al. 2022). In the last 15 years, genome-wide association studies have also identified genetic risk factors involved in pathogenesis of AMD (Seddon, Francis et al. 2007, Colijn, Meester-Smoor et al. 2021). The major challenge with diseases of multifactorial pathogenesis is disease prognostication. Various groups have proposed risk scores for AMD to solve this conundrum. However, the individual-level risk prediction for AMD progression to vision threatening disease or blindness remains a challenge. Moreover, response to treatment is also unpredictable. A crucial hurdle is our lack of understanding of the morphological diversity of AMD clinical phenotypes. It is becoming clear that AMD is not a single disease that progress through the known stages of disease progression. Instead, it consists of multiple phenotypes with varying outcomes within each major sub classification of dry and wet AMD and they may co-exist. The macular findings in an eye with AMD, irrespective of the severity stage are heterogeneous. Although

the findings in early and intermediate AMD (iAMD) correlate between eyes, one may progress to MNV or GA faster although they become symmetrical with time.

To date, all classification systems in AMD propose stages based on features identified on colour fundus photographs (CFP) (Thee, Meester-Smoor et al. 2020). With the advent of multimodal imaging and its increasing use in ophthalmology clinics and clinical trials, it has become imperative to understand heterogeneity of AMD features in these modalities as well. Spectral domain Optical Coherence Tomography (SD-OCT) is the current mainstay modality used for diagnoses and disease monitoring of AMD across several platforms including but not limited to clinics, community settings, clinical trials, research labs and to develop deep learning algorithms (Damian and Nicoară 2022). The high resolution of OCT allows cross-sectional analysis of the retinal layers that is closely comparable to retinal histology (Müller, Wolf et al. 2019). More importantly, OCT can identify first signs of cell loss and the beginning of atrophy in eyes with early or intermediate AMD before clinically apparent signs of late disease. These signs confer higher odds of disease progression (Sadda, Guymer et al. 2018). Moreover, OCT is the most accurate diagnostic modality to identify the presence of subretinal drusenoid deposits (SDD), a risk factor for progression to advanced AMD including higher rates of GA lesion expansion (Jaffe, Chakravarthy et al. 2021). In nAMD, several features on OCT imaging have been defined that were previously not captured on fundus fluorescein angiography (FFA) or CFP based description of nAMD for example., subretinal hyperreflective material (SHRM) and different types of pigment epithelial detachments (PED) (Muth, Toro et al. 2022). All these features are conspicuously absent from the current classification systems causing a noteworthy void in our outcome prediction for an individual.

The studies described in this thesis seek to better understand this phenotypic heterogeneity across varying stages of AMD and how they impact the visual and anatomical outcomes.

Chapter 1 will introduce the concepts central to this thesis:

- It will begin with an overview of the structure and physiology of the retina and choroid, changes in the ageing retina, followed by a brief discussion of AMD pathogenesis, diagnosis and current and pipeline management options (Sections 1.2 and 1.3)
- Next is a review of OCT-based imaging biomarkers and their risk for progression to advanced AMD (Section 1.4).
- The third section will discuss established classification systems of AMD and the rationale for new classification systems based on phenotypic and functional heterogeneity (Section 1.5).
- The chapter will be concluded with the overall aims of this thesis (Section 1.6).
- The thesis will then progress to the following chapters, and each will have a relevant introduction, specific methods, results and discussion:
  - The methodology that applies to all the studies in this thesis (Chapter 2).
  - Phenotypic heterogeneity in early and iAMD and derivation of a classification based on multimodal imaging and structure-function correlation (Chapter 3).
  - Phenotypic heterogeneity in nAMD and its impact on short- and long-term treatment outcomes (Chapter 4).
  - Heterogeneity of GA progression and its implications in measurement of outcome measures in clinical trials (Chapter 5).
  - An overall discussion of the body of work and conclusion including propositions for future work in this area (Chapter 6)

1.2 Overview of Relevant Anatomy and Physiology

1.2.1 Retinal structure and physiology

The retina forms the innermost coat of the posterior segment of the eye and is situated internal to the vascular choroid and the outermost fibrous sclera. It is the visible area of the posterior segment of the eye on clinical examination and consists of 10 layers of cells that capture incoming light as photons and transmits them through the nerve pathways for the brain to form the visual image. The transmission occurs via both electrical and chemical signals. On fundoscopy we can visualize the clear landmark of the optic nerve head (papilla) with blood

vessels radiating from it. Fovea is localized temporal to the optic disc at a distance of about 3.4 mm or 2.5 optic disc diameters away as a brownish-yellow area. Figure 1.1 shows the optic nerve head (papilla), retinal blood vessels and the fovea. The fovea is located temporal to the optic nerve head at a distance of approximately 3.4mm (2.5 disk diameter) *(Image source: Author's own)*.

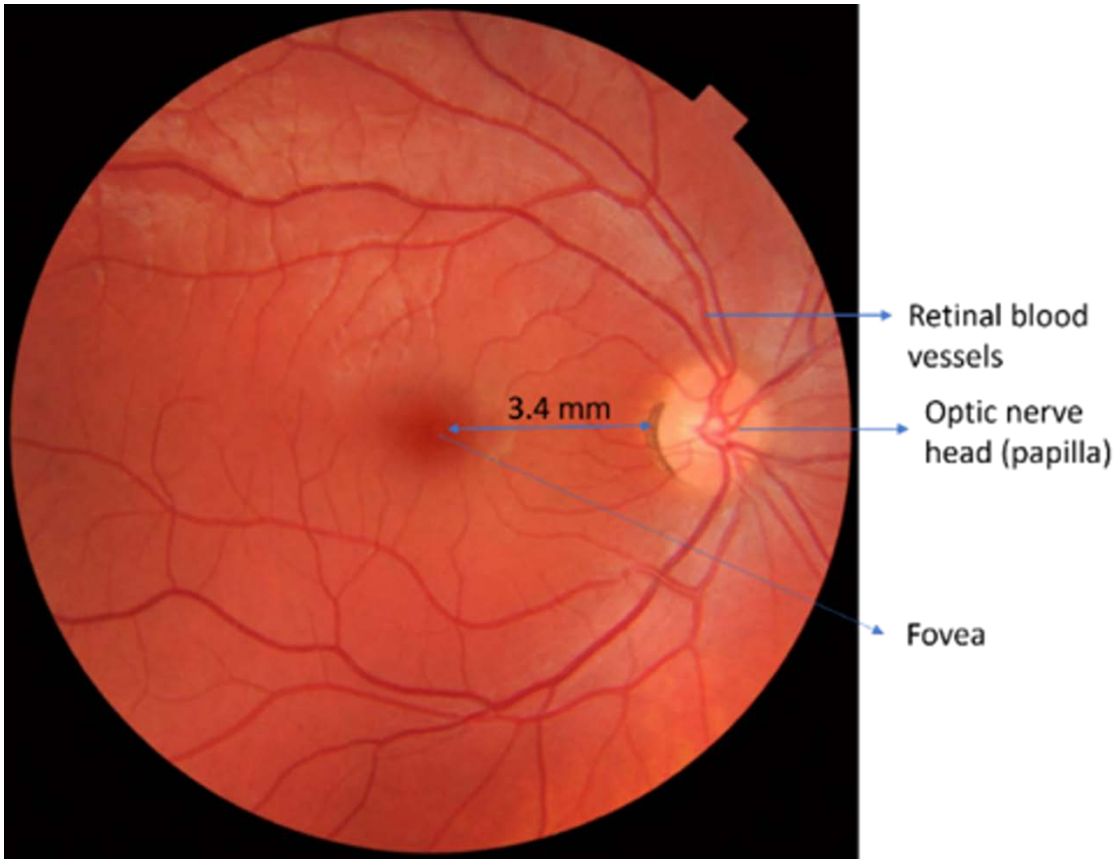

Figure 1.1 Colour photograph of a normal fundus.

An area of 5.5 mm diameter around the fovea is referred to as the macula whereas macula lutea is the yellow pigmentation that extends beyond the fovea into the parafovea with an approximate diameter of 2.5 mm. The fovea itself has a diameter of 1.5 mm, with the centre-most point called foveal pit or umbo (diameter 0.15 mm across). At the foveal pit, most retinal layers are absent except those beneath the cone photoreceptors. At the edges of the pit, the foveal slope may have some cell bodies of retinal interneurons, bipolar, horizontal and some amacrine cells. The nearest ganglion cells from the foveal pit appear only at the diameter of 0.35. The foveal avascular zone (FAZ) measures 0.5 mm across the fovea. Immuno-stained images of the central fovea have confirmed

that even the smallest capillaries do not intrude into the foveal centre (Figure 1.2) (Helga Kolb 2020 Feb 7 [Updated 2020 May 20]).

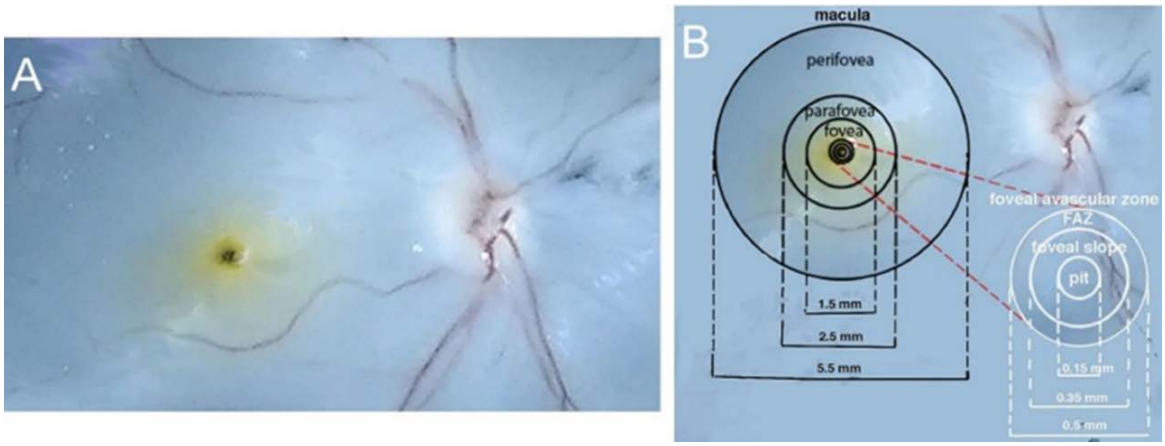

Figure 1.2 Human retina showing the fovea and optic nerve.
(A) the optic nerve (right), blood vessels and the fovea (centre) with surrounding macula lutea (yellow). (B) A map of the whole macular area to show the dimensions of the foveal pit, FAZ, parafovea, perifovea, and the limits of the macula. Inset shows the dimensions of the FAZ. Image Source (Helga Kolb 2020 Feb 7 [Updated 2020 May 20]).

As mentioned before the retina consist of 10 layers that are mentioned in order from inner (towards the vitreous) to outer (towards the choroid) (Tadi. 2023 Jan [Updated 2023 Aug 8]). With reference to the thesis, I have described the outer retinal layers in further detail.

Inner Limiting Membrane (ILM): This is the innermost layer of the retina and is formed of astrocytes and Müller cells.

Retinal Nerve Fiber Layer (RNFL): The retinal nerve fibre layer as the name suggests consists of axons of ganglion cells. These fibres travel along the surface of the retina towards the optic nerve head where they exit to travel towards the brain. This layer also contains the inner capillary plexus of the retinal circulation.

Ganglion Cell Layer (GCL): This layer contains the cell bodies of retinal ganglion cells interspersed by Müller cells and amacrine cells.

Inner Plexiform Layer (IPL): This layer contains the dendrites of the cell bodies in the inner nuclear layer.

Inner Nuclear Layer (INL): Bipolar, horizontal and amacrine cell bodies form the substance of this layer.

Outer Plexiform Layer (OPL): This is a synaptic layer like the inner plexiform layer and connects the bipolar cells from the INL to photoreceptors in outer nuclear layer.

Outer Nuclear Layer (ONL): the layer containing the cell bodies of both rods and cones. Thinning of this layer is an indirect marker for photoreceptor degeneration.

External Limiting Membrane (ELM): This layer separates the inner and outer segments of rods and cones from the cell bodies and is composed of gap-junctions between the Muller cells and photoreceptor cells. The ELM is seen as a thin hyperreflective line running inner to the ellipsoid zone (EZ) on the OCT scans.

Photoreceptor Layer (PRL): This layer contains both the outer and inner segments of the rods and cones. The inner segment house the numerous mitochondria and outer segments contain membrane bound discs filled with light sensitive pigments (Narayan, Chidlow et al. 2017). On OCT, the outer segments (OS) are called the myoid zone and inner segments (IS) are called the EZ layers. It is seen as a hyperreflective line inner to the RPE.

RPE: the outermost retinal layer that spans a width of a single cell located between the neural retina and the Bruch's membrane (BrM), adjacent to the highly vascularized choroid layer. The RPE contributes to the blood-retinal barrier in conjunction with the inner blood retinal barrier, the endothelium of the retinal vessels and has many functions including ion and water transport and secretion of growth factors and cytokines (Spencer, Abend et al. 2017). The RPE cells intermingle with the OS of the rods and cones. This proximity allows for the recycling of all-*trans*-retinal back into 11-*cis*-retinal and its delivery back to the cones and rods to be used again for phototransduction (Strauss 1995). RPE cells are crucial in the support and maintenance of both photoreceptor cells and the underlying capillary endothelium. The RPE anatomy and physiology is explained in further detail in section 1.2.2.

BrM: The BrM is 2-4 microns thin, and it composed of extracellular matrix that lies between the RPE and choroid. The BrM has 5 layers which are RPE basement membrane, inner collagenous layer, central elastic layer, outer collagenous layer and choroidal endothelial cell basement membrane from RPE to CC respectively (Hammadi, Tzoumas et al. 2023). These layers together act as a semi permeable membrane for exchange of nutrients, oxygen, minerals and visual cycle by-products. BrM is the primary regulator of this passive diffusion of nutrients from choroid to retina. This is particularly relevant for ageing retina and in AMD where BrM acts as a barrier especially for complement proteins (Guymer, Luthert et al. 1999). Even in young and healthy eyes, only a limited number of complement proteins namely factor H like 1 protein (FHL-1), factor D, and C5a, are allowed to diffuse through. However, in ageing and AMD this compartmentalisation may be exacerbated. BrM undergoes several alterations in an ageing eye, including but not limited to overall thickening due to increased deposition of collagen, lipids, tissue inhibitor of metalloproteinase (TIMP-2), matrix metalloproteinase (MMPs) 2 and 9, calcium phosphate, and advanced glycation end-products (AGEs). Additionally, basal laminar and basal linear deposits are observed with age, and there is a reduction in heparan sulphate. These changes to BrM contribute to the pathogenesis of several retinal diseases, including AMD. Due to increased lipid deposition in AMD there is reduced FHL-1 diffusion leading to creation of 2 separate compartments for complement activation and regulation, namely the retinal and choroidal sides, with complement proteins remaining on their side of origin (Hammadi, Tzoumas et al. 2023). This is of particular value in complement therapies for AMD.

1.2.2 Retinal Pigment Epithelium: anatomy and physiology

As mentioned above, the RPE is a single later of cells closely related to the outer segments of photoreceptors. It is responsible for multiple essential functions of retinal physiology namely: phototransduction cascade through regeneration of chromophore, trophic support for photoreceptors, transport barrier between CC and neurosensory retina, ocular immune response, binding of reactive oxygen species and absorption of excess radiation by the melanin granules (Wong, Ma et al. 2022). In normal ageing, the RPE cells decrease in density and some RPE cells become multinucleated particularly in the periphery. This is due to abnormal

or failed attempts at cell division process. The RPE cytoskeleton also changes with ageing where the cells become more irregular, elongated and lose their hexagonal shape. However, the monolayer remains intact with normal ageing. In AMD though the changes in RPE morphology differ. Cells become more concave and rounder; there is abnormal thinning or thickening or separation or splitting due to fragmentation of the cytoskeletal component (Ach, Tolstik et al. 2015). This leads to worsening of the blood retinal barrier formed by BrM and RPE (Figure 1.3). This is evident by the presence of toxic plasma components (that are usually excluded by the blood retinal barrier) in eyes with intermediate AMD (iAMD) indicating a compromised blood retinal barrier. These include plasma proteins like albumin, fibrinogen, IgG (Schultz, Song et al. 2019). Even in advanced stages of AMD like GA and nAMD this is apparent. Especially in nAMD it has been shown that the upregulation of vascular endothelial growth factor (VEGF) is not enough for new vessel formation and the breakdown of RPE tight junctions is an essential component (Oshima, Oshima et al. 2004).

Altogether these results show that breakdown of RPE blood retinal barrier in AMD eyes is an important pathological occurrence. The role of RPE in immune regulation also takes a hit in AMD eyes. A pro-inflammatory environment develops due to upregulation of complement factors and chemokines and associated receptors in the RPE leading to AMD progression (Demirs, Yang et al. 2021). There is decrease in phagocytic activity of the RPE leading to decreased renewal of photoreceptors outer segments as well. Additionally, autophagy dysfunction of RPE cells may be responsible for triggering inflammatory cascade that contributes to cell death in AMD (Mitter, Song et al. 2014). Lipid cycling has been shown by many to be the driver of AMD progression. The accumulation of lipid-derived components occurs in the RPE cell. These lipid droplets and components form a ‘lipid-wall’ between the RPE cell and the inner collagenous layer of the BrM (Curcio, Johnson et al. 2009). This ‘lipid-wall’ acts as an impediment to nutrient exchange impairing RPE function. The location and content of these basal linear deposits is suggested to represent soft drusen and highlights the importance of lipid cycling in the RPE in AMD. Lipofuscin associated with melanosomes is called melanolipofuscin and accumulates in the RPE in the ageing retina. In AMD there is excess accumulation of this

melanolipofuscin which interferes with RPE function by damaging mitochondrial DNA in RPE cells through lipid peroxidation. Chronic oxidative stress as well promotes RPE cell dysfunction (Olchawa, Furso et al. 2017).

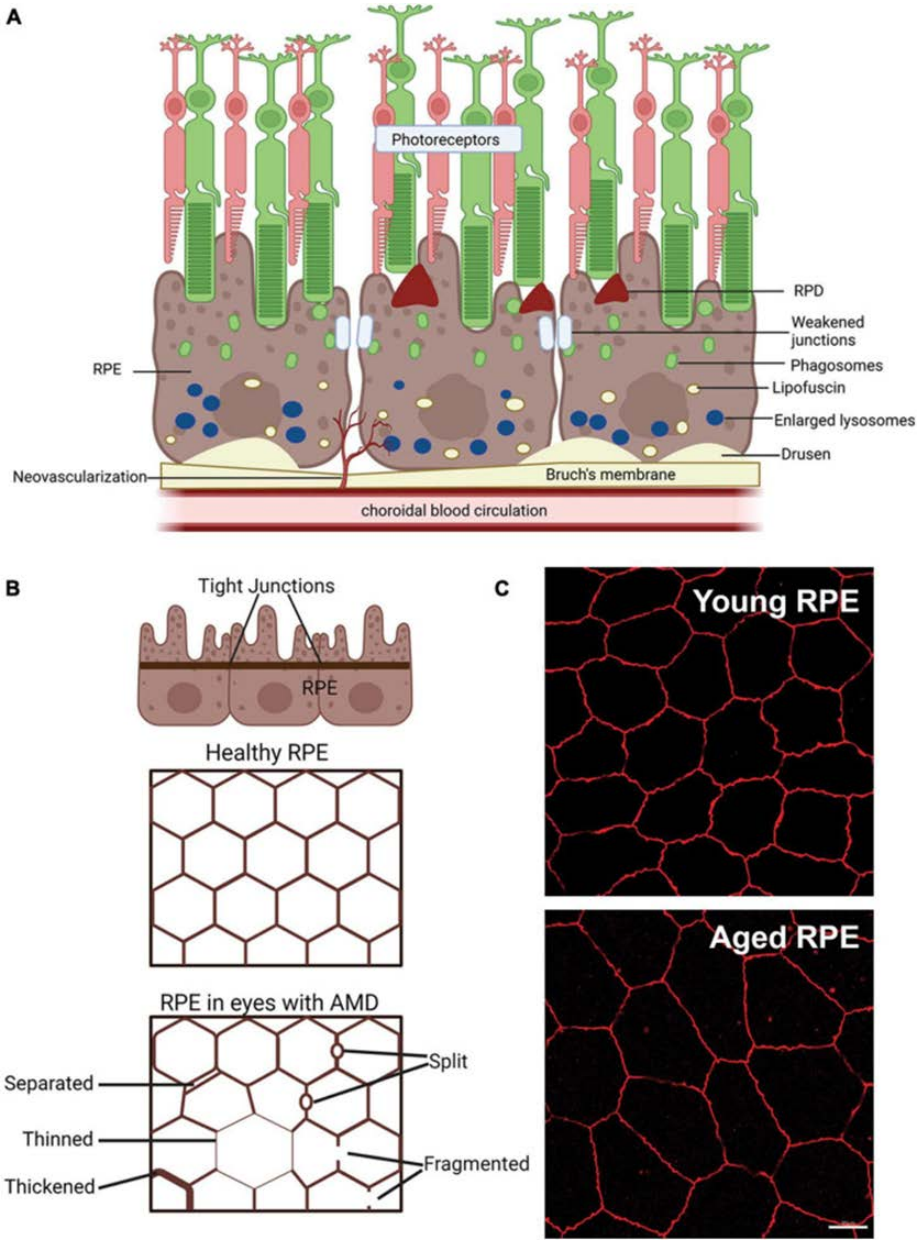

Figure 1.3 Schematic showing changes in RPE in healthy ageing and AMD. (A) RPE changes in late-stage AMD, including weakening of tight junctions, deposition of lipofuscin and enlarged failed lysosomes. (B) RPE tight junctions in AMD in flat mount view. (C) Aging mouse RPE. Tight junction ZO-1 (zonula occludens) labelling of young (3 month) and old (22 month) mouse RPE, shows increased RPE cell size in the aged tissue, suggesting cell loss with age. Image Source: (Wong, Ma et al. 2022).

1.2.3 Choroid: anatomy and physiology

The choroid forms the vascular layer sandwiched between the retina and sclera and it extends from the margins of the optic nerve to the pars plana and ciliary body. It is bound by the BrM forming its innermost layer and the suprachoroid on the outside. Based on the histological appearance the choroid has a complex 5-laminar structure: starting from the retinal (inner) side, these are the outer lamina of the BrM, the choriocapillaris, the two vascular layers (Haller's and Sattler's), and the suprachoroidea (Figure 1.4) (Nickla and Wallman 2010).

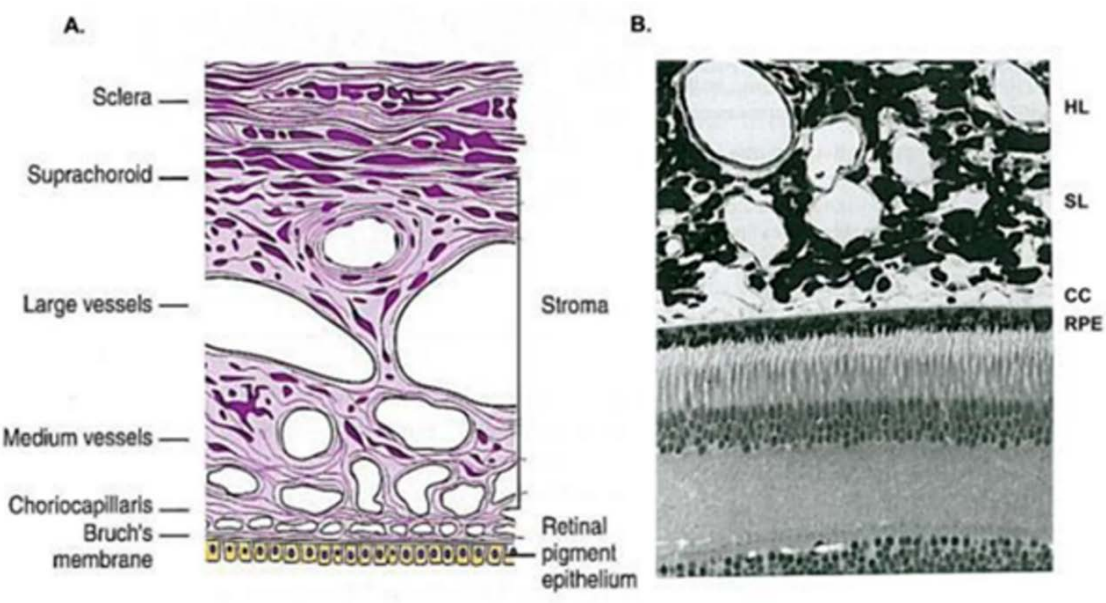

Figure 1.4 Histology of the choroid.
A. Layers of the choroid schema. B. Semithin resin section of the outer retina and choroid in the primate eye. RPE: retinal pigment epithelium; CC, choriocapillaris; SL: Sattler's layer; HL: Haller's layer. Image Source: (Nickla and Wallman 2010).

The choriocapillaris (CC) is a thin sheet of highly anastomosed capillary network opposed to the BrM. The outermost layer of BrM is formed by the fibrous basement membrane of the capillary endothelial cells. The CC is thickest subfoveally with the highest density of capillaries measuring about 10µm in thickness. It thins peripherally to about 7µm. The patchy structure of the CC is due to the lobular or hexagonal shaped domain of single layer of capillaries arising from the arterioles in Sattler's layer (Nickla and Wallman 2010). The capillaries have large fenestrations in them (20-40µm) that are highly permeable to proteins (Bill, Törnquist et al. 1980). The major blood supply to the retina is via the choroid especially the outer retinal layers and at the fovea. Due to high

metabolic activity of the photoreceptors over 90% of the oxygen delivered to the retina from the choroid is consumed by the photoreceptors (Linsenmeier and Braun 1992). In dark, the light gated channels for active transport of ions, most of the oxygen comes from the choroid. To obtain this high oxygen transport despite the BrM and RPE as barriers the choroid maintains a steep gradient of oxygen tension (Figure 1.5) (Yu and Cringle 2001). This is achieved by high blood flow per unit tissue weight. Consequently, the oxygen tension in the choroid stays high, with an arterial/venous difference of only 3% versus 38% for the retinal circulation.

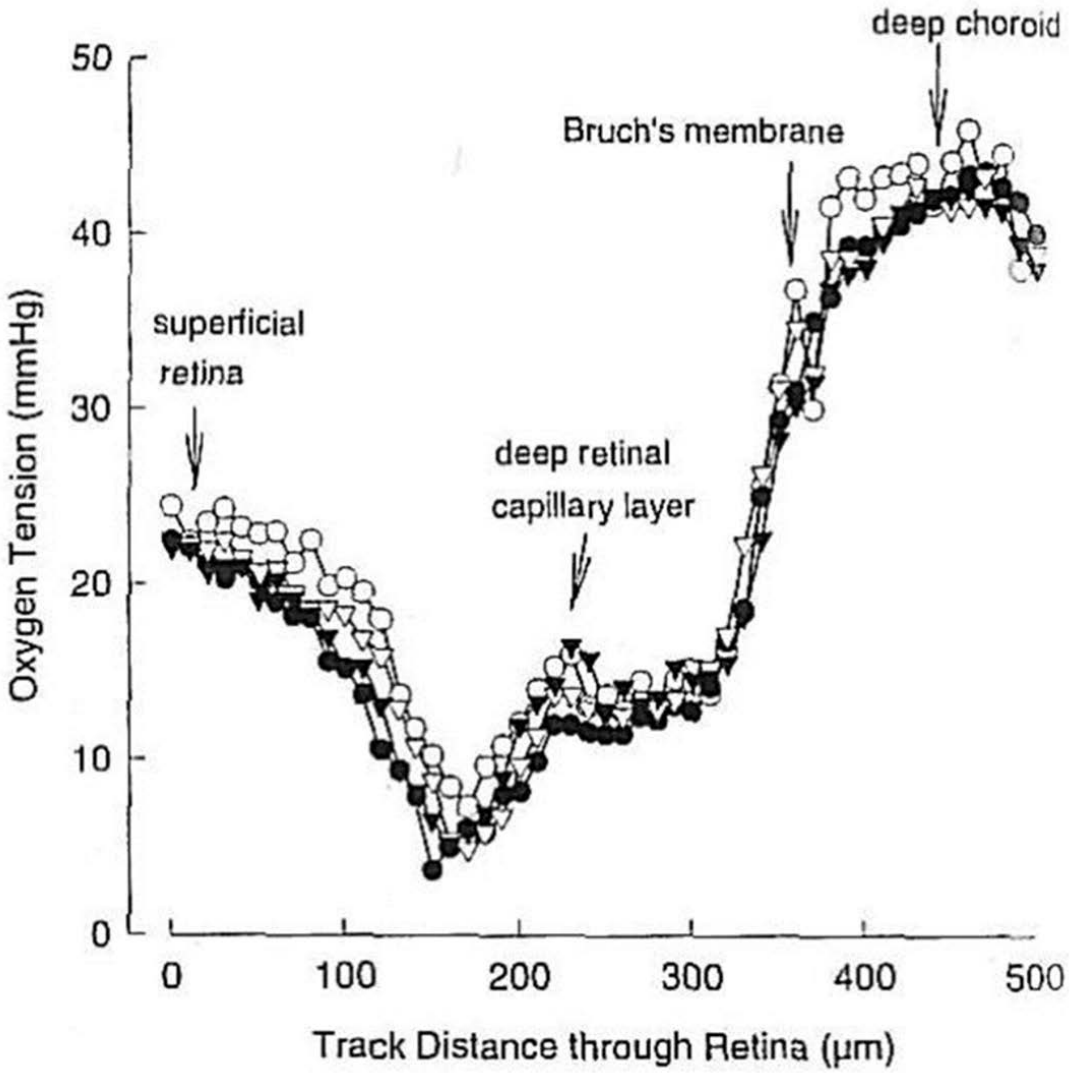

Figure 1.5 Oxygen tension profile through a vascular retina (rat).
The measurements are from two sequential penetrations (circles) and withdrawals (triangles) of the electrode. Image Source (Nickla and Wallman 2010).

1.2.4 Ageing retina and choroid versus Age related macular degeneration.

The ageing RPE becomes increasingly pleomorphic. Macular RPE becomes narrower with increased height and the peripheral RPE cells become broader, shorter and more vacuolated (Friedman and Ts'o 1968). Lipofuscin and other fluorophores accumulate in the cytoplasm of RPE, and apolipoprotein E (A2E) epoxides are toxic to the RPE (Sparrow, Vollmer-Snarr et al. 2003). There is significant clinical and research interest in lipofuscin related autofluorescence patterns in AMD; however, the histologic correlations with retinal imaging remain unclear (Bindewald, Bird et al. 2005, Rudolf, Vogt et al. 2013). Ageing retina also shows accumulation of sub RPE excrescences or drusen that form on the inner aspect of BrM and are composed of various substances including protein, crystalline calcium deposits, lipids and residual bodies (Spraul and Grossniklaus 1997). There are several histopathologic and imaging subtypes of drusen that vary from hard, soft, confluent, cuticular and SDD (Spraul and Grossniklaus 1997). It is important to note that hard drusen are nonspecific and age-related whereas soft, confluent drusen and SDD are associated with AMD (Sarks, Cherepanoff et al. 2007, Chen, Messinger et al. 2020). Basal laminar deposits are eosinophilic, brush-like material that accumulated external to the basement membrane of the RPE, and it contains granular material non coated and coated vesicles and wide spaced collagen (Sarks 1973). These deposits are associated with both aging and AMD, they are thicker in eyes with AMD (Sarks, Cherepanoff et al. 2007). In contrast basal linear deposits accumulate between the basement membrane and plasma membrane of the RPE and are a specific ultrastructural marker for AMD (Curcio and Millican 1999). The SDDs are identified as dollops or mounds of a granular extracellular material interspersed with tufts of RPE apical processes i.e., they appear internal to the RPE unlike other drusen morphologies (Curcio, Messinger et al. 2013, Chen, Messinger et al. 2020). This material contains histochemical detectable unesterified cholesterol, A2E, vitronectin, complement factor H (CFH), and CD59. Chen et al in their study on histologic insights of SDD have presented a theory of AMD deposit pathogenesis encompassing both SDD and other drusen (Chen, Messinger et al. 2020). They propose that both these deposits are a result of dysregulation of lipid transfer and cycling pathways that are essential for specialized physiology of photoreceptors, along with RPE, Muller glia and CC epithelium. This theory is supported by the

distinct lipid composition and topographies of SDD and soft drusen that resemble that of rods and cones (Curcio 2018). Drusen formation is linked to impaired BrM-choriocapillaris complex (BrM-CC) leading to large lipoprotein secretions of RPE getting accumulated in the BrM (Curcio 2018). Drusen enlargement occurs due to inefficient clearance of RPE secretions eventually leading to drusen collapse and associated RPE migration or death. SDD accumulate due to protein mediated transfer of unesterified cholesterol, fatty acids, retinoids and xanthophyll carotenoids. Changes in the BrM include thickening and calcification with ageing. These changes can be focal and diffuse thickening of the inner aspect of BrM and resemble changes in the arterial intima including the deposition of lipoproteins (Sivaprasad, Bailey et al. 2005).

Alteration in hemodynamics of the choroid, the main blood supply of the outer retina has been postulated to contribute to the pathogenesis of AMD (Gelfand and Ambati 2016). Therefore, the survival of the CC for nutrition and clearance of by-products of retinal metabolism is essential to the health of the outer retina (Farazdaghi and Ebrahimi 2019). Additionally, the choroid supplies the central 250 to 600 μm of the macula (FAZ), which lacks retinal blood vessels (Margolis and Spaide 2009). Given the high metabolic rate of the photoreceptors, the choroid per-unit mass is one of the most vascularized structures in the body (Zhu, Zheng et al. 2006, Zouache, Eames et al. 2016). Progressive involutional changes occur in the CC with normal aging. While some atrophy of the CC is expected with age, CC atrophy in AMD exceeds the amount attributable to normal aging (Bhutto, Uno et al. 2008, Seddon, McLeod et al. 2016). It has been suggested that the degree of CC pruning is related to the number of drusen present. Mullins et al observed an inverse relationship between choroidal thickness and the density of deposits (Mullins, Johnson et al. 2011). They showed that in early AMD (Age related Eye Disease Study [AREDS] grades 2 and 3), as the number of ghost vessels increases, CC density decreases, suggesting that CC dropout is due to endothelial loss and precedes RPE atrophy. In addition, an inverse relationship has been observed between the extent of drusen within the macula and choroidal blood flow beneath the fovea. Alten et al showed SDD tend to occur within or very near to choroidal watershed zones, which are at the border between two or more separate regions of perfusion,

which have comparatively poor vascularity and are vulnerable to ischemia (Alten, Clemens et al. 2013). Before any observable retinal alterations, early RPD development coincides with choroidal thinning, as well as an increase in the ratio of stromal to total choroidal area. Thorell et al showed that intermediate AMD patients with SDD had thinner choroid below the fovea compared with age-matched controls (Thorell, Goldhardt et al. 2015). These data support the idea that reduced blood flow within the macular CC is involved in early AMD pathophysiology especially in eyes with SDD.

1.3 Age related macular degeneration

1.3.1 Pathogenesis

The pathogenesis of AMD is highly complex and not completely understood. However, multiple triggers and processes that lead to degeneration of RPE and/or neovascularization have been identified (Garcia-Garcia, Usategui-Martin et al. 2022). The schematic below attempts to summarize the various components in play (Figure 1.6).

The main issues include an altered proteostasis and lipid homeostasis, uncontrolled oxidative stress, and mitochondrial dysfunction. These form an internal feedback loop leading to RPE dysfunction, deposition of misfolded proteins, lipid and lipid peroxidation products forming drusen. Over time, the deposition of aberrant drusen material increases due to a poor antioxidant response, deficiencies in autophagy systems, and dysregulation of the extracellular matrix (ECM). The complement system is an important part of the chronic inflammation of the subretinal region that is caused by the drusen, which also operate as inflammatory centres to recruit macrophages and microglia. Nutritional factors and choriocapillaris degeneration are additional well-known pathophysiologic components of AMD. The identification of the risk or protective polymorphisms of a few complement and ECM-related genes like CFH and ARMS2 (Age Related Maculopathy Susceptibility 2)/HTRA1 (High-Temperature Requirement protein A1) represents the genetic component of the disease. Therefore, those who carry the risk haplotype at ARMS2/HTRA1 are more likely to experience the onset of late AMD at a younger age. Lastly, gut microbiota and epigenetics may modulate the progression to progressive AMD.

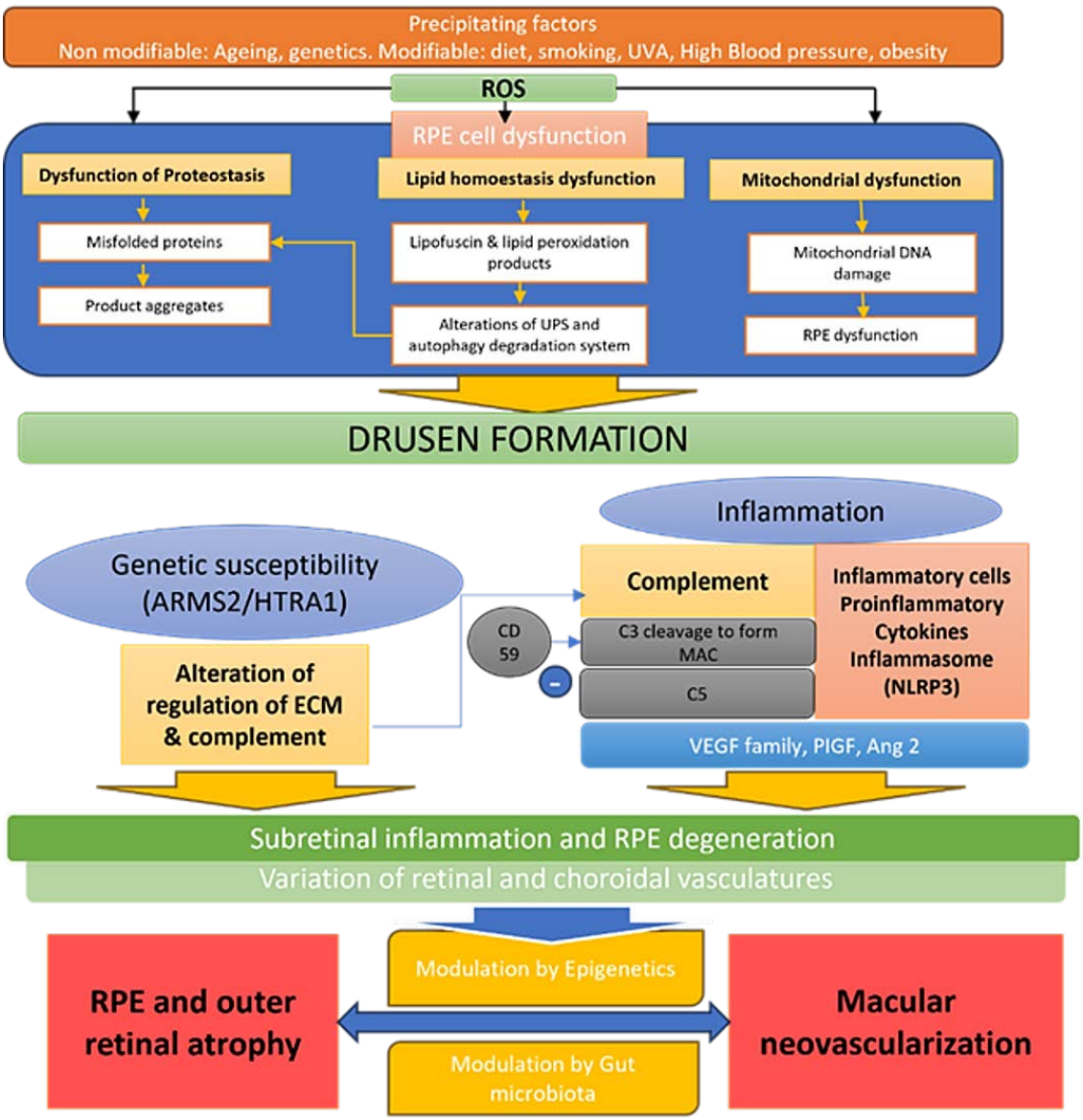

Figure 1.6 Summary of the pathophysiology of AMD.
NLRP3, NACHT, LRR and PYD domains-containing protein 3; ROS, reactive oxygen species; RPE, Retinal pigment epithelium; UPS, ubiquitin-proteosome system; UVAs, ultraviolet A; HBP, high blood pressure; RPE, retinal pigment epithelium; CFH, complement factor H gene; ECM, extracellular matrix; VEGF, vascular endothelial growth factor; PIGF, placental growth factor; Ang2, angiopoietin 2; ARMS2/HTRA1, age-related maculopathy susceptibility 2 gene/high-temperature requirement protein A1. Image source: Author's own.

Given the number of involved processes, a variety of complex treatment combinations will likely be the best choice to achieve the best visual outcomes; these combinations will then vary based on the type and severity of the disease affecting each patient individually or the stage of the disease in each patient at a given time. Personalised treatment for prevention and, perhaps, eventual cure will need to be programmed with better understanding of these combinations

and permutations. To develop therapeutic combinations for various concurrent or future issues, it is necessary to continue unravelling all the processes involved in the pathogenesis of AMD.

1.3.2 Risk factors

The main modifiable and non-modifiable risk factors for AMD are summarized in Table 1.1.

Table 1.1 Non-modifiable and modifiable risk factors for AMD.

Non-modifiable risk factors	
Increasing drusen area and volume	Larger drusen volume (>0.03 mm^3) within 3mm circle centred at fovea have a four-time higher risk of progressing to late AMD than those with smaller drusen volume (Yehoshua, Wang et al. 2011, Abdelfattah, Zhang et al. 2016).
Subretinal Drusenoid Deposits (SDD)	SDD or RPD is an independent risk factor for progression to late AMD (Zweifel, Imamura et al. 2010, Huisingh, McGwin et al. 2016).
Genetics	There is no genetic score defined to assess risk for AMD and although 52 genetic variants have been identified for AMD, almost 15% of patients with AMD have no risk variants (Haines, Hauser et al. 2005, Cascella, Strafella et al. 2018).
Fellow eye of nAMD eyes	Incidence of nAMD in fellow eyes: up to 12.2% by 12 months and 26.8% by 4 years (Wong, Chakravarthy et al. 2008).
Fellow eye of unilateral GA	Estimated median time to second eye involvement in AREDS was 7 years (Fleckenstein, Mitchell et al. 2018)
Double layer sign (DLS) and non-exudative macular neovascularization (neMNV)	Eyes with DLS have a four times greater hazard of progression to exudation over three years (Csincsik, Muldrew et al. 2023). The risk of exudation can be as high as 15.2 times (95% confidence interval, 4.2-55.4) greater in eyes with neMNV compared with

	eyes without subclinical MNV (de Oliveira Dias, Zhang et al. 2018).
Modifiable risk factors	
Smoking History	Smoking quadruples the risk of progression to late AMD in current smokers and there is a synergistic effect between smoking and genetic risk factors (Tan, Mitchell et al. 2007, Jabbarpoor Bonyadi, Yaseri et al. 2017). Current smokers develop nAMD at an average 5.5 years younger than those who never smoked and 4.4 years younger than past smokers (Detaram, Joachim et al. 2020).
Body Mass Index (BMI)	A higher BMI (>30) increases the risk for progression to advanced AMD (RR 2.35) (Jaisankar, Swaminathan et al. 2018). A twofold increased risk for progression is associated with a wider waist circumference (Seddon, Cote et al. 2003).
Nutrition	A diet low in omega-3 and -6 fatty acids, antioxidant vitamins, carotenoids and minerals are risk factors for AMD. Adherence to a Mediterranean diet is associated with a 41% reduced risk of incident late AMD (Merle, Colijn et al. 2019).
Sunlight exposure	Meta-analysis on the association between sunlight exposure and AMD indicated no relationship between exposure to sunlight and increased risk of AMD (Zhou, Zhang et al. 2018).

Abbreviations: AMD – Age related macular degeneration; BMI – Body mass index; DLS Double layer sign; nAMD – neovascular AMD; neMNV – non exudative macular neovascularization; SDD – Subretinal drusenoid deposits.

1.3.3 Clinical features of AMD

The fundus examination in eyes with AMD depends on the stage and severity of disease. The clinical examination in early and intermediate stage reveals presence of yellowish subretinal deposits aka drusen and/or retinal pigmentary changes which can be hypo or hyper-pigmentary changes. The various subtypes of drusen are: (i) soft drusen – these drusen are large (>125µm) with distinct or

indistinct edges, dome shape and are located at sub RPE level; the soft drusen may coalesce to form confluent drusen or large drusenoid pigment epithelium detachment (PED) (ii) hard drusen – small drusen (<63 µm) with distinct edge, round shape and sub RPE location; (iii) cuticular drusen – small drusen (25-75 µm) with triangular shape (saw tooth appearance) and sub RPE location; (iv) RPD/SDD are relatively large drusen (100-250 µm) with irregular borders in different shapes based on the stage of drusen (Khan, Mahroo et al. 2016). These are located above the RPE, below the neurosensory retina.

Advanced stages of AMD include GA and nAMD. GA lesions are visible on fundus examination as sharply delineated round or oval area of hypo- or depigmentation with visible underlying choroidal vessels due to absence of RPE (Maguire and Vine 1986). In contrast, nAMD is characterized by presence of MNV seen on clinical examination as subretinal greyish-green tissue along with fluid and or blood in the subretinal or intraretinal space (Bressler, Bressler et al. 1987, Group 2001). There can be presence of PED which can be serous, fibrovascular or haemorrhagic based on the sub RPE contents of fluid, fluid with fibrovascular tissue or blood respectively (Zayit-Soudry, Moroz et al. 2007).

Based on clinical examination the Age-related Eye Disease Study (AREDS) group proposed various levels of AMD as shown in Table 1.2 (Group 2001).

Table 1.2 AREDS classification of AMD based on clinical features.

AMD Level	Criteria
1	Drusen maximum size < circle C-0 (63 µm diameter) and total area < circle C-1 (125 µm diameter)
2	Presence of one or more of the following:
	(a) Drusen maximum size ≥ circle C-0 but < circle C-1
	(b) Drusen total area ≥ circle C-1
	(c) Retinal pigment epithelial pigment abnormalities consistent with AMD, defined as one or more of the following in the central or inner subfields:
	(1) Depigmentation present
	(2) Increased pigment ≥ circle C-1
	(3) Increased pigment present and depigmentation at least questionable
3	Presence of one or more of the following:
	(a) Drusen maximum size ≥ circle C-1
	(b) Drusen maximum size ≥ circle C-0 and total area > circle I-2 and type is soft indistinct
	(c) Drusen maximum size ≥ circle C-0 and total area > circle O-2 and type is soft distinct
	(d) Geographic atrophy within grid but none at centre of macula
4 (Advanced)	Presence of one or more of the following:
	(a) Geographic atrophy in central subfield with at least questionable involvement of centre of macula
	(b) Evidence of neovascular AMD
	(1) Fibrovascular/serous pigment epithelial detachment
	(2) Serous (or haemorrhagic) sensory retinal detachment
	(3) Subretinal/subretinal pigment epithelial haemorrhage
	(4) Subretinal fibrous tissue (or fibrin)
	(5) Photocoagulation for AMD

Abbreviations: AMD – Age related macular degeneration.

1.3.4 Management of AMD

1.3.4.1 Diagnosis

History

It is essential to document symptoms of AMD (blurring, scotoma, metamorphopsia), smoking and family history and advise patients of controlling any modifiable risk factors.

Clinical examination and colour fundus photographs

Clinical examination should include visual acuity (VA) assessment, fundoscopy, and examination of both eyes.

Best corrected Visual Acuity (BCVA)

VA is an essential measure in patients with AMD both in the clinical as well as research setting in clinical trials. However recent studies have shown VA might be a poor differentiating factor between healthy controls, varying levels of AMD severity and advanced AMD (Owsley, Clark et al. 2016). This is mainly because in eyes with early or iAMD there can be significant test-retest variability and it may be difficult to note incremental drop in visual acuity. In late AMD especially in eyes with foveal involvement due to disease process the BCVA assessment has poor yield (Hogg and Chakravarthy 2006). Studies by Mayer et al have proven the limited function of longitudinal BCVA assessment in eyes that progressed to nAMD (Mayer, Ward et al. 1994). Nevertheless, BCVA continues to be used as an indicator of patient's visual function both in clinics and research due to ease of measurement and minimal technical skills to perform the test. More importantly in the UK, National Institute for Health and Care Excellence (NICE) guidelines use VA as a metric to determine initiation of anti VGF treatment in eyes with nAMD (NICE 2018).

OCT

OCT is the first diagnostic test for patients with AMD and it is being increasingly employed to diagnose and monitor disease progression in AMD. The advantage with OCT is that it is a non-invasive test which provides extensive information on the structure of the retina. Additionally, it has been reported to have high sensitivity and specificity in detecting late AMD. SD-OCT acquires retinal images

at rates up to 20,000 axial scans per second with almost 5 µm resolution, with some state-of-the-art machines even managing 40–70,000 scans per second (Hanson, Airody et al. 2023). The details of imaging biomarkers across various stages of AMD are mentioned in section 1.4. It is crucial to remember that both eyes should have an OCT scan. Individuals with unilateral nAMD who are receiving therapy run the risk of developing nAMD in their second eye. OCT is the greatest tool for tracking the disease's progression because individuals may not exhibit any symptoms when it converts. The most sensitive method for evaluating therapy response, including disease reactivation, is OCT.

Optical coherence tomography –angiography (OCT-A)

OCT-A is now more commonly recognised as a quick, sensitive, non-invasive imaging technique for nAMD diagnosis and treatment. When MNV on OCT-A is detected, it is deemed sufficient evidence to start therapy when structural OCT reveals characteristics suggestive of nAMD. However, because of the presence of artefacts (such as motion, blink, and projection), the technology requires high-end computers for data storage, analysis, and skilled scan interpretation. Nonetheless, the diagnosis of MNV is not ruled out by a negative OCT-A scan. Invasive testing may be required in certain situations, where structural OCT indicates the presence of nAMD but OCT-A imaging does not support the existence of MNV. The preferred invasive test is FFA, however ICGA could be beneficial as well.

FFA

FFA has traditionally been used to diagnose nAMD. Now that structural OCT and OCT-A have been developed, FFA is currently used less frequently for clinical diagnosis. FFA, on the other hand, is a helpful technique that supports precise diagnosis in cases that are unclear. FFA in conjunction with ICGA is particularly recommended for patients who have partial or poor response to anti-VEGF medication, equivocal scans on OCT-A, and in whom other retinal symptoms may be confounding factors.

ICGA

In order to validate the diagnosis of MNV subtypes such polypoidal vasculopathy (PCV) and retinal angiomatous proliferation (RAP) and to reevaluate the

diagnosis, particularly in poor or non-responders, additional ICGA validation of the diagnosis may be necessary at baseline or at some other point.

Other relevant investigations

The test mentioned here are specific to research settings and are not routinely performed in the clinical setting for patients with AMD.

Low luminance visual acuity (LLVA)

LLVA is a simple, inexpensive and a rapid measure of visual function in dim light. It has been shown by Sunnes et al as a strong predictor for visual acuity loss across all levels of baseline VA in eyes with AMD (Sunness, Rubin et al. 2008). It is tested under standard visual acuity light conditions and low light is simulated by adding a 2.0 log unit neutral density filter (i.e., a filter that lowers luminance by 100 times) (Kodak Wratten filter, Rochester, NY) in front of the eye being tested. This is performed with the patient wearing their best corrected VA refraction. Grewal et al in their study found that compared with healthy participants, BCVA and LLVA scores were significantly reduced in the atrophic AMD group ($p < 0.0001$ and $p = 0.00016$, respectively) and in patients with SDD ($p = 0.028$ and $p = 0.045$, respectively). Participants with atrophy also had reduced BCVA ($p = 0.001$) and LLVA ($p = 0.009$) compared with the intermediate AMD no SDD group (Grewal, Chandra et al. 2020). Also, BCVA and LLVA correlated well in eyes with non-neovascular AMD. Wu et al showed LLVA to be more effective at detecting foveal deficits than BCVA in eyes with increasingly worsening retinal sensitivity in eyes with AMD (Wu, Ayton et al. 2014).

Dark Adaptation (DA)

Dark adaptation is the measure of the time taken during slow recovery of visual sensitivity in darkness following exposure to intense or prolonged illumination, which bleaches a significant amount of the rhodopsin. The process of DA involves phototransduction taking place mainly between the photoreceptor outer segments and RPE. Relationship of this retinoid cycle with visual function in humans was first explained by Lamb and Pugh (Lamb and Pugh 2004).

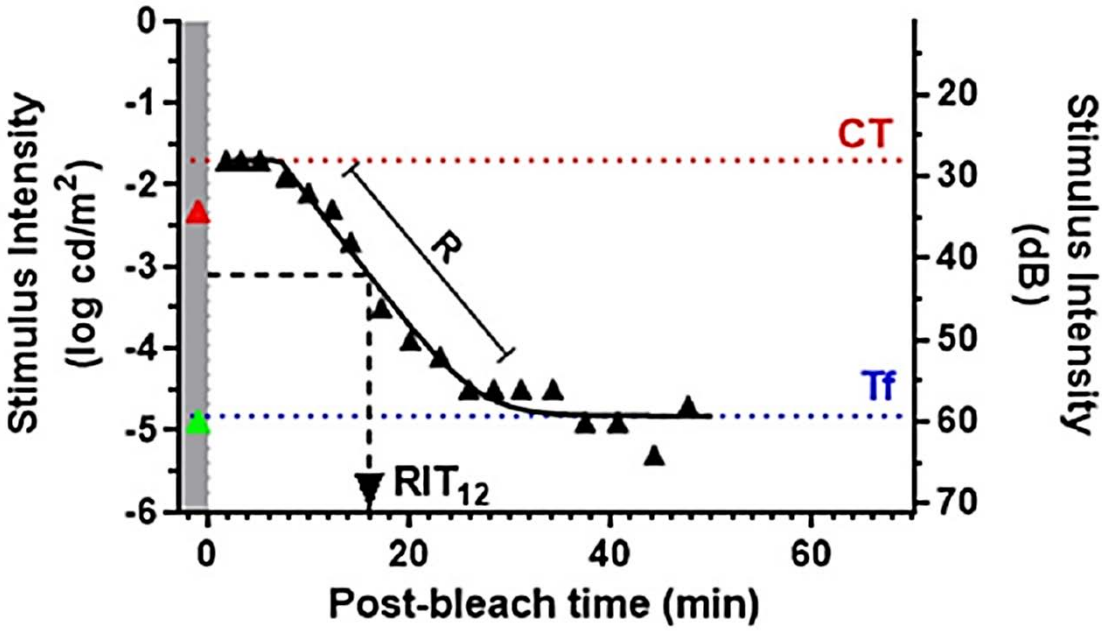

Figure 1.7 Dark Adaptation curve.
Green and red triangles illustrate scotopic thresholds at 505 nm and 625 nm respectively before delivery of bleach. Following exposure to a bleaching light, retinal sensitivity reaches an initial plateau mediated by cones (CT). Once rods become more sensitive to cones (Cone-rod break), retinal sensitivity continues to improve at a fixed rate (R dec/min) before reaching final asymptotic rod threshold (Tf). Image Source: (Nigalye, Hess et al. 2022).

Figure 1.7 shows the DA curve in humans. The observed visual response in DA is as follows: after the bright light exposure, the cones begin to recover first as the earlier part of recovery is guided by the cone response, but this cannot go beyond a threshold value which corresponds to the later part of mesopic vision, and hence the cone response plateaus. Next is the rod recovery which takes longer to start and is slower in progress as the rods that are saturated by the exposure to bright light (photopigment bleaching) become active only in the early mesopic phase. The slowed recovery is due to the presence of free opsin the rods following the bleaching. With time the rods take over the cone pathway (piggybacking) and eventually the visual response is completely rod driven (scotopic vision). This continues till rods reach their absolute threshold sensitivity. Rod intercept time (RIT), the time taken to detect a stimulus of −3.1 log phot cd/m^2 has been widely used to assess DA in AMD. Since a Muller cell-based visual cycle is believed to be able to sustain cone function and account for rapid recovery of cone visual pigment after bleaching for continuous daylight

vision, the measurement of rod-mediated adaptation (and associated curve–parameters) is thought to be more relevant to pathology associated with the RPE -BrM complex and photoreceptor function (Nigalye, Hess et al. 2022). Impaired rod function and kinetics of DA process in eyes with AMD has been shown by Owsley et al (Owsley, Jackson et al. 2000, Owsley, Jackson et al. 2001). This means that rate of photoreceptor sensitivity recovery reflected in DA are associated with and sensitive in detecting the presence of AMD. In a study by Grewal et al, compared with healthy participants, BCVA, LLVA, scotopic thresholds were depressed, and DA measured as Rod Intercept Time (RIT) was prolonged in iAMD patients with SDD ($p = 0.028$, $p = 0.045$, $p = 0.014$ and $p < 0.0001$ respectively). Patients with SDD also had reduced scotopic function and delayed RIT compared to iAMD without SDD ($p = 0.005$ and $p < 0.0001$) (Grewal, Chandra et al. 2022). Applicability of DA as a screening tool for AMD has been shown by Jackson et al where obtaining DA kinetics instead of absolute thresholds was a more sensitive, easier, rapid and more feasible option in elderly patient population with AMD (Jackson and Edwards 2008). However, the most significant impact of DA as a visual function in context of AMD is that DA is impaired in AMD eyes even prior to any structural changes on retinal imaging (Owsley, Huisingh et al. 2014).

Fundus Autofluorescence (FAF)

Fundus autofluorescence provides a reproducible technique for semi-automated image analysis and accurate identification of GA areas in high contrast images. It is the most commonly employed imaging modality across all clinical trials for GA and primary outcome measures for most trials is change in GA area measured on FAF (Holz, Steinberg et al. 2015). Also, patterns of hyper autofluorescence at the margin of GA have been considered to precede cell death and growth of GA (Figure 1.8). The rate of progression of GA was slowest in eyes with no abnormal pattern on FAF in the area around the lesion (median 0.38 mm2/year), followed by eyes with focal increased FAF (median 0.81 mm2/year). The highest rates of GA enlargement were noted in eyes with banded (median 1.81 mm2/year) or diffuse (median 1.77 mm2/year) patterns. The difference between the rates of progression between eyes without any FAF changes and those with pronounced

FAF patterns was statistically significant. ($p < 0.0001$) (Holz, Bindewald-Wittich et al. 2007).

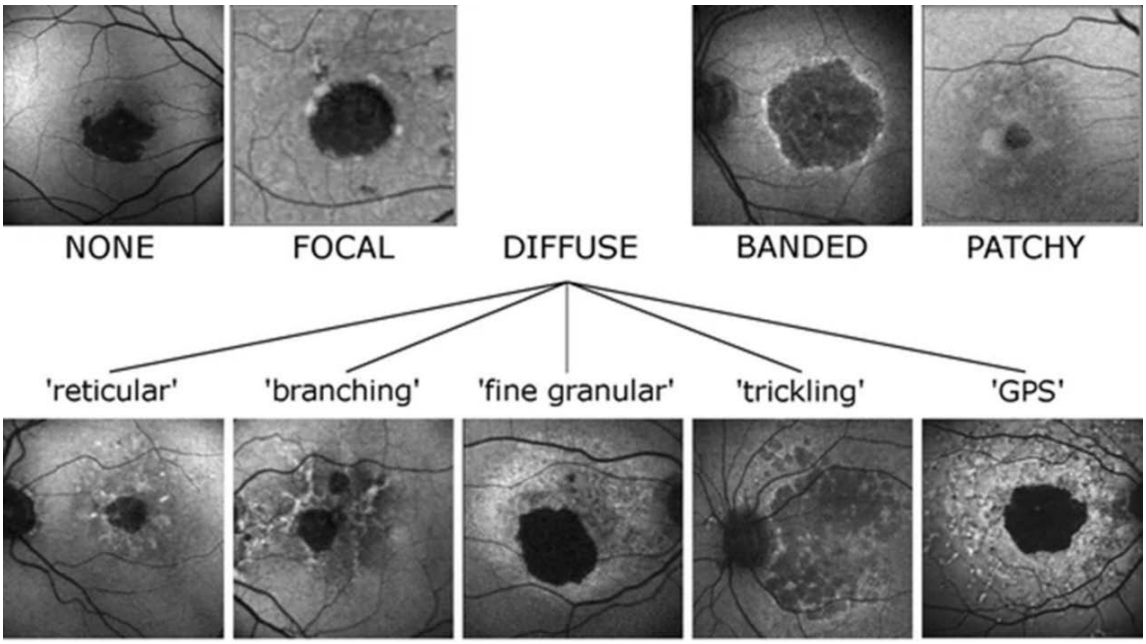

Figure 1.8 Patterns of abnormal FAF in the junctional zone of GA. GPS- fine granular with peripheral punctate spots. Image Source: (Holz, Steinberg et al. 2015).

Even though these FAF lesion phenotypes reflect heterogeneity on a molecular, cellular or genetic level these are not always reproducible (Figure 1.9 and Figure 1.10) (Scholl, Fleckenstein et al. 2009). OCT reflects changes and adds information at cellular level that precede FAF changes.

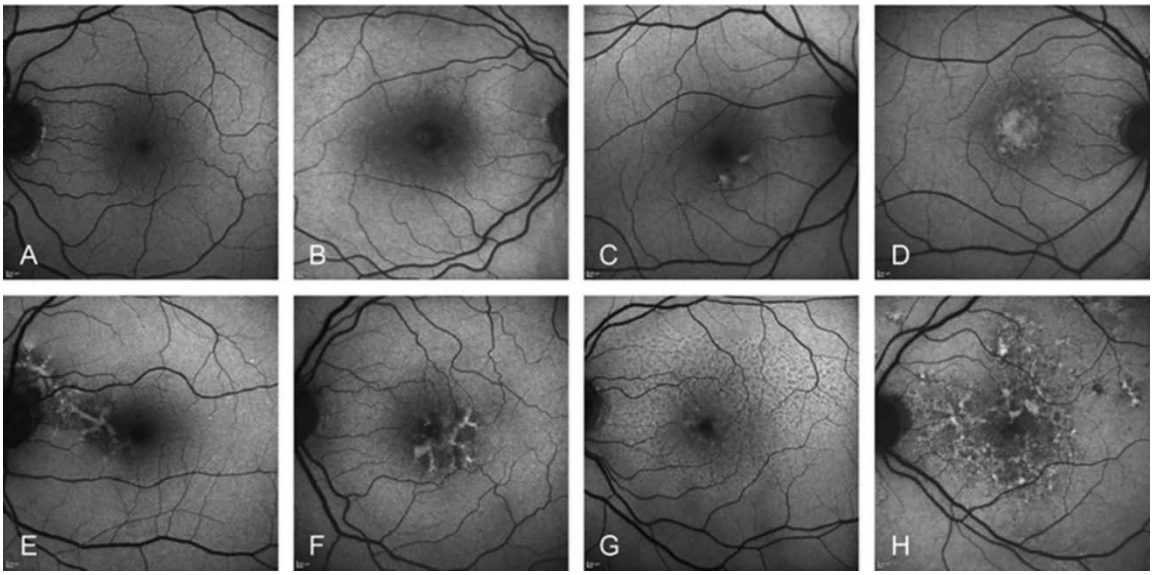

Figure 1.9 Different FAF patterns in early and intermediate AMD. Normal (a), minimal change (b), focal increased (c), patchy (d), linear (e), lacelike (f), reticular (g), and speckled (h).Image Source: (Holz, Steinberg et al. 2015).

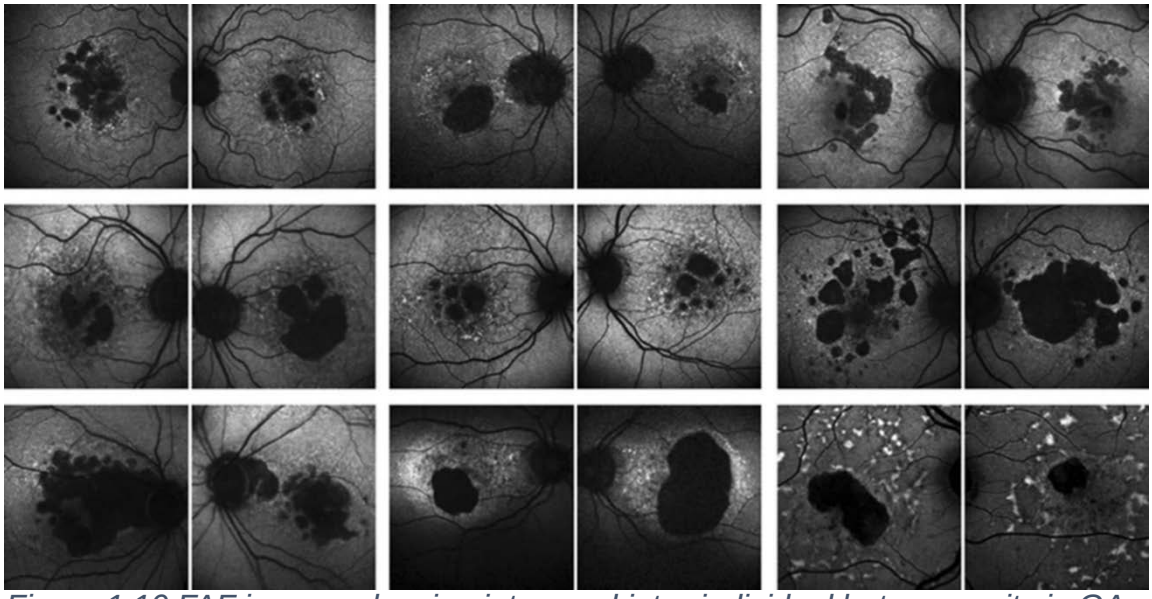

Figure 1.10 FAF images showing inter- and intra-individual heterogeneity in GA. Image Source: (Holz, Steinberg et al. 2015)

Quantitative autofluorescence (qAF)

Fundus autofluorescence has historically been used to monitor progression to late AMD as evidence of hypo autofluorescence indicates onset of atrophy. However, FAF has its disadvantages as absorption of blue light by the luteal pigment makes detection of foveal involvement quite tricky. Also, it is affected by pseudo autofluorescence phenomenon caused by light absorption by natural lens (Sepah, Akhtar et al. 2014). But most importantly FAF detects hypo autofluorescence which is an area of RPE cell loss and death. This is the area where the disease has run its course and will not benefit from therapies. To circumvent this issue, patterns of hyper autofluorescence at the margin of GA has been considered to precede cell death and growth of GA (Bindewald, Schmitz-Valckenberg et al. 2005). However, these FAF lesion phenotypes are not always reproducible. Therefore, the focus is diverted to other imaging modalities that can identify changes before RPE cell loss and can complement FAF.

qAF enables the in vivo quantification of FAF signals from diseases eyes to be compared with an internal standard. It has been concluded that eyes with increased qAF levels may benefit from anti-lipofuscin therapies. Studies have reported qAF levels in AMD eyes and its correlation with factors such as age, sex, ethnicity, smoking status, type and volume of drusen (Greenberg, Duncker

et al. 2013, Gliem, Müller et al. 2016, Reiter, Schwarzenbacher et al. 2021). These reports consistently showed either normal or reduced qAF levels in AMD eyes compared with age-matched controls. It is unclear whether the reduced qAF levels is associated with loss of function and integrity of RPE cells or is it because less lipofuscin is produced due to abnormalities in the visual cycle (Ach, Huisingh et al. 2014). This is particularly relevant in eyes with SDD which are associated with prolonged RIT; it may be a surrogate for impaired visual cycle. Deciphering the relation of qAF to the RPE and the visual cycle is important as there are interventional trials for GA aimed to modulate the visual cycle or reduce lipofuscin.

1.3.4.2 Treatment

There are several approved treatments (Table 1.3) and pipeline therapies for nAMD (Table 1.4).

Table 1.3 Current therapies for nAMD.

Generic	Brand name, manufacturer	Target/mechanism
Bevacizumab	Avastin; Genentech, San Francisco, California	All isoforms of VEGF-A
Ranibizumab	Lucentis; Genentech, San Francisco, California	All isoforms of VEGF-A
Aflibercept	Eylea; Regeneron, Tarrytown, New York	VEGF-A and B, placental growth factor (PGF)
Brolucizumab	Beovu; Novartis, Logo, Basel	VEGF-A
Faricimab	Vabysmo; F. Hoffmann-La Roche Ltd	VEGF-A and Ang-2 inhibitor
Ongavia	Teva Pharmaceutical Industries Ltd., UK	Ranibizumab biosimilar
Ximluci	STADA Arzneimittel and Xbrane Biopharma	Ranibizumab biosimilar
Byooviz	Biogen and Sansung Bioepis Co., Ltd.	Ranibizumab biosimilar

Abbreviations: Ang -2 – Angiopoetin 2; PGF – Placental growth factor; VEGF – vascular endothelial growth factor.

Table 1.4 Pipeline therapies for nAMD.

Class	Manufacturer	Mechanism of Action	Current status
Biosimilars	Razumab (Intas Pharmaceuticals Ltd., Ahmedabad, India)	Ranibizumab biosimilar	Approved
	FYB 201 (Formycon AG, Munich, Germany and Bioeq Gmbh Holzkirchen, Germany)	Ranibizumab biosimilar	Phase III trial completed
	SB-11 (Samsung Bioepsis, Incheon, South Korea)	Ranibizumab biosimilar	Phase III trial completed
	Xlucane (Xbrane Biopharma, Solna, Sweden)	Ranibizumab biosimilar	Phase III trial underway
	PF582 (Pfnex, San Diego, California)	Ranibizumab biosimilar	Phase I/II trial completed
	CHS3551 (Coherus BioSciences, Redwood City, California)	Ranibizumab biosimilar	Pre-clinical investigation
	FYB203 (Formycon AG, Munich, Germany and Bioeq Gmbh Holzkirchen, Germany)	Aflibercept biosimilar	Pre-clinical investigation
	ALT-L9 (Alteogen, Deajeon, South Korea)	Aflibercept biosimilar	Entering phase I trial
	MYL1710 (Momenta Pharamaceuticals, Cambridge, MA, and Mylan Pharmaceuticals, Canonsburg, PA)	Aflibercept biosimilar	Phase III trial underway
	CHS-2020 (Coherus BioSciences, Redwood City, California)	Aflibercept biosimilar	Pre-clinical investigation
	ONS-5010 (Lytenava, Outlook Therapeutics, Cranberry Township, New Jersey)	Bevacizumab biosimilar	Phase III trial completed
Anti-VEGF	OPT-302 (Opthea; OPTHEA limited; Victoria, Melbourne)	VEGF-C and VEGF-D	Phase IIb trial completed

Class	Manufacturer	Mechanism of Action	Current status
	Conbercept (Lumitin; Chengdu Kanghong Pharmaceutical Group, Chengdu, Sichuan)	VEGF-A, VEGF-B, and PGF	Phase III trial underway
Anti- PDGF	CLS-AX (Ataxinib; Clearside Biomedical, Alpharetta, Georgia)	VEGF and PDGF	Pre-clinical investigation
	DE-120 (Santen Pharmaceuticals, Kita-Ku, Osaka)	VEGF-A and PDGF	Pre-clinical investigation halted
Anti-tissue factor (TF)	ICON-1 (Iconic Therapeutics, San Francisco, California)	TF and natural killer cells	Phase II trial completed
Tie-2 receptor	ARP-1536 (Aerpio Therapeutics, Blue Ash, Ohio)	VE-PTP	Pre-clinical investigation
	DE-122 (Carotuximab; Santen, Kita-Ku, Osaka, and TRACON Pharmaceuticals, San Diego, CA)	Endoglin	Phase II trial completed
	AXT-107 (AsclepiX Therapeutics, Jersey City, New Jersey), inhibits both	VEGFR2	Pre-clinical investigation
Sustained treatments	OTX-TKI, a hydrogel depot of the tyrosine kinase inhibitor, sunitinib (Ocular Therapeutix; Bedford, Massachusetts)	VEGF and PDGF	Phase I underway
	Durasert Bioerodible TKI (Durasert; EyePoint Pharmaceuticals, Watertown, Massachusetts)	VEGF and PDGF	Pre-clinical investigation
	ENV1305 (Envisia Therapeutics, Morrisville, North Carolina)	VEGF-A	Pre-clinical investigation
	NT-503 (Neurotech, Cumberland, Rhode Island)	VEGF-A	Pre-clinical investigation

Class	Manufacturer	Mechanism of Action	Current status
Gene therapy	Adeno-associated virus type 2 (AAV2)-sFlt-1 (Genzyme, Cambridge, Massachusetts)	Produces sFlt-1, a soluble isoform of VEGFR-1, and an antagonist of VEGF	Phase I trial completed
	rAAV.SFLT-1 (AVA-101; Avalanche Biotechnologies, Redwood City, California)	Produces sFlt-1, a soluble isoform of VEGFR-1, and an antagonist of VEGF	Phase II trial completed
	ADVM-022 and ADVM-032 (Adverum Biotechnologies, Redwood City, California)	Produces aflibercept-like protein and ranibizumab-like protein	Phase I trial completed
	RGX-314 (REGENXBIO, Rockville, Maryland)	Vector expressing a protein similar to ranibizumab	Phase I/II underway
	Retinostat (Oxford Biomedica, Cowley, Oxford)	Codes for endostatin and angiostatin	Phase I completed
	AAVCAGsCD59 (HMR59; Hemera Biosciences, Waltham, Massachusetts)	Produces CD59	Phase I underway
Oral	AKST4290 (Alkahest, San Carlos, California)	Targets CCR3	Phase II completed

Class	Manufacturer	Mechanism of Action	Current status
treatments			
Topical treatments	Pazopanib (GlaxoSmithKline, Brentford, London)	VEGF-A and PDGF	Phase II completed
	OHR-102 (Squalamine lactate, Ohr Pharmaceutical, New York, New York)	VEGF, PDGF, and b-FGF	Phase II completed
	LHA510 (Alcon, Geneva, Switzerland)	Tyrosine kinase	Phase II completed

Abbreviations: AAV – Adenoviral vector; b-FGF – basic fibroblast growth factor; CCR3 - C-C chemokine receptor 3; PGF- placental derived growth factor; sFlt-1 - soluble fms-like tyrosine kinase-1; TF – tissue factor; VEGF – vascular endothelial growth factor; VE-PTP - Vascular endothelial tyrosine phosphatase. (Arepalli and Kaiser 2021).

Exploring treatments for geographic atrophy is an area of active clinical research. Table 1.5 summarises the current ongoing and approved therapies for geographic atrophy and also outlines the outcome measures used in each trial.

Table 1.5 Current trials for Geographic Atrophy

Intervention	Target pathway	Clinical trial	Molecule	Route	Outcome Measure
Human embryonic stem cells (hESC)	Cell based therapies	Open-label, single-arm, multi-centre, dose-escalation trial Phase 1/2a (NCT05626114)	OpRegen (RG6501)	Subretinal	Safety &Efficacy
hESC	Cell based therapies	Single arm prospective Phase 1/2a NCT02590692	California Project to Cure Blindness Retinal Pigment Epithelium (CPCB-RPE1)	Subretinal implant	Safety &Efficacy
Induced pluripotent stem cells (iPSCs)	Cell based therapies	Phase 1/2a NCT04339764	Autologous iPSC-derived RPE on PLGA (poly(d,l-lactide-co-glycolide)	Subretinal	Safety &Efficacy
iPSCs derived RPE cells	Cell based therapies	Phase 1/2a NCT02464956	iPSC Derived RPE Cells	Subretinal	Safety &Efficacy
Human umbilical tissue-derived cells (hUTC)	Cell based therapies	Multicentre, open-label phase 2b (PRELUDE) NCT02659098	Palucorcel (human umbilical tissue-derived cells)	Subretinal	Change in GA lesion growth as measured by FAF (secondary endpoint)
C3 inhibitors	Complement pathway	Phase 3, randomized, double-masked, sham-controlled studies. OAKS (NCT03525613) and	Pegcetacoplan	Intravitreal	Change in GA lesion size from baseline to Month 12 measured by FAF

Intervention	Target pathway	Clinical trial	Molecule	Route	Outcome Measure
		DERBY (NCT03525600)			
C5 inhibitor	Complement pathway	International, prospective, randomized, double-masked, sham-controlled, pivotal phase 2/3 clinical trial. NCT02686658	Avacincaptad pegol (Zimura/Izervay)	Intravitreal	Mean rate of change in GA over 12 months measured by FAF at 3 timepoints: baseline, month 6, and month 12.
C1q inhibitor	Complement pathway	Phase 2, Multicentre, Randomized, Parallel-Group, Double-Masked, 4-Arm, Sham-Controlled Study NCT04656561 (ARCHER)	ANX007	Intravitreal	Change in GA lesion area as assessed by FAF at month 12
Complement factor H recombinant	Complement pathway	Phase 1, multicentre, open-label, single-dose, dose-escalation study (ReGAtta) NCT04246866	Recombinant human complement factor H (CFH) GEM103	Intravitreal	Safety &Efficacy
Complement factor B inhibitor	Complement pathway	Phase 2, Randomized Placebo-Controlled, Double-Masked Study (GOLDEN) NCT03815825	Antisense Inhibitor of Complement Factor B – IONIS-FB-LRx	Intravitreal	Absolute Change from Baseline in the GA Area at Week 49, as Assessed by Retinal Imaging
CD59 Inducer	Complement pathway	Phase 2 Multi-Centre Trial NCT04358471	AAVCAGsCD59	Intravitreal	Evaluate the change in GA area (mm2) measured at Day 0 and compared to the measurement at Month 24
Anti HtRA1 antibodies	serine protease HtrA1 pathway	Phase II, Multicentre, Randomized, Single-Masked, Sham-Controlled Study (GAllego) NCT03972709	Galegenimab (FHTR2163)	Intravitreal	Mean Change in GA Area from Baseline to Week 72 as Measured by FAF

Intervention	Target pathway	Clinical trial	Molecule	Route	Outcome Measure
Mitochondrial targeted drug	Mitochondrial metabolism	Phase 2 Randomized, Double-Masked, Placebo-Controlled Clinical Study (ReCLAIM 2) NCT03891875	Elamipretide	Intravitreal	To evaluate the efficacy of elamipretide in looking at the change in LLVA To evaluate the efficacy of elamipretide through the change in GA area as measured by OCT

Abbreviations: hESC - Human embryonic stem cells; HTRA1 - High-Temperature Requirement protein A1 ; hUTC - Human umbilical tissue-derived cells ; iPSCs - Induced pluripotent stem cells; PGLA - poly(d,l-lactide-co-glycolide); RPE – retinal pigment epithelium.

1.4 Role of imaging biomarkers

Imaging biomarkers especially on OCT have recently shown great promise in disease diagnosis and risk predictions across all AMD severity levels. Some of these biomarkers on multimodal imaging relevant to the thesis are shown in Table 1.6.

Table 1.6 Current established & potential structural biomarkers on OCT, OCT-A and FAF for disease progression in AMD.

Imaging Modality	Biomarker	Description	High risk for progression to nAMD?	High risk for progression to atrophy?
	Intraretinal Fluid (IRF)	IRF is seen in nAMD eyes as either diffuse thickening in the ONL or large oval/round cystoid spaces with or without septae across all retinal layers when exudation increases (Keane, Patel et al. 2012).	N/A	Yes (Llorente-González, Hernandez et al. 2022)
	Subretinal fluid (SRF)	Seen in nAMD eyes as presence of hypo reflective space	N/A	No

Imaging Modality	Biomarker	Description	High risk for progression to nAMD?	High risk for progression to atrophy?
		between the photoreceptors and RPE tips i.e., neurosensory detachment (Keane, Patel et al. 2012).		
	PED	Several forms of elevation of the RPE monolayer from the underlying BrM (Spaide, Jaffe et al. 2020). These include drusenoid, serous, and fibrovascular. Many cases of serous PED show evidence of MNV called serous vascularized PED (svPED). svPEDs show hyperreflectivity beneath the RPE that partly fills the cavity (Clemens, Wolf et al. 2017). OCT-A is particularly useful in detecting the presence of neovascularization. Fibrovascular PED (fPED) are seen with type 1 MNV where entire sub RPE space is filled out with hyperreflective material (Clemens, Wolf et al. 2017). The cavity may also contain hyporeflective space which could be serous fluid and/or haemorrhage. Haemorrhagic PED (hPED) appear as sub RPE hyporeflective spaces with significant back shadowing where the haem comes from proliferating sub RPE MNV (Keane, Patel et al. 2012).	N/A	No
	SHRM	Seen in eyes with nAMD as fluffy material, well/ill-defined and isoreflective to inner retina, boundaries of which are clearly separate from the surrounding neurosensory retina, located between retina and RPE (Spaide, Jaffe et al. 2020).	Yes (Willoughby, Ying et al. 2015)	No, however increased risk for fibrosis (Cheung, Grewal et al. 2019)
	Retinal Thickness (RT)	RT is measured by software inbuilt in various OCT machines. Central retinal thickness (CRT) measured from ILM to inner boundary of the RPE. Foveal centre point thickness (FCPT) is	N/A	N/A

Imaging Modality	Biomarker	Description	High risk for progression to nAMD?	High risk for progression to atrophy?
OCT		the CRT measured at fovea. Central subfield thickness (CSFT/CST) is measured from ILM to BrM within the 1mm circle of ETDRS grid.		
	Drusen volume/RPE-drusen complex thickness (RPE-DC)	Drusen volume is measured by inbuilt OCT software on most machines. Drusen volume greater than 0.03 mm^3 is indicative of progression to late AMD (Nassisi, Lei et al. 2019). Progression to MNV is characterized by higher drusen volume near the fovea and progression to atrophy is characterised by drusen volume peaking at 0.5 mm eccentricity (Waldstein, Vogl et al. 2020).	Yes (Waldstein, Vogl et al. 2020)	Yes (Waldstein, Vogl et al. 2020, Hirabayashi, Yu et al. 2023)
	SDD or RPD	Presence of minimum of 5 SDD on different line scans on OCT confirmed on near infrared reflectance (NIR) has been used by studies to confirm presence of SDD (Zweifel, Spaide et al. 2010): Stage 1 - defined as diffuse deposition of granular hyperreflective material between the RPE-BrM band and the EZ. Stage 2 - mounds of accumulated material sufficient to deflect inwardly the contour of the EZ. Stage 3 - presence of a conical appearance and breaking through the EZ.	Yes (Lei, Balasubramanian et al. 2017)	Yes (Hirabayashi, Yu et al. 2023)
	Optical coherence tomography-reflective drusen substructures (ODS) including Hyporeflective drusenoid cores (hDc)	The four main phenotypes of ODS include: low reflective cores, high reflective cores, conical debris, and split drusen (Veerappan, El-Hage-Sleiman et al. 2016). hDC were defined as hyporeflective spaces within the sub-RPE compartment of the druse (Goh, Abbott et al. 2022).	No (Veerappan, El-Hage-Sleiman et al. 2016)	Yes (Hirabayashi, Yu et al. 2023)

Imaging Modality	Biomarker	Description	High risk for progression to nAMD?	High risk for progression to atrophy?
	Complete retinal pigment epithelium and outer retinal atrophy (cRORA)	Defined by the following criteria (i) Zone of hyper transmission of ≥250 µm (ii) Zone of attenuation or disruption of RPE band of ≥250 µm (iii) Evidence of overlying PR degeneration characterised by features that include ONL thinning, ELM loss, and EZ or interdigitation zone (IZ) loss (Sadda, Guymer et al. 2018).	No	Yes
	Incomplete retinal pigment epithelium and outer retinal atrophy (iRORA)	Defined by the following criteria: (1) a region of signal hyper transmission into the choroid and (2) a corresponding zone of attenuation or disruption of the RPE, with or without persistence of basal laminar deposits (BLamD), and (3) evidence of overlying photoreceptor degeneration, i.e., subsidence of the INL and OPL, presence of a hyporeflective wedge in the Henle fibre layer (HFL), thinning of the ONL, disruption of ELM, or disintegrity of the EZ, and when these criteria do not meet the definition of cRORA (Sadda, Guymer et al. 2018).	No	Yes (Guymer, Rosenfeld et al. 2020, Jaffe, Chakravarthy et al. 2021) HR 12.1
	Outer Retinal Tubulation (ORT)	ORTs are round hyporeflective lesions, which may contain a few focal hyperreflective spots and are always delineated by a hyperreflective ring, in contrast to the completely hyporeflective retinal cystoid lesions. They are always located at the level of the ONL, and in AMD, they are classically found very close to areas of neovascular fibrosis or retinal atrophy (Iaculli, Barone et al. 2015).	N/A	Yes (Haensli, Sugiura et al. 2021)

Imaging Modality	Biomarker	Description	High risk for progression to nAMD?	High risk for progression to atrophy?
	Hyperreflective foci (HRF)	Discrete punctate lesions with equal or greater reflectivity than that of the RPE within the retina (Jaffe, Chakravarthy et al. 2021).	Yes (Waldstein, Vogl et al. 2020)	Yes (Jaffe, Chakravarthy et al. 2021)
	Nascent geographic atrophy (nGA)	Defined as presence of (i) subsidence of INL and OPL and/or (ii) the presence of a hyporeflective wedge-shaped band within HFL, both indicating a loss of the PRL. These features were often, but not always, present with signs of attenuated or disrupted RPE and hyper transmission of signal through to the choroid (Wu, Goh et al. 2023).	No	Yes (Wu, Luu et al. 2020, Wu, Goh et al. 2023) HR 78.1
	Persistent Hyper transmission defects (hyperTDs)	Described on en face OCT-A scans as bright regions having a ≥250 μ diameters in any en-face direction. This defect appears brighter in contrast with the surrounding area on the en-face due to increased light signal transmission towards choroid through the attenuated or absent RPE (Liu, Shen et al. 2023).	No	Yes (Laiginhas, Shi et al. 2022)
	Changes in photoreceptor (PR) thickness	PRL thinning overlying drusen: thinning of ONL and IS+OS thickness at peak drusen height was noted prior to development of drusen collapse and atrophy (Sadigh, Cideciyan et al. 2013). PRL loss at the edge of GA lesion: deep learning-based automated PR quantification to calculate the PR loss/RPE loss ratio. PR core anatomy measured as area between the top of the EZ and the outer boundary of the IZ (Riedl, Vogl et al. 2022).	No	Yes (Sadigh, Cideciyan et al. 2013, Riedl, Vogl et al. 2022)

Imaging Modality	Biomarker	Description	High risk for progression to nAMD?	High risk for progression to atrophy?
	Changes in EZ reflectivity	EZ appears as a hyperreflective line on the OCT and represents the mitochondria rich PR IS (Gin, Wu et al. 2017). The reflectivity measured indirectly post processing of OCT images is therefore a reflection of photoreceptor health (Gin, Wu et al. 2017).	No	Yes (Toprak, Yaylalı et al. 2017, Thiele, Wu et al. 2022)
	DLS/ Shallow irregular RPE elevation (SIRE)	DLS is defined as shallow irregular PED. The upper hyper reflective band of the double layer is of the RPE, and the bottom band is of the BrM (Sheth, Anantharaman et al. 2018). SIRE is defined as RPE elevations with a greatest transverse linear dimension of ≥1000 µm, an irregular RPE layer with a height of predominantly <100 µm, and a nonhomogeneous internal reflectivity as characteristic features of the DLS when neMNV was present (Narita, Wu et al. 2020).	Yes (Narita, Wu et al. 2020)	No
	Choroidal changes on OCT	Choroidal thickness (CT) is measured using enhanced depth imaging (EDI) module on the SD-OCT or swept source OCT (SS OCT) (Hirano, Muraoka et al. 2023). It is measured from the BrM to the choroidoscleral interface. Reduced choroidal thickness and in particular CC thickness has been shown to be associated with AMD progression (Capuano, Souied et al. 2016, Amato, Arrigo et al. 2022).	Yes (Amato, Arrigo et al. 2022)	Yes (Amato, Arrigo et al. 2022)

Imaging Modality	Biomarker	Description	High risk for progression to nAMD?	High risk for progression to atrophy?
OCT-A	CC deficits	Defined as hyporeflective spaces in the CC slab of the OCT-A (Camino, Guo et al. 2019). Need to perform post image processing. Flow deficits increase as AMD progresses and have been shown to be linked to the development of iRORA and cRORA (Tiosano, Corradetti et al. 2021).	No	Yes (Borrelli, Uji et al. 2017, Corvi, Tiosano et al. 2021)
	neMNV	Defined on OCT-A as presence of neovascular network without signs of exudation (IRF, SRF or SHRM) on corresponding OCT scan (Thottarath, Chandra et al. 2023). Eyes with neMNV have a higher risk of exudation (Laiginhas, Yang et al. 2020).	Yes (Laiginhas, Yang et al. 2020)	No, neMNV has been shown to be protective against GA expansion (Hwang, Agrón et al. 2021).
FAF	Patterns of hypo or hyper fluorescence in iAMD and at junctional zone of GA lesions	iAMD FFA patterns: normal, minimal change, focal increased, patchy, linear, lacelike, reticular, and speckled (Holz, Steinberg et al. 2015). GA lesion junctional zone patterns: Focal, diffuse (reticular, branching, trickling, granular, GPS), banded and patchy (Holz, Steinberg et al. 2015). Banded has been shown to have the highest rate of GA progression.	No	Yes, faster rate of GA progression (Holz, Bindewald-Wittich et al. 2007).

Abbreviations: AMD – age related macular degeneration; cRORA - complete retinal pigment epithelium and outer retinal atrophy; hDC – hyporeflective drusenoid cores; HRF – hyperreflective foci; iRORA – incomplete retinal pigment epithelium and outer retinal atrophy; IRF – intraretinal fluid; neMNV – non exudative macular neovascularization; nGA – Nascent geographic atrophy; ODS - OCT reflective drusen substructures; ORT – outer retina tubulation; PED – pigment epithelium detachment; PRL – photoreceptor layer; RPE DC – retinal pigment epithelium drusen complex; RT – retinal thickness; SDD- subretinal drusenoid deposits; SHRM - subretinal hyperreflective material; SIRE – shallow irregular epithelium detachment; SRF – subretinal fluid.

1.5 Heterogeneity in AMD

1.5.1 Traditional classification systems

*1.5.1.1 **Epidemiological classification***

Table 1.7 Epidemiological classification for AMD.

Early AMD	Large (≥125μm) drusen or pseudodrusen or pigment irregularities
Late AMD	nAMD or GA

Abbreviations: GA – geographic atrophy; nAMD – neovascular AMD

*1.5.1.2 **AREDS 9-step severity scale** (Davis, Gangnon et al. 2005) (Table 1.8)*

Table 1.8 AREDS 9-step severity scale for AMD

Grade	Largest Drusen Size	Drusen Area	Increased Pigment	Depigmentation	Geographic Atrophy	Predominance of Soft Indistinct Drusen
0	None	None, Q,* or <C-0	None	None	None	None
1	Questionable*	≥C-0, <C-1	Questionable*	Questionable*	Questionable*	Questionable*
2	<C-0	≥C-1, <C-2	<C-0	<I-2	<I-2	Present, not predominant
3	≥C-0, <C-1	≥C-2, <I-2	≥C-0, <C-1	≥I-2, <O-2	≥I-2, <O-2	Predominant in 1 of 3 zones
4	≥C-1,<C-2	≥I-2, <O-2	≥C-1,<C-2	≥O-2, <0.5 DA	≥O-2, <0.5 DA	2 of 3 zones
5	≥C-2	≥O-2, <0.5 DA	≥C-2, <O-2	≥0.5, < 1.0 DA	≥0.5, <1.0 DA	3 of 3 zones
6	NA	≥0.5, <1.0 DA	≥O-2	≥1.0, <2.0DA	≥1.0, <2.0 DA	MA
7	NA	≥1.0 DA	Unrelated to AMD	≥2.0 DA	≥2.0 DA	NA
8	Cannot grade	Cannot grade	Cannot grade	Cannot grade	Cannot grade	Cannot grade

1.5.1.3 **AREDS classification (2001)** (Table 1.9)

Table 1.9 AREDS classification for AMD.

AREDS category 1 (no AMD)	- No or small drusen (<63µm) - Drusen area <125µm diameter - No pigment abnormalities Second eye: same as first eye
AREDS category 2	Presence of one or more of the following - Small (<63µm) or medium-sized (≥63; <125µm) drusen - Drusen area ≥125µm diameter - Retinal pigment epithelial pigment abnormalities consistent with AMD, defined as one or more of the following in the centre or inner subfields: depigmentation present; increased pigment circle ≥125µm; increased pigment present and depigmentation at least questionable Second eye: same as first eye or category 1
AREDS category 3	Presence of one or more of the following - Large drusen (≥125µm) - Soft, indistinct drusen, drusen size ≥63µm and drusen area ≥360µm diameter - Soft, distinct drusen, drusen size ≥63µm and drusen area ≥656µm diameter - Non-central geographic atrophy (outside 500µm radius from foveal centre) Second eye: same as first eye or category 1 or 2
AREDS category 4 (advanced AMD)	Presence of one or more of the following - Geographic atrophy in central subfield (inside 500µm radius from foveal centre) with at least questionable involvement of centre of macula - Evidence of nAMD: fibrovascular/serous pigment epithelial detachment. serous (or haemorrhagic) sensory retinal detachment; subretinal/sub-retinal pigment epithelial haemorrhage; subretinal fibrous tissue (or fibrin); photocoagulation for AMD Second eye: category 1, 2 or 3

1.5.1.4 ***AREDS Simplified severity scale*** *(Ferris, Davis et al. 2005)*

The scoring system developed for patients assigns to each eye 1 risk factor for the presence of 1 or more large (> or = 125-micron, width of a large vein at disc margin) drusen and 1 risk factor for the presence of any pigment abnormality (Figure 1.11).

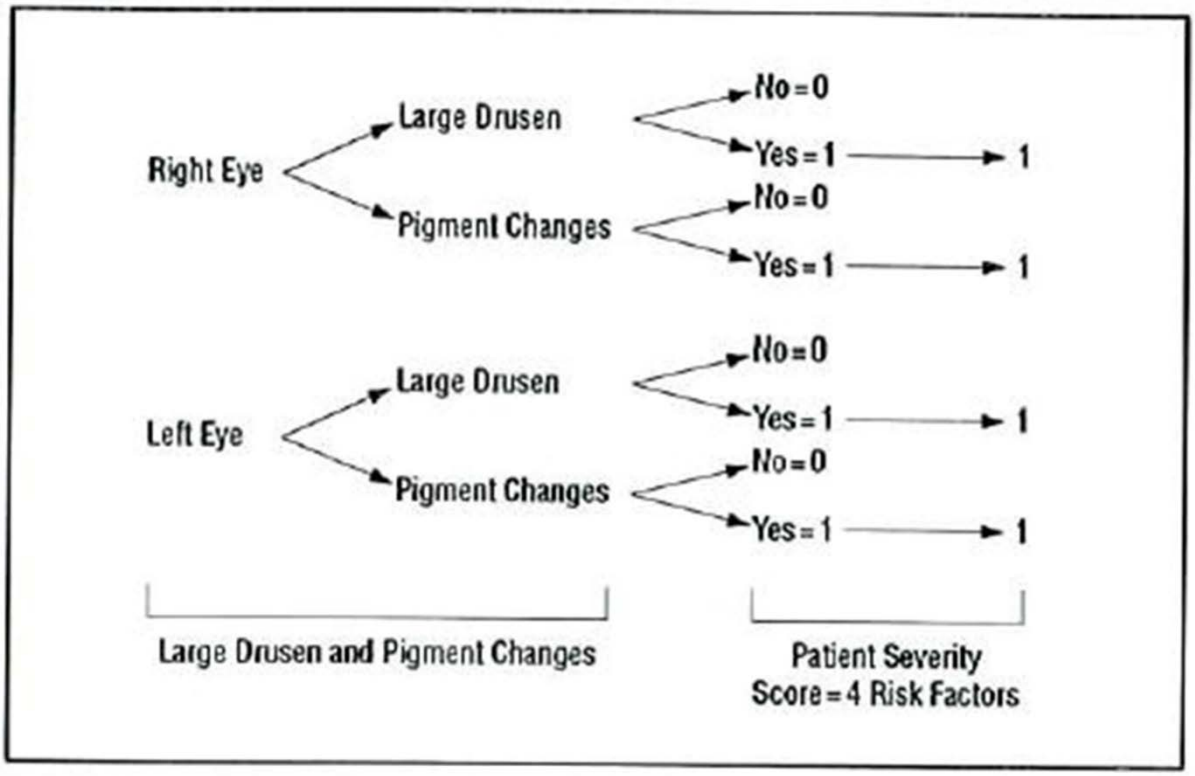

Figure 1.11 AREDS Simplified severity scale for AMD.

1.5.1.5 ***Classification Committee of the Beckman Initiative for Macular Research 2013*** *(Ferris, Wilkinson et al. 2013)*

Lesions are assessed within two-disc diameters of the fovea in either eye (Table 1.10).

Table 1.10 Beckman Initiative for Macular Research classification for AMD.

No apparent ageing changes	- No drusen, and - No AMD pigmentary abnormalities[a]
Normal ageing changes	- Only drupelets (small drusen ≤63µm), and - No AMD pigmentary abnormalities[a]
Early AMD	- Medium drusen >63µm and ≤125µm, and - No AMD pigmentary abnormalities[a]
Intermediate AMD	- Large drusen >125µm, and/or - Any AMD pigmentary abnormalities[a]
Late AMD	- Neovascular AMD, and/or - Any geographic atrophy

[a] *AMD pigmentary abnormalities: any definite hyperpigmentary or hypopigmentary abnormalities associated with medium or large drusen but not associated with known disease entities.*

*1.5.1.6 **NICE Classification of AMD (NICE 2018)** (Table 1.11)*

Table 1.11 Classification of AMD proposed by NICE.

AMD classification	Definition
Normal eyes	No signs of age-related macular degeneration (AMD) Small ('hard') drusen (less than 63 micrometres) only
Early AMD	Low risk of progression: medium drusen (63 micrometres or more and less than 125 micrometres) or pigmentary abnormalities Medium risk of progression: large drusen (125 micrometres or more) or reticular drusen or medium drusen with pigmentary abnormalities High risk of progression: large drusen (125 micrometres or more) with pigmentary abnormalities or reticular drusen with pigmentary abnormalities or vitelliform lesion without significant visual loss (best-corrected acuity better than 6/18) or atrophy smaller than 175 micrometres and not involving the fovea
Late AMD (indeterminate)	Retinal pigment epithelial (RPE) degeneration and dysfunction (presence of degenerative AMD changes with subretinal or intraretinal fluid in the absence of neovascularisation) Serous pigment epithelial detachment (PED) without neovascularisation
Late AMD (wet active)	Classic choroidal neovascularisation (CNV) Occult (fibrovascular PED and serous PED with neovascularisation) Mixed (predominantly or minimally classic CNV with occult CNV) Retinal angiomatous proliferation (RAP) Polypoidal choroidal vasculopathy (PCV)
Late AMD (dry)	Geographic atrophy (in the absence of neovascular AMD) Significant visual loss (6/18 or worse) associated with: dense or confluent drusen or advanced pigmentary changes and/or atrophy or vitelliform lesion

AMD classification	Definition
Late AMD (wet inactive)	Fibrous scar Sub-foveal atrophy or fibrosis secondary to an RPE tear Atrophy (absence or thinning of RPE and/or retina) Cystic degeneration (persistent intraretinal fluid or tubulations unresponsive to treatment) Note that eyes may still develop or have a recurrence of late AMD (wet active)

1.5.1.7 ***Three Continent AMD Consortium age-related macular degeneration severity scale 2014*** *(Klein, Meuer et al. 2014)(Table 1.12)*

Table 1.12 Three Continent AMD Consortium AMD severity scale.

Level	Label	Description
10	No AMD	No, questionable, small, or intermediate sized drusen (<125 µm in diameter) only, regardless of area of involvement, and no pigmentary abnormalities (defined as increased retinal pigment or RPE depigmentation present) OR No definite drusen with any pigmentary abnormality.
20	Mild early AMD	Small to intermediate sized drusen (<125 µm in diameter), regardless of area of involvement, with any pigmentary abnormality OR Large drusen (≥125 µm in diameter) with drusen area <331,820 μm^2 (equivalent to O-2 circle, defined as a circle with diameter of 650 µm) and no pigmentary abnormalities.
30	Moderate early AMD	Large drusen (≥125 µm in diameter) with drusen area <331,820 μm^2 and any pigmentary abnormality OR Large drusen (≥125 µm in diameter) with drusen area ≥331,820 μm^2, with or without increased retinal pigment but no RPE depigmentation.
40	Severe early AMD	Large drusen (≥125 µm in diameter) with drusen area ≥331,820 μm^2 and RPE depigmentation present, with or without increased retinal pigment.
50	Late AMD	Pure geographic atrophy in the absence of exudative macular degeneration OR Exudative macular degeneration with or without geographic atrophy present.

1.5.2 Relevance of phenotypic heterogeneity

The classification of AMD based on anatomical changes in the BrM-choroid have gone through several reiterations based on the numbers, size, area and location of drusen and the presence or absence retinal pigmentary changes in the macula as shown in the previous section. The Wisconsin age-related maculopathy grading system was proposed in the early 1990s and set forth the diagnostic criteria for individual AMD lesions based on a macular grid on CFP. The international consensus on AMD lesions by the International Age-Related Maculopathy Epidemiological Study Group also proposed a classification of lesions on CFP. However, both these systems lacked a severity scale which led to the establishment of the Rotterdam Study Group system in 2001 and various classifications by the AREDS group. One of the latest and more commonly employed classification is the Beckman classification that discriminates early from iAMD by the size of drusen and pigmentary changes (Ferris, Wilkinson et al. 2013). Intermediate AMD is defined as the presence of drusen of size > 125 µm and/or any retinal pigmentary abnormalities. The 3CC study in 2014 harmonized the grading of 4 large cohort AMD studies namely the Rotterdam Study, the Beaver Dam Eye Study, the Los Angeles Latino Eye study and the Blue Mountain Eye study.

The question is why has there been a need to reclassify AMD? It is important to note that all these systems are based on lesions identified on CFP, but with the emergence of multimodal imaging, several novel features have been identified and these need to be risk-stratified and incorporated into future classification to refine risk scores. Even within CFP classifications, there are heterogeneity and are designed for different utilities. For example, the AREDS simplified scale is quick and easy to interpret system for purposes of screening and referral clinics. Beckman classification is easy too but would require more technical knowledge as drusen need to be divided based on their size. But this system does not provide any information on progression rates and therefore would be inadequate measures in a trial setting while recruiting patients for intervention studies. The Rotterdam study was designed for or a more elaborate risk prediction using the AREDS 9-step scale or the 3-continent harmonization scale. Again, these are all limited in their applicability as they do not convey the true microstructural

changes and uses features seen only on CFP. Therefore, risk prediction using the current systems is not accurate and highly subjective. With the advent of artificial intelligence(AI) and extensive research in drug development for both non-neovascular and nAMD, we need more in-depth level lesion analysis to be better at-risk prediction for future events. There is a need for a more granular classification system.

The SD-OCT is being increasingly employed to diagnose and monitor progression in AMD, both in the clinical setting as well as in research. The high resolution allows cross-sectional analysis of the retinal layers with close histologic comparison of what appear to be the first signs of cell loss and the beginning of atrophy in eyes with AMD that only have drusen and pigmentary abnormalities (i.e., in patients with early/iAMD) before clinically apparent signs of late disease. OCT has also been used to evaluate morphological characteristics that confer higher odds of progression to advanced disease. Of significant interest among these are SDD or otherwise termed RPD that are located internal to the RPE (Reiter, Told et al. 2020). These deposits are best seen on NIR and B-scans on OCT (Spaide, Ooto et al. 2018). Unlike drusen, these change locations, appear and disappear and have a predilection for the superior temporal quadrant of the posterior pole. Eyes with SDDs are more at risk of progression to GA and nAMD. In most cases, they are also associated with a thin choroid (Cheng, Kaszubski et al. 2016). So, the definition of AMD has now got to involve not only the BrM-choroid complex as it has to broaden to include SDD, so AMD is defined better as abnormalities of the outer retina-BrM-choroid complex. Interestingly, SDD is not represented in any of the currently used AMD classifications. Both patient selection as well as selection of clinical trial endpoints are critical to the success or failure of an intervention. Therefore, phenotypic heterogeneity needs to be reflected in the eligibility criteria for interventional studies. Use of an OCT based granular classification might allow improve ex-ante identification of progressors versus non progressors or responders versus non-responders.

Phenotypic heterogeneity on imaging finds its role in all stages of disease – iAMD, GA and nAMD. To begin with iAMD, Appendix 1, Table S1.1 in the appendix summarizes the key endpoints for various ongoing clinical trials in

iAMD. The wide variation in key end points is striking. The LEAD study is using the development of nGA as an end point (Guymer, Chen et al 2021). nGA is a feature exclusively detected on OCT, therefore inclusion of a patient into the trial using any of the existing classification systems is most likely going to be inaccurate as based on a CFP classification all iAMD might be grouped together but they would be phenotypically different on OCT level, including those that have a pre-existing nGA. Similarly changes in EZ, drusen volume and development of iRORA or cRORA lesions are all OCT based key end points. Another significant reason to include phenotypic heterogeneity on imaging into classification systems is that it impacts functional outcomes. Presence of SDD is an apt example for this. Eyes with SDD have delayed RIT. This is understandable as the SDD are internal to the RPE and are often seen physically abutting the EZ on OCT. However, Owsley et al showed that delayed RIT can indeed be used as a screening tool to differentiate normal ageing from any AMD (Owsley, McGwin et al. 2016). This raises the question as to whether outer retinal changes correlate with delayed RIT or whether RIT could be used to stratify AMD. One could also argue that diseases such as Sorsby's fundus dystrophy that primarily affects the BrM also causes delayed DA and so DA changes may in fact occur without visible known anatomical changes in the outer retina in AMD (Christensen, Brown et al. 2017). Studies such as ALSTAR and DUKE FEATURE have DA as their key endpoints and here again inclusion of SDD eyes, which is absent from current classification systems would impact the outcomes. Therefore, there is an imminent need for a well-established universally applicable granular classification system that incorporates the phenotypic heterogeneity among these eyes.

GA, a previously untreatable disease has recently moved into the realm of active research interest. This is due to emerging evidence from multiple clinical trials developing therapies that can reduce the progression of GA over time. However, several pivotal trials targeting similar pathways in pathogenesis have failed. This point is accurately illustrated by the trials directed at complement pathway in AMD. For over two decades the role of complement pathway in AMD has been researched substantially and very recently, anti-complement agents have shown some evidence of success in reduction of growth rate of GA lesion compared to sham in pivotal trials. Previous complement inhibitors have either failed to begin

with or after promising results in early phase trials. This begs the question: Is GA one disease?

To elaborate the question further, are the investigational products only biologically effective in certain GA phenotypes and if so, was by random and spontaneous selection that these phenotypes represented a larger cohort in some trials and not others? Undoubtedly, both basic and clinical research have increased our understanding of the pathogenesis and progression of GA. Nevertheless, there are lacunae in our knowledge of the disease that has been highlighted through the results of clinical trials. The primary question that remains unanswered is: Can we assume that failed clinical trials in GA are due to ineffective interventions or should we dwell deeper into the heterogeneity of GA growth and measurement of GA.

The second major issue explaining the possible failure of trials in GA is poorly defined clinical trial endpoints – both functional and anatomical. Table 1.5 shows the variations in key clinical trial endpoints adopted across various interventional studies in GA. One of the most frequently employed anatomical measure is rate of GA progression. Understanding GA progression and its individual variability is critical in the design of clinical studies, in the interpretation and application of clinical trial results, and for counselling patients on how disease progression may affect their individual prognosis. Mones and Biarnes demonstrated three GA phenotypes with different progression rates at ≥ 6 months based on data driven cluster analysis of GA lesions in 77 eyes (Monés and Biarnés 2018). Therefore, with new reports on OCT classification of atrophy, as discussed in the previous subsections there is a need for incorporation of these markers while designing clinical trial inclusion criteria all the while bearing in mind the risk attributed by these towards disease progression.

The impact of phenotypic heterogeneity extends to nAMD as well. For most landmark clinical trials in nAMD change in CRT has been a key end point. Results from comparative effectiveness trials like VIEW 1&2, HAWK and HARRIER studies confirmed that irrespective of variations in central retinal thickness, the VA outcomes were identical at final time point. In contrast Chakravarty U et al used the CATT and IVAN study data and showed that higher

fluctuations in RT resulted in lower VA improvement and higher odds of fibrosis and atrophy. But CRT does not find relevance in most guidelines for treatment recommendations. The EURETINA 2014 guideline on management of nAMD defines disease activity as IRF, SRF and RPE detachments and mentions that these signs of activity are independent of CRT. It also advocates a 'zero tolerance' approach towards OCT criteria rapid disease progression and vision loss due to delayed treatment. Therefore, there is a role for phenotyping these eyes based on presence of these imaging biomarkers as they would determine how the eye responds or remains refractory to treatment both in the short and long term as well. More recently presence of SHRM on OCT has gained significance as a marker of disease activity and predictor of worse morphological outcomes. These eyes tend to develop fibrosis more frequently than those without SHRM. Thus, including eyes with and without SHRM in an interventional study that has a key end point of fibrosis development would impact the success or failure of intervention. In the CATT study, almost 50% of the patients had a VA of 20/40 or better, however the visual gains at the end of first 2 years were not maintained at 5 years (Maguire, Martin et al. 2016). Similarly, in the SEVEN-UP study, half of the eyes continued to remain stable but almost one third declined by 15 letters or more at 7 years (Rofagha, Bhisitkul et al. 2013). Thus, these studies confirm the long-term therapeutic advantage offered by anti-VEGF therapy for nAMD but also show that recurrent exudation remains a risk even in the late stages of therapeutic course. Importantly outcomes from real life studies also reflect a similar trend and in fact fall short of those reported in clinical trials. Why do some eyes respond well to treatment, and some do not both in the short and long term? I believe this can be attributed to the phenotypic heterogeneity in these eyes both at baseline and during the course of treatment as well, specifically at landmark stages like post loading. Therefore, it is relevant to investigate phenotypic heterogeneity determining visual and morphological outcomes in these eyes are various strategic time points during the course of treatment.

1.6 Rationale and PhD objectives

Development of potential treatments for non-neovascular AMD is challenging due to phenotypical heterogeneity of the disease and the lack of validated clinical

biomarkers. The challenge extends to eyes with GA due to heterogeneity in lesion characteristics and GA phenotypes. This may partly explain the negative outcomes in clinical trials for GA. Although anti-VEGF therapy has revolutionised treatment of nAMD, prediction of response to treatment continues to remain a challenge mainly due to phenotypic variations at diagnosis and heterogeneity in disease progression while on treatment. Imaging is an essential component of the clinical assessment of AMD. It is used to diagnose disease, define disease severity and progression, assess treatment response, and complements mechanistic laboratory science to understand AMD pathobiology. Diagnostic imaging tools can assist in deep phenotyping AMD eyes and may identify novel risk factors that are associated with certain morphological features. These morphological features may define imaging phenotypes of AMD that may differ with respect to progression and explain variations in treatment response. However, structure-function correlation also needs to be considered to fully explain the diagnosis and prognosis to patients with any severity level of AMD and inform drug development for this condition. Therefore, this thesis aims to answer these challenges by deep phenotyping eyes with non-neovascular AMD, nAMD and GA and studying structure-function correlation.

Objectives

- Establish effect of phenotypic heterogeneity in eyes with non-neovascular AMD both in terms of structure and visual function.
- To understand phenotypic heterogeneity in baseline features in eyes with nAMD that determine heterogeneity in treatment response both in the short- and long-term.
- To explain phenotypes of GA that affect progression and propose better definition of clinical trial eligibility criteria or clinical trial end points.

2 Chapter 2: Methodology

2.1 General methods

The general methods apply to the three main sections of my thesis examining heterogeneity in assessment of patient population or outcomes and the associations or risk factors that explain these differences. The three sections are:

- Phenotypic heterogeneity in early and iAMD and derivation of a classification based on multimodal imaging and structure-function correlation (Chapter 3).
- Phenotypic heterogeneity in nAMD and its impact on short- and long-term treatment outcomes (Chapter 4).
- Heterogeneity of GA progression and measurement techniques and their implications on outcome measures in clinical trials (Chapter 5).

Table 2.1 shows all the studies that have been done in each section. Each chapter will describe the study-specific methods.

Table 2.1 Studies, sample size, study design & approvals under each chapter.

Section	Study	Participant numbers	REC/ Clinical effectiveness references/ R&D reference numbers	Study design
Phenotypic heterogeneity in early and intermediate AMD and derivation of a classification based on multimodal imaging and structure-function correlation	Optical Coherence tomography-based classification for non-neovascular AMD – PEONY study data	254 participants (476 eyes)	London-Chelsea Research Ethics Committee London REC 19/LO/0931.	Prospective single centre cross sectional observational study
	Dark adaptation in OCT based classification of non-neovascular AMD – PEONY study data	209 eyes of 209 patients	London-Chelsea Research Ethics Committee London REC 19/LO/0931.	Prospective single centre cross sectional observational study
	Quantitative autofluorescence in OCT based classification of non-nAMD – PEONY study data	254 participants (476 eyes)	London-Chelsea Research Ethics Committee London REC 19/LO/0931.	Prospective single centre cross sectional observational study
Phenotypic heterogeneity in nAMD and its impact on short- and long-term treatment outcomes	Associations of presenting visual acuity with morphological changes on OCT in nAMD – PRECISE study data	2,274 eyes of 2,128 patients	REC number 19/LO/1385 (ISRCTN 28276860)	Multicentre Prospective longitudinal cohort study

	Baseline characteristics of eyes with early residual fluid post loading phase of aflibercept therapy in nAMD -PRECISE study data	2,274 eyes of 2,128 patients	REC number 19/LO/1385 (ISRCTN 28276860)	Multicentre Prospective longitudinal cohort study
	A multi-modal AI-driven cohort selection tool to predict suboptimal non-responders to aflibercept loading-phase for nAMD - PRECISE study data	2,274 eyes of 2,128 patients	REC number 19/LO/1385 (ISRCTN 28276860)	Multicentre Prospective longitudinal cohort study
	10-year visual and morphological outcomes of anti VEGF therapy for nAMD	149 eyes of 149 patients	Clinical Effectiveness Department at Moorfields (CA18/MR/15-141.	Retrospective cohort study
	Impact of injection frequency on five-year real-world visual acuity outcomes of aflibercept therapy for nAMD	512 eyes of 468 patients	Clinical Effectiveness Department at Moorfields (CA18/MR/15-141)	Retrospective cohort study
Heterogeneity of GA progression and measurement techniques and their implications on outcome measures in clinical trials	Measurement of GA using OCT-heterogeneity in growth OCT	50 eyes of 50 patients	Only anonymised images were analysed so institutional review board approval was not required.	Retrospective cohort study
	Translational value of new OCT based GA classification.	50 eyes of 50 patients	Only anonymised images were analysed so institutional review board approval was not required.	Retrospective cohort study

	Pilot analysis on detection of photoreceptor loss as a novel endpoint for assessing disease progression.	15 eyes of 11 patients	Only anonymised images were analysed so institutional review board approval was not required.	Retrospective cohort study
	Imaging based clinical trial outcomes in eyes undergoing intervention for GA	Analysed both control and study eye of 2 patients	Retrospective analysis of images from Phase 1/2 clinical trial R&D reference number SIVS1059	Retrospective cohort study

Abbreviations: AMD – age related macular degeneration; GA – geographic atrophy; ISRCTN - International Standard Randomised Controlled Trial Number; nAMD – neovascular AMD; OCT – optical coherence tomography; REC – Research Ethics Committee.

2.2 Study Procedures for prospective studies

2.2.1 Informed Consent

The patient received a participation invitation letter and a participant information sheet (PIS) before they could attend a screening or baseline appointment. After receiving a thorough explanation of the study and having a chance to ask questions, volunteers were asked to participate. The screening visit was utilised as a baseline visit if participants were interested and had verified their eligibility on that particular day. After the consent form was signed, assessments unique to the study were completed.

2.2.2 Sequence of study assessments and Imaging

Participants underwent a structured ocular and medical history. BCVA and LLVA were measured using the EDTRS chart at 4 meters. Following pupil dilation with 2.5% phenylephrine and 1% tropicamide, functional tests relevant to the study vis-à-vis DA, qAF were carried out. Following these, retinal imaging of both eyes including CFP, ultrawide field (UWF) photographs, NIR, SD-OCT and OCT-A, blue light autofluorescence (BAF) images were taken.

2.2.3 Visual Acuities

For all participants, BCVA was measured for each eye using an ETDRS test chart (number of letters seen recorded). LLVA was measured by placing a 2.0-log neutral density filter over the eye and have participants read the same chart, with the aim of the filter to lower background luminance by 100-fold. These tests were performed monocularly (right eye tested first, followed by the left eye) with alternating charts for each eye to avoid repetition and memorisation at 4 m distance. Subsequently, the difference between BCVA and LLVA in ETDRS letters was defined as the low luminance deficit (LLD) score.

2.2.4 Dark Adaptation

DA was measured for the PEONY Study. For measuring DA, the AdaptDx (MacuLogix, Hummelstown, PA) was used which is a computer-automated dark adaptometer. The procedure began with dark adapting participants in the room for 40 minutes after mydriasis and confirming pupil size of minimum 6mm. The participants were provided with a black sleeping mask on their eyes to avoid any light reaching their eyes. Following dark adaptation, they were requested to place

their chin and forehead on the instrument, focusing on the red central light. As per their refractive error, corrective lenses were inserted in the lens holder for a viewing distance of 30 cm. The non test eye was covered and test eye monocularly was exposed to the equivalent rhodopsin bleach of 82% with the delivery of a 505 nm photoflash subtending 4° and centred at 5° on the inferior vertical meridian (~ 0.80 ms duration). Light stimuli were presented for 200 ms using a 3-down/1-up staircase and thresholds were measured until the rod-intercept (time taken to recover 5.0 × 10−3 scotopic cd/m2 or 3.1 log units of stimulus attenuation) was reached, or up to 20 minutes post-bleach, which ever was shorter. Instructions given to the participants were to press on the response button when light stimuli were seen and had 15 seconds rest between each threshold measurement. Monitoring of fixation was done using an infrared camera and also with the instrument's fixation error output. A test was deemed unreliable when fixation error exceeded 30% and these were not included in the analysis. No validation assessment was performed for the dark adaptometry functional outcome as it has previously been shown to have good reliability with the diagnostic sensitivity of 88% and 100% specificity (Jackson and Edwards 2008).

2.2.5 Fundus Autofluorescence

2.2.5.1 Quantitative Autofluorescence

qAF images were acquired for the PEONY Study by two trained operators (*Shruti Chandra and Sash Y Jeetun*) after mydriasis. For all patients a standard operating procedure was followed. In summary, with room lights turned off, NIR image was recorded first. In the qAF mode, the image was refocused to ensure a uniform signal over the entire field. During set-up and focusing in qAF mode, the fundus was exposed for 20 seconds to reduce visual pigment absorption. Each image was acquired in high-speed video mode; at least 2 images were recorded, each being 12 frames. All video images were examined for image quality and at least 9 of the 12 frames were selected. Selected frames were aligned, and mean image saved. The image quality was graded based on the criteria defined by von der Emde et al (poor, acceptable or excellent) and all images with quality acceptable or above were included (von der Emde, Guymer et al. 2021).

qAF images were analysed with HEYEX software. First, intergrader agreement for qAF was measured in five participants (κ-0.89). qAF8 values were measured using the qAF8 segment. The qAF8 segment refers to the mid-ring of the Delori grid centered on the fovea in the range of 9°–11° eccentricity from the fovea. Vessels were automatically excluded from analysis by the software. The operator manually adjusted the threshold settings as needed. Phakic eyes were then corrected for standard age-related optical media densities (van de Kraats and van Norren 2007, Greenberg, Duncker et al. 2013). No age adjustment was performed for ocular media absorption in pseudophakic eyes. The normalized gray values from the central eight segments of the qAF8 image were averaged to provide the main outcome measure (qAF8) for this study.

2.2.5.2 Blue light Autofluorescence

These images were obtained on the Spectralis Heidelberg Retina Angiograph HRA2 (Heidelberg Engineering, Heidelberg, Germany) using a confocal scanning laser ophthalmoscope and blue light excitation (wavelength of 488 nm, delivered using an argon blue or optically pumped solid-state laser). The images were acquired in a mydriatic pupil prior to acquisition of OCT or OCTA scans. All images were centred on the fovea. The image details of BAF on Spectralis HRA 2 had the following specifications 5 μm/pixel lateral digital resolution, 768 × 768 pixels minimum image size and 30° field of view. The measurement of area on the fundus autofluorescence images was done using both automated method with Region finder software and manually using the inbuilt free-hand drawing overlay tool, provided by Spectralis.

2.2.6 Colour Fundus photographs and Ultrawidefield Colour photographs

Fundus photography was performed using the Topcon TRC-50DX (Topcon Corporation, Tokyo, Japan). As per the imaging protocol, a 35° stereo pair centred on the fovea was acquired. A fundus reflex photograph (anterior segment) was captured as well to document media opacities.

UWF fundus imaging was performed in both modes (colour and autofluorescence) in mydriatic pupils, using the Optos® (Optos, Dunfermline, Scotland, UK). All the images were centered on the macula and anonymized prior to being exported for analysis.

2.2.7 SD -OCT and OCTA

All NIR, OCT and OCTA scans analysed and graded in the thesis were acquired using the Spectralis HRA system (Heidelberg Engineering, Heidelberg, Germany) by a trained operator. All images were acquired in a mydriatic pupil, and all images were centred on the fovea. The participant was explained that they are required to place their chin on the chin rest and look directly into the camera lens. They would see a bright blue dot that represents the internal fixation target. In addition to the blue fixation target, a set of red lines would also be visible. While the OCT images are taken, the red light would move, and the patient was told to make a conscious effort to keep looking at the fixation target. One minute resting time was allowed between scan acquisitions. The confocal scanning laser ophthalmoscopy (cSLO) fundus reference image was aligned for even fundus illumination edge to edge and adjusted for sharp focus. It was also ensured that baseline scans were centred on the fovea. All scans for subsequent images were acquired in the follow-up mode.

For the PRECISE study, the image acquisition and data export details were compiled in the Manual of Operations (v 1.0 dated 31st October 2019) for PRECISE study and was prepared by *Shruti Chandra* in consultation with the chief investigator (*Sobha Sivaprasad*) for the study. This was distributed across all participating sites (Appendix 2 Section A).

For the PEONY study, dense raster volume scans covering a retinal area of 6 x 6mm^2 (20° x 20° visual angle) comprising of 97 parallel OCT B-scans were acquired for both eyes. Using the automated real-time (ART) function, 15 images were averaged for each scan. The 97-line volume scan allowed for generation of en-face OCT images.

The OCT-A images were acquired using the same general principles. Only HS 20 scans were acquired with the following specifications: 20°x 20°, 512 Sections (distance between 2-line scans -11 microns), High Speed, 5 Frames (ART).

2.3 Image grading

2.3.1 Multimodal image grading for non-neovascular AMD

All images were graded by single grader (*Shruti Chandra*). A subset was graded by a senior grader (*Sobha Sivaprasad*) and the intergrader agreement was Kappa 0.95.

2.3.1.1 Colour photographs

Various stages of AMD on colour photographs were graded based on the Beckman classification (Ferris, Wilkinson et al. 2013) (Table 2.2).

Table 2.2 Beckman Initiative for AMD classification system.

Classification of AMD	**Features (lesions assessed within 2-disc diameters of fovea of either eye)**
No apparent aging changes	No drusen and No AMD pigmentary abnormalities
Normal aging changes	Only drupelets (small drusen ≤63 µm) and No AMD pigmentary abnormalities
Early AMD	Medium drusen >63 µm and ≤125 µm and No AMD pigmentary abnormalities
Intermediate AMD	Large drusen > 125 µm and/or Any AMD pigmentary abnormalities
Late AMD	Neovascular AMD and/or Any geographic atrophy

AMD pigmentary abnormalities = any definite hyper- or hypopigmentary abnormalities associated with medium or large drusen but not associated with known disease entities.

2.3.1.2 OCT grading

1. SDD: Participants with a minimum of 5 SDD on different line scans on OCT confirmed on NIR were identified as a separate category irrespective of the size of drusen present. Eyes with SDD were further divided into stages (Zweifel, Spaide et al. 2010):

Stage 1 - defined as diffuse deposition of granular hyperreflective material between the RPE-BrM band and the EZ layer.

Stage 2 - mounds of accumulated material sufficient to deflect inwardly the contour of the EZ.

Stage 3 - presence of a conical appearance and breaking through the EZ.

2. nGA: was defined as presence of either of two features (i) subsidence of the OPL and INL and (ii) a hyporeflective wedge shaped band within the limits of the OPL (Wu, Goh et al. 2023). They could be associated with (i) Subsidence of the

OPL and INL: disruption of IS and the RPE band, break in ELM, traces of increased signal transmission below BrM; (ii) Hyporeflective wedge-shaped band: vortex like subsidence of OPL and INL, drusen regression, traces of increased signal transmission below BrM.

3. cRORA: was defined by the following criteria (i) Zone of hypertransmission of ≥250 µm (ii) Zone of attenuation or disruption of RPE band of ≥250 µm (iii) Evidence of overlying photoreceptor degeneration characterised by features that include ONL thinning, ELM loss, and EZ or IZ loss (Sadda, Guymer et al. 2018).

4. iRORA: was defined by the following criteria: (1) a region of signal hypertransmission into the choroid and (2) a corresponding zone of attenuation or disruption of the RPE, with or without persistence of BLamD, and (3) evidence of overlying photoreceptor degeneration, i.e., subsidence of the INL and OPL, presence of a hyporeflective wedge in the HFL, thinning of the ONL, disruption of the ELM, or disintegrity of the EZ, and when these criteria do not meet the definition of cRORA (Sadda, Guymer et al. 2018).

5. Intraretinal HRF: Discrete punctate lesions with equal or greater reflectivity than that of the RPE within the retina (Jaffe, Chakravarthy et al. 2021).

6. Choroidal hypertransmission: Linear and continuous vertical streaks of hyper-reflectivity extending into the choroid and obscuring the choroidal markings (Laiginhas, Shi et al. 2022).

7. hDC: Hyporeflective spaces within the sub-RPE compartment of the druse (Veerappan, El-Hage-Sleiman et al. 2016). Also referred to as hyporeflective drusenoid lesions (HDL).

8. Drusen Enface OCT classification: On en-face OCT, large drusen was defined as drusen diameter ≥145 µm, medium drusen diameters 100 µm to 144 µm, and small drusen had diameters <100 µm on OCT (Kim, Loo et al. 2021).

9. Drusen volume in mm^3: Drusen volume was measured using the Spectralis in-built segmentation software (post manual correction of segmentation of all layers

where required). It was defined as the average volume across ETDRS grid with segmentation lines between RPE layer and BrM.

10. ONL volume in mm^3: ONL volume was measured using the Spectralis in-built segmentation software (post manual correction of segmentation of all layers where required).

11. Subfoveal choroidal thickness (SFCT): Measured on the enhanced depth imaging (EDI) OCT scan. Defined as the vertical distance in microns from the BrM to the sclerochoroidal junction at the fovea.

2.3.1.3 OCT-based AMD classification proposed in the study

Based on the en-face OCT drusen classification and the features graded on OCT, I designed a multimodal imaging-based classification of AMD (Table 2.3). This was done to further dissect the role of phenotypic heterogeneity in intermediate eyes while performing structure-function correlation.

Table 2.3 Proposed new OCT classification system.

AMD Stage	**Features on OCT**
Early	defined as maximum druse diameter <100 µm with no SDD or atrophy.
Intermediate	defined as having more than 1 druse with diameter 100-145 µm or at least 1 druse (>145 µm) without SDD or atrophy (cRORA) but may have HRF or iRORA.
Eyes with SDD	Presence of SDD as per grading definition, any stage.
Eyes with atrophy (cRORA)	Presence of cRORA as per grading definition.

Abbreviations: cRORA – complete retinal pigment epithelium and outer retinal atrophy; HRF – hyperreflective foci; iRORA – incomplete retinal pigment epithelium and outer retinal atrophy; SDD – subretinal drusenoid deposits.

2.3.2 Multimodal image grading for nAMD

All images collected across 10 centres were anonymized and sent to Moorfields Eye Hospital NHS Foundation Trust as the reading centre. I screened and quality checked all the images received prior to grading. I also prepared a pre-defined OCT grading manual which was used to grade the OCT scans. Finally based on the grading manual, I trained 4 medical retina fellows to grade the scans in detail after grading on a test set of 50 OCT images. Each scan was corrected for any segmentation errors and foveal centration before CSFT was recorded.

2.3.2.1 OCT grading

Image Focus and method of analysis – Foveal versus extrafoveal

The images were graded for the presence of defined OCT parameters within the volume scan of the macula. The line scans protocols on Heidelberg Spectralis scans ranged from 19 to 49 (19, 25, 31 or 49). As per plan for response assessment, all parameters were graded in for presence in the fovea or extra-foveal or both. Primary step for this is to identify the fovea and place the ETDRS grid accurately at the fovea (Figure 2.1).

Fovea was defined as the central 1 mm area around the foveal depression as seen on the ETDRS grid.

Extra-foveal was defined as scan area beyond the central 1 mm zone (excluding the central 1 mm).

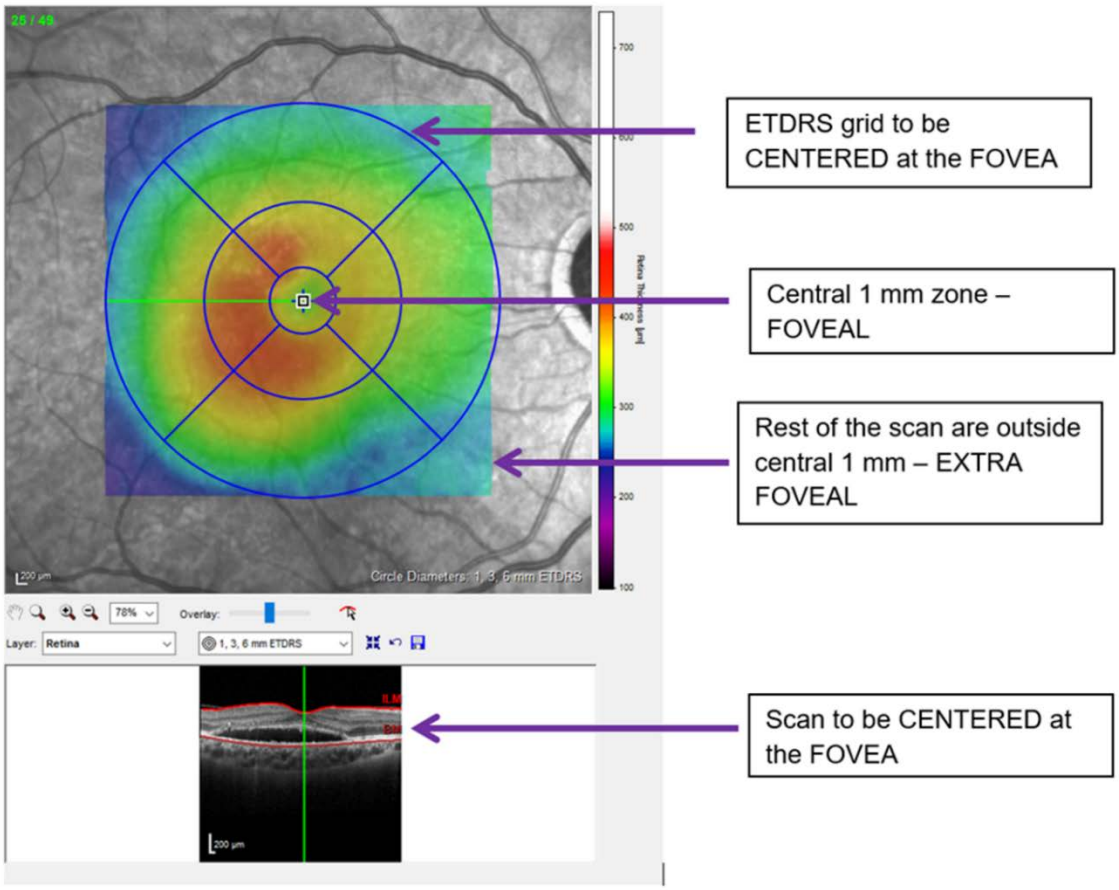

Figure 2.1 Methodology for foveal and extrafoveal grading. (Image source: Authors own).

2.3.2.2 Grading definitions of OCT parameters

Grading sheet of all parameters is attached in Appendix 2 Section B.

1. SRF: Presence of hypo reflective space between the photoreceptors and RPE tips i.e., neurosensory detachment (Keane, Patel et al. 2012).

2. IRF: Intra-retinal hypo reflective cyst like spaces usually seen above the OPL, not associated with underlying atrophy. IRF can occur either diffusely, creating increased retinal thickness and reduced retinal reflectivity, or appear localized in non-reflective well-defined cysts (cystic macular oedema) (Keane, Patel et al. 2012).

3. MNV: Defined as presence of SHRM or PED on OCT scan with or without presence of SRF or IRF (Spaide, Jaffe et al. 2020).

4. Components of MNV: Defined as fluid or contiguous blood or PED or fibrosis.

5. MNV type: The MNV subtypes on OCT were defined based on the Consensus on Neovascular Age-Related Macular Degeneration Nomenclature Study Group (CONAN) classification (Spaide, Jaffe et al. 2020).

    i. Type 1 MNV represents areas of neovascular complexes arising from the choroid and imaged with OCT as an elevation of the RPE by material with heterogeneous reflectivity; vascular elements may be seen. OCT-A shows vessels below the level of the RPE.

    ii. Type 2 MNV was defined as neovascular complex located in the subretinal space, above the level of the RPE. May be associated with SHRM and separation of the neurosensory retina from the RPE. OCT-A demonstrates vascular elements above the level of the RPE.

    iii. Type 3 or RAP was defined as extension of hyperreflectivity from the middle retina toward to level of the RPE associated with intraretinal oedema, haemorrhage, and telangiectasis. OCT-A shows the downgrowth of new vessels toward or even penetrating the level of the RPE.

iv. PCV was defined as presence of notched/tall peaked/ thumb like PED with a DLS or haemorrhage with or without presence of sub RPE hyperreflective oval structure of a polyp.

6. PED: Several forms of elevation of the RPE monolayer from the underlying BrM. This includes drusenoid, serous, and fibrovascular. Some forms of early type 1 neovascularization produce a relatively flat elevation. Many cases of serous PED show evidence of MNV. OCT-A is particularly useful in detecting the presence of neovascularization (Spaide, Jaffe et al. 2020).

7. SHRM was defined as fluffy material, ill-defined and isoreflective to inner retina located between retina and RPE (Spaide, Jaffe et al. 2020).

8. Fibrosis: was defined as subretinal hyper-reflective thickening, well defined and dense as RPE, better observed by reducing the contrast, may have a multilaminar appearance (Spaide, Jaffe et al. 2020).

9. Atrophy: Presence of atrophy was defined as per CAM meeting definition (Zone of hyper transmission of ≥250 μm; Zone of attenuation or disruption of RPE band of ≥250 μm; Evidence of overlying photoreceptor degeneration characterised by features that include ONL thinning, ELM loss, and EZ or IZ loss (Sadda, Guymer et al. 2018).

10. ORT: ORTs are round hyporeflective lesions, which may contain a few focal hyperreflective spots and are always delineated by a hyperreflective ring, in contrast to the completely hyporeflective retinal cystoid lesions. They are always located at the level of the ONL, and in AMD, they are classically found very close to areas of neovascular fibrosis or retinal atrophy (Iaculli, Barone et al. 2015)

11. Vitreomacular traction (VMT): Vitreomacular traction is characterized by anomalous posterior vitreous detachment accompanied by anatomic distortion of the fovea, which may include pseudocysts, macular schisis, cystoid macular oedema, and subretinal fluid (Duker, Kaiser et al. 2013).

12. Epiretinal Membrane (ERM): ERM as an irregular, hyper-reflective layer on the ILM commonly associated with retinal wrinkling and hypo-reflective spaces between the ERM and ILM (Fung, Galvin et al. 2021).

13. CST: Measured after correction of segmentation where necessary. The CST was measured from ILM to the BrM.

2.3.3 Multimodal image grading for GA

Grading of all images was performed by single grader (*Shruti Chandra*). A smaller subset was re-graded by a senior grader (*Sobha Sivaprasad*) and the intergrader agreement was Kappa 0.97.

2.3.3.1 Fundus autofluorescence

1. Junctional changes: The junctional changes in the FAF were graded into 5 phenotypes as defined by the FAM group (Bindewald, Schmitz-Valckenberg et al. 2005) (Table 2.4).

2. Focality: Unifocal lesions were defined as single demarcated lesion of hypoautofluorescence, whereas multifocal lesions were defined as those with multiple scattered or confluent hypoautofluorescent areas of atrophy.

3. Area of atrophy: The area of atrophy was measured in mm^2.

Table 2.4 Junctional zone patterns on FAF (FAM study group).

Junctional FAF pattern	Description
None	No increase in FAF intensity at the junction.
Minimal change	Change at the junctional zone was minimal without a definite pattern.
Focal	Presence of at least one spot of hyperautofluorescence at the junction, diameter <200 microns.
Patchy	More than one spot of hyperautofluorescence or single spot diameter >200 microns at the junctional zone.
Banded	Presence of definite, continuous, ring-shaped hyperautofluorescence around the atrophy.
Diffuse	Presence of areas with increased FAF directly adjacent to the margin of the atrophic patch and elsewhere.

2.3.3.2 OCT grading for GA

1. Presence of iRORA/cRORA: as defined in 2.3.1

2. Foveal involvement: defined as atrophic lesion involving the central 1mm of the macular volume scan when centered on the fovea.

3. Presence of SDD: As defined in 2.3.1

3 Chapter 3: Phenotypic heterogeneity in early and intermediate AMD and derivation of a classification based on multimodal imaging and structure-function correlation

3.1 Introduction

Preventing progression of early and iAMD to late stages is an area of current active research. Several new developments including clinical trial end point and interventions instituted at early and intermediate stages are underway to evaluate strategies to prevent disease progression. Another notable development is the incorporation of deep learning algorithms in monitoring progression of early disease and use of automated image grading for screening (Ting, Peng et al. 2019, Waldstein, Vogl et al. 2020). Crucially, both these developments require robust classifications systems of AMD. The purpose for classifying AMD also varies based on the stakeholder requirements (i.e., clinicians, clinical trialist, community optometrists or AI engineers) (Thee, Meester-Smoor et al. 2020). For example, in the context of clinical trials, well-defined inclusion criteria are required to achieve high rates of outcome events while AI scientists developing automated screening tools need accurate information in the form of 'ground truth'. Irrespective of the user need, the classification needs to accurately represent risk stratification of AMD. Multiple studies have identified OCT biomarkers such as subretinal drusenoid deposits (SDD) that can predict progression to late AMD however; the current classification systems do not reflect these high-risk characteristics (Brandl, Zimmermann et al. 2018). Therefore, although iAMD on colour photographs is considered one category defined as presence of at least 1 large drusen and RPE changes, it is clear on OCT that this category is heterogeneous with varying rates of progression. Further stratification is therefore required to ensure that clinical trials of novel agents are not declared negative due to lack of refinement of study cohort.

Aims and justification:

In this chapter, I propose a new framework for classifying non-neovascular AMD that incorporates the phenotypic heterogeneity in OCT imaging. I then explored how the phenotypic heterogeneity represented in this classification affects

functional changes in non-neovascular AMD. In addition, I examined how this classification relates to macular qAF.

My first aim was to design a framework for an OCT based classification of non-neovascular AMD severity. There are risk scores based on anatomical changes on CFP that can predict disease progression to advanced AMD. Despite this initiative, there are significant inter-individual variations. For example, fellow eyes of patients with nAMD have a 10% risk of converting to nAMD per year (Gehrs, Anderson et al. 2006). So, two eyes with similar anatomical characteristics may convert at different time points. Although genetic susceptibility and modifiable risk factors such as smoking also play a role, these do not seem to provide more information at an individual level. Therefore, more elaborate risk prediction analysis requires intricate phenotyping on multimodal imaging that can discriminate progression rate among categories. In the first section of this chapter, I incorporate OCT classification integrating SDD in the AMD severity staging. I also compare my OCT classification with the Beckman classification.

My second aim was to correlate the OCT based classification with DA in eye with varying severity of AMD because DA has been proposed as a possible functional biomarker for AMD (Owsley, McGwin et al. 2016). The degree of outer retinal involvement also indicates that associated visual function changes may be used to stratify AMD. There may be different subgroups of AMD based on rod function. The RIT measures the ability of rods to recover from stress of bleaching. Therefore, studying the relation of function to the structure of the outer retina-BrM- choroid complex in categories of people with and without abnormal DA may help us understand the pathogenesis of AMD.

My third and final aim in this chapter was to correlate qAF levels across varying severity of AMD based on the OCT classification proposed in section 3.2. Lipofuscin is a major contributor of signals in FAF. qAF enables in vivo quantification of these FAF signals compared with an internal standard. Excessive lipofuscin could adversely affect essential RPE functions and contribute to the pathogenesis of AMD (Young 1987, Delori, Fleckner et al. 2000, Moreno-García, Kun et al. 2018). Therefore, eyes with increased qAF8 levels may benefit from anti-lipofuscin therapies as in Stargardt disease and metabolic

studies (Delori, Fleckner et al. 2000, Burke, Duncker et al. 2014, Sparrow, Duncker et al. 2020). In this study I evaluate whether quantitative autofluorescence levels vary with OCT based stages of AMD progression. I also probe whether OCT risk features of RPE cell death influence qAF8 levels thereby exploring its efficacy as a clinical trial end point for anti-lipofuscin therapy trials in AMD. Table 3.1 summarizes the sections in this chapter with their aims.

Table 3.1 Summary table of the studies that reflect the aims of this chapter.

Section	Title	Aims
3.2	Optical Coherence tomography-based classification for non-neovascular AMD	To propose an OCT based classification of AMD incorporating phenotypic heterogeneity and to compare it with Beckman classification.
3.3	Dark adaptation in OCT based classification of non-neovascular AMD	To study phenotypic heterogeneity determining prolonged dark adaptation in OCT based stages of AMD progression.
3.4	Quantitative autofluorescence in OCT based classification of non-neovascular AMD	To evaluate whether quantitative autofluorescence levels vary with OCT based stages of AMD progression and interrogate whether OCT risk features of RPE cell death influence qAF8 levels.

3.2 Optical Coherence tomography-based classification for non-neovascular AMD

3.2.1 Purpose

To propose an OCT based classification of AMD incorporating phenotypic heterogeneity and to compare it with Beckman classification.

3.2.2 Methods

In this prospective study (PEONY study) I recruited 254 participants who met the eligibility criteria for the study. The PEONY study was a single centre study and patients were recruited from 09/09/2019 to 30/05/2023.

Inclusion criteria included Caucasians aged ≥50 years with varying severity of non-neovascular AMD in at least one eye and age-matched controls with healthy

maculae were recruited for this study from August 2020 to July 2022. Inclusion criteria for non-neovascular AMD in at least one eye were Snellen visual acuity of ≥6/18 with media clarity for qAF8 and other imaging.

Exclusion criteria were any condition that in the opinion of the investigator could affect or alter visual acuity or retinal imaging such as vitreous opacities, epiretinal membrane and other comorbid conditions such as diabetic retinopathy.

The aim was to study the OCT characteristics of non-neovascular AMD so as to describe the features that determine the heterogeneity to inform an OCT-based classification and structure-function correlation. The imaging methods used in the PEONY study are described in detail in Chapter 2 in section 2.3.1.

Statistical Analysis

Data were summarised using mean ± standard deviation (SD) or median, interquartile range (IQR) for continuous variables and number (%) for categorical variables. Differences between the controls and individual AMD groups by multimodal imaging OCT and Beckman classification were compared. Stage of SDD and drusen volume were summarised based on varying severity of RPE cell loss in AMD. Generalised Estimating Equations (GEE) with an exchangeable working correlation structure were used to account for the within-participant correlation among those with data from both eyes.

3.2.3 Results

The participant flow for the study is shown in Appendix 3, Figure S3.1. A total of 353 eyes of 239 patients were analyzed. Of these, 248 eyes of 176 participants had varying severity of non-neovascular age related macular degeneration and 105 eyes of 63 participants aged at least 50 years were included as controls in the study analysis. Based on the en-face OCT drusen classification and the features graded on OCT, Table 3.2 shows the definitions for the stages of multimodal imaging-based classification of AMD.

Table 3.2 Definitions for stages of AMD severity in the OCT classification.

AMD Stage	**Features on OCT**
Normal	Defined as no evidence of AMD changes on OCT
Early AMD	Defined as maximum druse diameter <100 µm with no SDD or atrophy (cRORA). If there is iRORA, then intermediate stage
Intermediate AMD	Defined as having more than 1 druse with diameter 100-145 µm or at least 1 druse (>145 µm) without SDD or atrophy (cRORA) but may have HRF or iRORA.
Eyes with SDD	Presence of SDD as per grading definition, any stage of AMD except cRORA i.e., early or intermediate
Eyes with atrophy (cRORA)	Presence of cRORA as per CAM grading definition.

Abbreviations: AMD – age related macular degeneration; cRORA – complete retinal pigment epithelium and outer retinal atrophy; HRF – Hyperreflective foci; iRORA – incomplete retinal pigment epithelium and outer retinal atrophy; OCT – Optical Coherence Tomography; RPE – Retinal pigment epithelium; SDD – subretinal drusenoid deposits

Table 3.3 shows the distribution of participant and imaging characteristics in Beckman versus OCT classification. This table includes controls, aged 50 years or older and AMD eyes categorised based on the Beckman Classification on CFP. We also include the OCT based classification to highlight the incorporation of SDD and other parameters to each category.

Table 3.3 Participant and imaging characteristics in AMD categories based on the Beckman and OCT classification.

	Beckman AMD classification			**AMD classification based on multimodal imaging**			
Variable	**Early, N=59 eyes of 50 participants**	**iAMD, N=161 eyes of 125 participants**	**GA, N=28 eyes of 22 participants**	**Early, N = 47 of 38 participants**	**iAMD, N = 76 of 58 participants**	**SDD, N = 97 of 75 participants**	**cRORA, N = 28 of 22 participants**
Participant level[a]							
Number of bilateral participants	9 (18.0%)	36 (28.8%)	6 (27.3%)	9(23.7%)	18(31.0%)	22(29.3%)	6(27.3%)
Age, years	69.5 (8.5)	73.1 (7.1)	74.0 (5.1)	69.0 (8.2)	71.5 (7.0)	73.8(7.6)	74.0 (5.1)
Age, years							
< 60	5 (10.0%)	5 (4.0%)	1 (4.6%)	4 (10.5%)	4(6.9%)	3(4.0%)	1(4.6%)
60-69	21 (42.0%)	30 (24.0%)	1 (4.6%)	17 (44.7%)	17(29.3%)	14(18.7%)	1(4.6%)
70-79	17 (34.0%)	68 (54.4%)	17 (77.3%)	14 (36.8%)	30(51.7%)	41(54.7%)	17(77.3%)
>=80	7 (14.0%)	22 (17.6%)	3 (13.6%)	3 (7.9%)	7(12.1%)	17(22.7%)	3(13.6%)
Gender							
M	21 (42.0%)	42 (33.6%)	11 (50.0%)	18(47.4%)	20(34.5%)	24(32.0%)	11(50.0%)
F	29 (58.0%)	83 (66.4%)	11 (50.0%)	20(52.6%)	38(65.5%)	51(68.0%)	11(50.0%)

Eye level[b]							
Pseudophakia	12 (20.3%)	35 (21.7%)	6 (21.4%)	9 (19.1%)	16 (21.1%)	22 (22.7%)	6 (21.4%)
Stage of SDD							
No SDD	41 (69.5%)	82 (50.9%)	28 (100.0%)	47 (100.0%)	76 (100.0%)	0 (0%)	28 (100.0%)
Stage 1	1(1.7%)	4 (2.5%)	0 (0.0%)	0 (0%)	0 (0%)	5 (5.2%)	NA
Stage 2	1 (1.7%)	14 (8.7%)	0 (0.0%)	0 (0%)	0 (0%)	15 (15.5%)	NA
Stage 3	16 (27.1%)	61 (37.9%)	0 (0.0%)	0 (0%)	0 (0%)	77 (79.4%)	NA
Drusen volume (RPE-BrM) mm^3 in those without cRORA	-	-	-	0.3 (0.3, 0.4)	0.5 (0.4, 0.5)	0.5 (0.4, 0.6)	NA
SFCT, microns				246.0 (195.0, 309.8)	223.0 (155.2, 274.0)	200.2 (107.3, 231.7)	176.0 (125.8, 234.5)
ONL volume, mm3				1.8	1.7	1.7	1.6
Stages of RPE cell integrity							
Absence of HRF without evidence of iRORA or cRORA	-	-	-	46 (97.9%)	54 (71.1%)	53 (54.6%)	NA
Presence of HRF without evidence of iRORA or	-	-	-	1 (2.1%)	8 (10.5%)	7 (7.2%)	NA

cRORA							
Presence of iRORA without any evidence of cRORA	-	-	-	0 (0%)	14 (18.4%)	37 (38.1%)	NA
Presence of cRORA	-	-	-	0 (0%)	0 (0%)	0 (0%)	28 (100.0%)

a Participant level characteristics were based on total cohort of 231 participants, the number of participants across Beckmann categories do not add up to 231 (total number of participants in the cohort) due to bilateral eligibility in the cohort where eyes from the same participant belong in different Beckmann classification groups.
b Eye level characteristics based on total analysed sample of 353 eyes.
Abbreviations: AMD – age related macular degeneration; cRORA – complete retinal pigment epithelium and outer retinal atrophy; GA – Geographic atrophy; HRF – Hyperreflective foci; iAMD – intermediate AMD; IR- Infrared reflectance; iRORA – incomplete retinal pigment epithelium and outer retinal atrophy; IQR – Interquartile range; OCT – Optical Coherence Tomography; qAF8 – quantitative autofluorescence; RPE – Retinal pigment epithelium; SDD – subretinal drusenoid deposits.

On comparison with Beckman, I noted that 40% of eyes classified as early AMD as per Beckman had SDD on OCT and likewise 30% with iAMD as per Beckman had SDD on OCT. Of the eyes that had SDD almost 80% had stage 3 SDD, including 2 eyes from the early AMD group. Interestingly 20% of eyes had stage 1 or 2 SDD that are known to be either invisible or poorly visible on CFP, emphasizing the need for OCT classification for more phenotypically homogeneous cohorts. Similarly, 40% of SDD eyes and 20% of iAMD eyes had confirmed iRORA on OCT. When considering HRF, about 10% eyes in SDD and iAMD group had HRF and importantly there was 1 eye classified as early by Beckman that had confirmed HRF on OCT. It might also be worthy to mention here that all iRORA and HRF were not detectable on CFP as pigmentary changes.

3.3 Dark Adaptation in OCT based classification of non-neovascular AMD

3.3.1 Purpose

To study how phenotypic heterogeneity relates to changes in DA in OCT based stages of AMD progression.

3.3.2 Methods

The relevant methods are mentioned in Chapter 2: Methodology (Section 2.2 and 2.3). In addition to OCT imaging classification shown in Table 3.2, I also studied the DA in the whole cohort. For the DA analysis, patients with unreliable DA test were excluded from the analysis.

The visual function and structural markers were studied in the cohort as stratified by Beckman classification as well as the OCT classification. The visual function markers studied were BCVA, LLVA, Low luminance deficit (LLD) and dark adaptation as RIT. Among structural markers we looked at ONL, RPE-BrM volume and SFCT. RIT in one eligible eye of each participant was measured using AdaptDx (Maculogix, Hummelstown, PA, USA Ltd). After dark adaptation for 30 minutes, participants were exposed to a bleach of 83% with 505nm photoflash centred at 5^{o} in the inferior vertical meridian. RIT was measured as time to reach a threshold of $5x10^{-3}$ cd/m^2 or to a maximum test duration of 20 minutes. Delayed RIT was defined using 2 thresholds of RIT >6.5 and >12.5 minutes. We also studied the odds of delayed RIT based on detailed imaging

phenotyping of non-neovascular AMD. For the purposes of studying associations a threshold of ≥8 minutes was used. In addition, as markers of outer retinal integrity nGA and hypertransmission defects were graded. These are defined in Chapter 2 methodology in section 2.3.1.

Statistical analysis

Descriptive and inferential statistics were done for comparison. Spearman coefficient was used for correlation. Analysis of variance overall test was used for BCVA, ONL volume and SFCT analysis followed by post-hoc pairwise t-tests. Kruskal Wallis test overall used for BCVA, LLVA and RPE-BM volume followed by duns test for pairwise comparisons. For proportions Chi-squared test was used, followed by pairwise chi2 tests. Univariate and multivariable associations between structural markers and RIT threshold of ≥8 minutes were reported using Odds Ratio (OR) with 95% confidence interval (95% CI) and P-value.

3.3.3 Results

A total of 209 eyes of 209 patients were analysed for this study. Normal, 50; Early AMD without SDD, 22; Early AMD with SDD, 15; iAMD without SDD, 56; iAMD with SDD, 49; cRORA, 17. Table 3.4 shows the demographic and clinical characteristics of the patients.

Table 3.4 Demographic & clinical characteristics of the DA cohort.

Variable	**Overall, N = 209**
Age, years	70.6 (9.2)
Gender	
M	79 (37.8%)
F	130 (62.2%)
BCVA, ETDRS letters	82.4 (6.2)
LLVA, ETDRS letters, median(IQR)	70.0 (64.0,75.0)
RIT, minutes	
<=6.5 minutes	91 (43.5%)
>6.5 minutes	118 (56.5%)

Variable	Overall, N = 209
RIT, minutes	
< 8.0 minutes	101 (48.3%)
>=8.0 minutes	108 (51.7%)
RIT, minutes	
<=12.5 minutes	114 (54.5%)
>12.5 minutes	95 (45.5%)
Age, years	
< 60	31 (14.8%)
60-69	51 (24.4%)
70-79	91 (43.5%)
>=80	36 (17.2%)
BCVA, ETDRS letters	
54-67	3 (1.4%)
>=68	206 (98.6%)
LLVA, ETDRS letters	
<54	14 (6.7%)
54-67	75 (35.9%)
>=68	120 (57.4%)
LLD, median(IQR)	13.0 (10.0, 17.0)
AMD	
Normal	50 (23.9%)
Early AMD without SDD	22 (10.5%)
Early AMD with SDD	15 (7.2%)
Intermediate AMD without SDD	56 (26.8%)
Intermediate AMD with SDD	49 (23.4%)
cRORA	17 (8.1%)
SFCT, microns	217.6 (87.8)
ONL volume, mm3	1.70 (0.22)
RPE BrM volume, mm3, median(IQR)	0.41 (0.37,0.49)

Abbreviations: iAMD – intermediate AMD; BCVA – best corrected visual acuity; IQR – Interquartile range; LLD – Low luminance deficit ; LLVA – low luminance visual acuity ; OCT – Optical Coherence Tomography; qAF8 – quantitative autofluorescence; RPE-BrM – Retinal pigment epithelium; SDD – subretinal drusenoid deposit; SFCT – subfoveal choroidal thickness.

Table 3.5 and Table 3.6 show the visual and structural markers in the cohort stratified by AMD disease severity as per Beckman and OCT classification respectively. The sample size for the Beckman classification is 192 as 17 eyes with GA were not included in the analysis. LLVA was significantly different between normal versus early in Beckman classification (p value 0.004), and normal versus early with SDD (p=0.001); however, it was not significantly different between normal versus early without SDD (p= 0.25) emphasizing the inclusion of SDD in the classification has an influence on functional and structural markers. Similarly, ONL volume was not significantly different across the Beckman groups of normal, early, and intermediate (p =0.055).

Table 3.5 Visual function and structural markers in the eyes that underwent dark adaptation testing summarized for all participants and stratified by AMD disease severity (Beckman classification).

Variable	**N**	**Normal, N = 50**	**Early, N = 37**	**iAMD, N = 105**	**p-value**	**Normal vs. Early**	**Normal vs. iAMD**	**Early vs. iAMD**
BCVA, ETDRS letters[a]	192	87.5 (4.7)	83.5 (4.8)	80.7 (5.3)	<0.001	<0.001	<0.001	0.004
LLVA, ETDRS letters[b]	192	74.5 (71.2, 78.0)	72.0 (64.0, 75.0)	67.0 (61.0, 73.0)	<0.001	0.004	<0.001	0.04
RPE-BM volume[b]	192	0.4 (0.4, 0.4)	0.4 (0.3, 0.4)	0.5 (0.4, 0.5)	<0.001	0.19	<0.001	<0.001
ONL volume (mm3)[a]	192	1.8 (0.2)	1.7 (0.3)	1.7 (0.2)	0.055			
SFCT (microns)[a]	192	271.1 (75.6)	200.2 (107.3)	201.2 (77.1)	<0.001	<0.001	<0.001	>0.9
RIT, minutes[c]	192				<0.001	<0.001	<0.001	0.2
<=6.5 minutes		46 (92.0%)	15 (40.5%)	28 (26.7%)				

Variable	N	Normal, N = 50	Early, N = 37	iAMD, N = 105	p-value	Normal vs. Early	Normal vs. iAMD	Early vs. iAMD
>6.5 minutes		4 (8.0%)	22 (59.5%)	77 (73.3%)				
RIT, minutes[c]	192				<0.001	<0.001	<0.001	0.5
<=12.5 minutes		48 (96.0%)	19 (51.4%)	45 (42.9%)				
>12.5 minutes		2 (4.0%)	18 (48.6%)	60 (57.1%)				
LLD[b]	192	12.5 (10.0, 16.0)	13.0 (9.0, 16.0)	13.0 (10.0, 18.0)	0.6			

[a] Analysis of variance overall test, followed by post-hoc pairwise t-tests; [b] Kruskal Wallis test overall, followed by duns test for pairwise comparisons; [c] Chi-squared test, followed by pairwise chi2 tests. Abbreviations: BCVA- Best corrected visual acuity; LLD – low luminance deficit; LLVA - Low luminance visual acuity; ONL- Outer nuclear layer; RIT – Rod intercept time; RPE-BM –Retinal pigment epithelium Bruchs membrane; SFCT- Subfoveal choroidal thickness; RIT- Rod Intercept time

Table 3.6 explains the visual function and structural markers in eyes that underwent DA stratified by OCT classification. In the OCT classification LLVA was not significantly different in in eyes with early AMD (with or without SDD) versus normal (p value 0.25). However, when we looked at LLD, this was significant in eyes with early AMD +SDD versus normal eyes (p value 0.03) indicating the impact of SDD. ONL volume was significantly different in normal versus early with SDD (p = 0.012) and not when comparing normal versus early without SDD (p =0.5) demonstrating the influence of SDD. The RPE-BM complex volume was similar in normal versus early AMD cohort, irrespective of presence of SDD which is intuitive as SDD are seen above the RPE and therefore so not contribute to this measurement. With reference to dark adaptation, RIT>6.5 minutes could discriminate early AMD without SDD from normal (p=0.03) but not RIT>12.5 minutes (p=0.12). Only 8% and 4% of the normal eyes had RIT>6.5 and >12.5 minutes respectively. SDD was an independent risk factor for delayed DA, irrespective of AMD stage.

Table 3.6 Visual function and structural markers in the eyes that underwent dark adaptation testing summarized for all participants and stratified by AMD disease severity (OCT classification).

Variable	N	Normal, N = 50	Early without SDD, N = 22	Early with SDD, N = 15	iAMD without SDD, N = 56	iAMD with SDD, N = 49	cRORA, N = 17	p-value	Normal vs. Early without SDD	Normal vs. Early with SDD	Normal vs. iAMD without SDD	Normal vs. iAMD with SDD	Normal vs. cRORA
BCVA, ETDRS letters[a]	209	87.5 (4.7)	83.6 (4.9)	83.3 (4.7)	81.2 (5.7)	80.1 (4.8)	75.8 (6.4)	<0.001	0.003	0.006	<0.001	<0.001	<0.001
LLVA, ETDRS letters[b]	209	74.5 (71.2, 78.0)	74.0 (68.0, 76.5)	66.0 (62.0, 71.0)	69.0 (64.0, 75.0)	65.0 (59.0, 70.0)	63.0 (55.0, 66.0)	<0.001	0.25	<0.001	<0.001	<0.001	<0.001
RPE - BrM, volume, mm3	209	0.4 (0.4, 0.4)	0.3 (0.3, 0.4)	0.4 (0.3, 0.4)	0.4 (0.4, 0.5)	0.5 (0.4, 0.6)	0.5 (0.4, 0.6)	<0.001	0.17	0.60	<0.001	<0.001	<0.001
ONL volume, mm3	209	1.8 (0.2)	1.7 (0.2)	1.6 (0.3)	1.7 (0.2)	1.7 (0.2)	1.6 (0.3)	0.044	0.5	0.012	0.12	0.022	0.015
SFCT, microns	209	271.1 (75.6)	237.1 (108.4)	146.1 (81.8)	204.8 (80.0)	197.0 (74.2)	199.2 (79.9)	<0.001	0.10	<0.001	<0.001	<0.001	0.002
LLD[b]	209	12.5 (10.0, 16.0)	12.5 (8.2, 14.8)	16.0 (13.5, 22.5)	12.0 (10.0, 16.0)	14.0 (11.0, 19.0)	15.0 (12.0, 18.0)	0.008	0.29	0.03	0.84	0.04	0.11

Variable	N	Normal, N = 50	Early without SDD, N = 22	Early with SDD, N = 15	iAMD without SDD, N = 56	iAMD with SDD, N = 49	cRORA, N = 17	p-value	Normal vs. Early without SDD	Normal vs. Early with SDD	Normal vs. iAMD without SDD	Normal vs. iAMD with SDD	Normal vs. cRORA
RIT, minutes[c]	209							<0.001	0.026	<0.001	<0.001	<0.001	<0.001
<=6.5 minutes		46 (92.0%)	15 (68.2%)	0 (0.0%)	23 (41.1%)	5 (10.2%)	2 (11.8%)						
>6.5 minutes		4 (8.0%)	7 (31.8%)	15 (100.0%)	33 (58.9%)	44 (89.8%)	15 (88.2%)						
RIT, minutes[c]	209							<0.001	0.12	<0.001	<0.001	<0.001	<0.001
<=12.5 minutes		48 (96.0%)	18 (81.8%)	1 (6.7%)	37 (66.1%)	8 (16.3%)	2 (11.8%)						
>12.5 minutes		2 (4.0%)	4 (18.2%)	14 (93.3%)	19 (33.9%)	41 (83.7%)	15 (88.2%)						

[a] Analysis of variance overall test, followed by post-hoc pairwise t-tests; [b] Kruskal Wallis test overall, followed by duns test for pairwise comparisons; [c] Chi-squared test, followed by pairwise chi2 tests.

Abbreviations: BCVA- Best corrected visual acuity; LLD – low luminance deficit; LLVA - Low luminance visual acuity; ONL- Outer nuclear layer; RIT – Rod intercept time; RPE-BM –Retinal pigment epithelium Bruchs membrane; SFCT- Subfoveal choroidal thickness; RIT- Rod Intercept time

Thinner SFCT and higher RPE-BrM volume were significantly correlated with increasing AMD severity across both RIT thresholds (p<0.01) (Figure 3.1).

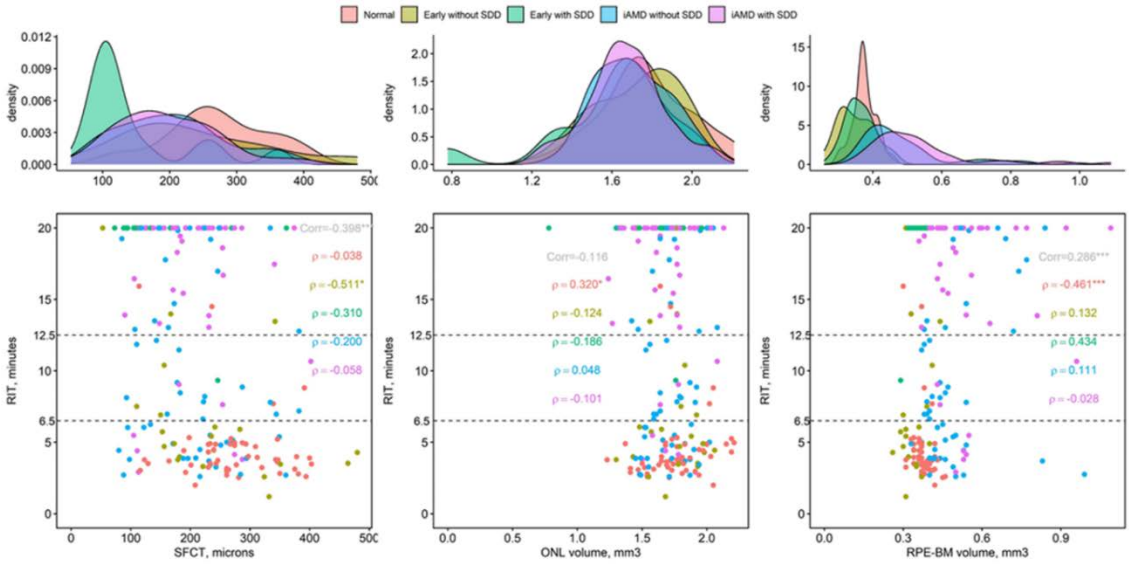

Figure 3.1 Correlation plots for SFCT, ONL vol & RPE-BM with RIT.
iAMD – intermediate AMD; ONL – outer nuclear layer; RIT – rod intercept time; RPE-BM – Retinal pigment epithelium Bruch's membrane; SDD – subretinal drusenoid deposits; SFCT - subfoveal choroidal thickness.

Table 3.7 shows the univariate analysis of age-gender adjusted OR of RIT ≥8 minutes with various structural biomarkers like RPE-BM changes, choroidal thickness (SFCT) and drusen characteristics e.g., subtypes including SDD, HDL, cuticular drusen, refractile drusen and drusen volume as RPE-BM volume.

Table 3.7 Univariate analysis of age-gender adjusted OR of RIT ≥8 minutes with structural biomarkers.

Characteristic	**OR (95% CI)**	**P value**
Presence of SDD No Yes	 - 20.0 (8.03 - 50.0)	 <0.001
Presence of Refractile drusen No Yes	 - 10.6 (1.36 - 82.9)	 0.024
Presence of Cuticular drusen No Yes	 - 2.03 (0.12 - 34.8)	 0.63
Presence of HDL No Yes	 - 3.65 (1.35 - 9.87)	 0.011
ONL volume (mm3), per 0.1mm^3 decrease	1.15 (1.03 - 1.29)	0.010

RPE-BrM volume, per 10% increase	1.35 (1.17 – 1.56)	<0.001
SFCT, per 100 microns decrease	2.40 (1.69 - 3.41)	<0.001
Presence of nGA or Hypertransmission No nGA with No Hypertransmission nGA or Hypertransmission	 - 2.11 (1.07 - 4.14)	 0.030
Presence of cRORA No Yes	 - 4.82 (1.09 - 21.3)	 0.039
Presence of HypoAF No Yes	 - 9.42 (2.69 - 33.0)	 <0.001

Abbreviations: cRORA – complete retinal pigment epithelium and outer retinal atrophy; HDL – hyporeflective drusenoid lesions; HypoAF – hypoautofluorescence; nGA – nascent geographic atrophy; ONL – outer nuclear layer; RPE – BrM – Retinal pigment epithelium Bruchs membrane; SDD – subretinal drusenoid deposits; SFCT – subfoveal choroidal thickness.

On multivariable analysis, the significant features placed in order of OR were presence of SDD OR 18.6 (95% CI 6.31 - 54.7), p value <0.001; presence of HDL OR 4.29 (95% CI 1.12 - 16.5), p value 0.034 and SFCT pre 100 micron decrease OR 1.92 (95% CI 1.09 - 3.35), p value 0.023. It is important to note that presence of nGA or hypertransmission also had higher odds of prolonged RIT (OR 2.11).

3.4 Quantitative autofluorescence in OCT based classification of non-neovascular AMD

3.4.1 Purpose

To evaluate whether quantitative autofluorescence levels vary with OCT based stages of AMD progression and interrogate whether OCT risk features of RPE cell death influence qAF8 levels.

3.4.2 Methods

The relevant methods are mentioned in Chapter 2. Methodology for acquisition of qAF images and calculation of qAF8 are detailed in section 2.2.5.1 and that for OCT grading are detailed in section 2.3.1.2.

Statistical Analysis

Data were summarised using mean (SD) or median (IQR) for continuous variables and number (%) for categorical variables. Statistical differences in $\log_e$ Mean qAF8 levels between the controls and individual AMD groups by multimodal imaging OCT and Beckman classification, were compared after adjustment for the potential confounders age, sex and lens status (pseudophakic vs phakic). Stage of SDD, qAF8 and drusen volume were summarised based on varying severity of RPE cell loss in AMD. Associations after adjusting for age, sex and lens status were quantified with odds ratio (95% CI) and P-value. GEE with an exchangeable working correlation structure were used to account for the within-participant correlation among those with data from both eyes. qAF8 levels were $\log_e$-transformed to avoid estimating misleading associations from outliers. Model coefficient estimates were therefore interpreted in relation to relative percentage increase rather than the absolute increase in qAF8 values. Where log-transformations were applied to the independent variable qAF8 in the GEE models, model estimates were interpreted in relation to relative percentage increase in the independent variable. Spearman correlation coefficient for clustered data, using the within-cluster resampling (WCR)-based method and standard errors based on fixed denominator was used to test the correlation between age and mean qAF8 levels.

3.4.3 Results

The participants had a mean age of 70.3 years (SD 8.5), 138 were females (59.7%) and 60 (17%) eyes were pseudophakic.

Comparison of qAF8 levels in AMD versus control eyes aged ≥50 years

The spearman correlation coefficient between age and qAF8 values in controls ≥50 years was ρ_{WCR}=-0.21; P=.08, in AMD eyes ≥50 years was ρ_{WCR}=-0.05; P=.49 (Figure 3.2) and in ≥65 years was ρ_{WCR}=-0.05; P=.54. Compared with controls ≥50 years, qAF8 values were significantly reduced in eyes with any AMD (241.6 [IQR 185.4 - 294.4] vs 163.5[IQR 122.6 - 216.6]; unadjusted difference= -25.2% [95% CI -33.0%, -16.5%]; P<0.001; GEE model).

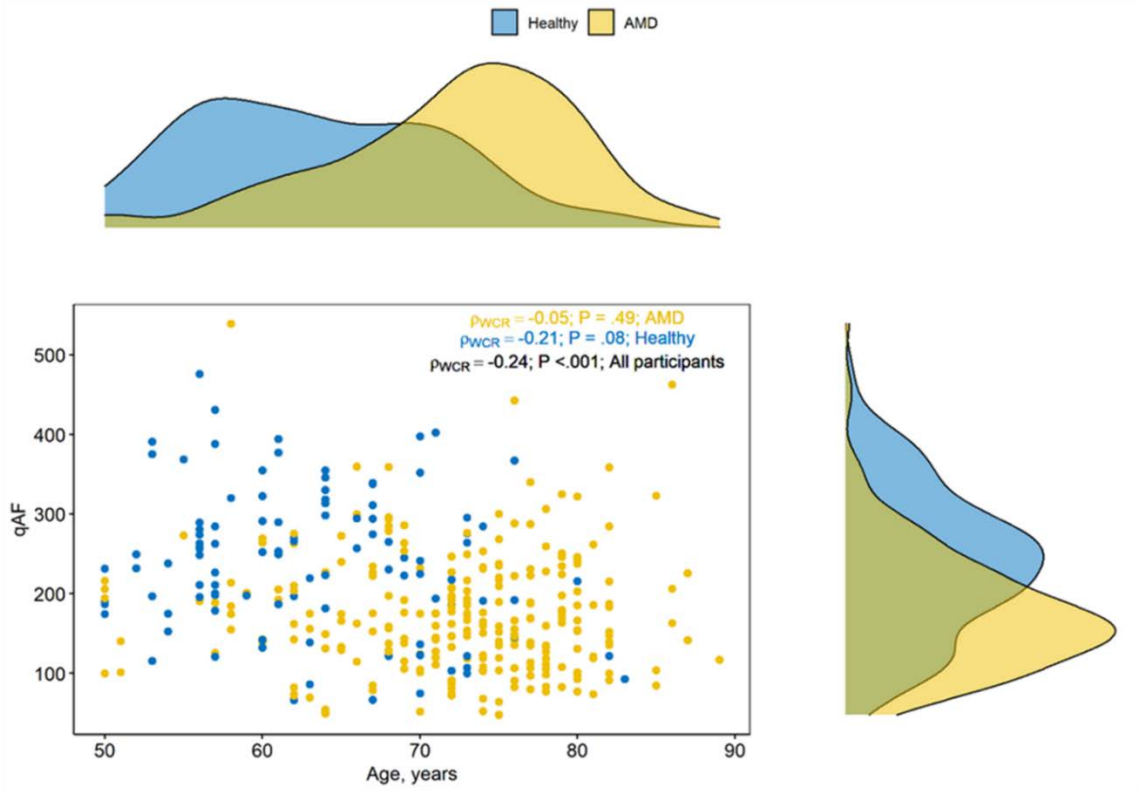

Figure 3.2 Correlation between Age and qAF8 levels in AMD & controls.
AMD – age related macular degeneration; qAF – quantitative autofluorescence; wcr – within cluster resampling; ρ – spearman correlation.

Comparison of qAF8 levels in AMD categories – Beckman classification

There was a significant reduction in qAF8 in AMD eyes versus control (-19.7% [95% CI-28.8%, -10.4%]; P <0.001, Table 3.8). Statistical differences were found among all Beckman subgroups relative to control eyes, in both univariate analysis and following adjustment for age, gender and lens status (adjusted % differences; Early AMD, -13.1% (-24.4%, -1%), P=0.04; iAMD, -22.9% (-32.3%, -13.1%), P<0.001; and GA -25.2% (-38.1%, -10.4%), P=.002). Significant differences were identified comparing early AMD with iAMD (% adjusted difference -11.4% [95% CI -0.10%, -21.3%]; P= 0.048, while the comparison between GA and early AMD failed to reach statistical significance in both univariate and adjusted analysis (% adjusted difference -14.0% [95% CI -28.7%, 3.6%]; P=.11). No statistically significant differences were found between iAMD and GA.

Table 3.8 Parameters associated with log-qAF8 mean adjusted for age, gender and lens status using GEE models.

Characteristics	**N**	**Coefficient in log-qAF8 units**	**qAF8 difference in %**	**p-value**
Controls vs AMD	353			
Controls		—	-	
AMD		-0.22 (-0.34 - -0.11)	-19.7% (-28.8%,-10.4%)	<.001
Beckman classification	353			
Normal		—	-	
Early		-0.14 (-0.28 - -0.01)	-13.1% (-24.4%,-1%)	.04
iAMD		-0.26 (-0.39 - -0.14)	-22.9% (-32.3%,-13.1%)	<.001
GA		-0.29 (-0.48 - -0.11)	-25.2% (-38.1%,-10.4%)	.002
AMD classification based on multimodal imaging	353			
Normal		—		
Early without SDD		-0.06 (-0.21 - 0.08)	-5.8% (-18.9%, 8.3%)	.40
iAMD without SDD		-0.31 (-0.45 - -0.17)	-26.7% (-36.2%,-15.6%)	<.001
SDD		-0.27 (-0.41 - -0.13)	-23.7% (-33.6%,-12.2%)	<.001
cRORA		-0.31 (-0.50 - -0.12)	-26.7% (-39.3%,-11.3%)	.001
Stage of SDD in those with SDD	97			
Stage 1 or 2		-		
Stage 3		-0.05 (-0.28-0.18)	-4.9% (-24.4%, 19.7%)	.67
Stage of SDD	248			
0		—		
1		0.01 (-0.17 - 0.19)	1% (-15.6%, 20.9%)	.88
2		0.05 (-0.22 - 0.33)	5.1% (-19.7%, 39.1%)	.71
3		-0.05 (-0.17 - 0.07)	-4.9% (-15.6%, 7.3%)	.38
Drusen volume	220	-0.01	-1.4%	.40

in those without cRORA, per 0.1-unit increase		(-0.05 - 0.02)	(-4.6%, 1.9%)	
Combination of presence of HRF, iRORA and cRORA	248			
Absence of HRF without evidence of iRORA or cRORA		—		
Presence of HRF without evidence of iRORA or cRORA		-0.18 (-0.43 - 0.07)	-16.5% (-34.9%, 7.25%)	.16
Presence of iRORA without any evidence of cRORA		-0.16 (-0.28 - -0.03)	-14.8% (-24.4%, -3.0%)	.01
Presence of cRORA		-0.13 (-0.30 - 0.05)	-12.2% (-25.9%, 5.1%)	.15

Abbreviations: AMD – age related macular degeneration; cRORA – complete retinal pigment epithelium and outer retinal atrophy; GA – Geographic atrophy; GEE – Generalised estimating Equation; HRF – Hyperreflective foci; iAMD – intermediate AMD; IR- Infrared reflectance; iRORA – incomplete retinal pigment epithelium and outer retinal atrophy; IQR – Interquartile range; OCT – Optical Coherence Tomography; qAF8 – quantitative autofluorescence; RPE – Retinal pigment epithelium; SDD – subretinal drusenoid deposits

Comparison of qAF8 levels in AMD categories – OCT classification

The qAF8 levels were found to be reduced in eyes with AMD compared to normal eyes while iAMD, SDD and GA groups are in close correspondence (Figure 3.3). In the adjusted analysis, differences were found between OCT AMD subgroups relative to controls, except early AMD (adjusted % differences; Early AMD, -5.8%(-18.9%,8.3%); P=.40; iAMD, -26.7%(-36.2%,-15.6%); P<.001; SDD, -23.7%(-33.6%,-12.2%); P<.001; and cRORA, -26.7%(-39.3%,-11.3%), P=.001, Table 3.8). Significant differences were found on comparing early AMD to other categories of AMD based on MMI classification (iAMD; % adjusted difference of -21.9% [95% CI -32.6%, -9.5%]; P=.001), SDD; -19.0% [95% CI -30.4%, -5.7%]; P=.006), cRORA -22.0% [95% CI -36.1%, -4.8%]; P=.01). No significant

differences were found on comparing non-early categories of AMD. Figure 3.4 shows example qAF8 images of participants with same age across different AMD groups.

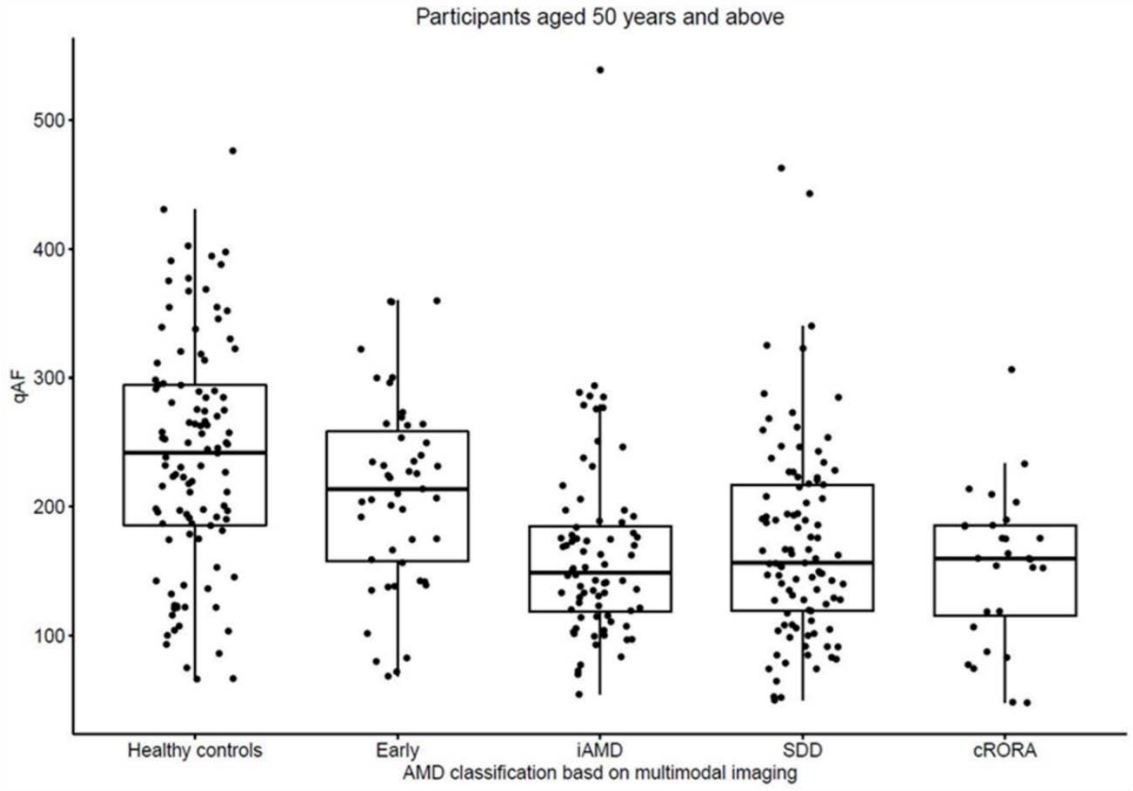

Figure 3.3 Mean qAF8 values in OCT categories of AMD versus controls.
The multimodal imaging AMD classification shown on the x-axis. Comparison was with age-matched controls. Early -drusen diameter <100 µm and no SDD, intermediate - drusen diameter 100-144 µm or 1 drusen 145 µm or more and no SDD, SDD -eyes with SDD with no cRORA and final group- cRORA. Abbreviations: AMD – age related macular degeneration; cRORA – complete retinal pigment epithelium and outer retinal atrophy; iAMD – intermediate AMD; qAF8 – quantitative autofluorescence; SDD – subretinal drusenoid deposits.

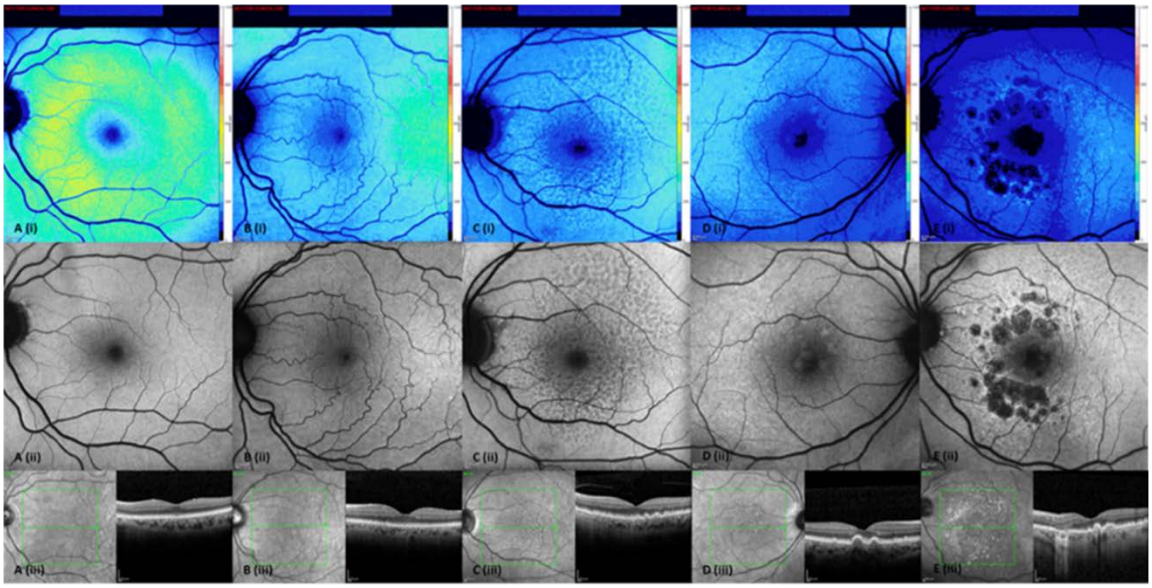

Figure 3.4 Multimodal imaging showing qAF8 changes in AMD.
A –Controls; B – Early AMD; C – Subretinal drusenoid deposit; D – Intermediate AMD; E – Multifocal geographic atrophy. Images (i), (ii) and (iii) show the qAF8 image, fundus autofluorescence and IR+OCT images respectively for all groups. Abbreviations: AMD – age related macular degeneration; cRORA – complete retinal pigment epithelium and outer retinal atrophy; GA – Geographic atrophy; iAMD – intermediate AMD; IR- Infrared reflectance; OCT – Optical Coherence Tomography; qAF8 – quantitative autofluorescence; SDD – subretinal drusenoid deposits.

Comparison of qAF8 levels in AMD eyes with and without risk factors of progression to GA or cRORA.

Table 3.9 shows that an increase in qAF8 levels was associated with a reduction in the odds of presenting with HRF, iRORA or cRORA (OR 0.91 [95% CI 0.85-0.97] per 10% increase in qAF8; P =.006). Increasing drusen volume in those without cRORA was associated with an increase in the odds of presenting with HRF, iRORA or cRORA (OR 2.00 [95% CI 1.47-2.73] per 0.1 unit increase in drusen volume; P<.001).

Table 3.9 Age, gender and lens status adjusted associations between stage of SDD, qAF8 levels and drusen volume on risk factors of RPE cell death in AMD eyes.

AMD eyes only				
Variable	**Absence of HRF or iRORA or cRORA, N = 153 eyes [total No] of 117 participants**	**Presence of HRF, iRORA or cRORA, N = 95 eyes [total No] of 70 participants**	**Adjusted odds ratio (95% CI)[a]**	**P-value**
Stage of SDD				
stage 0	100 (65%)	51 (54%)	Ref	-
stage 1 or 2	11 (7.2%)	9 (9.5%)	0.27 (0.03-2.16)	.22
stage 3	42 (27%)	35 (37%)	1.44 (0.87-2.38)	.16
Median qAF8, (IQR) or per 10% increase in qAF8	175 (135, 231)	152 (117, 188)	0.91 (0.85-0.97)	.006
Drusen volume in those without cRORA, median (IQR) or per 0.1-unit increase	0.40 (0.34, 0.47) [153]	0.54 (0.46, 0.68) [67]	2.00 (1.47-2.73)	<.001

a Adjusted for age, gender and lens status.
Abbreviations: AMD – age related macular degeneration; CI – Confidence Interval; cRORA – complete retinal pigment epithelium and outer retinal atrophy; GA – Geographic atrophy; HRF – Hyperreflective foci; iRORA – incomplete retinal pigment epithelium and outer retinal atrophy; IQR – Interquartile range; qAF8 – quantitative autofluorescence; RPE – Retinal pigment epithelium.

3.5 Discussion

The following are the main results of this chapter. About 40% of eyes with early AMD and half of the eyes in the intermediate AMD group as per Beckman classification had presence of SDD. Among SDD group, 7.2% and 38.1% eyes had markers of loss of RPE integrity, HRF and iRORA respectively. DA was significantly worse in eyes with SDD. SDD was an independent risk factor with highest odds for prolonged DA in early and intermediate AMD. Using a RIT threshold of ≤6.5 minutes was effective in discriminating between normal eyes and those with early AMD without SDD as those with SDD had higher RIT irrespective of their Beckman stage. Finally, qAF8 levels were not significantly different in eyes with and without SDD. These findings highlight the phenotypical variations seen within the Beckman classification in non-neovascular AMD.

The proposed OCT based classification focussed on the relevance of incorporating SDDs and outer retinal changes into the Beckman classification of AMD. The study shows that SDD is present even in early AMD in keeping with reports that early and intermediate AMD patients represent a heterogeneous population with variable risk of progression to advanced stages (Flores, Carneiro et al. 2021). Unlike drusen, these SDDs are dynamic in nature as they appear and disappear and have a predilection for the superior temporal quadrant of the posterior pole. These deposits were best seen on NIR and B-scans on OCT as previously established by Spaide et al. (Spaide, Ooto et al. 2018). Of the eyes that had SDD in this study, almost 80% had stage 3 SDD, including 2 eyes from the early AMD group. Interestingly 20% of eyes had stage 1 or 2 SDD that are known to be either invisible or poorly visible on CFP. In addition to including SDD as an independent classification stage irrespective of drusen size, I also included features indicating RPE disruption or loss i.e., HRF and iRORA into the classification definitions and atrophy as defined using the CAM definition of cRORA. Almost 40% of SDD eyes and 20% of iAMD eyes had confirmed iRORA on OCT. When considering HRF, about 10% eyes in SDD and iAMD group had HRF and importantly there was 1 eye classified as early by Beckman that had confirmed HRF on OCT. These results indicate that signs of RPE cell loss like HRF and iRORA can be seen a sub cohort of eyes that are classified as early using CFP. It is important to note that HRF may be noted on CFP as hyperpigmentation however; hyperpigmentation is not evident in all cases as shown by Khanifar et al that discuss non-RPE origins of HRF (Khanifar, Koreishi et al. 2008). The HRF might in some cases may be representative of migrating microglia that are engorged with lipid droplets or cholesterol. These HRF that are indicative of microglial activation might be particularly relevant in non-neovascular AMD eyes progressing to neovascular stage (Coscas, De Benedetto et al. 2013). Additionally, OCT classification-based identification of HRF also gives added value to risk prediction for the following reasons. First, association of HRF with drusen i.e., overlying a drusen is a risk factor for MNV versus its presence in the 0.5mm of eccentricity edging the foveal pit without drusen in the foveal centre where it is a risk factor for atrophy (Fragiotta, Abdolrahimzadeh et al. 2021). Second, different hyperreflective structures on OCT have been correlated to RPE phenotypes on histology and among these phenotypes, the RPE plume denoted

a peculiar OCT feature with a comma-shaped configuration of HRF, believed to represent grouped migrating RPE cells within the Henle fiber layer indicating loss of RPE integrity and dysfunction.

Eyes classified as intermediate AMD on Beckman had another important finding that when we consider ONL volume between normal, early and intermediate AMD using the Beckman classification, there is no significant change between groups. However, when SDD is incorporated to the classification, eyes with SDD (whether with early or intermediate AMD) had significantly lower ONL volume than those without SDD. ONL thinning in SDD eyes may explain the functional abnormalities seen in these cohort of patients i.e., prolonged RIT. These findings highlight the need for OCT structures to be incorporated to AMD classification for better phenotypic classification.

I then also show that OCT classification has better discriminatory power in differentiating people with non-neovascular AMD with losses in visual function. If we consider BCVA and LLVA, I found no significant difference among controls versus eyes with early AMD irrespective of presence of SDD. However, the LLD was significantly worse in eyes with early AMD and SDD versus controls. This is an important finding as LLD is a derivative of BCVA and LLVA that are easy and quick to perform in the clinic and may aid in discriminating eyes with early AMD with SDD. It is important to note that it still cannot differentiate between early AMD without SDD and normal, therefore OCT imaging would still be required.

Early or iAMD eyes with SDD have prolonged RIT compared to those without SDD. (Reiter, Told et al. 2020). Even in the early stages of disease these patients have worse function (Nigalye, Hess et al. 2022). This is understandable as the SDD are internal to the RPE and are often seen physically abutting the EZ on OCT. Our findings complement reports by Owsley et al that show that delayed RIT can indeed be used as a screening tool to differentiate normal ageing from any AMD (Owsley, McGwin et al. 2016). I also found that RIT was significantly prolonged in eyes with early AMD versus controls. This is indicative that DA is impaired in AMD eyes even prior to any significant structural changes on imaging. This raises the question as to whether outer retinal changes correlate with delayed RIT or whether RIT could be used to stratify AMD. One could also

argue that diseases such as Sorsby's fundus dystrophy that primarily affects the BrM also causes delayed DA and so dark adaptation changes may in fact occur without visible homogeneous anatomical changes in the outer retina (Christensen, Brown et al. 2017). Although such differentiation cannot be made using the OCT classification, eyes with SDDs are more at risk of progression to GA and nAMD and so they should be included in predictive models of disease progression. Additionally, I found that eyes with SDD were associated with significantly thinner choroid across all AMD severity and per 100 microns decrease in SFCT significantly increased the risk for prolonged RIT (OR 2.40, p value <0.001) suggesting a role of choroidal element in AMD pathogenesis .

In addition to SDD, I studied multiple outer retinal and choroidal structural biomarkers and their correlation with dark adaptation. Prolonged RIT was associated with RPE-BM changes (nGA, hyper transmission), choroidal thickness (SFCT) and drusen characteristics e.g., subtypes including SDD, HDL, cuticular drusen, refractile drusen and drusen volume as RPE-BM volume. On multivariable analysis, the most significant features were SDD, presence of HDL/hDc and decrease in SFCT. Of all functional tests in non-neovascular AMD, RIT is the parameter that has shown the greatest reliability. RIT can discriminate early AMD from healthy eyes suggesting that drusen sizes as small as <63um may be sufficient to cause a delayed RIT if SDD is present. Presence of nGA and/hypertransmission significantly increased the odds of prolonged DA (OR 2.11, p value 0.03). It is important to mention that there is significant overlap in the OCT features defining nGA and iRORA and both the features are indicative of loss of outer retinal integrity. Together, the novel OCT structural changes that correlate with visual function changes highlight the need for better classification system for AMD with better predictive ability of disease progression.

The other layer significantly involved in pathogenesis and progression of disease in eyes with early and intermediate AMD is the RPE-BM complex. Theoretically, excessive accumulation of lipofuscin in the RPE could adversely affect essential functions and contribute to the pathogenesis of AMD. Lipofuscin is the major contributor for signal in FAF and its levels can be quantified using imaging modality qAF (Delori, Fleckner et al. 2000, Moreno-García, Kun et al. 2018). In

section 3.4 I evaluated whether qAF levels vary with OCT based stages of AMD progression and interrogate whether OCT risk features of RPE cell death influence the qAF levels. The mean qAF8 levels significantly decreased in AMD eyes (all AMD categories taken together) compared with age-matched controls. Decrease in qAF8 may be explained by a change in the configuration of bisretinoids produced in AMD that may be less autofluorescent. Alternatively, I infer that the photodegradation of bisretinoids may be more rapid than the accumulation of photooxidised bisretinoids in AMD. I also observed that RPE cell dysfunction appears early in AMD. Each AMD category were associated with reduced qAF8 compared to age matched controls with no significant differences in qAF8 levels between them. These observations reflect early RPE dysfunction. Exocytosis may play a role. As more RPE cell death occurs, more and more new RPE cells may undergo dysfunction so mean qAF8 may not be different between AMD groups (Ach, Huisingh et al. 2014).

I also found that decreased qAF8 values are associated with eyes at risk of continuing RPE cell death (Jaffe, Chakravarthy et al. 2021). Bird hypothesised that the reduced ability of the RPE cells to degrade outer segments may reduce lipid availability to the photoreceptor cells to produce outer segments and shortening of outer segments would follow (Grewal, Chandra et al. 2022). In turn, there may be reduced shedding and decreased phagosomal load in the RPE and reduced lipofuscin formation. Another hypothesis is that reduced qAF8 levels may suggest abnormal visual cycle as the spatial location of lipofuscin reflects those of the rods. However, there was no statistical difference in qAF8 levels between AMD eyes with and without SDD. As SDDs are markers of delayed rod intercept time, our findings do not suggest that rod dysfunction or changes in the visual cycle influences qAF8 levels (Owsley, Huisingh et al. 2014). Although anti-lipofuscin interventions may be useful to reduce the toxicity of lipofuscin on the RPE cells, my study implies that very early intervention is required to prevent RPE dysfunction in people aged less than 70 years. After 70 years, there seems to be a normal decline in RPE cell function based on the qAF8 values. Although late onset Stargardt disease can be confused with GA, there were no eyes with GA and high qAF8 in this study. These findings suggest that rod dysfunction or changes in the visual cycle are not related to qAF8 levels and therefore,

modulating the visual cycle or decreasing lipofuscin load is of questionable benefit in AMD.

In conclusion, this chapter elucidates the phenotypic heterogeneity among structural and functional markers in eyes with non-neovascular AMD. The structure – function correlation revealed eyes with SDD irrespective of the stage of AMD, behave functionally similar to advanced disease than eyes with early or iAMD without SDD. Presence of SDD therefore is an independent risk factor for poor visual function. Similarly outer retinal changes like HRF and iRORA/nGA are indicators of worsening visual function even prior to onset of advanced disease. The key message therefore is that granular phenotyping of non-neovascular AMD eyes would aid improved clinical trial selection and designing of clinical trial outcomes.

4 Chapter 4 Phenotypic heterogeneity in neovascular AMD and its impact on short- and long-term treatment outcomes

4.1 Introduction

Neovascular AMD is characterised by the presence of MNV. On OCT, active MNV is defined as presence of exudation, that may include SRF, IRF or SHRM. The current mainstay of treatment for exudative MNV is intravitreal injections of anti-VEGF therapy. The injections are initiated as a loading phase of 3 injections when most eyes have the maximal visual gains and fluid resolution. The aim of continuing treatment is to maintain the visual anatomical outcomes after the loading phase. However, response to this treatment is heterogeneous without definite clinical explanation.

Heterogeneity in response to anti-VEGF is also seen in the maintenance phase and the long-term outcomes show inter-individual variations. Multiple factors determine and modulate both visual and morphological outcomes. Some of these include time from disease onset to presentation, baseline clinical and imaging data, treatment protocol and the drug used. The key treatment outcomes of nAMD include change in visual acuity, fluid resolution, development or progression of atrophy and/or fibrosis.

This chapter aims to explore the heterogeneity that exists at baseline among patients presenting with treatment naïve nAMD and its impact on both post-loading and long-term outcomes. The chapter is divided into two major sections:

Section 4.2 - 4.4: Heterogeneity at presentation before treatment is initiated to study factors that influence short term outcomes after post loading phase. All three studies included in this section are based on the data collected in the PRECISE study.

Section 4.5 – 4.6: Heterogeneity in OCT features and treatment regimen associated with long term outcomes at 5 and 10 years after initiation of anti-VEGF therapy. Data for both studies in this section was collected retrospectively from the electronic medical records database.

Aims and justification:

Firstly, I assessed whether there were variations in baseline anatomical features that determine presenting VA. Eyes with MNV due to nAMD present with a wide range of VA loss. It is well-established that presenting VA is the strongest predictor of final visual outcome at 12 months (Ying, Huang et al. 2013, Ying, Maguire et al. 2015, Ho, Albini et al. 2017). Identifying anatomical surrogates of presenting VA may help to explain short- and long-term outcomes.

As VA is a foveal function, classification of each OCT feature based on its location within and outside 1-mm of the fovea also provides further information. The Comparison of Age-related macular degeneration Treatment Trials (CATT) study group concentrated on foveal involving OCT features to study association and prediction of visual outcome while the VIEW study group showed that extrafoveal SRF may indeed be a visual prognostic indicator (Waldstein, Simader et al. 2016, Jaffe, Ying et al. 2019). Therefore, both foveal and non-foveal involving OCT parameters have to be considered to explain presenting VA (Rim, Lee et al. 2021). No study to date has examined in detail the OCT features that determine presenting in these patients. The section 4.2 aims to identify morphological features of the MNV on OCT that best explain presenting VA in nAMD.

Secondly, in section 4.3, I studied the relation between heterogeneity in baseline factors and fluid resolution post loading phase. Most anti-VEGF treatment regimens are initiated with a loading phase (LP) of monthly injections for 3 doses. The macular fluid status on OCT at the first appointment post LP is a decision point to assess early treatment response and customize future treatment regimen for each patient. A proportion of eyes have early residual fluid (ERF) following LP irrespective of the anti-VEGF agent used or the protocol followed. This persistent fluid has been described in literature as ERF. Clinical trial results from VIEW 1&2, TENAYA & LUCERNE and HAWK and HARRIER indicate that although most patients with new nAMD respond rapidly to anti-VEGF treatment, ERF is seen in a proportion of patients irrespective of the agents used (Waldstein, Simader et al. 2016, Dugel, Koh et al. 2020, Cheung CMG 2022, Heier, Khanani et al. 2022). These patients who are suboptimal responders to treatment likely to require more

aggressive treatment compared to ERF-free eyes. Therefore, this subsection aimed to explore the heterogeneity in baseline characteristics that determine persistence of fluid post loading phase and also the visual acuity outcomes among these eyes.

Thirdly, taking the learning from my previous work on the ability to identify suboptimal responders based on baseline heterogeneity, in section (4.4), AI was employed to automate identification of non-responders based only on non-annotated baseline scans, CST, baseline VA and demography of patients. The aim was to see if identification of early suboptimal responders by AI at baseline could inform the design of randomised controlled trials (RCTs) of novel investigational agents by enriching the study cohort with treatment-naïve patients predicted to have a suboptimal response to aflibercept (predictive enrichment). This in turn will help in effective personalization of treatment for this condition in the future (Harrer, Shah et al. 2019, Bhatt 2021, Maharjan, Ektefaie et al. 2021). Therefore, in this study I collaborated with AI researchers at IBM, Melbourne to train a multi modal AI system to identify suboptimal responders to the loading-phase of aflibercept with minimal number of baseline OCT variables.

Fourth, I then explored outcomes of anti-VEGF therapy for nAMD at 10 years. My hypothesis was that long-term outcomes are affected by heterogeneity in disease activity and progression throughout the course of treatment as well as the variations in treatment regimens. Furthermore, among the baseline features, I examined phenotypic variations in SRF in detail and its impact on outcomes.

My fifth aim was to examine how injection frequency within a 5-year period of treatment of nAMD can influence both visual and anatomical outcomes in the real-world. The VIEW trials for aflibercept recommended fixed dosing in the first year of treatment and this has widely been adopted in the UK as the protocol for treatment of nAMD with fairly good outcomes (Talks, Lotery et al. 2016). From the second year, there is a need for proactive treatment that introduces heterogeneity due to subjectivity in assessing disease activity (Eleftheriadou, Vazquez-Alfageme et al. 2017, Eleftheriadou, Gemenetzi et al. 2018). Therefore, I studied the influence of injections on heterogeneity of outcomes over 5 years. A summary of all studies done within this chapter is shown in Table 4.1.

Table 4.1 Summary table of the studies that reflect the aims of this chapter.

Section	Title	Aims
4.2	Associations of presenting visual acuity with morphological changes on OCT in nAMD	To investigate how OCT features, attributing phenotypic heterogeneity at baseline, are associated with presenting VA in treatment naïve eyes with nAMD.
4.3	Baseline characteristics of eyes with early residual fluid post loading phase of aflibercept therapy in nAMD	To examine baseline features that determine the phenotypes –with early residual fluid (ERF) and without ERF after aflibercept loading phase (LP) in patients with treatment naïve nAMD.
4.4	A multi-modal AI-driven cohort selection tool to predict suboptimal non-responders to aflibercept loading-phase for neovascular age-related macular degeneration.	To identify suboptimal responders to the loading-phase of the anti-VEGF agent aflibercept from baseline characteristics using a multi-modal artificial intelligence system.
4.5	10-year visual and morphological outcomes of anti VEGF therapy for nAMD	To investigate the role of phenotypic heterogeneity in determining visual outcomes, atrophy and fibrosis over 10 years of anti VEGF therapy for nAMD.
4.6	Impact of injection frequency on five-year real-world visual acuity outcomes of aflibercept therapy for neovascular age-related macular degeneration	To evaluate the impact of injection frequency on yearly heterogeneity in visual outcomes of patients treated with intravitreal aflibercept for nAMD over a period of five years

4.2 Associations of presenting visual acuity with morphological changes on OCT in neovascular age related macular degeneration

4.2.1 Purpose

To investigate the OCT features that may explain the presenting VA in treatment naïve eyes with nAMD.

4.2.2 Methodology

This study used the PRECISE database. The PRECISE study was a 10-centre study (ISRCTN 28276860). I conducted the site initiation visits across the 10 sites

individually and assisted them in study set up. Patients were recruited for this study from 18/12/2019 to 04/08/2021.

Inclusion criteria included patients aged 50 years or above presenting with treatment naïve MNV due to nAMD initiated on aflibercept loading phase. The OCT scans had to be captured on Spectralis OCT (Heidelberg Engineering GmbH, Heidelberg, Germany) and MNV was confirmed by clinicians at the local sites. Both eyes of an individual were recruited, if eligible.

Exclusion criteria were co-existent ocular disease that, in the opinion of the investigator, could affect or alter VA during the study, poor image quality and missing baseline OCT scans.

I received all images from the 10 centres participating in the study; quality checked the images and reviewed all scans for eligibility into the study. I graded all scans (minimum 2 visit scans per patient and 4 visit scans for a few sites) for presence or absence of foveal and macular fluid. I also graded all the OCT-A scans for presence or absence of neovascular membrane. The details of eligibility criteria, data collection, image analysis and grading are mentioned in Chapter 2.

The baseline OCT features associated with presenting VA ≥68 ETDRS letters (Snellen equivalent ≥6/12) and those with VA <54 letters (Snellen <6/18). Comparisons between VA 54-67 (Snellen ≥6/18 & <6/12) vs VA≥68 and VA 54-67 (Snellen ≥6/18 & <6/12) vs VA<54 letters were also conducted.

Statistical Analysis

Data were summarised with mean ± SD or median (IQR) for normally and non-normally distributed continuous variables, respectively and n (%) for categorical variables. Univariate and multivariable associations between MNV features and the categorical outcomes for visual acuity (VA≥68 ETDRS letters and VA<54 ETDRS letters) were reported using Odds Ratio (95% CI) and P-value. Features associated with VA 54-67 ETDRS letters vs VA>=68 letters and VA 54-67 vs VA<54 letters were also reported. GEE with an exchangeable working correlation structure were used to account for the within-participant correlation among those

with data from both eyes. *P*-values < 0.05 were considered statistically significant. Statistical analysis was undertaken using the R version 4.1.2 statistical software package.

4.2.3 Results

In the PRECISE study a total of 2,274 eyes of 2,128 patients were enrolled which included 138 (7.3%) patients whose both eyes were included in the study. For the final analysis, 2,039 eyes of 1,901 patients were included. The study flow diagram from recruitment to analysis sample is shown in Appendix 4, figure S4.1.

Baseline demographic, ocular and clinical characteristics

The mean age of the study participants was 79.4 (SD 7.8) years. The female-to-male ratio was 3:2 and the study population were predominantly of white ethnic background (1,808 [95%]). Table 4.2 shows the demographic and OCT characteristics in the whole population and in the three baseline vision categories: VA ≥68; VA 54-67 and those with VA <54 ETDRS letters. The mean presenting visual acuity of the study population was 58.0 (SD 14.5) ETDRS letters. The proportions of eyes with initial VA of >70, 61-70, 51-60, 41-50, 31-40, 30 ETDRS letters were 342(16.8%), 622(30.5%), 488(23.9%), 301(14.8%), 213(10.4%), 73(3.6%) respectively.

Table 4.2 Demographic, ocular and OCT characteristics of study participants overall and by visual acuity categories.

		Visual Acuity, ETDRS letter score		
Variable	**Overall, N = 2,039 eyes of 1,901 patients**	**<54 letters, N = 660 eyes of 644 patients[a]**	**54-67 letters, N = 729 eyes of 710 patients[a]**	**≥68 letters, N = 650 eyes of 629 patients[a]**
Patient level (N=1,901)				
Age, mean(SD)	79.4 (7.8)	80.3 (7.8)	79.6 (7.6)	78.3 (7.8)
Age, years				
< 60	27 (1.4%)	9 (1.4%)	9 (1.3%)	9 (1.4%)
60-69	175 (9.2%)	43 (6.7%)	65 (9.2%)	74 (11.8%)
70-79	672 (35.3%)	213 (33.1%)	246 (34.6%)	244 (38.8%)

		Visual Acuity, ETDRS letter score		
Variable	**Overall, N = 2,039 eyes of 1,901 patients**	**<54 letters, N = 660 eyes of 644 patients[a]**	**54-67 letters, N = 729 eyes of 710 patients[a]**	**≥68 letters, N = 650 eyes of 629 patients[a]**
>=80	1,027 (54.0%)	379 (58.9%)	390 (54.9%)	302 (48.0%)
Gender				
Female	1,155 (60.8%)	394 (61.2%)	436 (61.4%)	374 (59.5%)
Male	746 (39.2%)	250 (38.8%)	274 (38.6%)	255 (40.5%)
Ethnicity				
Black	12 (0.6%)	5 (0.8%)	5(0.7%)	2 (0.3%)
Other	56 (2.9%)	22 (3.4%)	18 (2.5%)	17(2.7%)
Other Asian	9(0.5%)	2 (0.3%)	5 (0.7%)	2(0.3%)
South Asian	16 (0.8%)	6 (0.9%)	6 (0.8%)	4(0.6%)
White	1,808 (95.1%)	609 (94.6%)	676 (95.2%)	604 (96.0%)
Number of patients with two eyes	138 (7.3%)	16 (2.5%)	19 (2.7%)	21 (3.3%)
Eye level (N=2,039)				
Location of MNV				
Subfoveal (central 1mm region)	1,951 (95.7%)	652 (98.8%)	703(96.4%)	596 (91.7%)
Non-foveal location	88 (4.3%)	8 (1.2%)	26 (3.6%)	54(8.3%)
MNV Type (CONAN OCT Classification)				
Type 1	802 (39.3%)	185(28.0%)	282 (38.7%)	335 (51.5%)
Type 2 and mixed	667(32.7%)	262 (39.7%)	230 (31.6%)	175(26.9%)
RAP	442 (21.7%)	150 (22.7%)	177 (24.3%)	115(17.7%)
PCV	128 (6.3%)	63 (9.5%)	40 (5.5%)	25 (3.8%)
Subfoveal presence of any component of MNV complex	1,983 (97.3%)	655 (99.2%)	713 (97.8%)	615 (94.6%)
CST in microns, Median (IQR)	414.0 (339.5, 525.0)	504.0 (395.0, 632.0)	413.0 (339.0, 500.0)	362.5 (312.0, 430.0)
Presence of IRF				
No	1,008 (49.4%)	241 (36.5%)	366(50.2%)	401 (61.7%)

		Visual Acuity, ETDRS letter score		
Variable	**Overall, N = 2,039 eyes of 1,901 patients**	**<54 letters, N = 660 eyes of 644 patients[a]**	**54-67 letters, N = 729 eyes of 710 patients[a]**	**≥68 letters, N = 650 eyes of 629 patients[a]**
Yes, Foveal involving	771 (37.8%)	350 (53.0%)	262(35.9%)	159 (24.5%)
Yes, Non-Foveal involving	260(12.8%)	69 (10.5%)	101 (13.9%)	90 (13.8%)
Presence of SRF				
No	351 (17.2%)	118 (17.9%)	136(18.7%)	97 (14.9%)
Yes, Foveal involving	973 (47.7%)	262 (39.7%)	357 (49.0%)	354 (54.5%)
Yes, Non-Foveal involving	715 (35.1%)	280 (42.4%)	236(32.4%)	199 (30.6%)
Presence of PED				
No	103 (5.1%)	46 (7.0%)	37 (5.1%)	20 (3.1%)
Yes, Foveal involving	1,593 (78.1%)	535 (81.1%)	573 (78.6%)	485 (74.6%)
Yes, Non-Foveal involving	343(16.8%)	79 (12.0%)	119 (16.3%)	145 (22.3%)
Presence of Atrophy				
No	1,609 (78.9%)	485 (73.5%)	586 (80.4%)	538 (82.8%)
Yes, Foveal involving	138 (6.8%)	109 (16.5%)	22 (3.0%)	7 (1.1%)
Yes, Non-Foveal involving	292 (14.3%)	66(10.0%)	121 (16.6%)	105 (16.2%)
Presence of fibrosis				
No	1,740 (85.3%)	438(66.4%)	667(91.5%)	635 (97.7%)
Yes, Foveal involving	266 (13.0%)	212 (32.1%)	47 (6.4%)	7 (1.1%)
Yes, Non-Foveal involving	33 (1.6%)	10 (1.5%)	15 (2.1%)	8(1.2%)
Presence of SHRM				
No	849(41.6%)	191 (28.9%)	306 (42.0%)	352 (54.2%)
Yes, Foveal involving	966 (47.4%)	417 (63.2%)	341(46.8%)	208 (32.0%)
Yes, Non-Foveal involving	224 (11.0%)	52 (7.9%)	82 (11.2%)	90 (13.8%)
Presence of ORT				
No	1,987 (97.4%)	636 (96.4%)	714 (97.9%)	637(98.0%)

		Visual Acuity, ETDRS letter score		
Variable	**Overall, N = 2,039 eyes of 1,901 patients**	**<54 letters, N = 660 eyes of 644 patients[a]**	**54-67 letters, N = 729 eyes of 710 patients[a]**	**≥68 letters, N = 650 eyes of 629 patients[a]**
Yes, Foveal involving	23 (1.1%)	13 (2.0%)	5(0.7%)	5 (0.8%)
Yes, Non-Foveal involving	29(1.4%)	11 (1.7%)	10 (1.4%)	8 (1.2%)
Presence of SDD	612 (30.0%)	166 (25.2%)	235 (32.2%)	211 (32.5%)
Presence of HRF	1,431(70.2%)	471 (71.4%)	517(70.9%)	443 (68.2%)
Loss of EZ				
No	591 (29.0%)	79 (12.0%)	220 (30.2%)	292(44.9%)
Yes, Foveal involving	386(18.9%)	303(45.9%)	70(9.6%)	13(2.0%)
Yes, Non-Foveal involving	213(10.4%)	29(4.4%)	92(12.6%)	92(14.2%)
Ungradable	849 (41.6%)	249(37.7%)	347(47.6%)	253 (38.9%)
Loss of ELM				
No	900 (44.1%)	167 (25.3%)	332 (45.5%)	401 (61.7%)
Yes, Foveal involving	330 (16.2%)	273(41.4%)	51(7.0%)	6(0.9%)
Yes, Non-Foveal involving	218 (10.7%)	38(5.8%)	93(12.8%)	87(13.4%)
Ungradable	591 (29.0%)	182(27.6%)	253 (34.7%)	156(24.0%)
EZ loss / ELM loss				
Neither Foveal-involving	1,073 (52.6%)	175 (26.5%)	414 (56.8%)	484 (74.5%)
Either or both ELM and EZ loss Foveal-involving	387 (19.0%)	304 (46.1%)	70 (9.6%)	13 (2.0%)
Both Ungradable	579 (28.4%)	181 (27.4%)	245 (33.6%)	153 (23.5%)
Presence of ERM				
No	1,821 (89.3%)	584 (88.5%)	644 (88.3%)	593 (91.2%)
Yes, Foveal involving	70 (3.4%)	28(4.2%)	23 (3.2%)	19 (2.9%)
Yes, Non-Foveal involving	148 (7.3%)	48 (7.3%)	62 (8.5%)	38(5.8%)

Abbreviation: CONAN - Consensus Nomenclature for Reporting Neovascular AMD; CST – central subfield thickness; ELM – external limiting membrane; ERM – Epiretinal membrane; EZ – ellipsoid zone; HRF – hyperreflective foci; IRF – intraretinal fluid; MNV – macular neovascularization; PCV – polypoidal choroidal vasculopathy; ORT – outer retinal tubulation; PED – pigment epithelium detachment; RAP – retinal angiomatous proliferation; SDD – subretinal drusenoid deposits; SHRM – subretinal hyperreflective material; SRF – Subretinal fluid.

The median CST was 504.0 µm (IQR 395.0 – 632.0 µm) in those presenting with VA<54 ETDRS letters, 413 µm (IQR 339.0 – 500.0 µm) in those with VA 54-67 ETDRS letters and 362.5 µm (IQR 312.0 – 430.0 µm) in those with VA≥68 ETDRS letters.

Baseline phenotype associations of presenting visual acuity

Univariate and multivariable analysis of demographic and OCT characteristics were done to study the associations of VA≥68 ETDRS letters and VA<54 ETDRS letters at presentation (Figure 4.1). The odds ratio and 95% CI are mentioned in a tabular form in Appendix 4, Table S4.1 and Table S4.2.

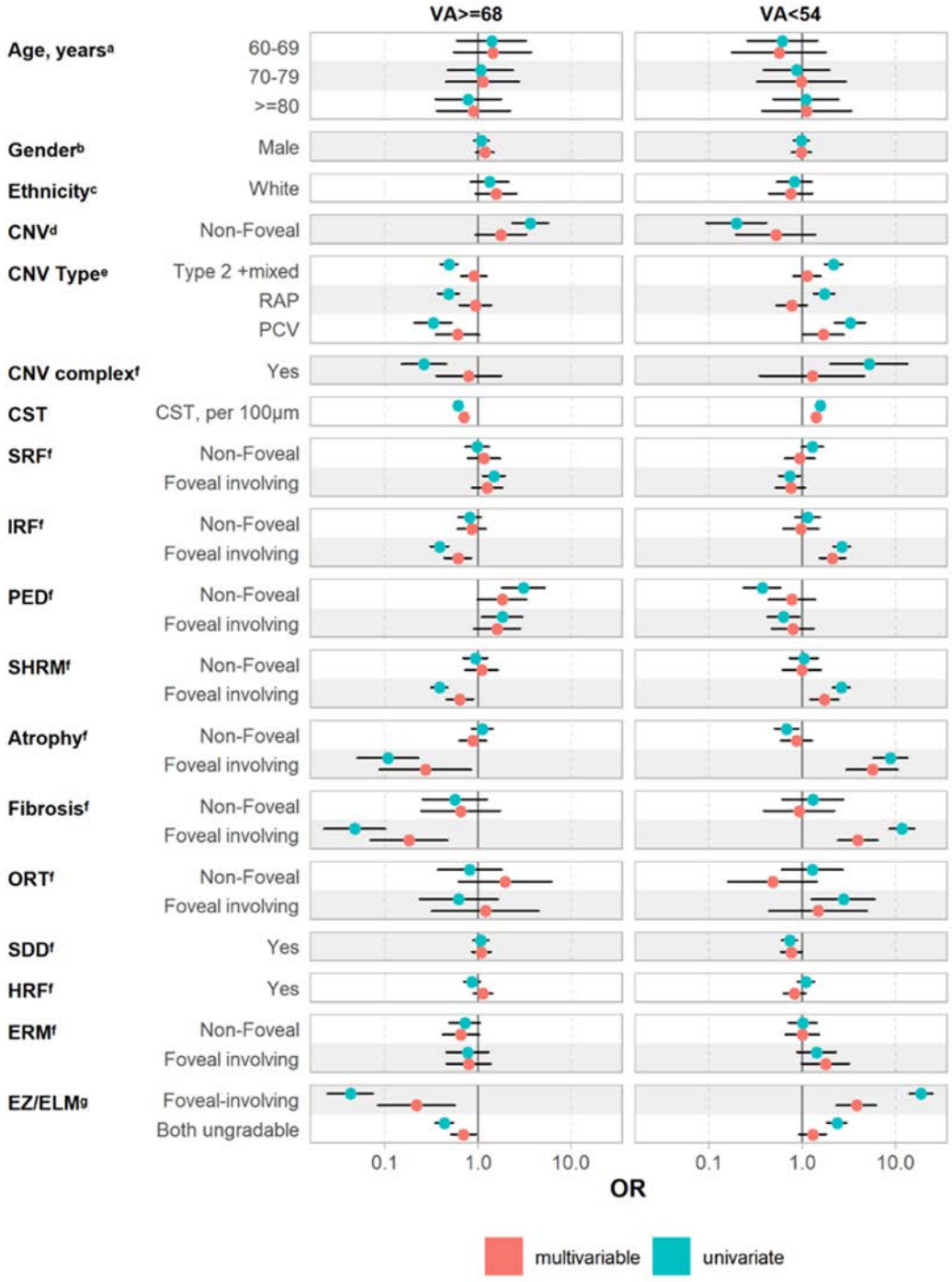

Figure 4.1 Odds Ratio plot for associations of good and poor baseline VA. Abbreviations: OCT- Optical coherence tomography; ETDRS- Early Treatment Diabetic Retinopathy Study; GEE -Generalised Estimating Equation; VA- Visual Acuity; OR- Odds Ratio; CI- Confidence interval; MNV – Macular neovascularisation; PCV-polypoidal vasculopathy; RAP-retinal angiomatous proliferation. The ratio axis is displayed on the logarithmic scale to provide a visual description of the uncertainty associated with each estimate. Reference categories were: a <60 years, b Female, c Non-White (Black/South Asian/other Asian/other), d CNV foveal involving, e Type 1, f Absent, g Neither foveal involving.

None of the demographic factors were associated with presenting visual acuity. Primary statistically significant associations for poor presenting VA (VA<54 letters) in descending order of odds ratio were: presence of foveal atrophy (OR 5.54), foveal fibrosis (OR 3.85), loss of integrity of foveal EZ/ELM (OR 3.83), presence of foveal IRF (OR 2.14), presence of foveal SHRM (OR 1.73) and finally increased CST (OR 1.73). Associations for intermediate visual acuity i.e., reduced odd of VA≥ 68 letters in descending order of odds ratio were: increased CST (OR 0.71), presence of foveal SHRM (OR 0.63), presence of foveal IRF (OR 0.60), presence of foveal atrophy (OR 0.27), presence of foveal involving ELM or EZ loss (OR 0.22) and finally presence of foveal fibrosis (OR 0.18).

4.3 Baseline characteristics of eyes with early residual fluid post loading phase of aflibercept therapy in neovascular AMD

4.3.1 Purpose

To examine baseline features that predict eyes with and without early residual fluid (ERF) and after aflibercept loading phase (LP) in patients with treatment naïve nAMD.

4.3.2 Methodology

This study used the PRECISE database. The details of eligibility criteria, data collection, image analysis and grading are mentioned in Chapter 2, section 2.3.2.1 and as mentioned in section 4.2.2.

The primary outcome of the study was OCT features associated with presence of ERF at the final visit.

Secondary outcomes included (1) features associated with phenotype presence of early subretinal fluid (eSRF) or early intraretinal fluid (eIRF) at the final visit and (2) VA outcomes among the three phenotypes – ERF, eSRF and eIRF

Statistical Analysis

Data were summarised with mean ± SD or median (IQR) for normally and non-normally distributed continuous variables, respectively and n (%) for categorical variables. Univariate and multivariable associations between demography and OCT features and the binary outcomes for ERF, eSRF and eIRF were reported

using Odds Ratio (95% CI) and P-value. GEE with an exchangeable working correlation structure were used to account for the within-participant correlation among those with data from both eyes. CST was analysed in quartiles, ranging from low CST (quartile 1) to high CST (quartile 4). Receiver operating characteristic (ROC) curve analysis was performed for CST using clustered bootstrap with 1000 replicates to estimate the bias corrected 95% confidence intervals for the area under the curve (AUC), and optimal thresholds for CST were selected based on maximising Youden's index, defined as sensitivity + specificity - 1. Bootstrapping allows for probability-based inference for the AUC and corrects for the inter-eye correlation with respect to the estimation of the standard error of the estimated AUC. *P*-values < 0.05 were considered statistically significant. Statistical analysis was undertaken using R version 4.1.2 statistical software package and Stata MP 15.

4.3.3 Results

For this study 1,999 eyes of 1,862 patients were derived to form the sample for analysis. The flowchart for patient selection is given in Appendix 4, Figure S4.2.

The demography of the patients and ocular characteristics of the included eyes are shown in Table 4.3 Mean age was 79.3 (SD 7.8) years, 1,126 (60.5%) were women and 1,772 (95.2%) participants were white. The median time interval between the first aflibercept injection and the final visit was 112 days (IQR 98 to 119 days) in the total cohort (median 112 days [IQR 91 to 118] for participants without ERF and 113 days [IQR 110-119] in those with ERF), and modes located at 86.7 (~12 weeks) and 114 days (~16 weeks). CST was categorised as less than 340µm in quartile 1 (Q1), 341µm to 415µm in quartile 2 (Q2), 416µm to 525µm in quartile 3 (Q3) and greater than 525µm in quartile 4 (Q4). Median CST was 416µm (IQR 340µm to 526µm).

Table 4.3 Demography, baseline clinical and ocular characteristics overall and by fluid status/type.

Variable	Overall, N = 1,999 eyes of 1,862 patients	Visit 4 [a]					
		ERF status		eSRF status		eIRF status	
		No ERF, N = 999 eyes of 950 patients	ERF, N = 1,000 eyes of 973 patients	No eSRF, N = 1,253 eyes of 1,174 patients	eSRF, N = 746 eyes of 734 patients	No eIRF, N = 1,571 eyes of 1,481 patients	eIRF, N = 428 eyes of 417 patients
Patient level (N=1,862)							
Age, years	79.3 (7.8)	80.4 (7.7)	78.3 (7.6)	80.4(7.7)	77.7 (7.5)	79.3 (7.9)	79.8 (7.3)
Age, years							
< 70	198 (10.6%)	88 (9.3%)	116 (11.9%)	108 (9.2%)	96 (13.1%)	164 (11.1%)	36 (8.6%)
70-79	662 (35.6%)	286 (30.1%)	398 (40.9%)	360 (30.7%)	319 (43.5%)	526 (35.5%)	150 (36.0%)
>=80	1002 (53.8%)	576 (60.6%)	459 (47.2%)	706 (60.1%)	319 (43.5%)	791 (53.4%)	231 (55.4%)
Gender							
Female	1126 (60.5%)	606 (63.8%)	560 (57.6%)	739 (62.9%)	415 (56.5%)	904 (61.0%)	243 (58.3%)
Male	736 (39.5%)	344 (36.2%)	413 (42.4%)	435 (37.1%)	319 (43.5%)	577 (39.0%)	174 (41.7%)
Ethnicity							
Black	11 (0.6%)	5 (0.5%)	6 (0.6%)	6 (0.5%)	5 (0.7%)	10 (0.7%)	1 (0.2%)
Other	54 (2.9%)	22 (2.3%)	34 (3.5%)	28 (2.4%)	28 (3.8%)	42 (2.8%)	13 (3.1%)
Other Asian	9 (0.5%)	3 (0.3%)	6 (0.6%)	4 (0.3%)	5 (0.7%)	6 (0.4%)	3 (0.7%)
South Asian	16 (0.9%)	8 (0.8%)	8 (0.8%)	11 (0.9%)	5 (0.7%)	12 (0.8%)	4 (1.0%)
White	1772 (95.2%)	912 (96.0%)	919 (94.5%)	1125 (95.8%)	691 (94.1%)	1411 (95.3%)	396 (95.0%)
Number of patients with 2 eyes	137 (6.9%)	49 (4.9%)	27 (2.7%)	79 (6.3%)	12 (1.6%)	90 (5.7%)	11 (2.6%)
Eye level (N=1,999 eyes)							
Time since first aflibercept injection	112 (98, 119)	112 (91, 118)	113 (110, 119)	112 (93, 118)	114 (112, 120)	112 (96, 119)	113 (112, 119)

Variable	Overall, N = 1,999 eyes of 1,862 patients	Visit 4 [a]					
		ERF status		eSRF status		eIRF status	
		No ERF, N = 999 eyes of 950 patients	ERF, N = 1,000 eyes of 973 patients	No eSRF, N = 1,253 eyes of 1,174 patients	eSRF, N = 746 eyes of 734 patients	No eIRF, N = 1,571 eyes of 1,481 patients	eIRF, N = 428 eyes of 417 patients
Visit 1 visual acuity, ETDRS	58.0 (14.5)	57.9 (14.3)	58.1 (14.9)	57.0 (14.5)	59.5 (14.6)	59.1 (14.1)	53.5 (15.6)
Visit 1 visual acuity categories, ETDRS							
<54	648 (32.4%)	318 (31.8%)	330 (33.0%)	433 (34.6%)	215 (28.8%)	449 (28.6%)	199 (46.5%)
54-67	715 (35.8%)	373 (37.3%)	342 (34.2%)	459 (36.6%)	256 (34.3%)	573 (36.5%)	142 (33.2%)
>=68	636 (31.8%)	308 (30.8%)	328 (32.8%)	361 (28.8%)	275 (36.9%)	549 (34.9%)	87 (20.3%)
Presence of MNV							
Yes, Foveal involving	1,914 (95.7%)	955 (95.6%)	959 (95.9%)	1,196 (95.5%)	718 (96.2%)	1,506 (95.9%)	408 (95.3%)
Yes, Non-Foveal	85 (4.3%)	44 (4.4%)	41 (4.1%)	57 (4.5%)	28 (3.8%)	65 (4.1%)	20 (4.7%)
MNV Type based on OCT CONAN criteria							
Type 1	781 (39.1%)	346 (34.6%)	435 (43.5%)	403 (32.2%)	378 (50.7%)	672 (42.8%)	109 (25.5%)
Type 2	652 (32.6%)	314 (31.4%)	338 (33.8%)	396 (31.6%)	256 (34.3%)	500 (31.8%)	152 (35.5%)
RAP	440 (22.0%)	291 (29.1%)	149 (14.9%)	390 (31.1%)	50 (6.7%)	307 (19.5%)	133 (31.1%)
PCV	126 (6.3%)	48 (4.8%)	78 (7.8%)	64 (5.1%)	62 (8.3%)	92 (5.9%)	34 (7.9%)
Presence of any component of MNV complex	1,945 (97.3%)	971 (97.2%)	974 (97.4%)	1,218 (97.2%)	727 (97.5%)	1,530 (97.4%)	415 (97.0%)
CST in microns	416 (340, 526)	393 (322, 492)	437 (362, 567)	401 (326, 509)	436 (364, 567)	404 (334, 510)	467 (366, 596)
CST quartiles in microns							

Variable	Overall, N = 1,999 eyes of 1,862 patients	Visit 4 [a]					
		ERF status		eSRF status		eIRF status	
		No ERF, N = 999 eyes of 950 patients	ERF, N = 1,000 eyes of 973 patients	No eSRF, N = 1,253 eyes of 1,174 patients	eSRF, N = 746 eyes of 734 patients	No eIRF, N = 1,571 eyes of 1,481 patients	eIRF, N = 428 eyes of 417 patients
[137-340]	503 (25.2%)	313 (31.3%)	190 (19.0%)	370 (29.5%)	133 (17.8%)	426 (27.1%)	77 (18.0%)
(340,415]	496 (24.8%)	261 (26.1%)	235 (23.5%)	313 (25.0%)	183 (24.5%)	412 (26.2%)	84 (19.6%)
(415,525]	499 (25.0%)	233 (23.3%)	266 (26.6%)	295 (23.5%)	204 (27.3%)	390 (24.8%)	109 (25.5%)
(525, 1423]	501 (25.1%)	192 (19.2%)	309 (30.9%)	275 (21.9%)	226 (30.3%)	343 (21.8%)	158 (36.9%)
Presence of IRF	1,017 (50.9%)	594 (59.5%)	423 (42.3%)	822 (65.6%)	195 (26.1%)	668 (42.5%)	349 (81.5%)
Presence of SRF	1,654 (82.7%)	753 (75.4%)	901 (90.1%)	920 (73.4%)	734 (98.4%)	1,318 (83.9%)	336 (78.5%)
Distribution of macular fluid							
SRF and IRF	672 (33.6%)	348 (34.8%)	324 (32.4%)	489 (39.0%)	183 (24.5%)	415 (26.4%)	257 (60.0%)
SRF only	982 (49.1%)	405 (40.5%)	577 (57.7%)	431 (34.4%)	551 (73.9%)	903 (57.5%)	79 (18.5%)
IRF only	345 (17.3%)	246 (24.6%)	99 (9.9%)	333 (26.6%)	12 (1.6%)	253 (16.1%)	92 (21.5%)
Presence of PED							
No	101 (5.1%)	53 (5.3%)	48 (4.8%)	70 (5.6%)	31 (4.2%)	76 (4.8%)	25 (5.8%)
Yes, Foveal involving	1,558 (77.9%)	774 (77.5%)	784 (78.4%)	958 (76.5%)	600 (80.4%)	1,234 (78.5%)	324 (75.7%)
Yes, Non-Foveal	340 (17.0%)	172 (17.2%)	168 (16.8%)	225 (18.0%)	115 (15.4%)	261 (16.6%)	79 (18.5%)
Presence of Atrophy	421 (21.1%)	265 (26.5%)	156 (15.6%)	341 (27.2%)	80 (10.7%)	314 (20.0%)	107 (25.0%)
Presence of fibrosis	292 (14.6%)	128 (12.8%)	164 (16.4%)	189 (15.1%)	103 (13.8%)	183 (11.6%)	109 (25.5%)
Presence of SHRM	1,164 (58.2%)	576 (57.7%)	588 (58.8%)	722 (57.6%)	442 (59.2%)	896 (57.0%)	268 (62.6%)
Presence of ORT	51 (2.6%)	31 (3.1%)	20 (2.0%)	39 (3.1%)	12 (1.6%)	38 (2.4%)	13 (3.0%)

Variable	Overall, N = 1,999 eyes of 1,862 patients	Visit 4 [a]					
		ERF status		eSRF status		eIRF status	
		No ERF, N = 999 eyes of 950 patients	ERF, N = 1,000 eyes of 973 patients	No eSRF, N = 1,253 eyes of 1,174 patients	eSRF, N = 746 eyes of 734 patients	No eIRF, N = 1,571 eyes of 1,481 patients	eIRF, N = 428 eyes of 417 patients
Presence of Drusen	1,833 (91.7%)	920 (92.1%)	913 (91.3%)	1,148 (91.6%)	685 (91.8%)	1,448 (92.2%)	385 (90.0%)
Presence of SDD	598 (29.9%)	337 (33.7%)	261 (26.1%)	429 (34.2%)	169 (22.7%)	466 (29.7%)	132 (30.8%)
Presence of HRF	1,401 (70.1%)	697 (69.8%)	704 (70.4%)	883 (70.5%)	518 (69.4%)	1,082 (68.9%)	319 (74.5%)
Presence of VMT	39 (2.0%)	13 (1.3%)	26 (2.6%)	25 (2.0%)	14 (1.9%)	24 (1.5%)	15 (3.5%)
Presence of ERM	217 (10.9%)	114 (11.4%)	103 (10.3%)	158 (12.6%)	59 (7.9%)	155 (9.9%)	62 (14.5%)
Presence of VMT or ERM	251 (12.6%)	125 (12.5%)	126 (12.6%)	179 (14.3%)	72 (9.7%)	176 (11.2%)	75 (17.5%)
Loss of EZ							
No	578 (28.9%)	267 (26.7%)	311 (31.1%)	315 (25.1%)	263 (35.3%)	506 (32.2%)	72 (16.8%)
Yes	584 (29.2%)	313 (31.3%)	271 (27.1%)	427 (34.1%)	157 (21.0%)	401 (25.5%)	183 (42.8%)
Not gradable	837 (41.9%)	419 (41.9%)	418 (41.8%)	511 (40.8%)	326 (43.7%)	664 (42.3%)	173 (40.4%)
Loss of ELM							
No	883 (44.2%)	394 (39.4%)	489 (48.9%)	471 (37.6%)	412 (55.2%)	764 (48.6%)	119 (27.8%)
Yes	536 (26.8%)	291 (29.1%)	245 (24.5%)	398 (31.8%)	138 (18.5%)	364 (23.2%)	172 (40.2%)
Not gradable	580 (29.0%)	314 (31.4%)	266 (26.6%)	384 (30.6%)	196 (26.3%)	443 (28.2%)	137 (32.0%)
EZ and ELM combination							
Intact EZ and ELM	847 (42.4%)	378 (37.8%)	469 (46.9%)	451 (36.0%)	396 (53.1%)	736 (46.8%)	111 (25.9%)
Either EZ or ELM loss	584 (29.2%)	313 (31.3%)	271 (27.1%)	427 (34.1%)	157 (21.0%)	401 (25.5%)	183 (42.8%)

Variable	Overall, N = 1,999 eyes of 1,862 patients	Visit 4 [a]					
		ERF status		eSRF status		eIRF status	
		No ERF, N = 999 eyes of 950 patients	ERF, N = 1,000 eyes of 973 patients	No eSRF, N = 1,253 eyes of 1,174 patients	eSRF, N = 746 eyes of 734 patients	No eIRF, N = 1,571 eyes of 1,481 patients	eIRF, N = 428 eyes of 417 patients
Both ungradable	568 (28.4%)	308 (30.8%)	260 (26.0%)	375 (29.9%)	193 (25.9%)	434 (27.6%)	134 (31.3%)

Abbreviations: CONAN-Consensus on Neovascular AMD Nomenclature; eIRF – Early intraretinal fluid; ERF – Early residual fluid; ERM- Epiretinal membrane; eSRF – Early subretinal fluid; ETDRS – Early treatment diabetic retinopathy study; ELM- External limiting membrane; EZ- Ellipsoid zone; HRF – Hyperreflective foci; IQR- interquartile range; IRF- Intraretinal fluid; MNV – Macular neovascularisation; OCT – Optical Coherence Tomography; OR- Odds Ratio; ORT – Outer retinal tubulation; PCV-polypoidal vasculopathy; PED – Pigment Epithelial Detachment; RAP-retinal angiomatous proliferation; SD-standard deviation; SDD- Subretinal drusenoid deposits; SHRM- Subretinal hyperreflective material; SRF- Subretinal fluid; VA- Visual Acuity; VMT-Vitreomacular traction.

[a] The same patients may be present in different residual macular fluid groups, hence the number of patients may not sum up to the total of 1,862 patients.

Baseline macular fluid status

At baseline, a third of eyes (672 of 1,999 [33.6%]) presented with both IRF and SRF. More than 80% had SRF (1,654 of 1,999 [82.7%]) and approximately half of the eyes had IRF (1,017 of 1,999 [50.9%]). A total of 982 (49.1%) had SRF without IRF at presentation.

Early residual fluid (ERF)

After LP, ERF was present in 1,000 eyes (50.0%, Figure 4.2). The proportion with eSRF and eIRF were 37.3% (N=746) and 21.4% (N=428) respectively. The proportion of eyes with co-existent eSRF and eIRF was 8.7% (N=174 eyes), and 50.0% of total cohort had no macular fluid (N=999 eyes).

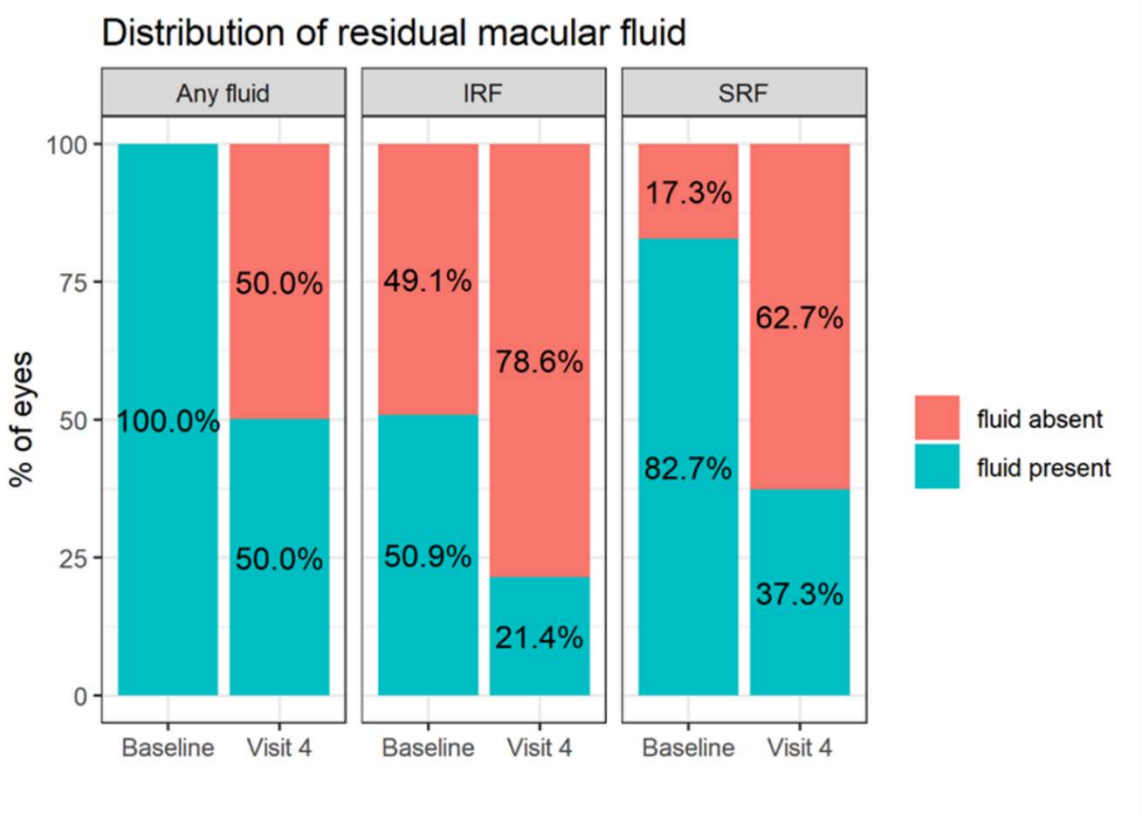

Figure 4.2 Distribution of fluid at baseline and post-loading. Abbreviations: IRF -Intraretinal fluid; SRF – subretinal fluid

Table 4.4 shows the baseline and post LP VA (unadjusted and adjusted) based on the distribution of ERF. Eyes with residual eIRF had the worst VA across all groups.

Table 4.4 Presenting and post-loading VA based on distribution of ERF at visit 4.

ERF at visit 4	**Baseline Mean VA (SD)**	**Post-loading (Visit 4)**	
		Mean VA (SD)	**Adjusted Mean VA (SE)[a]**
ERF	58.1 (SD 14.8)	61.3 (16.5)	61.7 (SE 0.35)
No ERF	57.9 (SD 14.3)	64.4 (16.0)	63.4 (SE 0.36)
eSRF (+/-eIRF)	59.5 (SD 14.5)	63.2 (13.9)	62.1 (SE 0.41)
eSRF only	61.5 (SD 13.4)	65.2 (12.8)	62.7 (SE 0.45)
No eSRF	57.1 (SD 14.5)	62.1 (16.0)	62.8 (SE 0.32)
eIRF (+/-eSRF)	53.6 (SD 15.5)	57.2 (16.4)	60.3 (SE 0.56)
eIRF only	54.0 (SD 15.0)	57.6 (17.0)	60.4 (SE 0.71)
No eIRF	59.2 (SD 14.0)	64.0 (14.6)	63.2 (SE 0.29)

Abbreviations: ERF – Early residual fluid, eSRF – early subretinal fluid, eIRF – early intraretinal fluid.[a]GEE model with visit 4 visual acuity as the outcome and adjusted for baseline visual acuity.

Associations of increased odds of ERF phenotype

Univariate and multivariable analysis of participant demographic and OCT characteristics were performed to study its associations with presence of ERF, eSRF and eIRF (Appendix 4, Table S4.3). Represented as a plot in Figure 4.3. The ERF phenotype had the following demographic associations – longer follow up from first injection (multivariable OR 1.03 per 1 day increase [95% CI 1.02 to 1.04]; P<0.001), participants of non-white ethnicity (Non-white vs white ethnicity; OR 1.62 [95% CI 1.02 to 2.58]; P=0.04), males (OR 1.23 [95% CI 1.01 to 1.50]; P=0.04) The baseline OCT features with increased odds of ERF phenotype were: SRF only (SRF only vs IRF only; OR 2.28 [95% CI 1.59 to 3.26]; P<0.001), vitreomacular traction (VMT) (OR 2.76 [95% CI 1.31 to 5.80]; P=0.007) and increased CST (Q2, 1.45 [95% CI 1.10 to 1.92]; P=0.009, Q3, 2.06 [95% CI 1.54 to 2.75]; P<0.001 and Q4, 3.11 [95% CI 2.27 to 4.26]; P<0.001).

Associations of reduced odds of ERF phenotype

Variables associated with a reduction of odds of ERF phenotype included: participants aged 80 years and above (age ≥ 80 years vs <70 years; OR 0.68 [95% CI 0.50 to 0.94]; P=0.02), eyes with retinal angiomatous proliferation (RAP) (RAP vs Type 1; OR 0.68 [95% CI 0.49 to 0.94]; P=0.02), atrophy (OR 0.68 [95% CI 0.47 to 0.99]; P=0.045) and ungradable EZ and ELM (ungradable EZ/ELM vs Intact EZ and ELM; OR 0.70 [95% CI 0.53 to 0.93]; P=0.01).

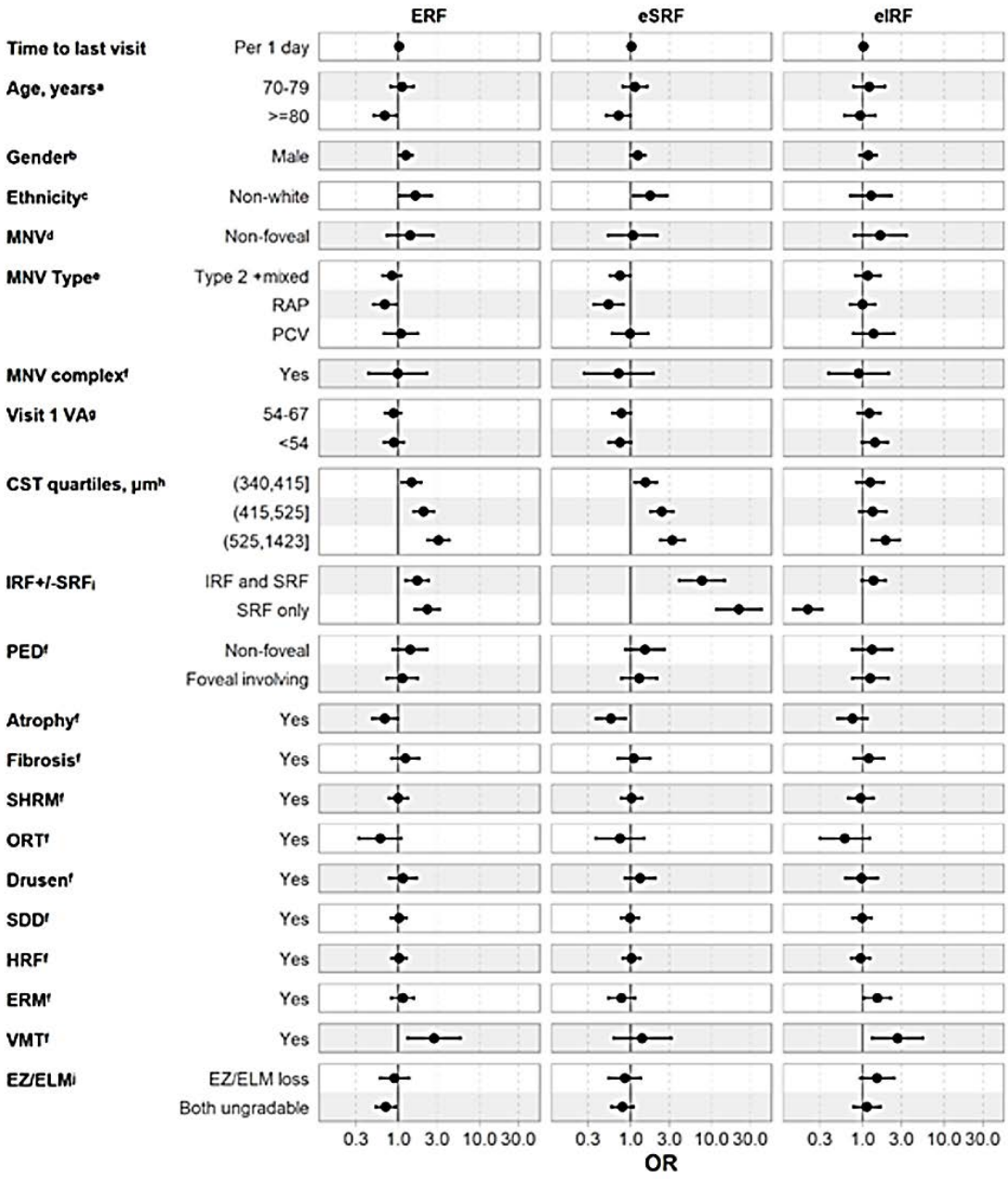

Figure 4.3 Odds Ratio plot for associations of early residual fluid.
Abbreviations:ERM- Epiretinal membrane; ETDRS – Early treatment diabetic retinopathy study; ELM- External limiting membrane; EZ- Ellipsoid zone; GEE - Generalised Estimating Equation; HRF – Hyperreflective foci; IRF- Intraretinal fluid; MNV – Macular neovascularisation; OCT – Optical Coherence Tomography; OR- Odds Ratio; ORT – Outer retinal tubulation; PCV-polypoidal vasculopathy; PED – Pigment Epithelial Detachment; RAP-retinal angiomatous proliferation; SDD- Subretinal drusenoid deposits; SHRM- Subretinal hyperreflective material; SRF- Subretinal fluid; VA- Visual Acuity; VMT- Vitreomacular traction. The ratio axis is displayed on the logarithmic scale to provide a visual description of the uncertainty associated with each estimate. Reference categories were: [a] <70 years; [b] Female; [c] White; [d] MNV foveal involving; [e] Type 1;[f] Absent or No; [g] VA>=68 ETDRS letters; [h] CST≤340µm; [i] IRF only; [j] EZ and ELM intact.

Optimal threshold for CST to discriminate the three phenotypes

ROC analysis was performed to find the optimal cut-off point for CST capable of discriminating presence of ERF, eSRF and eIRF at visit 4 (Figure 4.4). AUCs were comparable and ranged from 0.59 to 0.61 for distinguishing presence and absence of ERF, eSRF and eIRF. CST >= 418 microns had 57% sensitivity and 58% specificity to distinguish ERF from no ERF at visit 4. While CST >= 359 microns was able to distinguish eSRF from no eSRF at visit 4 with 78% and 36% sensitivity and specificity respectively. CST >= 448 microns identified eIRF with 54% sensitivity and confirmed no eIRF with 64% specificity.

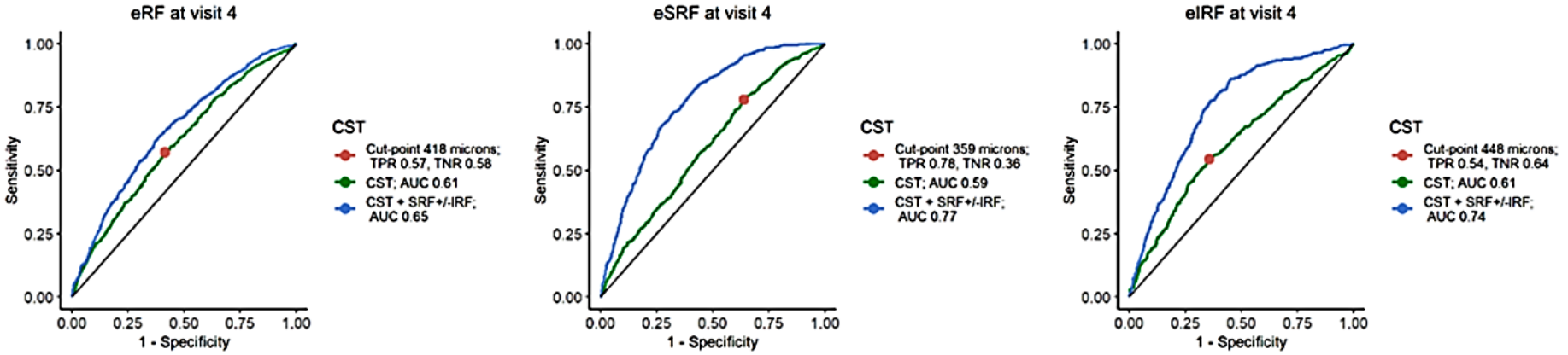

Figure 4.4 The ROC curves for CST in detecting eRF, eSRF and eIRF at visit 4.
Abbreviations: CST- Central Subfield Thickness; AUC- Area Under the Curve; TPR- True positive rate (Sensitivity); FPR – False positive rate (Specificity); eRF – early residual fluid; eSRF- early subretinal fluid; eIRF-early intraretinal fluid.

Optimal threshold points that maximise Youden's index indicated in red. AUC and bias corrected 95% confidence intervals were 0.61 (95% CI 0.58-0.63) for eRF, 0.59 (95% CI 0.56-0.62) for eSRF and 0.61 (95% CI 0.58-0.64).

4.4 A multi-modal AI-driven cohort selection tool to predict suboptimal non-responders to aflibercept loading-phase for neovascular age-related macular degeneration

4.4.1 Purpose

To identify suboptimal responders to the loading-phase of the anti-VEGF agent aflibercept from baseline characteristics using a multi-modal AI system.

4.4.2 Methods

This study used the PRECISE database. The details of eligibility criteria, data collection, image analysis and grading are mentioned in Chapter 2. Additional analysis performed in this study is described below.

Data collection

Demographic data included age at presentation, sex, and ethnicity. Clinical data collected in a web-based database included visual acuity using standardized ETDRS letter charts, CST, total retinal volume (TRV) and dates of OCT and injections at all visits. The AI system used only demography and these baseline features to predict post-loading outcome of presence or absence of macular fluid.

Study participants

Participants were divided based on two main treatment protocols: eyes belonging to the standard protocol sub-cohort had a therapy course of 105–135 days, and about 8 weeks between third injection and final observation. Eyes belonging to the short protocol sub-cohort had a therapy course of 75–104 days, and about 4 weeks between last injection and final observation.

Image setting and grading

Baseline and final visit images graded for the presence of any fluid (SRF or IRF) anywhere in the entire macular volume scan. The grading was done by single grader (Shruti Chandra) and a subset was graded by second grader (Sobha Sivaprasad). The intergrader agreement was κ 0.94. The baseline images were anonymized and saved as .xml as well as .E2E files for processing by IBM researchers.

Outcome definition

The outcome for this study were defined as follows: A good response to aflibercept loading-phase (denoted '0') was defined as total absence of both intra- and sub-retinal macular fluid in the macular volume scan at the final follow-up. A suboptimal response was defined as presence of any macular fluid (denoted '1') at the final follow-up.

Statistical Analysis

Univariate associations of clinical features and outcome were estimated using Fisher exact test for binary features and Mann–Whitney U-test for continuous features. We corrected for multiple hypotheses by employing the Benjamini–Hochberg's false discovery rate (FDR) correction. AUROC, sensitivity and specificity are reported with a 95% CI. A p-value <0.05 was considered to indicate a statistically significant difference.

AI system development

This part of the methodology was performed by researchers at IBM, Melbourne. The detailed methodology is available in Appendix 4 Section A.

4.4.3 Results

Final dataset consisted of 1720 eyes of 1612 patients across 10 clinics (Appendix 4, Figure S4.3). Older age was associated with good response to treatment (median age, 82 vs 79 years, FDR adjusted p-value $<3\times10^{-11}$; Table 4.5), as was female sex (67% vs 59%, p-value $<4\times10^{-3}$). CST was positively associated with suboptimal response (0.34 vs 0.38, p-value $<1\times10^{-7}$). Baseline absence or presence of fluid at the fovea was not associated with outcome (p-value >0.05).

Table 4.5 Association of features of interest with therapy response for the standard protocol sub-cohort.

	No. of eyes	Eyes with no macular fluid	Eyes with macular fluid	Adjusted p-value
Age*	1170 (100)	82 [77, 87]	79 [73, 84]	2.97×10^{-11}
Sex	1170 (100)	67%	59%	3.93×10^{-3}
CST*	1169 (99.9)	0.34 [0.27, 0.43]	0.38 [0.31, 0.48]	1.23×10^{-6}
Visual acuity*	1125 (96.2)	60 [50.00, 68.25]	60 [48.00, 70.00]	0.271

Data in parentheses are percentages. Median data and interquartile range.
*CST, central retinal subfield thickness. *Data are median [interquartile range]*

Treatment response prediction using the AI system based on baseline features

The AI system obtained an AUC of 0.71 (95% CI 0.64, 0.78) in the standard protocol sub-cohort (Figure 4.5, red dot on the ROC shows specificity and blue dot represents the sensitivity). The contribution of each model to the ensemble is summarised in

Table 4.6. The clinical features that contributed the most to response prediction in the standard protocol sub-cohort were age, CST, and sex, in descending order (Figure 4.6).

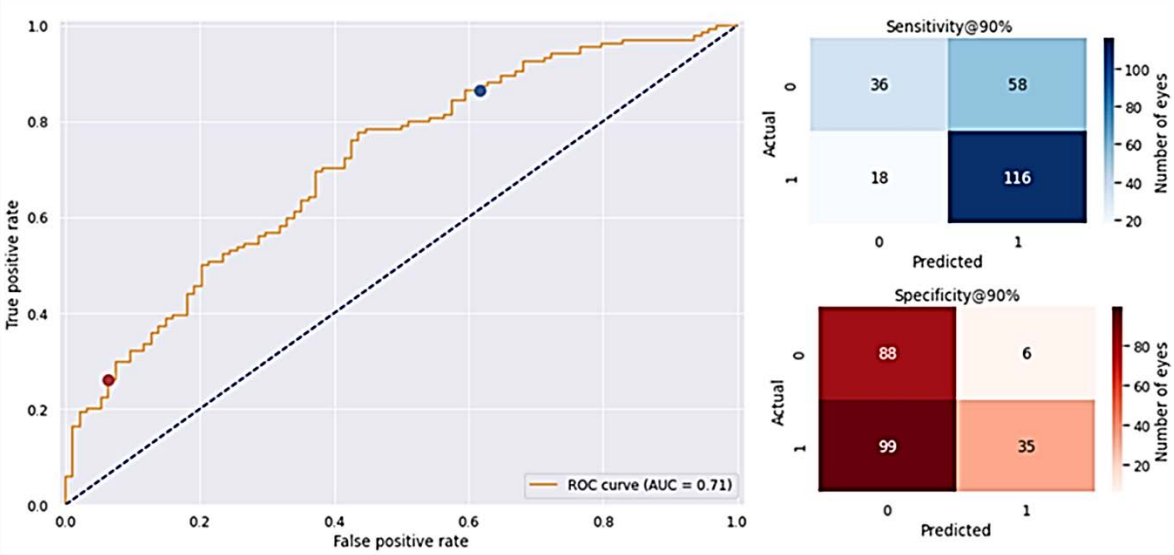

Figure 4.5 ROC curve and confusion matrices for the standard protocol sub-cohort.

Table 4.6 Performance summary of the AI system.

	Standard	**Standard applied to short**	**Standard tuned on short**
Logistic regression	0.63 [0.56, 0.71]	0.60 [0.55, 0.65]	0.64 [0.55, 0.72]
Convolutional neural network	0.70 [0.63, 0.77]	0.60 [0.55, 0.65]	0.67 [0.59, 0.75]
Final ensemble score	0.71 [0.64, 0.78]	0.62 [0.57, 0.66]	0.68 [0.61, 0.76]
90% sensitivity operating point			
Sensitivity	0.87 [0.81, 0.92]	0.86 [0.81, 0.91]	0.89 [0.82, 0.97]
Specificity	0.38 [0.29, 0.49]	0.23 [0.19, 0.28]	0.31 [0.23, 0.39]
90% specificity operating point			
Sensitivity	0.26 [0.17, 0.32]	0.26 [0.19, 0.31]	0.20 [0.16, 0.37]
Specificity	0.94 [0.88, 0.98]	0.85 [0.81, 0.88]	0.93 [0.85, 0.96]

The top three rows consist of AUROC values. Data in parentheses are 95% CI. AI, artificial intelligence; AUROC, area under the receiver operating characteristic curve.

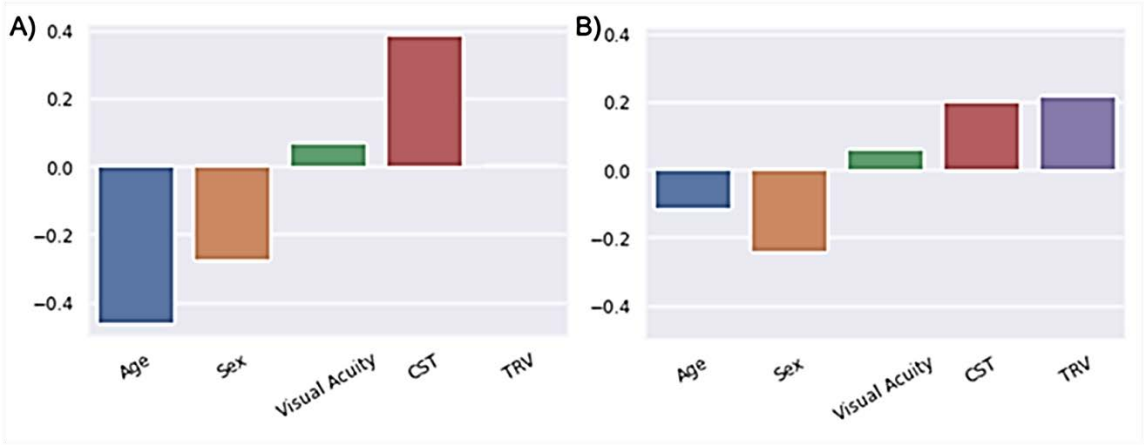

Figure 4.6 Feature contribution to the machine-learning model. A) standard and B) short protocol sub-cohorts.

Testing the model for candidate selection for a hypothetical trial preferring suboptimal responders to aflibercept.

First, we used the AI system to prioritise patients based on their individual model scores (interpreted as the odds of being a suboptimal responder). Similarly, we prioritised patients based on baseline CST (descending order) and age (ascending order). Lastly, we added a random selection method to the comparison, which is the current clinical standard. For each hypothetical trial size between 20 and 120 eyes (drawn from the test data of each protocol), the AI-based selection method resulted in more suboptimal responders than any other method. It obtained an 18.6–57.6% increase in suboptimal responders compared with random selection. It also achieved a 9.4–24.2% increase compared with any other biomarker-based selection method, given different cohort sizes based on the standard protocol sub-cohort (see Table 4.7 for full comparison).

Table 4.7 Fraction of suboptimal responders for the standard protocol sub-cohort in selected trial sizes

Cohort size (no. of eyes)	AI	CST	Age	Random	% AI increase	% AI increase from random
20	0.93	0.81	0.71	0.59	14.81	57.63
50	0.82	0.65	0.66	0.59	24.24	38.98
70	0.78	0.66	0.62	0.59	18.18	32.20
100	0.74	0.65	0.64	0.59	13.85	25.42
120	0.72	0.64	0.63	0.59	12.50	22.03
150	0.70	0.64	0.61	0.59	9.37	18.64

Candidates were selected from the held-out set of the standard protocol sub-cohort (228 patients). AI, artificial intelligence; CST, central retinal subfield thickness.

4.5 10-year visual and morphological outcomes of anti VEGF therapy for nAMD

4.5.1 Purpose

To investigate the role of phenotypic heterogeneity in determining visual outcomes, atrophy and fibrosis over 10 years of anti VEGF therapy for nAMD.

4.5.2 Methods

The data for this analysis was collected retrospectively. The details are mentioned in Chapter 2. Additional grading relevant to the section is mentioned here.

Statistical Analysis

Data was collected from the electronic medical records and entered manually onto an excel sheet. Data was analyzed using SPSS Statistics for Windows, Version 24.0. Armonk, NY: IBM Corp. Shapiro-Wilk test was used to check for normality of the data and the data was found to be not normally distributed. Wilcoxon signed rank test was used to compare means at baseline and final follow up. Chi-square test was used to explore differences in proportions among categorical data in independent groups. A p value of <0.05 was considered statistically significant. Groups were compared using one-way ANOVA test.

4.5.3 Results

A total of 149 eyes of 149 patients were included in the analysis. The participant flow is shown in Appendix 4, Figure S4.4. The mean age in years was 74.5 (±7.8) and almost two-third of the cohort was female. Mean visual acuity at baseline was 59.5 (±13.1) ETDRS letters. Baseline mean foveal thickness was 298.7 (±87.9) microns.

4.5.3.1 Variation in Vision outcomes

As shown in Table 4.8, mean change in visual acuity from baseline in ETDRS letters in the whole cohort was -2.1 letters (SD 19.9, p= 0.65). The change in VA in ETDRS letters was calculated individually for each patient and the data is shown in the form of a waterfall chart (Figure 4.7). There was a wide variation in visual acuity change with values ranging from a maximum gain of 45 letters to a maximum loss of 66 letters.

Table 4.8 Vision outcomes for all eyes at baseline and at 10-year follow up.

Outcome	Baseline	At 10-year follow up	p-value
Visual acuity score, letters Snellen equivalent, no. (%)			
	N = 149	N = 149	
83-97, 20/12-20/20	3 (2)	3 (2)	1
68-82, 20/25-20/40	55 (36.9)	47 (31.5)	0.39
53-67, 20/50-20/80	56 (37.5)	50 (33.6)	0.54
38-52, 20/100-20/160	20 (13.4)	28 (18.8)	0.27
37-18, 20/200-20/400	15 (10)	18 (12)	0.71
<17, <20/400	0 (0)	2 (2)	0.16
Mean letters (SD)	59.5 (13.1)	57.4 (17.8)	0.57
Mean change in visual acuity (SD)	-2.1 (19.9)		
Change in visual acuity score, from baseline, letters, no. (%)			
>15 increase	29 (19.5)		
5-14 increase	34 (22.8)		
<4 change	26 (17.5)		
5-14 decrease	25 (16.7)		
15-29 decrease	19 (12.8)		
>30 decrease	16 (10.7)		

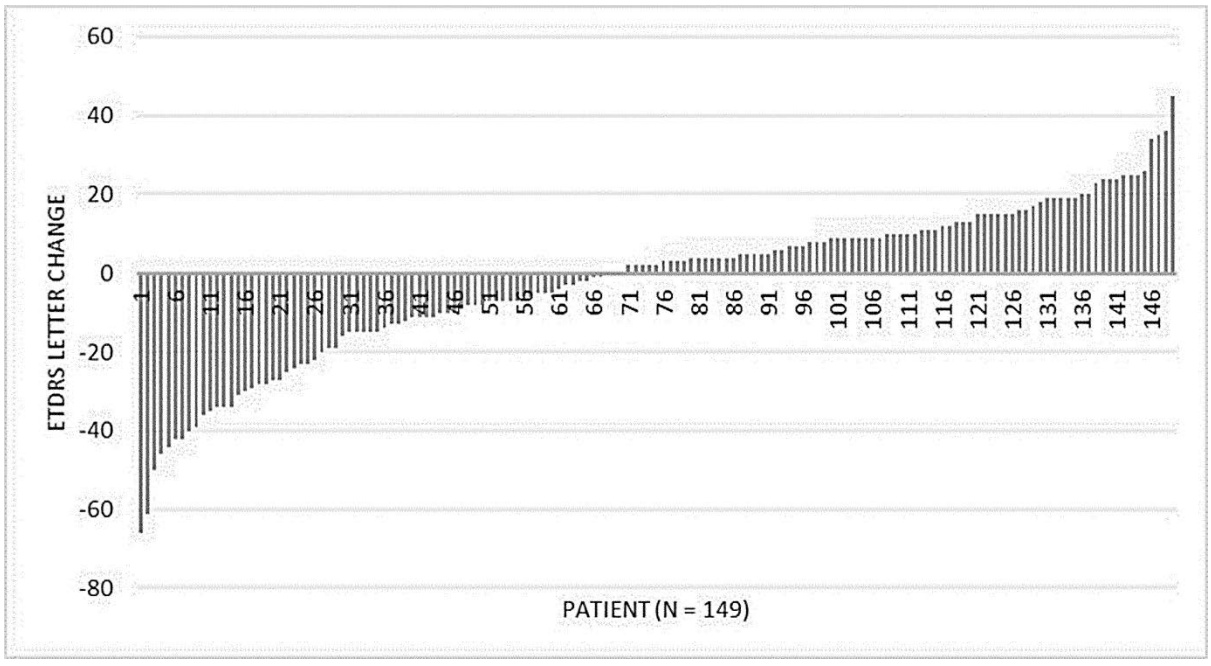

Figure 4.7 Letter change in VA per patient from baseline to final visit.

4.5.3.2 Variations in Anatomical outcomes -Subretinal fluid

Five patterns of SRF course over 10 years were identified. Table 4.9 shows the different phenotypes identified with their definitions and distribution of patients. The highest proportion of eyes fell in the late dry group (37.3%) and SRF throughout had the lowest proportion of eyes (7.0%).

Table 4.9 Definition of five patterns of SRF course.

Groups	**Definition**	**N (%age)**
SRF Throughout	SRF present throughout	10 (7.0)
Early Dry	SRF only at baseline	17 (12.0)
New SRF	SRF absent at baseline but noted during the course of treatment	24 (16.9)
Late Dry	SRF present at baseline and initial visits, but once dry no recurrence	53 (37.3)
SRF Fluctuation	Irregular course of SRF through follow-up	38 (26.8)

4.5.3.3 Variations in Anatomical outcomes – Atrophy and Fibrosis

Table 4.10 shows the proportion wise distribution of any atrophy and any fibrosis across three groups of each – baseline fibrosis or atrophy, new fibrosis or atrophy and no atrophy or fibrosis. The highest proportion of new atrophy 50/72 (69.4%) was noted in the eyes that developed new fibrosis. It is important to note that 15 eyes (10.6%) of the entire cohort did not develop atrophy or fibrosis even over 10 years of treatment and progression of natural history of disease.

Table 4.10 Proportion wise distribution of atrophy and fibrosis across 3 groups for each – baseline, new and no atrophy or fibrosis.

	Baseline fibrosis (n)	New fibrosis over follow-up (n)	No fibrosis (n)	Total n(%age)
Baseline atrophy (n)	3	1	5	8(5.6)
New Atrophy over follow-up (n)	7	***50***	31	89(62.7)
No Atrophy (n)	9	21	***15***	45(31.7)
Total n(%age)	19(13.4)	72(50.7)	51(35.9)	**142(100)**

4.5.3.4 Influence of anatomic outcomes on visual outcomes

Influence on visual outcomes

Figure 4.8 shows influence of SRF phenotypes on the visual outcomes over the course of 10 years. Best visual outcome was seen in eyes with presence of SRF throughout

66.4±9.3 letters and worse final VA was seen in eyes that developed new SRF 56.2±17.4 (p value 0.09). There was no statistically significant difference across the groups with respect to baseline VA also (p value 0.79).

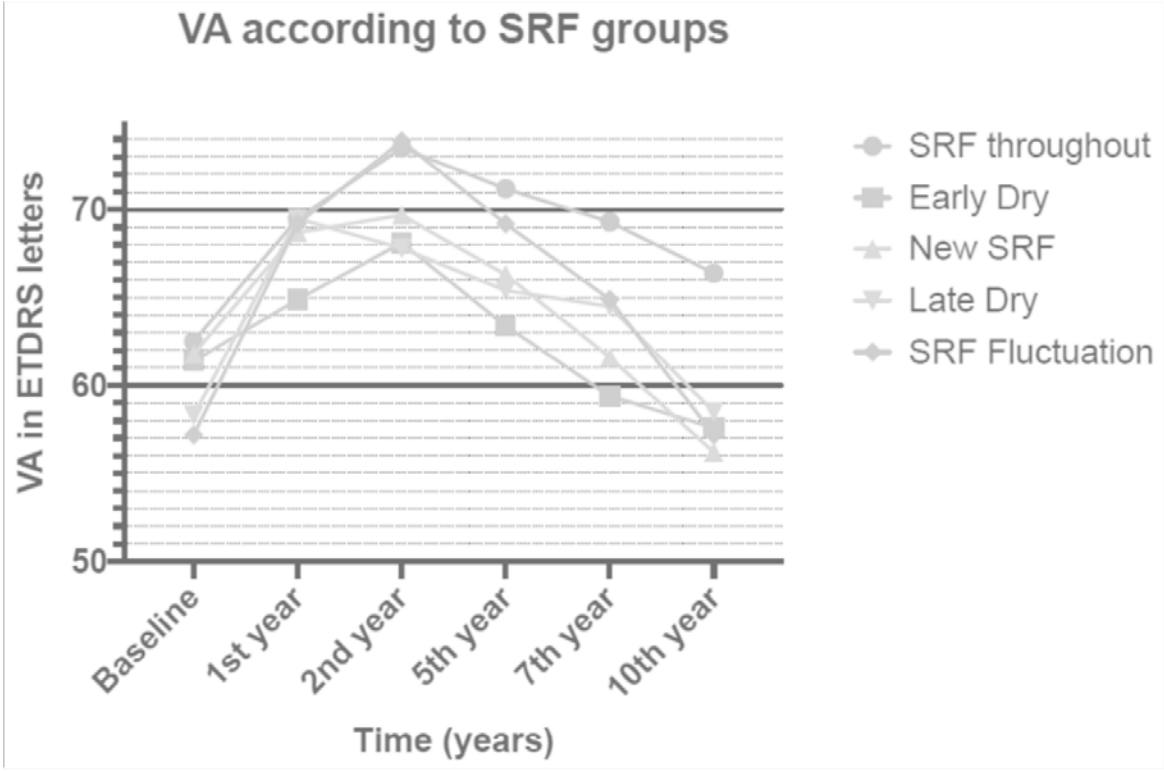

Group	N	1st year	2nd year	5th year	7th year	10th year
SRF throughout	10	69.5±13.6	73.5±9.7	71.2±11.5	69.3±7.8	66.4±9.3
Early Dry	17	64.9±12.9	68.1±11.7	63.4±12.1	59.4±12.9	57.6±17.3
New SRF	24	68.7±14.0	69.7±11.2	66.3±13.9	61.6±13.2	56.2±17.4
Late Dry	53	69.5±12.5	67.8±14.0	65.4±13.4	64.5±13.3	58.5±16.5
SRF Fluctuation	38	69.2±12.6	73.9±10.8	69.2±12.6	64.9±15.6	57.2±18.3
P value		0.79	0.16	0.39	0.37	0.58

Figure 4.8 Visual outcomes in various SRF phenotypes.

Influence of SRF phenotypes on atrophy and fibrosis

SRF had an impact on morphological outcomes over the long term. Based on survival analysis eyes with presence of SRF throughout 10 years had the highest probability of no atrophy at 10 years. In contrast the eyes that had early drying of SRF had the lowest probability of no atrophy at 10 years. Notably this group of Early Dry had the highest

probability of no fibrosis. Figure 4.9 shows the survival curves for (a) atrophy and (b) fibrosis for all SRF phenotypes.

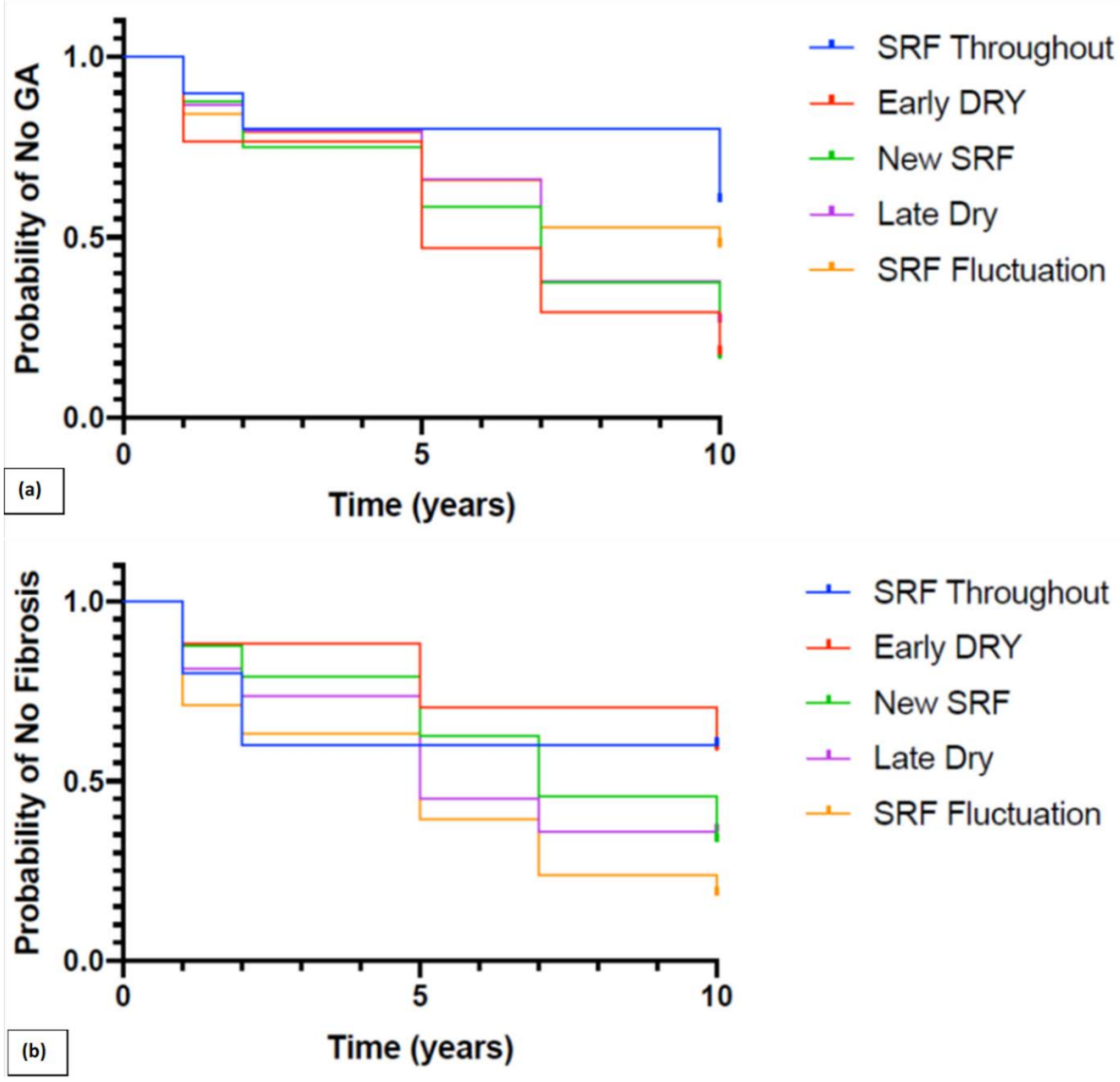

Figure 4.9 Survival curves for (a) atrophy and (b) fibrosis for all SRF phenotypes.

Influence of atrophy and fibrosis on visual outcomes

Figure 4.10 shows the distribution of final mean VA across the various groups of morphological outcomes. Eyes with no atrophy or fibrosis had the best final visual acuity outcome 61(±13.7), followed by fibrosis only (58.7±15.6), both fibrosis and atrophy present (57.9±18.2) and then only atrophy (57.3±16.9) had the worst final VA. However, these differences were not statistically significant (p value 0.45)

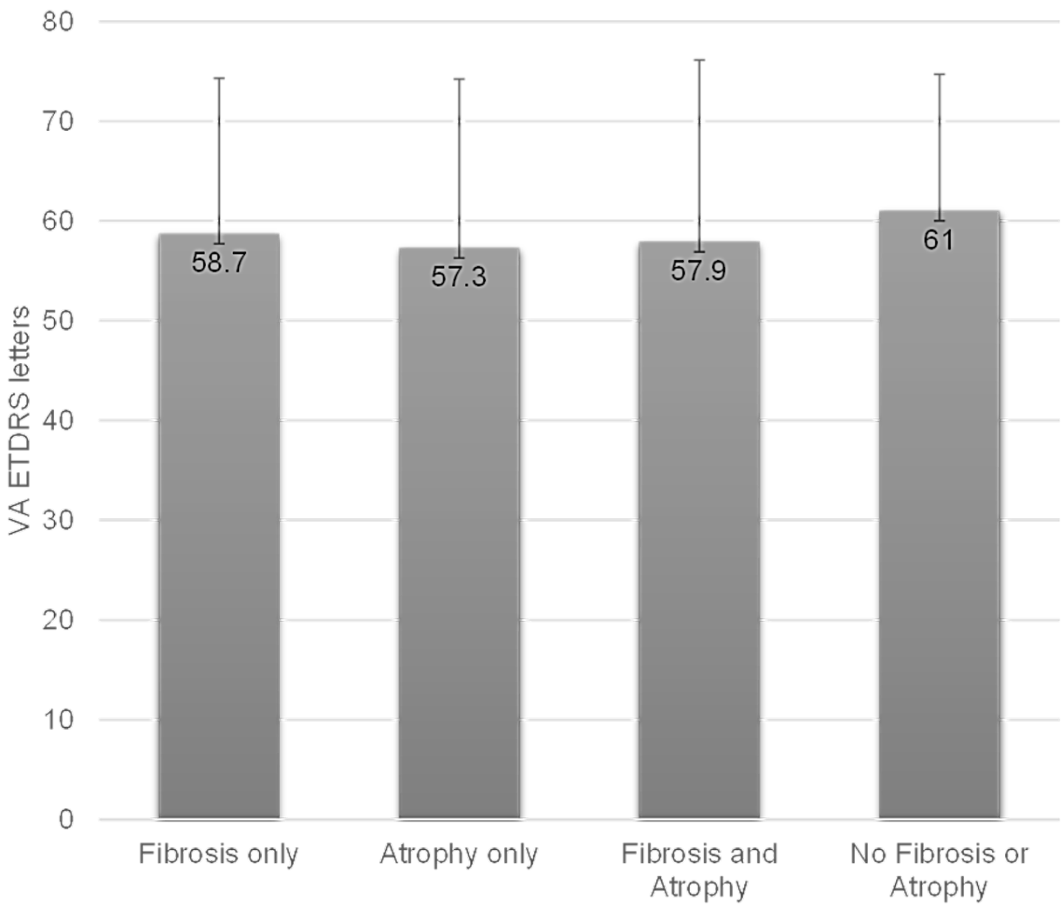

Figure 4.10 Distribution of final VA across groups of morphological outcomes.

4.6 Impact of injection frequency on five-year real-world visual acuity outcomes of aflibercept therapy for neovascular age-related macular degeneration

4.6.1 Purpose

To evaluate the impact of injection frequency on yearly visual outcomes of patients treated with intravitreal aflibercept for nAMD over a period of five years.

4.6.2 Methods

The data for this analysis was collected retrospectively. The details are mentioned in Chapter 2. Additional methods relevant to the section are mentioned here.

Statistical Analysis

The analysis was done for (a) the whole cohort defined as every patient initiated on intravitreal aflibercept therapy in 2013 and (b) the completers defined as the sub-sample who completed 5-year follow-up. For missed visits, an average VA score was calculated using the observations before and after the missed visits. No observations were carried

forward in patients lost to follow-up. The last visit was considered as 60 months ± 3 months. All statistical tests were 2-sided (alpha < 0.05). Continuous variables were described by mean ± standard deviation. A patient-level analysis was done for age, sex, first or second eye involvement and patients who received bilateral injections on the same day. An eye-level analysis was also conducted to assess VA per visit, dates of injections and monitoring visits. The association between final VA to the frequency of aflibercept injections was calculated using Kruskal-Wallis and Dunnes test. While comparing the different VA categories with each other and the frequency of injections received, P-value was calculated from post-hoc Dunnes test (Bonferroni adjusted by multiplying p-value from each test by (m) total number of pairwise comparisons). The eyes of an individual were considered independent given the pathophysiology of nAMD. The 5-year completers were divided into 3 subgroups. Group A - eyes that continued to receive treatment throughout 5 years, Group B – eyes that stopped receiving treatment and stabilized requiring no further treatment until completion of 5 years and Group C – eyes that stopped receiving treatment for a minimum of 12 months and were re-initiated on treatment. The comparison among the groups was done using one –way analysis of Variance (ANOVA). All analyses were performed with the statistical software SPSS (SPSS, USA).

4.6.3 Results

A total of 512 eyes of 468 patients were initiated on aflibercept therapy for nAMD and constituted the whole cohort, 338 eyes of 309 (66%) patients had completed 5-year follow-up and were included within the completers cohort. Appendix 4, Figure S4.5 shows the flow of patients in the study period, the number of patients excluded from analysis and the reasons for exclusion, if provided.

Baseline Characteristics

Mean age of the whole cohort was 79.5 ± 8.5 years and 54% of the patients were female. Mean baseline VA for the study eyes was 58.3 ± 15.4 letters and fellow eyes was 57.3 ± 27.6 letters. Proportion of study eyes with baseline VA ≥ 70, 54 – 69, 37 – 53 and < 37 letters were 29.1%, 39%, 18.2% and 13.1 % respectively. Forty –four (9.4%) patients received injections in both eyes during the study period. Twenty-six (59%) of the 44 patients were initiated on bilateral injections on the same day.

Correlation between visual outcomes and frequency of injections

Table 4.11 shows that decrease in mean number of injections was associated with worsening final VA across all years. Significantly a greater number of injections were given in eyes with good final VA (≥ 70 letters) compared to those with poor final VA (<37 letters) and this was observed in each year from 2 to 5 years. By assessing association between total injections and adjusted change in VA from baseline to year 5, every additional injection resulted in a 0.6 letter gain in VA (p< 0.001). When adjusted for age and baseline VA, there was a statistically significant association between total number of injections given and change in VA. On an average, the adjusted mean difference in final VA in the group who received >=20 injections compared to the group <20 injections were +8.04 letters (p=0.001). Change in VA from baseline of those who received ≤3 injections in year 2,3,4,and 5 years was 1.2, -2.0, -7.5 and – 6.5 letters respectively while the change in VA observed in eyes that received ≤4 injections was 1.7, -0.4, -5.3 and -6.4 letters respectively. In contrast, eyes that received ≥5 injections had a mean change in VA of 5.4, 4.1, 3.52 and 3.76 letters in year 2, 3 4 and 5.

Table 4.11 Correlation between injection frequency, baseline VA and final visual outcomes.

N = 338	**Number of injections/year, Mean (SD)**					
Final VA at 5 years	1st year	2nd year	3rd year	4th year	5th year	Cumulative injections at 5 years
≥70 letters	8.1(1.2)	5.4(2.4)	4.6(3.1)	4.0(3.2)	3.8(3.5)	26.0(10.9)
54-69	7.9(1.5)	5.9(2.7)	4.6(3.1)	5.1(2.8)	4.3(2.9)	27.8 (10.8)
37-53	7.7(1.3)	4.2(2.6)	4.0(2.5)	3.7(3.1)	2.2(2.5)	21.9 (8.2)
<37 letters	7.8(1.2)	4.1(2.9)	2.1(2.6)	1.4(2.1)	1.5(2.4)	17.9 (7.6)
P-value (K-W) a	0.3	*0.0013*	*0.0001*	*0.0001*	*0.0001*	*0.0001*
P-value (K-W) b	0.1	*0.0007*	*0.0001*	*0.0001*	*0.0001*	*0.0001*
P-value (D-T) c						
Comparing <37 with 37-53	0.7	0.2	0.3	*0.04*	0.4	*0.07*
Comparing <37 with 54-69	0.3	*0.0006*	*0.0001*	*<0.0001*	*<0.0001*	*<0.0001*
Comparing <37 with >=70	0.3	*0.003*	*<0.0001*	*<0.0001*	*<0.0001*	*<0.0001*
Comparing 37-53 with 54-69	1	0.5	0.2	*0.006*	*0.0004*	*0.01*
Comparing 37-53 with >=70	1	1	0.2	0.2	*0.02*	0.1
Comparing 54-69 with >=70	1	1	1	1	0.3	0.6

Abbreviations: K-W; Kruskal-Wallis, D-T; Dunnes test, $_a$ P-value generated from Kruskal-Wallis test with ties assessing whether number of injections per year differed based on final VA groups. $_b$ P-value generated from Kruskal-Wallis comparing ≥ 70 with < 37 letters VA [n=208]. $_c$ P-value from post-hoc Dunnes test (Bonferroni adjusted by multiplying p-value from each test by (m) total number of pairwise comparisons; m=6)

Subgroup Analysis

Change in VA from baseline was significantly different among the three groups with the maximum letter loss seen in Group B (-11.2±25.8), followed by Group C (-3.8±26.8) ($p < 0.05$). Eyes with continued treatment (group A) throughout 5 years sustained a 3.2±18.8 letter gain at the end of 5 years and received significantly higher cumulative number of injections. Group B received less than half number of injections as compared to Group A (14.6±5.5 injections versus 31.8±7.7 injections respectively) ($p < 0.05$). Group C received a mean of 18.4±4.6 injections. Figure 4.11 shows the distribution of patients in each VA category in the Group B patients. The proportion of patients in the ≥70 letters category at baseline and at 5 years remained stable. The proportion of eyes with <37 letters increased while the patients were on treatment and then stabilized once treatment was stopped indicating probably development of disciform scarring or atrophy that was unlikely to benefit from further anti-VEGF therapy.

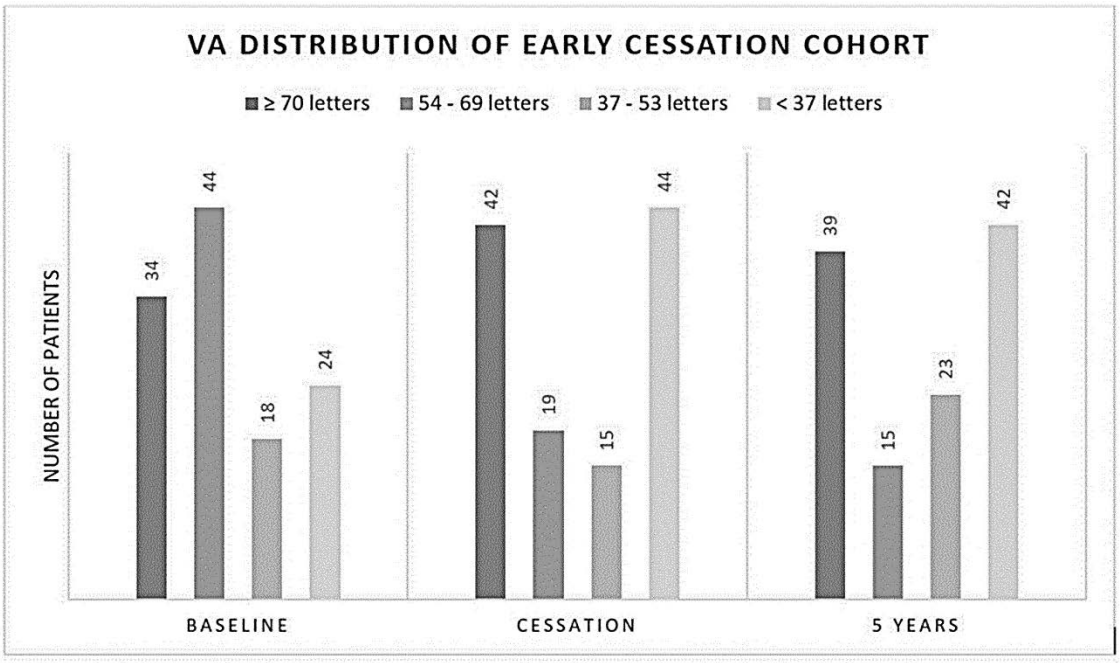

Figure 4.11 Visual acuity change among eyes in Group B (early cessation group).

4.7 Discussion

The highlights of this chapter are, first, presenting VA can be partly explained by certain OCT features. Increased CST, foveal IRF, fovea involving SHRM, foveal atrophy or fibrosis and the loss of EZ/ELM integrity at the fovea were associated with poor VA at presentation i.e., less than 54 letters (Snellen equivalent <6/18). Indeed, foveal fibrosis followed by foveal atrophy showed the strongest associations. Notably, fovea involving SRF or PED were not associated with poor presenting VA. This finding is in keeping with most previous reports that have shown that baseline presence of foveal SRF or PED do not influence final visual outcome at 12 months (Guymer, Markey et al. 2019, Kim, Lee et al. 2020, Ohji, Okada et al. 2021). Therefore, baseline OCT features of foveal intraretinal fluid, fibrosis or atrophy in a treatment naïve MNV provide significant information not only explaining poor presenting VA but also their poor visual outcome at 12 months. In fact, the recent analysis of the TENAYA and LUCERNE pooled data showed that those who required 8 weekly injections post-loading had poorer baseline VA compared to those who met the criteria for 12 or 16-weekly re-treatment (Timothy Lai 2022). Surprisingly, we found that eyes with SDD were unlikely to present with poor VA. SDD is a known poor prognostic indicator for both geographic atrophy and nAMD. One explanation may be that eyes with SDD usually present with RAP and these MNVs develop outside the fovea (Haj Najeeb, Deak et al. 2020). There were 21.7% of eyes with RAP in this study cohort. As these lesions are bilateral, it is likely that these eyes also present earlier (Haj Najeeb and Schmidt-Erfurth 2023).

Second, baseline factors associated with ERF phenotype included non-white ethnicity, males, high baseline CST, and eyes presenting with IRF and SRF or with SRF only. These results indicate that patients with these features are likely to require further monthly injections for complete fluid resolution. A key observation is that high baseline CST is associated with higher prevalence of ERF. Similar observations were noted in the VIEW 1 and 2 studies and HAWK and HARRIER studies (Waldstein, Simader et al. 2016, Dugel, Koh et al. 2020). Post-hoc exploration of baseline features in the ALTAIR study also showed that patients with increased central retinal thickness were more likely to have retinal fluid at week 16 (Ohji, Okada et al. 2021). Secondary analysis of the combined faricimab arms in TENAYA and LUCERNE also showed that eyes with increased CST at baseline were more likely to require 8 weekly dosing compared to the other two cohorts dosed at extended intervals (Timothy Lai 2022). These findings

highlight that irrespective of the drug used, eyes presenting with high CST are the ‘difficult to treat’ group and are likely to require frequent injections. In this study, a CST of >= 418 microns is likely associated with ERF. Considering the relationship of VA in eyes with ERF and its distribution, the findings in my study are comparable to the results of a post-hoc analysis of aflibercept LP in the ARIES study (Chaudhary, Holz et al. 2022, Chaudhary, Matonti et al. 2022). Both the presenting VA and the VA outcome adjusted for baseline VA and other potential confounders were numerically higher in eyes with eSRF. The converse was true for eIRF. The negative impact of IRF has been established in previous reports at various time-points (Sharma, Toth et al. 2016, Waldstein, Wright et al. 2016, Guymer, Markey et al. 2019, Ohji, Okada et al. 2021, Sadda, Holekamp et al. 2022). The results of high CST and poorer VA at baseline are associated with eIRF indicate that these eyes also need to be treated more aggressively.

The third highlight of this chapter is the development of an AI tool to automate ex ante identification of these suboptimal responders and improve trial selection. I evaluated our AI system, as a patient selection method by emulating hypothetical clinical trials of different sizes based on the PRECISE study data set and found that the tool detected up to 57.6% more suboptimal responders than random selection, and up to 24.2% more than any alternative selection criteria tested. Notably the previous analysis (section 4.3) which was based on manual grading also found 50% patients to have ERF post loading dose. Bogunovic et al. attempted to predict patients’ pro re nata requirements based on their loading-phase OCT (Bogunovic, Waldstein et al. 2017).In addition, Schmidt-Erfurth et al. examined the correlation of baseline visual acuity and OCT features with visual acuity measured 12 months post treatment in the HARBOR trial and obtained an R^2 of 0.34 (Schmidt-Erfurth, Bogunovic et al. 2018). However, this AI tool aimed to predict the disease trajectory under real-world non-singular protocol, and non-annotated baseline OCT scans, a qualitatively different task, and may therefore not be compared with many previously reported results of AI systems on OCT tasks.

The fourth highlight of this chapter is that there are significant variations in the long-term outcomes post anti VEGF treatment which are partly explained by phenotypic heterogeneity in imaging features and partly by variations in treatment regimen. I found significant variation in visual outcomes ranging from gain of 45 letters to loss of 66

letters even in a widely uniform cohort receiving treatment in a protocolised regimen over 10 years in the NHS. On comparing extremes of visual outcomes, I found that highest gainers had high baseline visual acuity and lower baseline foveal atrophy. Fibrosis and atrophy both impacted visual outcomes; however eyes with only atrophy had the worst visual outcomes. Interestingly, eyes with new fibrosis had the highest prevalence of macular atrophy indicating common factors for development of both morphological outcomes. A recent study by Gonzalez-Llorente reported that the risk of developing either of the two unfavourable anatomical changes (atrophy or fibrosis) doubles the risk of developing the other (Llorente-González, Hernandez et al. 2022).

Another significant finding was the role of SRF course in predicting visual and morphological outcomes. Visual acuity improvements are seen till 2nd year of treatment, thereafter the VA declines, however the decline is slowest in eyes with persistent SRF. The CATT, VIEW and FLUID study result showed that tolerating some amount of retinal fluid leads to better visual outcomes (Jaffe, Martin et al. 2013, Schmidt-Erfurth, Waldstein et al. 2015, Guymer, Markey et al. 2019). My results add to the evidence by replicating these results in a longer follow up in the real world. Remarkably the survival analysis revealed better morphological outcomes with persistent SRF where highest probability for no atrophy and second highest probability for no fibrosis was noted in the SRF throughout group. In contrast early drying of SRF had lowest probability for no atrophy and highest probability for no fibrosis. The FLUID study showed patients who tolerated some SRF with fewer injections had comparable outcomes to those in the treatment intensive group with complete resolution of SRF. However, FLUID study did not report the morphological outcomes for these groups.

Finally, I emphasize the role of treatment regimen on visual outcomes in the long term, with higher injection frequency and better adherence to treatment showing better visual acuity at 5 years. The study results emphasise the need for a proactive approach of an average of ≥5 injections each year up to 5 years to sustain initial VA gains and reduce the “efficacy-gap” seen between clinical trial results and real-world data. There is significant interest to decrease treatment burden by increasing dosing intervals with new trial designs attempting to extend injection frequency to 16 weeks under a T&E protocol (Ross, Downey et al. 2020). My study results caution against such extensions. To deliver 5 injections a year to maintain visual acuity over 5 years, an ideal treatment

interval is on average 10 weeks if disease activity does not mandate a shorter frequency. I also noted that best visual outcomes were noted in the group that received injections without interruption throughout the course of follow-up.

My work in this chapter has the following strengths. The sections 4.2-4.4 analysed a large real-world data of nearly 2000 eyes collected from 10 centres in UK, thereby representative of clinical practices across various centres. In addition, the data is uniform with all receiving 3 loading doses of aflibercept for treatment naïve neovascular AMD eyes and all imaging was with SD-OCT (Heidelberg, Spectralis). All eyes underwent exhaustive and meticulous grading after manual correction of segmentation, if required. As both eyes of some patients were included in the study robust analytical tools like generalised estimating equations were employed to account for any effect. The analyses were also adjusted for VA and time to follow-up to ensure strength of results. However, there are some limitations to this study. The classification of MNV subtypes is OCT based CONAN classification and we did not have concurrent fluorescein or ICGA to confirm the MNV subtype. The long-term outcome studies (section 4.5 and 4.6) analysed retrospective data and the study only included patients who were on follow-up for 10 years representing a best cared population. The VA measurements were done in the clinical scenario using ETDRS letters and could be considered as a limitation. However, the study was done to understand real-world outcomes.

5 Chapter 5: Heterogeneity of geographic atrophy progression and its implications in measurement of outcome measures in clinical trials

5.1 Introduction

Across all interventional trials for GA, there has been non-uniformity of inclusion criteria, and a wide range of GA sizes are included. There is significant heterogeneity in GA growth rates, not only due to the differences in baseline GA sizes but there seem to be other factors that influence growth in certain directions. For example, some non-foveal GAs grow towards the centre while most grow outwards. Similarly, GAs may progress as an annulus around the fovea, maintaining good visual acuity for considerable number of years while others may involve fovea quicker. Therefore, across different clinical trials, the mean growth rates of GA area show a wide range from 0.53 to 2.79 mm^2/y (Sunness, Gonzalez-Baron et al. 1999, Fleckenstein, Mitchell et al. 2018, Shen, Liu et al. 2018).

Change in GA area on FAF is traditionally used as the primary outcome measure in clinical trials on GA (Figure 5.1). Although FAF provides a reproducible technique for semi-automated image analysis, there is a need to study the growth rate of individual GA lesion on FAF to describe the expansion so that a more homogeneous cohort of patients could be evaluated in future clinical trials. Also, FAF only identifies RPE cell death while OCT of the junctional zone of GA shows significantly more changes that pre-date RPE cell death and may be of value to understand growth of GA. The CAM group have defined subtypes of outer retinal degeneration. These subtypes of GA also suggest that photoreceptor loss is a key distinguishing factor. There is a need to design clinical trials in a more homogeneous cohort to understand the true drug effect.

In this chapter, I focussed on understanding the variations in growth rate of GA. I looked at how heterogeneity may be introduced due to measurement techniques of GA and inter-grader assessments. I highlight the heterogeneity of GA progression rates to inform future clinical trials and investigated the prognostic factors associated with different GA phenotypes. I also show the translation of these measurements in a clinical trial and propose a new and earlier endpoint of disease progression.

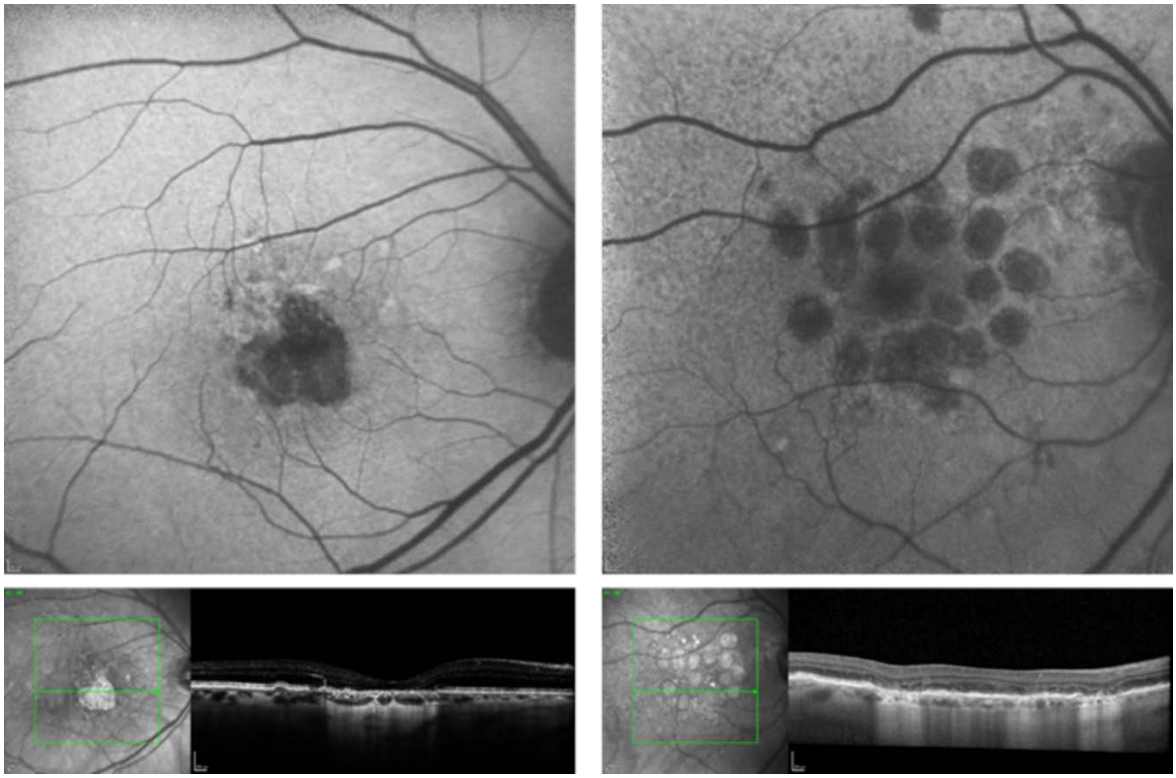

Figure 5.1 GA lesions on FAF and corresponding OCT.
Unifocal (left) and multifocal (right).

On FAF, GA area growth rate (in mm^2/y) is related to baseline morphological factors, including GA area, lesion number, and circularity index (Sunness, Gonzalez-Baron et al. 1999, Yehoshua, Rosenfeld et al. 2011, Domalpally, Danis et al. 2013, Schmitz-Valckenberg, Sahel et al. 2016, Fleckenstein, Mitchell et al. 2018, Keenan, Agrón et al. 2018, Shen, Liu et al. 2018, Pfau, Lindner et al. 2019, Shen, Sun et al. 2020, Shen, Sun et al. 2021). As area measures are mathematically affected by the distance between the centre of lesion to the edge, use of area measure by itself may not be sufficient (Yehoshua, Rosenfeld et al. 2011, Feuer, Yehoshua et al. 2013). Especially in centrifugally growing lesions, larger the lesion size, greater will be the progression in absolute area compared to a smaller lesion, assuming that the distance travelled outwardly from the lesion is the same. This is due to the larger perimeter of the larger lesion. Therefore, an apparently subtle advance in the border of a large GA lesion may manifest the same increase in area as a small GA lesion which has enlarged considerably (Uji, Nittala et al. 2019). So, if a trial uses change in area in mm^2 as a clinical end point to measure drug efficacy they might end up with a negative result, even though the drug might in fact be affecting the growth rate in a more homogeneous cohort.

To account for these discrepancies, Yehoshua et al proposed the square root of area (mm/y) method (also known as growth rate of effective radius) as it is considered to be independent of baseline size and time elapsed between baseline and final measurement (Yehoshua, Rosenfeld et al. 2011). However, it is still dependent on multifocality of lesion and circularity. Shen LL et al reported that after adjustment for GA perimeter, GA growth rate was not correlated with baseline GA area, lesion number, and circularity (Shen, Sun et al. 2021). Implication of these findings is that linear expansion rate of the leading edge of GA is independent of lesion morphology.

Aims and justification:

My aim was to investigate heterogeneity of GA lesion size and growth rates and the impact on clinical trials.

Firstly, I studied the variability in measurement of GA progression using FAF to decipher the challenges with measurement of GA growth using FAF. I compared area-based measures of GA to linear measure of GA growth and how they correlate with each other to answer this question. In my dataset of well characterised GA patients, I scrutinized how features such as focality, foveal involvement, presence of SDD and junctional FAF patterns affect GA expansion rate to explain the heterogeneity in growth rates. I evaluated the prognostic factors for disease progression so that they can be used to inform future models of disease progression. The reporting of this individual level variability in GA progression may inform better clinical trial designs. In addition, these variations in GA progression may also reflect differences in the pathophysiologic mechanisms of GA.

Secondly, I studied the reliability of the interpretation of current OCT classification of GA to evaluate its value as a future measurement technique for GA. This because OCT is the core diagnostic imaging modality used for macular diseases including AMD and is accessible to more doctors than FAF. Therefore, incorporating OCT into trial designs will enable the trial results to be reflected well in clinical practice. The high axial resolution of OCT is also an advantage as it offers a layer-by-layer evaluation of retinal and choroidal tissue (Fujimoto, Pitris et al. 2000), facilitating better cross-sectional phenotyping of GA lesions using OCT. Notably, OCT meets a previously unmet need with FAF images in GA progression i.e., longitudinal OCT scans can reveal temporal changes and identify

precursor lesions of GA (Holz, Sadda et al. 2017, Jaffe, Chakravarthy et al. 2021, Sayegh, Simader et al. 2011, Velaga, Nittala et al. 2022). In the light of these advantages, the CAM group proposed a new classification system based on OCT, unique to atrophy associated with AMD (Sadda, Guymer et al. 2018). The new classification system considered microstructural changes in the outer retina and RPE to define 4 phenotypes of atrophy based on the correlated histopathological changes in the retina (Sadda, Guymer et al. 2018). The components of cRORA were decided upon after extensive discussions and grading exercises conducted by a group of retinal experts from around the world, even though these qualities have been thoroughly characterised. The identification of these factors is based on the subjective interpretation of descriptive features because there are no objective quantification methods. It can be difficult to precisely determine the existence of these features due to their modulation observed in different OCT images, image artefacts, and changes in image quality. The agreement among clinicians in a real-world setting provides a measure of this challenge. Therefore, I evaluated the reliability of this classification for patient selection in trials and routine clinical practice.

My third aim was to study the extent of photoreceptor layer loss that may exceed the limits of RPE on OCT. As noted, although negative outcomes in large-scale GA treatment trials may partly be attributed to lack of biological efficacy, the use of change in size of atrophy as the primary endpoint may have masked the potential beneficial effects in the short-term effects unrelated to atrophy progression (Sivaprasad, Chandra et al. 2023). This may be particularly relevant in the context of certain phenotypes. For example, GA in the presence of SDD where progressive photoreceptor regeneration continues to take places even in the presence of an intact RPE and has been confirmed on both imaging as well as histopathological studies (Spaide 2013, Steinberg, Saßmannshausen et al. 2016, Chen, Messinger et al. 2020). Monitoring of photoreceptor degeneration over time outside of the junctional zone of GA would likely provide information not reflected by the end point RPE atrophy progression (Qu, Velaga et al. 2018). Quantifying these changes would also provide researchers the chance to examine treatment approaches aimed at slowing photoreceptor degeneration in patients with GA who have a better benefit-risk profile than those with iAMD (Pfau, von der Emde et al. 2020). As a result, additional research into the spatial distribution of photoreceptor degeneration (in terms of distance to the RPE atrophy boundary) and the progression of

this degeneration over time is necessary in eyes with GA associated with AMD. As manual analysis of photoreceptor (PR) loss in GA eyes is labour intensive and prone to errors, automating detection of this loss would allow expedited and robust analysis of GA expansion (Bui, Reiter et al. 2022). Recently, Riedl et al reported on an artificial intelligence-based tool to quantify photoreceptor degeneration on the FILLY trial dataset (Riedl, Vogl et al. 2022). They reported PR thinning was significantly reduced under pegcetacoplan treatment compared with sham within the GA junctional zone, as well as throughout the 20° scan area. A trend toward greater inhibition of PR loss than RPE loss was observed under therapy. For the purposes of their analysis, they trained the model to measure PR layer thickness. However, this measure is subject to errors due to directionality-dependent reflectivity i.e., PR loss detected where PR is present and vice-versa (Riedl, Vogl et al. 2022). Using longitudinal natural-history data, I performed a pilot study to develop a deep learning-based image segmentation and quantification map for PR loss. To avoid the limitation faced by Riedl et al I looked at the ratio of EZ to ELM as the primary end point. The ELM was selected for reference because this layer is considered to be the least altered in early disease and its intensities are relatively constant across a wide eccentricity (Gin, Wu et al. 2017). The third section of this chapter discusses the results of this pilot analysis of this endpoint across various GA phenotypes.

Lastly, as a follow up of my work on OCT based identification of GA and FAF measures of GA progression, I wanted to discern the translational relevance of the work I had done thus far in an interventional trial. I utilized my learning in a trial setting, i.e., on the images of two patients recruited for a phase 1 first in human trial for GA. The GA lesions of both patients were phenotypically different, and I wanted to study the applicability of my work on evaluation of outcomes. I describe my findings in the final section of this chapter. A summary of studies mentioned within this chapter is mentioned in Table 5.1.

Table 5.1 Summary Table of the studies that reflect the aims of this chapter.

Section	Title	Aims
5.2	Comparative analysis of measures of GA progression.	To compare the available methods used to measure GA enlargement rate to ascertain the interchangeability of these methods. To compare growth rates in GA phenotypes based on imaging features.
5.3	Translational value of new OCT based GA classification.	To evaluate the inter-rater reliability for identification of cRORA on SD-OCT images as defined by the CAM group.
5.4	Pilot analysis on detection of photoreceptor loss as a novel endpoint for assessing disease progression.	To develop an automated tool for detection of photoreceptor loss in conventional SD-OCT scans in eyes with GA.
5.5	Imaging based clinical trial outcomes in eyes undergoing intervention for GA.	To test the applicability of OCT based measures of GA expansion and compare them to the FAF measure.

5.2 Comparative analysis of measures of geographic atrophy progression

5.2.1 Purpose

To compare the available methods used to measure GA enlargement rate on FAF to ascertain the interchangeability of these methods and to describe growth rates of GA phenotypes based on imaging features.

5.2.2 Methods

The details of eligibility criteria, data collection, image analysis and grading are mentioned in Chapter 2. Additional analysis performed in this study is mentioned below.

Definitions of GA measures

1. Subtraction method: This was calculated as the ratio of difference in area (in mm^2) between final and baseline visits to time elapsed between visits (in years). It was expressed as mm^2/year (Figure 5.2).
2. Square root transformation method: The square root of the area on the final and baseline visits was calculated, subtracted, and the result was again divided by time between visits (in years). It was expressed as mm/year.
3. Geographic Area Circularity Index (GACI) method: This was measured as per the methodology described by Domalpally et al (Domalpally, Danis et al. 2013). The annotated FAF images (with area marked in mm^2) were exported to a Photoshop-based application (Adobe Photoshop CS3 Extended v10.0; Adobe Systems Inc,

San Jose, CA) for perimeter measurement. Calibration in Photoshop was performed by converting the pixel length of the greatest linear dimension line into known millimetres of measurement obtained from ImageNet. The length of the planimetry drawing was measured in millimetres and constituted the perimeter of the GA. By using the geometric formula for perimeter = 2πr, the radius(r) and the area of a circle expected for a given perimeter were calculated (expected area). GACI was calculated as the ratio of measured area of GA to the expected area and has a range of 0.0 to 1.0. A ratio closer to 0.0 indicates an irregular shape, and a ratio closer to 1.0 indicates a circular shape. For multifocal GA, cumulative area and perimeter of individual foci are taken into account for the calculations. For GA with an island of remnant RPE (e.g., ring shaped), both inner and outer perimeters are used to obtain a cumulative perimeter. The measured area in a ring shape includes the area of atrophy only.

4. Linear growth (distance mapping) method: This work was done along with my collaborator on this project, Dr. Joan M. Nunez do Rio. To quantify the linear expansion rate of the GA border, we registered GA border delineations from the baseline and final visit of each eye. We used the methodology explained by Uji et al to find the distance travelled by each point on the GA border over time (Uji, Nittala et al. 2019). In each eye, we applied a Euclidean distance map transformation to the mask of all GA lesions at the baseline visit so that every pixel beyond the baseline GA border was encoded with the shortest distance to the baseline GA border. The measure was expressed as microns/year and the depicted as a heat map (Figure 5.2).

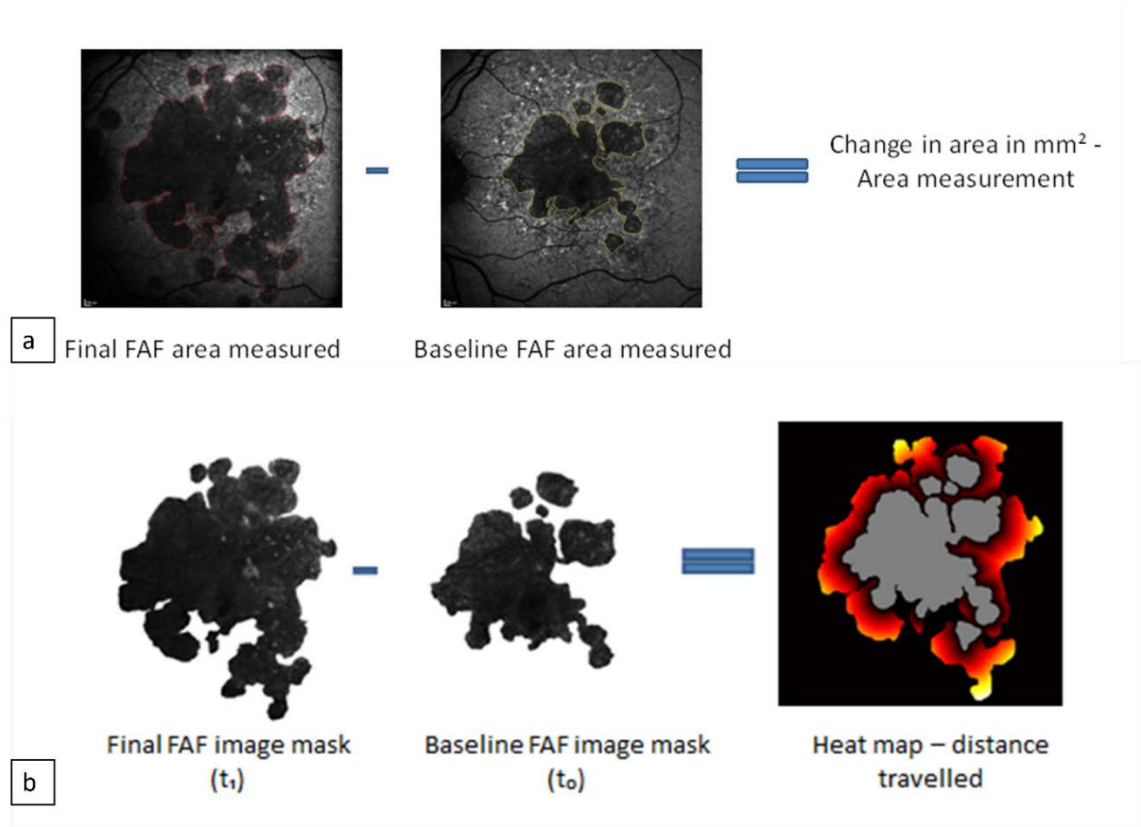

Figure 5.2 Methods of GA measurement.
(a)Subtraction method and (b) Linear distance method of measure of geographic atrophy expansion. The example is an anonymized image of an eye included in this study.

Statistical analysis

Values expressed as the mean ± SD. Bivariate correlations analysed with Spearman correlation coefficient. P value 0.05 was considered statistically significant. Analysis was performed using R version 4.1.2 statistical software package. Data visualization was done using ggplot2 package (v3.4.2, Wickham 2016)

5.2.3 Results

A total of fifty eyes of 50 patients were included in the study. The mean age of the cohort was 82.1 (SD 5.3) years. Mean baseline area was 3.48 ± 3.4 mm^2 and mean duration of follow-up was 3.53 ± 2.45 years.

Measures of growth outcomes

Mean rate of growth per year was 0.33 ± 0.18 mm/year with square root transformation, 1.5 ± 1 mm^2/year with area measurement, 66 ± 43µm/ year by distance mapping and mean GACI index was 0.57 ± 0.23.

There was positive significant correlation between baseline size and rate of growth /year in mm^2/year (r 0.56, P<0.001). The was no statistically significant correlation between baseline GA area and linear distance measure (r -0.14, P =0.3). However, the smaller lesion had higher growth rates by linear distance travelled.

On a continuous scale of GACI, there was significant correlation between subtraction method growth rate and GACI both for measurements in mm (r -0.53, P <0.001) and for square root transformed measurements (r -0.51, P < 0.001). However, there was poor correlation between square root transformation method and distance mapping (r 0.04, P = 0.73). There was a negative correlation between GACI and distance mapping, but it was not statistically significant (r -0.07, P = 0.65). Figure 5.3 demonstrates the correlation among various measures of GA expansion as (a) scatter plots and (b) correlogram.

On in-depth analysis of the heat maps, there were some edges that displayed minimal or no growth at all over time whereas some edges were rapidly advancing. This intra-lesion variability in growth is illustrated in Figure 5.4. Figure 5.4 shows the enlarged image of a heat map and corresponding OCT scans at certain points at the edge of the lesion.

Deep phenotyping and measures of growth outcomes

Foveal centre was involved 54% eyes. Multifocal configuration was seen in 36% eyes. Mean distance from fovea was 261.66 ± 363.86 µm. Multifocality, extrafoveal location of atrophy, presence of SDD and “trickling” or “patchy” junctional zone pattern on FAF were associated with higher growth rates across all measures. However, the difference was not statistically significant across all measures. Table 5.2 shows the variations in growth rates across area measures in the GA phenotypes based on imaging features.

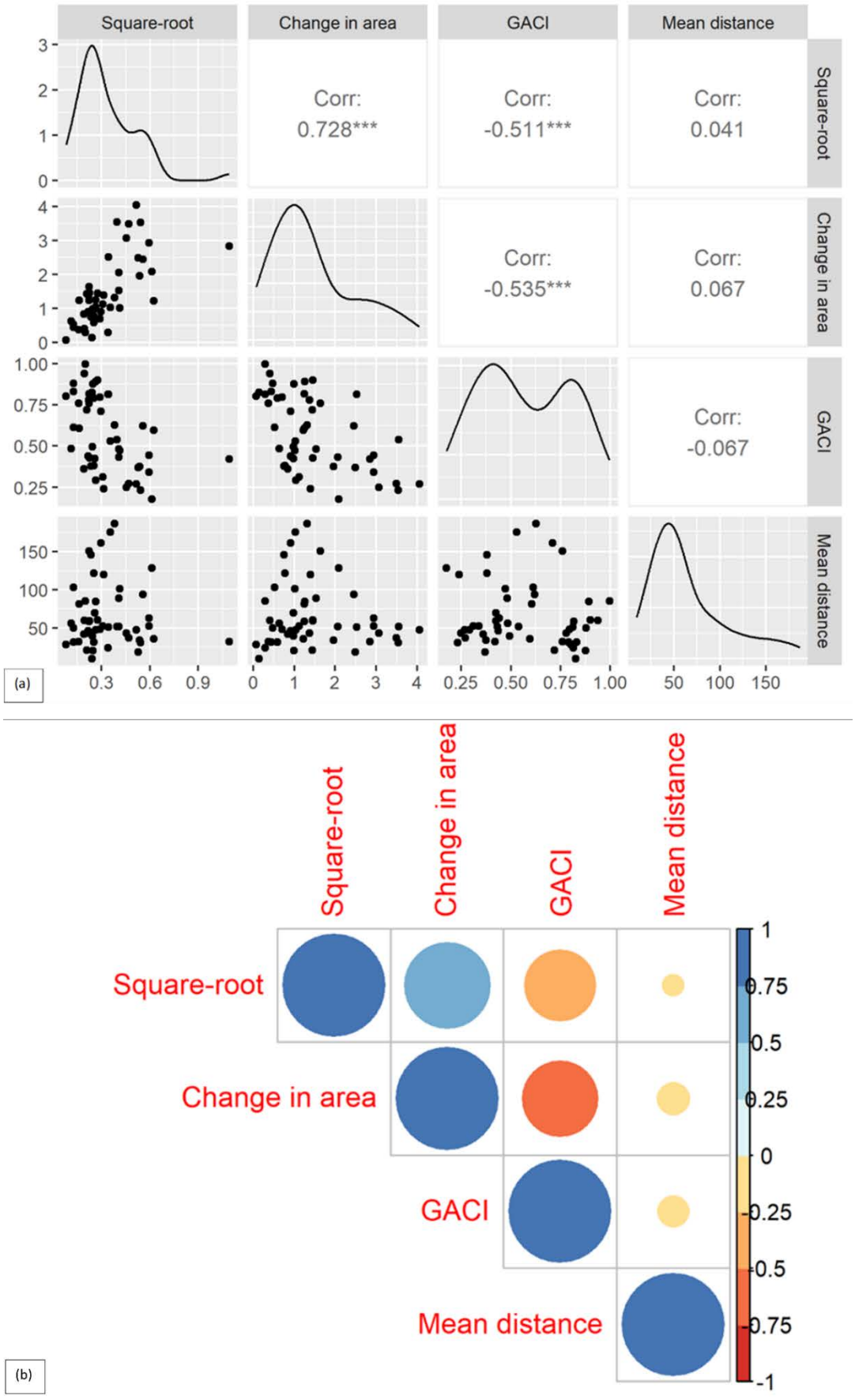

Figure 5.3 Correlation among various measures of GA expansion. (a) scatter plots and (b) correlogram.

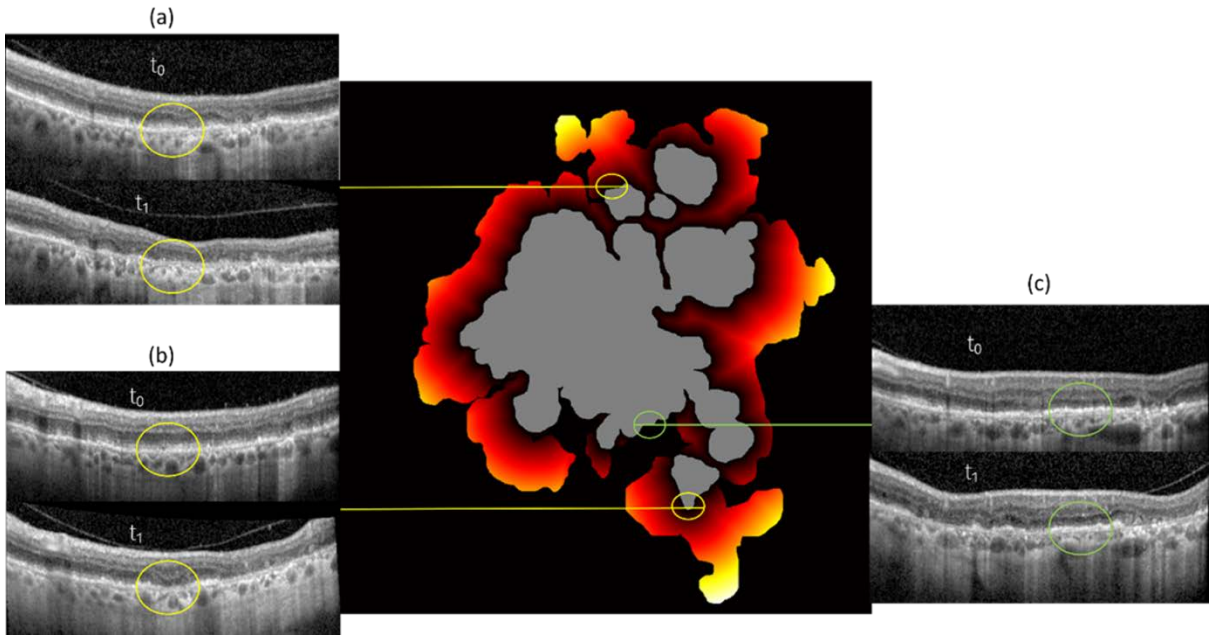

Figure 5.4 Heat map & corresponding OCT at certain points at the edge of the lesion. (a) and (b) are through rapidly advancing edges of the lesion and show development of new atrophy that met the criteria for cRORA. (c) illustrates preserved patch of RPE in an area of no lesion progression that lies between 2 moderately advancing edges.

Table 5.2 Variations in growth rates across area measures in GA phenotypes based on imaging features.

Imaging feature	**Baseline area (mm^2)**	**Area change (mm^2/year)**	**Sq. root transformation (mm/year)**	**GACI**
Focality				
Unifocal (n=32)	3.10 (2.94)	1.22 (0.87)	0.3 (0.2)	0.64 (0.22)
Multifocal (n=18)	4.16 (4.13)	1.87 (1.3)	0.4 (0.2)	0.34 (0.18)
p value	0.29	*0.02*	0.09	*0.0001*
Lesion Location				
Extrafoveal (n=23)	2.94 (3.38)	1.49 (1.19)	0.36 (0.22)	0.55 (0.25)
Foveal (n=27)	3.94 (3.44)	1.43 (0.84)	0.32 (0.14)	0.58 (0.21)
p value	0.3	0.83	0.44	0.64
SDD				
Present (n=28)	2.99 (3.3)	1.47 (1.34)	0.32 (0.2)	0.33 (0.15)
Absent (n=22)	4.46 (6.3)	1.09 (1.08)	0.25 (0.2)	0.54 (0.4)
p value	0.29	0.28	0.6	*0.013*
Junctional FAF pattern				
Trickling/patchy (n=24)	3.2 (2.1)	1.54 (1.2)	0.27 (0.2)	0.25 (0.3)
Other (n=26)	3.6 (3.3)	1.33 (1.1)	0.28 (0.3)	0.44 (0.4)
p value	0.6	0.52	0.89	0.06

Abbreviations: FAF – Fundus autofluorescence; GACI – geographic atrophy circularity index; SDD – Subretinal drusenoid deposits.

5.3 Translational value of new OCT based GA classification

5.3.1 Purpose

To evaluate the inter-rater reliability for identification of cRORA on SD-OCT images as defined by the CAM group.

5.3.2 Methods

The details of eligibility criteria, data collection, image analysis and grading are mentioned in Chapter 2. Additional details in grading procedure particular to work are mentioned below.

Grading procedure

The 50 pairs of images were interpreted by 5 clinicians (4 medical retina fellows and 1 consultant) who are skilled OCT readers from the same retina centre (Moorfields Eye Hospital, London, UK). Two of the 5 graders (Shruti Chandra and Sobha Sivaprasad) were more accustomed to the CAM grading. All graders were familiarized with the CAM grading and trained to identify the parameters on test-sets before grading the study images independently.

The five graders analysed the 50 pairs of SD-OCT horizontal cross-sectional scans without application of any image modifications. The images were presented in 2 separate data sets of 50 images each, and the readers were masked to the grading outcome. The readers were required to go through both the images and data sets in the same order. The graders were asked to document their response as Yes or No for presence or absence cRORA and each parameter that defines cRORA. The folders were then randomly re-numbered, and graders re-graded the images to evaluate intra-grader agreement. Additionally, they were asked to make a notation of whether WB or BW scans was most helpful in identifying each particular feature for a set of images. They could also choose that there was no difference in terms of setting, in their ability to evaluate respective OCT features.

Statistical analysis

Statistical analysis was performed using SPSS Statistics version 24 (IBM), Microsoft Excel for Mac version 15.33 (Microsoft), and the web-based Kappa Program. Inter-grader agreement was evaluated as a measure of reliability. The higher the intergrader

correlation coefficient, the more reliable was the identification and detectability of respective morphologic alteration**.** The responses being categorical variables, Fleiss' kappa (κ) was used for this purpose. To measure the intra-grader agreement and inter-grader agreement among 2 graders Cohen's kappa was used (Table 5.3). The significance was set at p≤ 0.05.

Table 5.3 Interpretation of Cohen's and Fleiss Kappa.

Cohen's Kappa Value	**Interpretation**	**Fleiss Kappa Value**	**Interpretation**
0 - 0.20	None	<0.00	Poor agreement
0.21 – 0.39	Minimal	0.00 – 0.20	Slight agreement
0.40 – 0.59	Weak	0.21 – 0.40	Fair agreement
0.60 – 0.79	Moderate	0.41 – 0.60	Moderate agreement
0.80 – 0.90	Strong	0.61 – 0.80	Substantial agreement
>0.90	Almost perfect	0.81 – 1.00	Almost perfect

5.3.3 Results

Fifty pairs of single SD-OCT horizontal scans were graded twice by each grader. Of the 50 images, 36 images demonstrated cRORA and the rest had iRORA as confirmed by 2 graders with previous experience in CAM grading.

The inter-grader and intra-grader Cohen's kappa values for cRORA diagnosis are shown for white-on-black (Table 5.4) and black-on-white images (Table 5.5). The intra-grader reliability by Cohen's kappa was in the range of 0.88 – 0.92 for white-on-black images which is strong to almost perfect agreement. The Cohen's kappa for black-on-white images ranged from 0.45 – 0.95, being >0.90 for 4 out of 5 graders. The inter-grader reliability varied from as low as 0.28 to almost perfect value of 0.92 for white-on-black images. Similarly, it ranged from 0.34 to 0.86 for black-on-white images. The inter-grader agreement was almost perfect for 2 graders (kappa WB 0.92, p value<0.0001; kappa BW 0.86, p value<0.0001) who were accustomed to the CAM criteria.

Table 5.4 Inter-grader and Intra-grader agreement (Cohen's Kappa) for cRORA in White on Black images.

Grader	#1	#2	#3	#4	#5
#1	0.88	0.64	0.44	0.28	0.30
#2	0.64	0.94	0.39	0.33	0.34
#3	0.44	0.39	0.94	0.65	0.68
#4	0.28	0.33	0.65	0.95	0.92
#5	0.30	0.34	0.68	0.92	0.92

Table 5.5 Inter-grader and Intra-grader agreement (Cohen's Kappa) for cRORA in Black on White images.

Grader	#1	#2	#3	#4	#5
#1	0.93	0.49	0.48	0.37	0.50
#2	0.49	0.90	0.55	0.39	0.34
#3	0.48	0.55	0.95	0.57	0.58
#4	0.37	0.39	0.57	0.93	0.86
#5	0.38	0.34	0.58	0.86	0.45

The Fleiss kappa values (κ) are shown in Table 5.6. There was moderate agreement in identifying cRORA using white-on-black images (κ 0.49, p value<0.0001) and fair agreement using BW images (κ 0.34, p value<0.0001). The RPE attenuation/loss was parameter detected most reliably in both sets of images whereas hypertransmission was the most poorly detected parameter.

Table 5.6 Fleiss Kappa showing Inter-grader agreement across 5 graders for all parameters.

Parameter	**Fleiss Kappa (95% CI)**	**Standard error**	**Level of Agreement**
White on Black Images			
cRORA overall	0.49 (0.22 – 0.45)	0.06	Moderate
Hypertransmission	0.36 (0.20 – 0.52)	0.08	Fair
Inner retinal changes	0.46 (0.30 – 0.62)	0.08	Moderate
RPE attenuation/loss	0.68 (0.52 – 0.84)	0.08	Substantial
Black on White Images			
cRORA overall	0.34 (0.33 – 0.65)	0.08	Fair
Hypertransmission	0.34 (0.22 – 0.48)	0.06	Fair
Inner layer changes	0.38 (0.30 – 0.56)	0.40	Fair
RPE attenuation/loss	0.72 (0.65 – 0.79)	0.60	Substantial

Overall, the agreement was better using WB images for all parameters except RPE attenuation/loss. The graders noted that RPE attenuation/loss was the relatively easier parameter to identify in the images, better detected on BW images. Hypertransmission was the least reliable parameter according to the graders and was particularly difficult to distinguish on BW images. Inner layer changes also were more clearly identified using WB versus BW images. However, the graders observed that to reliably detect the presence of cRORA it is better to analyse both images together. Examples of challenges in grading cRORA are shown in Figure 5.5.

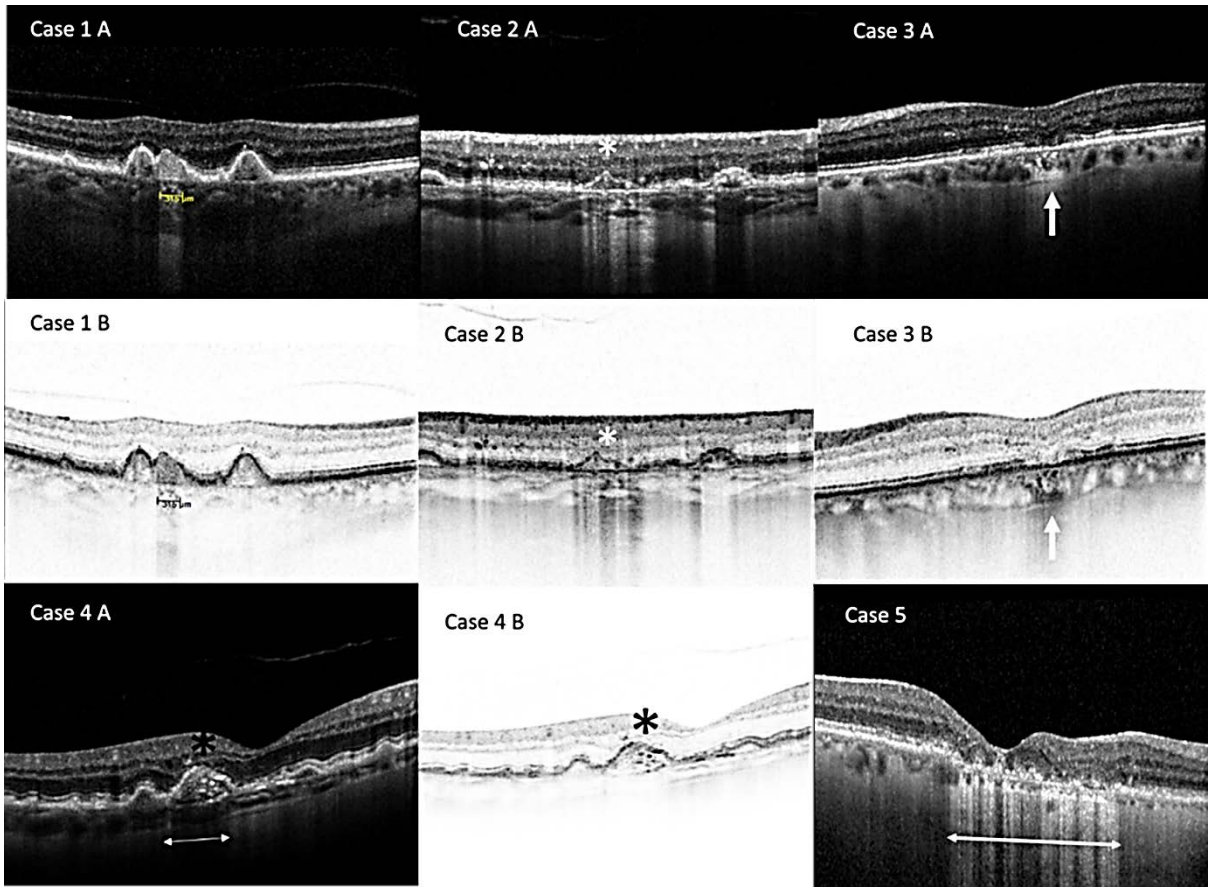

Figure 5.5 Examples of OCT images analysed in the study.
Case 1A: White on Black (WB) image showing hypertransmission of 315µm width and associated inner retinal changes overlying the PED. In the corresponding Black on White (BW) image (Case 1B), the RPE loss is better appreciated. Case 2A and 2B: This image shows the presence of a persistent hyper-reflective line in the bed of cRORA, which could be confused as attenuated RPE. This has been termed persistent basal laminar deposit (white asterisk) by the CAM classification. Case 3A: All signs of cRORA are noticeable (EZ/ELM layer changes and hypertransmission of 250µ), however the RPE is intact (white vertical arrow). This is again more evident in the BW image (white vertical arrow; Case 3B). Case 4A: There is loss of RPE and EZ and ELM layer changes overlying the PED (black asterisk), but the hypertransmission is absent (white horizontal arrow). Case 4B. The BW image confirms the definite absence of RPE (black asterisk). Case 5: This case shows an example of discontinuous transmission overlying a region of cRORA caused due to back shadowing secondary to dispersed pigmented cells (white horizontal arrow).

5.4 Pilot analysis on detection of photoreceptor loss as a novel endpoint for assessing disease progression

5.4.1 Purpose

To develop an automated tool for detection of photoreceptor loss in conventional SD-OCT scans in eyes with GA.

5.4.2 Methods

The study design was retrospective. The details of eligibility criteria, data collection, image analysis and grading are mentioned in Chapter 2. Additional details in image analysis procedure particular to work are mentioned below.

Development of EZ: ELM maps.

This work was performed along with my collaborator Dr. Edward Adams. We chose the EZ as the region of interest because it is the region of highest density mitochondria in photoreceptors and reflectivity of EZ in OCT is a function of mitochondria activity. Therefore, earliest sign of cell death would be reduction in mitochondrial activity. This in turn would lead to a decline in EZ reflectivity (Figure 5.6). The prerequisites for the measurements were accurate IS/OS segmentation and normalization of scans to allow case by case analysis. A stepwise approach to achieving this is mentioned below:

1. Segment IS/OS junction using semi-automatic segmentation algorithm.
2. Define offset from IS/OS junction above (for ELM) and below (for EZ).
3. Create two sub volumes based on the offset.
4. Extract A-scan peaks associated with ELM and EZ for the two volumes respectively - producing ELM and EZ enface reflectivity maps.
5. Normalise the EZ enface using the ELM enface by pixel-to-pixel (A-scan to A-scan) division - EZ/ELM. ELM is appropriate because it is located just above the EZ and therefore has a similar, if not the same, OCT structural artefact from the overlying vasculature.
6. Step 5 produces normalised maps EZ (EZ/ELM).
7. Interpolate EZ map across full 6mm (since only 49 or 97 B-scans are available).

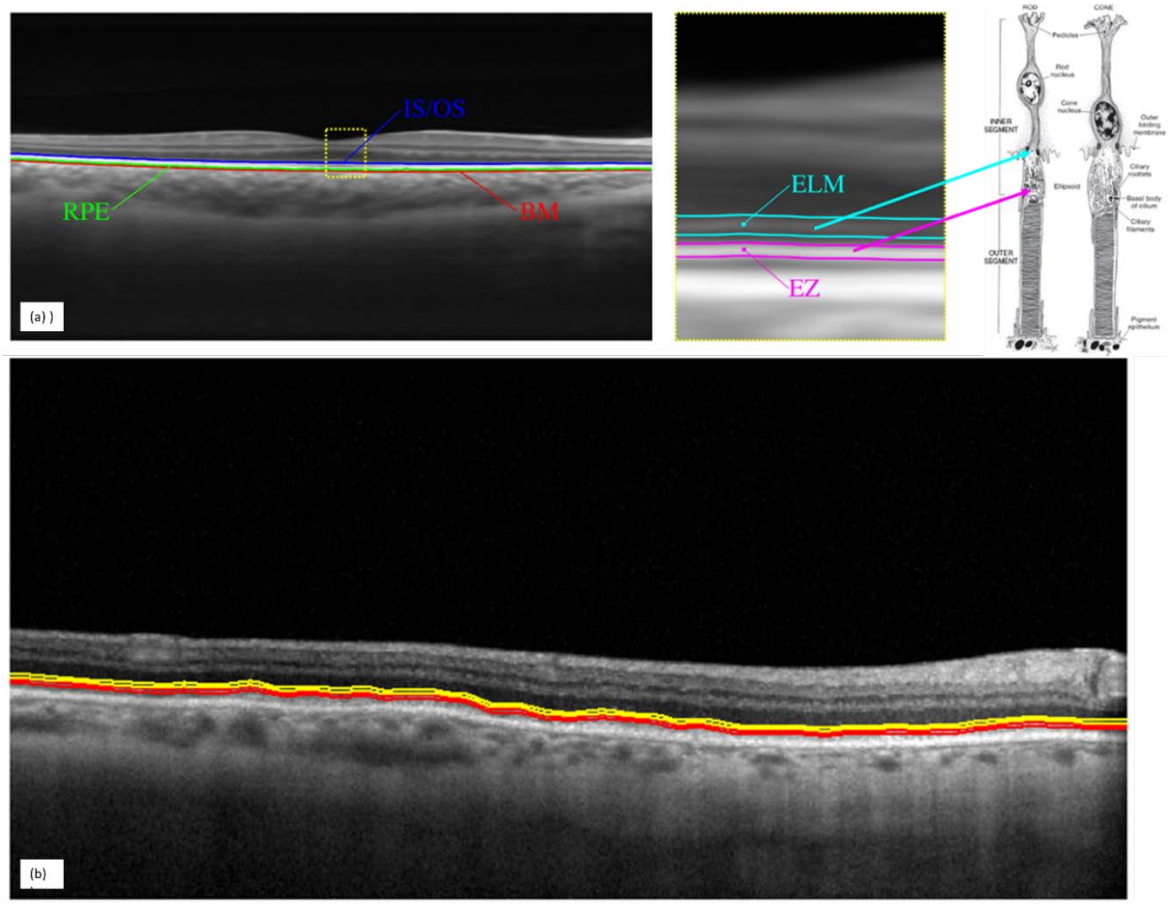

Figure 5.6 Methodology for EZ: ELM measurement.
(a) shows the IS/OS junction in an OCT scan of a normal eye. The enlarged image (central) shows the ELM (in blue) and EZ (in pink). The corresponding histopathological elements of the rod and cone receptors are shown in the image in extreme right. (b) Upper and lower boundaries of EZ (red) and ELM (yellow) for maximum projection.

The EZ: ELM ratio was calculated for the overall volume scan as well as for an annulus around the GA border (GA border + 500 microns) (Figure 5.7). This was done to focus on the junctional/transition zone around the GA lesion which shows the earliest activity during expansion.

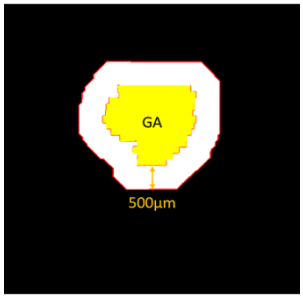

Figure 5.7 Schematic representation for EZ: ELM measurement region.
Measurement region (white) defined as 500µm from segmented GA region (yellow).

5.4.3 Results

A total of 15 eyes of 11 patients were selected for the study. 2 scan files were corrupted during data export and were excluded from the analysis. Of the 13 scans analysed, 9 scans were 49-line volume scans and 4 were 97-line volume scans. The 97-line volume scan produced better defined EZ maps than 49-line scans. The phenotypic characteristics of the eyes included in the pilot analysis are shown in Table 5.7.

Table 5.7 Baseline features of all the eyes included in the pilot analysis.

Pt no.	Study Eye	GA confirmed on OCT/FAF/both	Baseline area (mm^2) on FAF	Focality (Unifocal/ multifocal)	SDD (Present/ absent)	Foveal involvement (Yes/No)	Junctional changes on FAF	Fellow eye diagnosis
1	Right	Both	2.04	Unifocal	Absent	Yes	Patchy hyper AF	Unifocal foveal GA
2	Left	Both	2.22	Unifocal	Absent	Yes	None	Unifocal foveal GA
3	Right	Both	7.28	Multifocal	Present	No	None	Multifocal foveal GA
4	Left	Both	6.7	Multifocal	Present	Yes	None	Multifocal extrafoveal GA
5	Right	Both	22.17	Unifocal	Absent	Yes	Patchy hyper AF	Unifocal foveal GA
6	Left	Both	26.3	Unifocal	Absent	Yes	Patchy hyper AF	Unifocal foveal GA
7	Right	Both	16.92	Unifocal	Present	No	Banded hyper AF	Unifocal extrafoveal GA
8	Left	Both	18.56	Multifocal	Present	No	Banded hyper AF	Unifocal extrafoveal GA
9	Excluded from analysis- corrupted files during data transfer							
10	Left	Both	8.59	Multifocal	Present	No	Banded hyper AF	Multifocal foveal GA
11	Left	OCT alone	0	Multifocal	Present	Yes	Patchy hyper AF	Intermediate AMD
12	Excluded from analysis- corrupted files during data transfer							
13	Right	Both	2.53	Multifocal	Present	Yes	None	Intermediate AMD
14	Right	Both	1.38	Unifocal	Absent	Yes	None	Unifocal foveal GA
15	Left	Both	1.9	Multifocal	Present	No	Patchy	Intermediate AMD

The results of EZ: ELM ratio for the 13 eyes is shown in Figure 5.8. Two examples of EZ: ELM maps generated from the pilot dataset are shown in Figure 5.9.

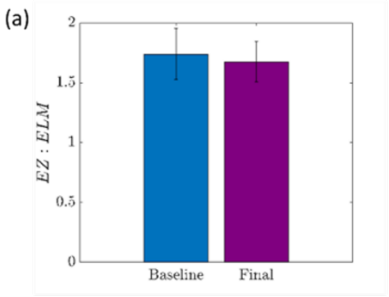

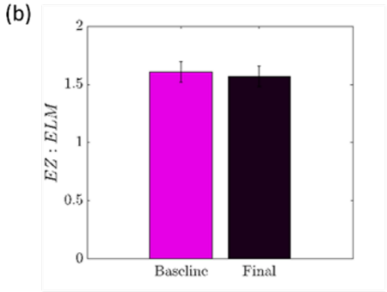

	Baseline	Final	p-value*
EZ:ELM	1.7407±0.212	1.676±0.170	0.0369

	Baseline	Final	p-value*
EZ:ELM	1.608±0.086	1.571±0.087	0.0162

Figure 5.8 Results for the pilot analysis of EZ:ELM measurement.
(a) EZ:ELM ratio for the entire volume scans (b) EZ:ELM ratio for the GA border + 500 microns annulus.

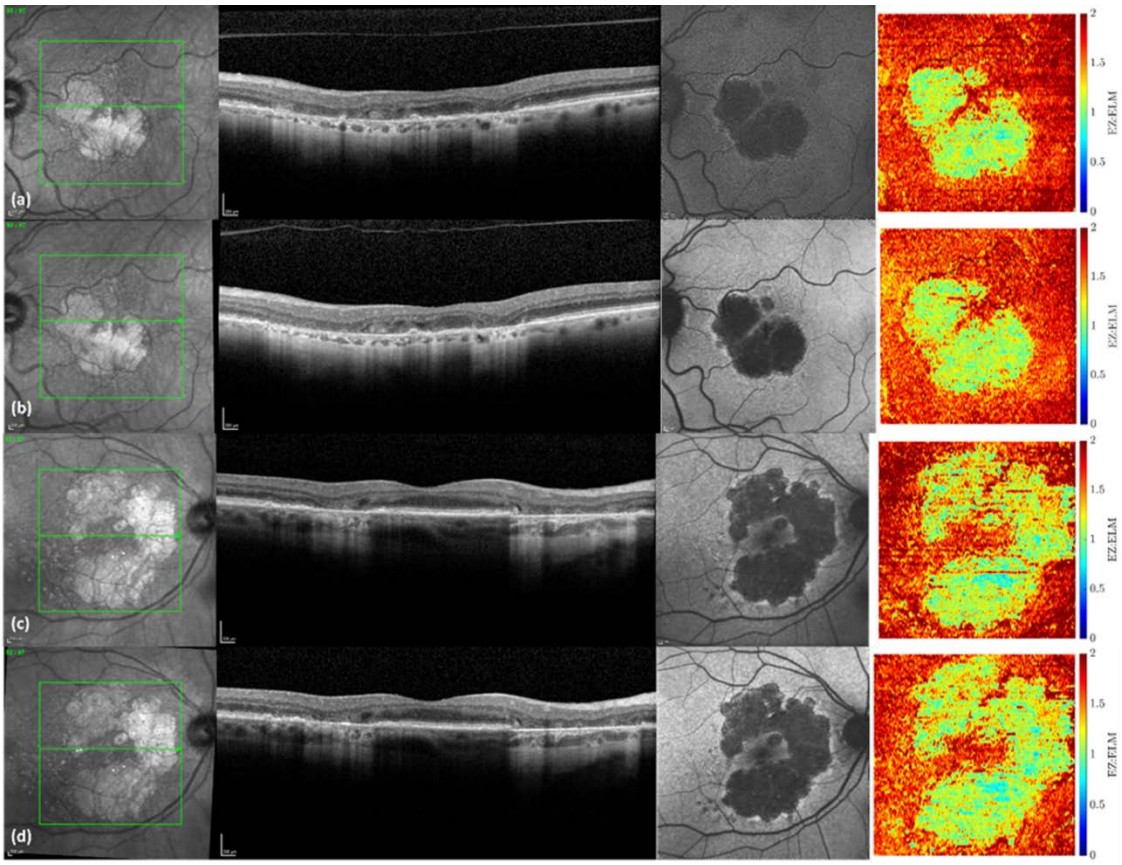

Figure 5.9 Examples for EZ:ELM maps.
Multimodal imaging shown are NIR image with OCT scan (section through the fovea) and FAF image. (a) and (b) show the baseline and final visit for the first example. The area by FAF was same at both time points. The EZ maps show and increase in area of EZ loss. (c) and (d) shows the baseline and final visit for the second example. The area by FAF was same at both time points. The EZ maps show and increase in area of EZ loss.

5.5 Imaging based clinical trial outcomes in eyes undergoing intervention for GA

5.5.1 Purpose

To test the applicability of OCT based measures of GA expansion and compare them to the FAF measure.

5.5.2 Methods

The study design was retrospective. The details of eligibility criteria, data collection, image analysis and grading are mentioned in Chapter 2. The additional methodology relevant to the study is mentioned below.

Intervention

This was a phase 1/2 first in human study for an intravitreally injectable investigational medical product for GA. It was given as a single dose injection of 0.05 ml in the vitreous. The patients were followed up for a total of 3 months with interim visits.

Measurement of GA area

Area of atrophy was measured on FAF images and defined as areas of definite hypo autofluorescence. This was done using the in-built overlay tool in Spectralis. In the eyes with multifocal lesions, each separate island of atrophy was measured and then sum of these was calculated as total area of atrophy in mm^2. The images with area measures for both eyes are shown in Figure 5.10.

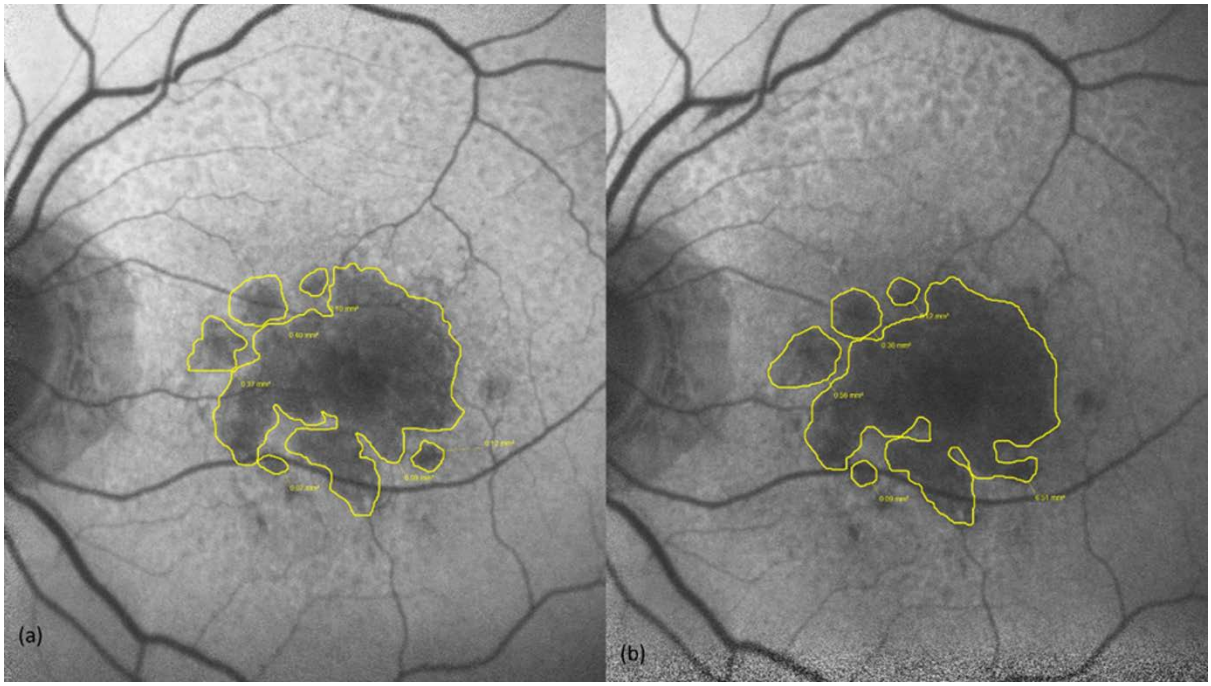

Figure 5.10 Method for measuring GA area using the overlay tool.
This is the study eye of the patient with multifocal GA lesions. (a) shows the area measurement at baseline – 7.15 mm^2 (b) shows the area measurement at 4 months – 7.56 mm^2.

Measurement of photoreceptor loss – Manual and Automated

Manual grading of photoreceptor loss was done by measuring the linear distance between visible photoreceptor at the edges of a cRORA lesion. This measurement was performed across all line scans in the volume scan spanning the region of atrophy. In case of multifocal lesions, EZ loss for calculated per lesion per scan. Figure 5.11 shows the measurement of EZ in unifocal as well as multifocal lesions. The total EZ loss was calculated as mean of all these values. In addition, the AI tool developed for pilot analysis was used to develop the EZ map for both patients.

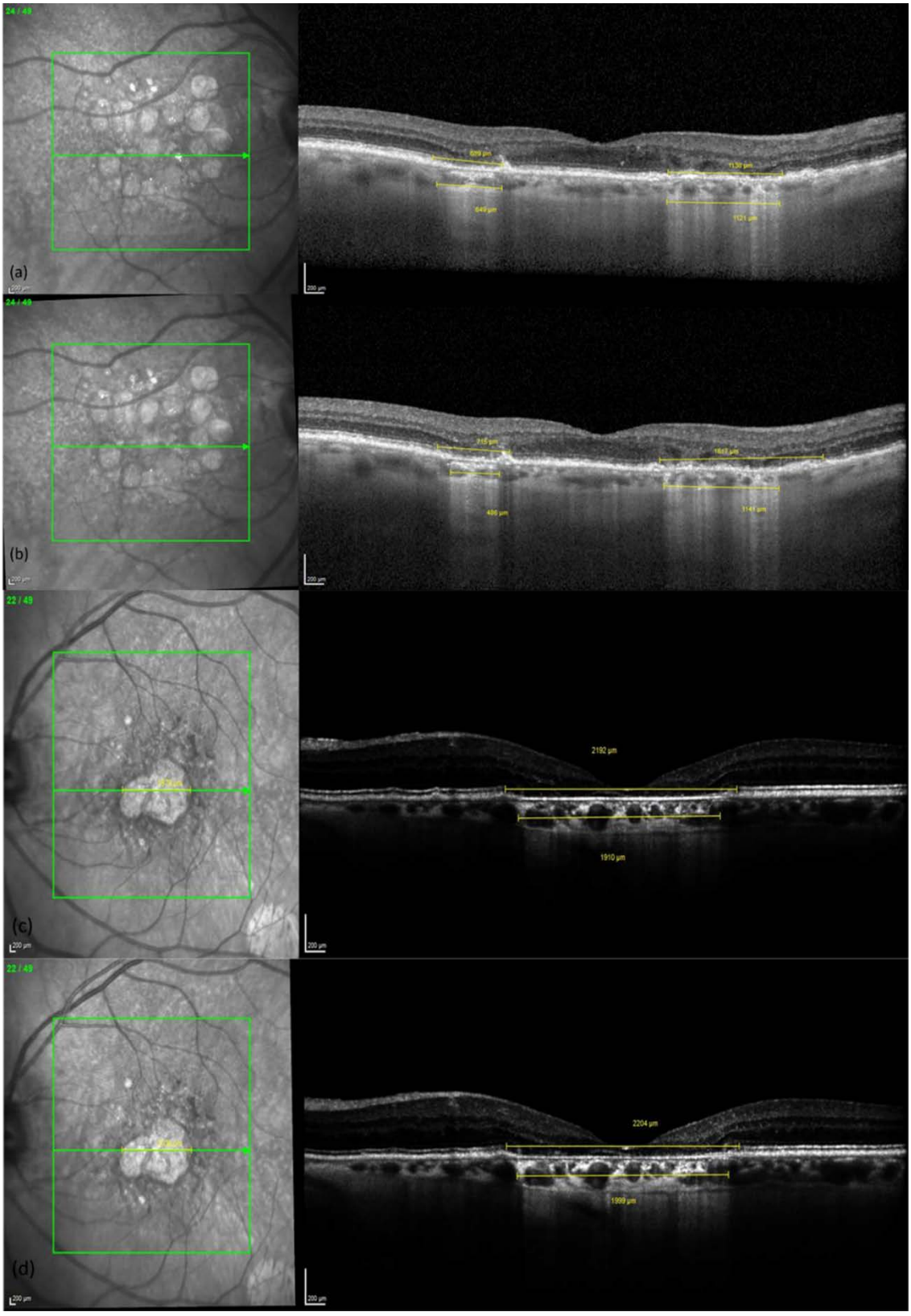

Figure 5.11 Method for manual measurement of photoreceptor loss.
In multifocal lesion (control eye) (a) at baseline and (b) at final visit. In unifocal lesion (study eye) at (c) baseline and (d) final visit. Each lesion was measured separately across all the entire volume scan and then averaged.

5.5.3 Results

The description of baseline and final features of two patients are shown in Table 5.8. Each visit data and analysis for patient 1 is shown in Figure 5.12.

Table 5.8 Baseline & final visit clinical characteristics for the patients analysed.

	Patient 1 – Study eye	**Patient 1 – Control eye**	**Patient 2 – Study eye**	**Patient 2 – Control Eye**
Laterality	Left	Right	Left	Right
Baseline BCVA (ETDRS letters)	50	50	45	76
Baseline GA area (mm^2)	2.22	2.04	7.15	7.69
Focality	Unifocal	Unifocal	Multifocal	Multifocal
SDD	Absent	Absent	Present	Present
Fovea involvement	Yes	Yes	Yes	No
Junctional changes in FAF	Patchy hyper	Patchy hyper	None	None
Change in GA area (mm^2)	+0.16	+0.16	+0.41	+0.45
Mean EZ loss (microns)	12	58	86	505
Change in retinal volume (mm^3)	+0.14	-0.03	+0.01	-0.09
Baseline EZ:ELM ratio at GA border +500 microns annulus	1.65	1.70	-	-
Baseline EZ:ELM ratio at GA border +500 microns annulus	1.33	1.58	-	-

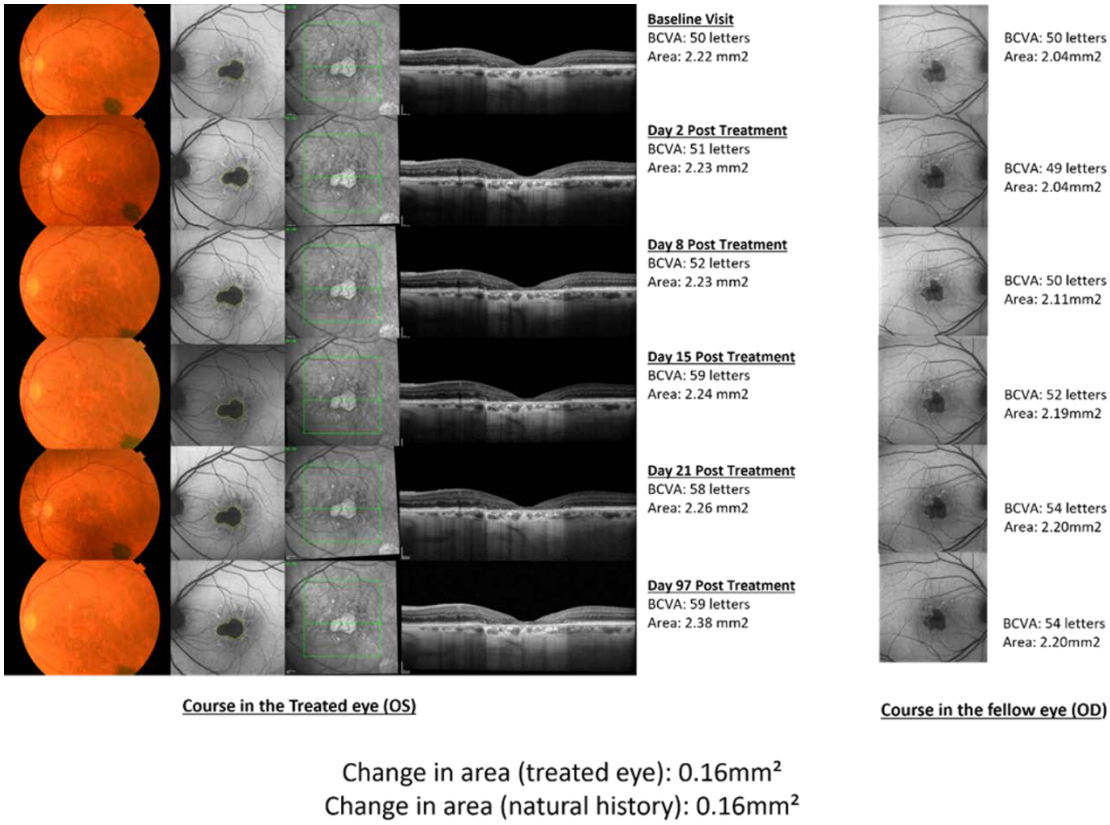

Figure 5.12 Detailed progression across multimodal imaging for patient 1.

The change in EZ:ELM ratio was higher in the control eye than study eye for patient 1 at the GA border + 500 microns region. However, for patient 2, the multifocality of lesion presented some issues in developing the EZ: ELM map. This was compounded by the fewer line scans in the volume scan. Therefore, the map for patient 2 was not accurate. The example of EZ maps against FAF images at baseline and final visits are shown in Figure 5.13 for study eye and Figure 5.14 for control eye for patient 1.

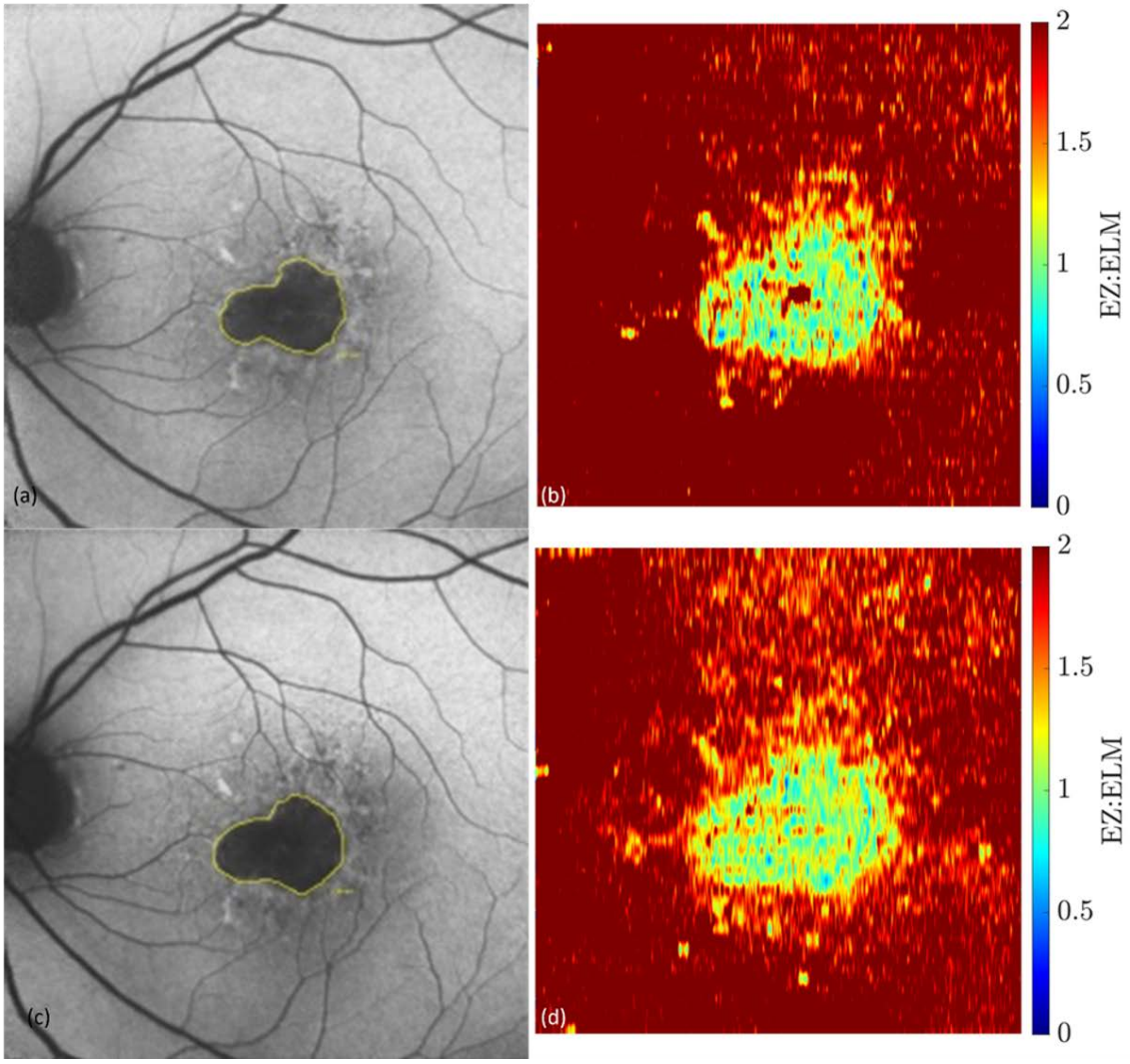

Figure 5.13 Examples of FAF and EZ:ELM ratio maps for study eye for patient 1. (a) and (b) are FAF and EZ: ELM ratio maps at baseline respectively, (c) and (d) are FAF and EZ: ELM ratio maps at final visit respectively.

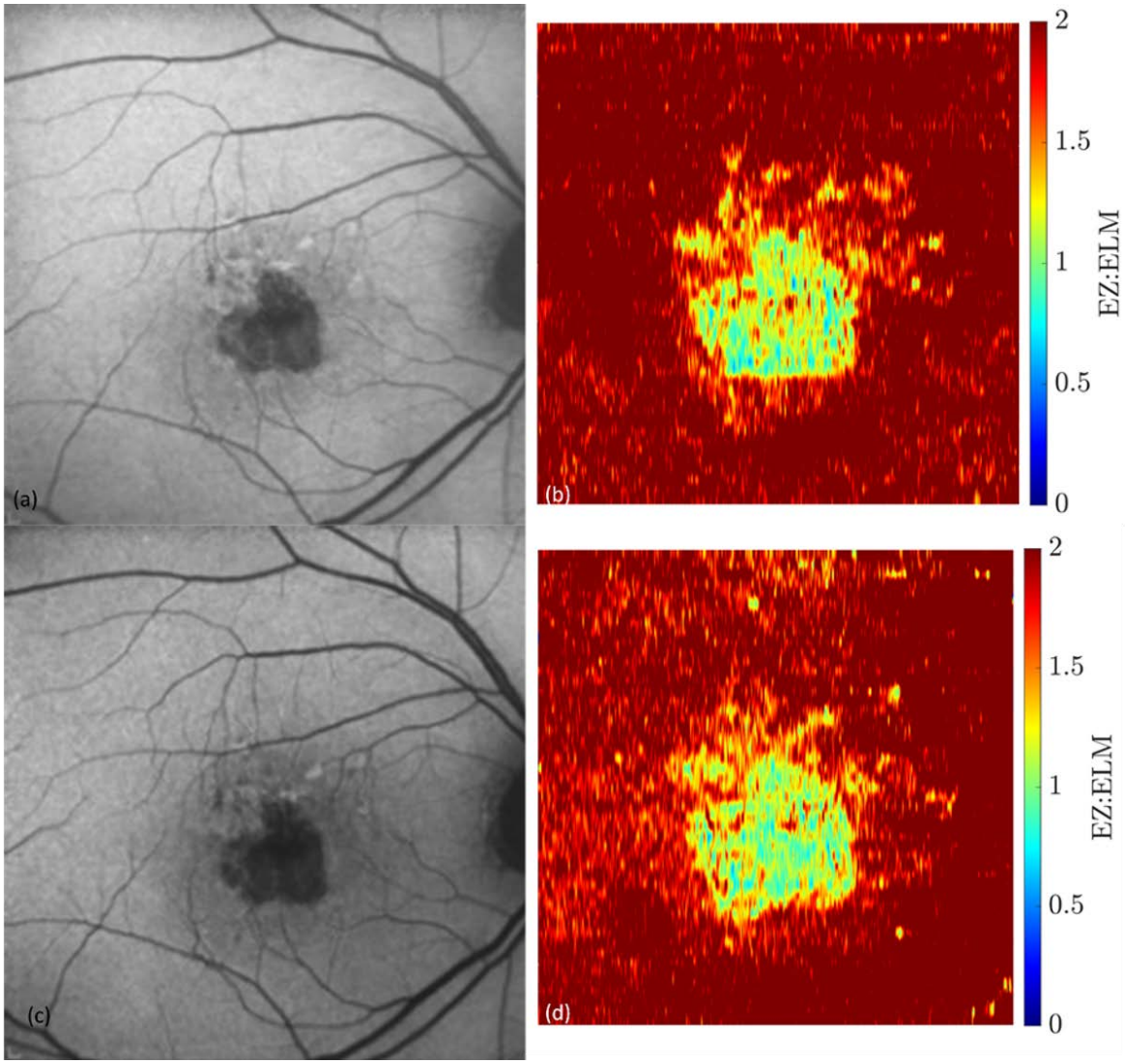

Figure 5.14 Examples of FAF and EZ:ELM ratio maps for control eye for patient 1. (a) and (b) are FAF and EZ: ELM ratio maps at baseline respectively, (c) and (d) are FAF and EZ: ELM ratio maps at final visit respectively.

5.6 Discussion

This chapter describes the various aspects of heterogeneity of progression of GA and the implications it has on outcome measures in clinical trials. The main findings from my work are, firstly that quantification of GA progression by area of enlargement and progression of GA border as a linear distance are not correlated due to high variability in GA phenotypes and therefore cannot be used interchangeably as an outcome tool. Secondly, there is significant inconsistency in diagnosis of cRORA (equivalent of GA), as evidenced by microstructural phenotypic variations in these lesions, highlighting the need for refinement of the criteria prior to its use as an inclusion criterion for clinical trials. Thirdly, automated quantification of maintenance/reduction in EZ:ELM ratio

especially in the transition zone around the GA border, is an effective indicator of GA progression (as early as 3 months) and has potential for use as an early clinical trial endpoint. Finally, a detailed analysis of data from an interventional trial reveals the caveats the current outcomes and the use of photoreceptor loss as an end point showed potential neuroprotective effects of the agent.

There exists large variation in the design characteristics of GA treatment trials nevertheless expansion of GA is the most frequently employed primary outcome. A review by Cheng et al in 2018 reported GA growth was the primary outcome in in 58% of phase 2 trials and 71% of phase 3 trials, and as a secondary outcome in 31% of phase 2 trials (Cheng, Gao et al. 2018). All trials quantify growth rate based on area change. Previous natural history studies as well focused on the growth rate of the total GA area which is a measure dependent on lesion morphology (Klein, Klein et al. 1995, Domalpally, Danis et al. 2016). As GA lesions exhibit significant heterogeneity in lesion morphology, this has bearings on use of area difference as an outcome in clinical trials. Use of linear distance growth instead has been reported as more independent measure of GA (Uji, Nittala et al. 2019, Shen, Sun et al. 2021). In my analysis, I found an expected significant positive correlation between area enlargement and baseline lesion size, but there was no correlation between linear growth and baseline lesion area. Notably though smaller lesions showed higher linear growth than larger GA lesions. Also, there no statistically significant correlation between area-based enlargement and linear growth of GA lesion. Therefore, there is a fundamental flaw in the way we report the most commonly use outcome measure for GA in interventional trials (Sivaprasad, Chandra et al. 2023).

The importance of lesion shape characteristics as prognostic variables has been reported by Pfau et al (Pfau, Lindner et al. 2019). They and demonstrated that descriptors of lesion morphology explain up to 24.4% of variance in progression rates in patients for whom there was no previous data and in 39.1% patients with available previous assessment. A potential influence of genetic variants has also been described in the AREDS2 Report Number 16 (Keenan, Agrón et al. 2018). Shen et al reported an increased effect of topographic location of GA lesions on rate of growth (Shen, Sun et al. 2020). In line with these reports, I found that multifocality, extrafoveal location junctional changes at GA border on FAF and presence of SDD lead to escalated growth

rates. Another and perhaps more important finding was that the advancement of the lesion border was not similar between cases and significant variation even within a case. Hence, heterogeneity in GA lesion morphology can significantly impact the measurement of growth as an outcome and thereby reflect on the efficacy if the intervention. There is a definite unmet need to redefine this outcome or develop newer end points that are independent of intrinsic lesion characteristics.

One of the key design characteristics of a clinical trial for GA is the eligibility criteria. For GA studies this would entail accurate identification of true atrophic lesions for inclusion in the trial. My work assessed the reliability of detection of these atrophic lesions on SD-OCT scans, termed cRORA by the CAM classification. There was significant subjectivity in the identification of the parameters used to define cRORA with high intra grader variation across both sets of images. Taken together these findings suggest that diagnosis of cRORA on OCT images may be quite subjective and have an impact on clinical diagnosis when treatment become available for this condition. The CAM group report 6 was study designed to determine the interreader agreement for iRORA and cRORA and their related features in AMD (Wu, Pfau et al. 2022). They reported moderate agreement for a 3-category classification of no atrophy, iRORA, and cRORA (AC1 = 0.53) and substantial or better interreader agreement for all qualitatively graded OCT features associated with atrophy (AC1 = 0.63–0.87), except for RPE attenuation (AC1 = 0.46) and disruption (AC1 = 0.26). These results were similar to my work with variations in agreement for each of these features. This could be attributed to the microstructural phenotypic heterogeneity that exists in OCT features defining atrophy.

Another reason for these inconsistencies could be the variation in prevalence of individual features in a designated cohort of cRORA lesions. This variability is evidence of the disease manifestation of atrophy itself and does not represent any selection bias while choosing the images for the analysis. The evidence comes from the dataset used in CAM report 6, where outer retinal layers changes like ONL thinning, EZ/ELM disruption was seen in over 85% readings whereas a hypo reflective wedge was noted in 25% of readings (Staurenghi, Sadda et al. 2014, Wu, Pfau et al. 2022). This indicates that atrophy on OCT has significant heterogeneity in features and may or may not present with the entire suite of defined features. Critically presence or absence of these

features may impact selection into trials and outcome assessment as well (Curcio and Millican 1999, Tan, Astroz et al. 2017).

An element of heterogeneity in GA expansion is directional kinetics in GA growth. It has been reported in clockwise direction by Uji et al and Shen LL et al reported an increase in linear growth from foveal centre to 3.5 mm retinal eccentricity (Uji, Nittala et al. 2019, Shen, Sun et al. 2020). The underlying mechanism responsible for the differential GA progression kinetics in the macula is unclear, but several hypotheses have been proposed ranging from protective effects of macular pigments, higher choriocapillaris flow deficits and higher vulnerability of rods to atrophy than cones (Owsley, Jackson et al. 2000, Beatty, Murray et al. 2001, Nassisi, Baghdasaryan et al. 2018, Zheng, Zhang et al. 2019, Kar, Clark et al. 2020, Moult, Alibhai et al. 2020). This directionality of growth is highly relevant while recruiting patients with preserved fovea in a clinical trial. Ex-ante identification of aggressive GA border towards fovea would aid selection of high-risk patients into clinical trials. This is also important keeping in mind the regional therapeutic approaches (stem cell injection and subretinal therapies) which may be delivered to a specific quadrant. Thus, the practical question is how we identify these edges on the most commonly performed imaging modality i.e., OCT. An element heterogeneity in GA expansion is directional kinetics in GA growth. Combining the learning from Section 5.2 and 5.3, I studied the features of rapidly and slowing advancing edges correlating it with the corresponding OCT scan at each point. I scrutinized the intact RPE layer adjacent to the edges which was likely to develop atrophy over time. I found that at baseline the RPE appeared similar at all points i.e., irrespective of whether the edge was rapidly advancing or slow the baseline OCT had an intact flat RPE adjacent to the edge. I therefore hypothesize that an intrinsic event at a particular GA edge occurred between baseline and final year visit that attribute its directionality and pace of growth. Probably a precursor lesion like photoreceptor disruption or loss could have led to this. But these precursor lesions were missed, partly due to sparse time points of analysis that are usually 12 months apart and in part due to end point measuring RPE loss and not photoreceptor loss.

Based on my hypothesis I used volumetric OCT scans to study photoreceptor loss in GA eyes at 3 months from baseline. Considering photoreceptor loss is a subtle change on OCT that may be difficult for human grading I employed an automated method to

perform this analysis to increase its precision and accuracy along with reproducibility (Csaky, Ferris et al. 2017). I found that photoreceptor loss, as indicated by a decrease in EZ:ELM ratio, was a predictor of progression in GA eyes, as early as 3 months into analysis even when there was no measurable change in GA area on FAF. This was seen through the entire volume scan as well as in the transition zone. The dataset included all phenotypes of GA with various combination of features as well as low density OCT volume scans to ascertain the applicability of the model in real world datasets as well.

Multiple factors corroborate the use of EZ: ELM loss as a potential clinical trial end point. First, the objective definition the parameter itself. On OCT the second hyperreflective band represents the photoreceptor layer and was previously known as the IS/OS junction, however the high reflectivity of this band originates from the photoreceptor inner segment ellipsoids and is now known as the EZ (Fernández, Hermann et al. 2008, Spaide and Curcio 2011, Staurenghi, Sadda et al. 2014). These photoreceptors IS ellipsoids are loaded with mitochondria making them responsible for essential metabolic and light guiding functions (Hayes, Tracey-White et al. 2021). Therefore, EZ would be the ideal layer to perceive the earliest decline in metabolic function and slowing of cellular processes leading to cell death (Tao, Wu et al. 2016). Qualitative description of EZ as present, absent or disrupted is highly subjective, subject to direction-dependent reflectivity and image quality. Therefore, in my study utilization of an automated analysis of relative reflectivity of EZ to ELM to circumvents both issues. Use of ELM layer as reference value controls for the variation in brightness and contrast of various OCT scans and being a non-neural layer, its intensity does not alter with age or stage of degeneration providing consistency across the retina (Wu, Ayton et al. 2013). Riedl et al used PR loss/RPE loss ratio for follow up where the RPE layer is subject to changes secondary to ageing and degeneration (Kaarniranta, Uusitalo et al. 2020, Riedl, Vogl et al. 2022). Secondly, the reduction in EZ:ELM ratio was noted in almost 500 microns annulus away from the GA border where RPE was still intact indicating early signs of progression. Thirdly, recent evidence supporting role of photoreceptor loss as an end point comes from the work by Riedl et al on the effect of pegcetacoplan on PR loss. Kim et al showed evidence of C3 deposits on photoreceptor activating glial cells like macrophages which explains the treatment arm in FILLY trial showed a reduction in PR loss (Kim, Mastellos et al. 2021). As most interventions in GA trials are based on

complement therapy, reduced EZ: ELM or its maintenance would be an ideal early end point. Fourth, the high correlation between PR loss and functional changes shown in various studies monitoring local GA progression is highly relevant (Csaky, Ferris et al. 2017). Above all use of EZ:ELM ratio as an end point is independent of heterogeneity in lesion morphology characteristics rendering it a better trial outcome end point than any other.

I tested the applicability of the work done in sections 5.2 to 5.4 in the dataset of an interventional Phase 1/2 first in human GA trial using an injectable intravitreal agent. The analysis supported our hypothesis. Using area difference as an outcome showed no effect of intervention, however the photoreceptor loss was lower in the treated eye than the control eye. Also, preservation of retinal volume was more in the treated eye than control. These two features might indicate neuroprotective properties of the agent which would have not been detected with the use of standard outcome measures.

There are a few limitations to my work in this chapter. The retrospective nature of data analysed in sections 5.2-5.4. In section 5.2 the small sample size combined with the high individual variability on GA lesions could have an impact on the results. In the study to determine reliability of CAM classification, the use of volume scans instead of .tiff images would probably have improved scores as it would allow dynamic manipulation of the scans to appreciate the features better. However, most reliability studies are done on static images due to ease of implementation. The pilot analysis included a very small number of patients. The scans used for preparing the maps were 49-line scans. Use of high-density scans would provide higher quality and better definition in these maps. Also, it was difficult to analyse the GA border + 500 microns annulus in very small multifocal lesions. These were scans acquired in a clinical setting and the future goal is to refine the model so that it can pick up EZ:ELM ratio even in these scans. Use of high-density scans acquired on swept source OCT that provide higher axial resolution may alone development of better-quality maps.

In conclusion, my work presents evidence of impact of heterogeneity in GA lesions and its effect on a primary outcome measure i.e., GA growth as measured on FAF. I also demonstrate the heterogeneity in identification of GA using OCT scans that can impact patient selection and eventually outcomes in interventional trials. I put forth a new clinical trial end point of EZ:ELM ratio, which is independent of lesion morphology, is

detectable at a time point as early as 3 months and can be calculated using our automated tool. Finally, I test the translational value of this work in an interventional trial data and confirm that photoreceptor loss indeed precedes RPE loss and is a valuable clinical trial end point.

6 Chapter 6 Discussion

6.1 Summary of findings

The overarching aim of this work was to identify and reinforce phenotypic heterogeneity among AMD disease categories based on current classification system. The aim was to demonstrate how anatomical differences, not related to drusen seen on multimodal imaging partly contribute to the diverse structural and functional outcomes of eyes in each category of AMD. My hypothesis was based on the scientific rationale that there is a need for a more granular classification of AMD to better explain natural history, identify fast-progressors in non-neovascular AMD and poor responders amongst people with nAMD treated with anti-VEGF therapies. By better stratification of patients with AMD, we are likely to explain why some patients progress to atrophy, fibrosis or have persistent fluid despite anti-VEGF treatment. In this way, we may be able to define better eligibility criteria for novel interventions in clinical trials, develop new clinical trial end points and provide new knowledge for drug discovery.

The results of the first chapter on eyes with early and iAMD show the relevance of incorporating SDDs and outer retinal changes into a novel classification system for AMD. In my new classification system, I included presence of SDD as an independent classification stage irrespective of drusen size. I also graded presence of outer retinal changes – HRF and iRORA in normal, early and iAMD groups and show that eyes with early and intermediate category on Beckman can be classified with more granularity that correlate with visual function better. I noted that 40% of eyes classified as early AMD as per Beckman had SDD on OCT and likewise 30% with iAMD as per Beckman had SDD on OCT. Of the eyes that had SDD almost 80% had stage 3 SDD, including 2 eyes from the early AMD group. Interestingly 20% of eyes had stage 1 or 2 SDD that are known to be either invisible or poorly visible on CFP, emphasizing the need for OCT classification for more phenotypically homogeneous cohorts. Similarly, 40% of SDD eyes and 20% of iAMD eyes had confirmed iRORA on OCT. When considering HRF, about 10% eyes in SDD and iAMD group had HRF and importantly there was 1 eye classified as early by Beckman that had confirmed HRF on OCT. It might also be worthy to mention here that all iRORA and HRF are not detectable on CFP. It was thought originally that HRF are intraretinally migrated RPE cells and hence associated with pigmentation which could be detected on CFP. However now it has been shown that HRF could be composed of

macrophages with engulfed RPE cells or even non-RPE origins and therefore not detectable on CFP. The importance of these findings is that we might be incorrectly classifying AMD based on CFP and in the process disregarding the presence of biomarkers like HRF and iRORA that are significant contributors to disease progression.

It is of course not enough if we phenotypically classify AMD and there is a need to correlate with visual function, a key end-point required by regulators for novel interventions for AMD. In the next section I looked at dark adaptation as a functional biomarker for non-neovascular AMD. My results show SDDs located internal to the RPE can classify non-neovascular AMD eyes into two groups with varying visual functions. On multivariable analysis, the most significant features were SDD, presence of hypo reflective drusenoid lesions and decreased SFCT. I tested the discriminatory power of RIT using my classification and employed two thresholds of RIT that have been proposed in literature as “normal” cut-offs for RIT. RIT>6.5 minutes could discriminate early AMD without SDD from normal (p=0.03) but not RIT>12.5 minutes (p=0.12). Importantly, only 8% and 4% of the normal eyes had RIT>6.5 and >12.5 minutes respectively and SDD was an independent risk factor for delayed DA, irrespective of AMD stage. Most studies using DA as a functional marker have used CFP based classification. I found that outer retinal changes on OCT like nGA and choroidal hypertransmission also led to significantly prolonged RIT.

A clinicopathologic correlate study of the lifecycle of SDD describing stage specific composition provides further insight into risk prediction in SDD eyes. For example, higher association of immune cells with stage 3 SDD versus stage 1 or 2 might indicate role of inflammation at this stage or presence of scattered RPE organelles in stage 3 SDD would be consistent with RPE degranulation as a degeneration pathway (Monge, Araya et al. 2022). Like basal linear deposits and soft drusen, SDD primarily consist of membranous debris; however, they form above the RPE. The futility of laser treatment and continued faster progression in SDD eyes as shown in the LEAD study further emphasises the point that eyes with SDD possess a divergent pathogenesis from that of AMD and therefore might respond differentially to an intervention (Guymer, Chen et al. 2021). The supporting knowledge regarding this comes from reports associating presence of SDD with cardiovascular diseases, indicating a predominant vascular influence (Gerardo, Oscar et al. 2022). Also, composition of SDD is different from

drusen consisting of lower lipid content therefore inclusion of these eyes in anti-lipid therapy trials might lead to poor results. Knowing the limits of SDD visibility on CFP and enhanced diagnostic accuracy of multimodal imaging to detect SDD are also important arguments in favour of including eyes with SDD as a distinct severity group of AMD. My results further elucidate these findings. Eyes with SDD in my cohort had significantly prolonged dark adaptation irrespective of their Beckman stage of AMD, they had significantly thinner SFCT and thinner ONL. I hypothesize that eyes with SDD behave akin to eyes with outer retinal atrophy and therefore will respond differentially to interventions targeted at pathways for drusen formation alone.

In addition, my results support previous studies that most eyes with SDD irrespective of their AMD classification have a thin choroid (Cheng, Kaszubski et al. 2016). This finds its relevance in elucidating the etiopathogenetic role of choroid in these eyes and re-emphasizing the vascular predominance. Alten et al showed SDD tend to occur within or very near to choroidal watershed zones, which are at the border between two or more separate regions of perfusion, which have comparatively poor vascularity and are vulnerable to ischemia (Alten, Clemens et al. 2013). Before any observable retinal alterations, SDD development coincides with choroidal thinning, as well as an increase in the ratio of stromal to total choroidal area. These data support the idea that reduced blood flow within the macular choriocapillaris is involved in early AMD pathophysiology especially in eyes with SDD. Keeping these findings in mind it can be proposed that drugs that improve vascular perfusion e.g., phosphodiesterase -5 inhibitors might play a role in delaying disease progression if given to patients with early AMD or stage 1 or 2 SDD. It is essential therefore to include these features in clinical trial inclusion criteria for interventions targeting choroidal blood flow.

Furthermore, I show that better definition of RPE changes rather than hypo or hyperpigmentation on CFP are useful to identify the faster progressors to atrophy. These include features of RPE disruption or loss on OCT i.e., HRF, iRORA, nGA and cRORA. HRF combined with foveal drusen in eyes with iAMD have shown to be associated with vision loss and RPE atrophy. Similarly, iRORA and nGA had a high predictive value for GA progression (adjusted HR 12.1 and 78.1 respectively). In the LEAD study 21 % of the eyes with iAMD had prevalent iRORA with an endpoint of nGA (Guymer, Chen et al. 2021). There is a subtle difference in the features that define

iRORA and nGA on OCT and therefore a CFP based grouping of these eyes in a study would be incorrect. But one common factor is that eyes with iRORA or nGA show the earliest signs of progression to advanced disease and therefore might be the ideal cohort to target for interventions aimed at preventing progression to GA. For example, clinical trials on complement pathway drugs or gene therapy trial might design their studies to include eyes with iRORA or nGA, to avoid progression to cRORA.

The question is if eyes with SDD or HRF or iRORA or a combination of these have a unique risk profile to those without, would be wise to group them together based on our current classification systems that do not acknowledge their presence? More importantly do we alter our clinical trial interventions and trial outcomes based on inclusion or exclusion of these high-risk characteristics? The answer is a definite yes where clinical trial inclusion needs to be based on a more detailed and granular classification. Additionally deep phenotyping of these eyes will aid design better interventions and study outcomes. Based on my findings propose a modified classification for non-neovascular AMD incorporating the microstructural as well as functional biomarkers studied (Table 6.1).

Table 6.1 Proposed imaging-based classification for non-neovascular AMD based on the results of this thesis.

	Drusen size	**Distinctive features**	**Additional markers**
Early AMD	Maximum druse diameter <100 µm on en face OCT	No SDD No outer retinal changes*	Normal or thick SFCT RIT ≤ 6.5 mins
Intermediate AMD – a (iAMD^{a})	More than 1 druse with diameter 100-145 µm or at least 1 druse (>145 µm)	No SDD No outer retinal changes*	Normal or thick SFCT (If thin SFCT – measure ONL thickness, to consider SDD regression) RIT ≤ 12.5 mins
Intermediate AMD – b (iAMD^{b})	More than 1 druse with diameter 100-145 µm or at least 1 druse (>145 µm)	No SDD Outer retinal changes present*	Normal or thick SFCT (If thin SFCT – measure ONL thickness, to consider SDD regression) RIT may be prolonged ≥ 12.5 but < 20 mins
SDD in early AMD (eAMD^{s})	Any stage of SDD. Maximum druse diameter <100 µm on en face OCT	Outer retinal changes may be present	Thin/Thick SFCT RIT prolonged ≥ 20 mins
SDD in intermediate AMD (iAMD^{s})	Any stage of SDD More than 1 druse with diameter 100-145 µm or at least 1 druse (>145 µm)	Outer retinal changes may be present	Thin SFCT RIT prolonged ≥ 20 mins

**Outer retinal changes – HRF, inner layer subsidence, ONL thinning*

Chapter 4 evaluated phenotypic heterogeneity in nAMD at baseline and variations in short- and long-term responses post anti VEGF therapy based on these phenotypic variations. Outcomes to treatment with nAMD vary significantly and in the real world, despite mandated protocols the treatment regimens are individualized to meet patient requirements. However, patients are lost to follow-up, some die, and some miss a significant number of treatment visits due to other reasons such as co-morbidities. Moreover, the definition of non-responders has not been crystallised. Although there is a significant emphasis on fluid resolution being a marker for response and modulating therapy, visual acuity outcomes at 12 or 24 months are based on several other known morphological characteristics, presenting visual acuity and age of the patient. Based on my results, heterogeneity in imaging features at presentation are significant determinants of good or poor baseline VA. Imaging factors associated with poor presenting VA defined as VA<54 letters, in descending order of odds for risk of poor VA were foveal atrophy, foveal fibrosis, loss of integrity of foveal EZ/ELM, foveal IRF, foveal SHRM and increase in CST. Once detected to have nAMD, most treatment regimens start with a loading phase of monthly injections for 3 months and the post-loading visit outcome is an important decision point to assess early treatment response as a proportion of these eyes will have residual fluid. My study found that presence of only SRF, CST >418 microns and presence of VMT were features associated with increased odds of residual fluid post loading.

This information is critical for various reasons. Primary utility is in disease prognostication. Presenting visual acuity is the strongest risk factor of poor visual outcomes. An essential unmet need to improving visual outcomes is reduction in “first eye gap” in terms of presenting visual acuity. Detection of aforementioned features on OCT prior to vision loss would help reduce this gap (Zarranz-Ventura, Liew et al. 2014). Additionally, as presenting VA is the best predictor of final VA outcome in these eyes, the morphological factors that determine baseline VA will help clinicians to relate the reasons for the presenting VA to the likely outcome while communicating with patients. This helps planning management pathway and prognostication for these patients. This evidence regarding features associated with poor VA strengthens the argument for close monitoring of second eyes for early detection of exudative nAMD. Secondly, these results find relevance in designing clinical management pathways for the suboptimal responder.

Eyes with residual fluid after loading phase need to continue on the loading phase of anti-VEGF therapy or be switched to another agent that has a combination of anti-VEGF and another anti-angiogenic agent such as anti-angiopoietin-2. For example, based on my results we know, a treatment naïve nAMD eye that shows evidence of increased CST on OCT, will have poor baseline VA and presence of residual fluid post loading dose of anti VEGF therapy. It might be prudent then to plan treatment at shorter intervals and not extend the patient too early or consider a sustained drug delivery system as this patient would require aggressive therapy. However, if the phenotype at presentation is increased CST with foveal fibrosis, then the approach would potentially change to combining an antifibrotic agent with the anti VEGF therapy. Thus, based on the heterogeneity in OCT features, the treatment pathways can be modulated for improved response.

Finally, these results find an additional relevance in patient selection for clinical trials. As per the results of the AI prediction tool used in the study, the lack of association between vision and post-treatment presence of macular fluid further strengthens the hypothesis that being able to identify baseline fluid is not sufficient for an accurate anatomic response prediction. Therefore, phenotypic heterogeneity in baseline OCT features (as mentioned in Chapter 4, section 4.2 and 4.3) are critical determinants of final visual and morphological outcomes. Applying this method to the entry process of candidates into randomised controlled trials may contribute to the success of such trials and further inform personalised care. Based on findings from the short-term response analysis, I propose a working classification for eyes with neovascular AMD which incorporates post loading outcome prediction (Table 6.2).

Table 6.2 Proposed imaging-based classification for nAMD based on the results of this thesis.

	Visual acuity	**Features in central 1 mm**	**CST**
Relevant features	Presenting VA <54 letters	Fibrosis or SHRM IRF	≥418 microns
Score	2	2 (1 each for fibrosis or SHRM), 1 for IRF	1
nAMD – Grade 3	Total score 4-6 : Highest odds of poor outcome post loading[#]		
nAMD – Grade 2	Total score 2-4 : Likely poor outcome post loading[#]		
nAMD – Grade 1	Total score < 2: Least odds of poor outcome post loading[#]		

 # Outcome defined as presence of early residual fluid or decrease in visual acuity from baseline.

The other highlight of my work in nAMD eyes was that I found significant variations in long term outcomes post anti VEGF treatment which could in part be explained by phenotypic heterogeneity both at baseline and during the course of treatment. The most substantial finding was that both fibrosis and atrophy impacted visual outcomes, however those with only atrophy had worst visual outcomes. Additionally, eyes with any new fibrosis also had the highest prevalence of macular atrophy. Querques et al discuss two distinct phenotypic subgroups of fibrosis: (1) fibrocellular group – development of scar and (2) fibrovascular group – absence of leakage, wherein the fibrocellular group which had residual vessels with reduced perfusion on OCTA leading to higher incidence of RPE atrophy and worse functional outcomes in these eyes (Querques, Parravano et al. 2020). Further research into the interdependence of these features might add to our understanding of their pathogenesis.

As both fibrosis and atrophy impact VA, I also studied what phenotypic feature is the primary determinant of these. Among the three indicators of disease activity i.e., RPE detachments, IRF and SRF, RPE detachments are largely refractory to treatment with anti-VEGF therapy and longstanding persistent IRF is considered a sign of irreversible retinal damage and therefore should not prompt treatment (Kodjikian, Parravano et al. 2021). Therefore, does SRF largely determine visual and morphological outcomes over long term therapy? I found that persistence of SRF had a protective effect on the retina, eyes with persistent SRF had the highest probability of no atrophy and 2nd highest probability of no fibrosis. These results are in line with those of the FLUID study (Guymer, Markey et al. 2019). But then again eyes with early drying of fluid had lowest risks for development of fibrosis. These findings support previous reports that significant heterogeneity exists within eyes with SRF, therefore it is imperative to tease out the associated characteristics present along with SRF as they all have varying natural histories and impact the VA outcome. Are there other associations on imaging to look for while deciding which patient would do well with a completely dry retina versus another who would be better with some residual SRF? For instance, the presence of SHRM along with persistent SRF may have differing outcomes compared to presence of IRF with persistent SRF. These factors were not studied my current work presented here but I plan to study them in this dataset in the future.

As discussed above, there is evidence that SRF may in fact be exuding from MNV that is nurturing the outer retina. So, would it be appropriate to aggressively treat these eyes, or would it be better to defer treatment in these cases? My results show that by and large tolerating some SRF led to better visual and anatomical outcomes. However, fluctuation in SRF did lead to highest probability of fibrosis and early drying was protective against fibrosis. Currently, it is difficult to decipher the protective effect of MNV or SRF on preserving the health of the outer retina. Therefore, in clinical practice it would be best to individualize the treatment regime keeping in mind the heterogeneity in response.

The various aspects of heterogeneity of progression of GA and the implications it has on outcome measures in clinical trials is discussed in Chapter 5. There exists large variation in the design characteristics of GA treatment trials nevertheless expansion of GA is the most frequently employed primary outcome. As GA lesions exhibit significant heterogeneity in lesion morphology, use of change in area - measure of growth rate as an outcome in clinical trials might not be ideal. Use of linear distance growth instead has been reported as more independent measure of GA (Uji, Nittala et al. 2019, Shen, Sun et al. 2020). I noted small lesions showed higher linear growth than larger GA lesions and there was no statistically significant correlation between area-based measures and linear measures. Therefore, there is a fundamental flaw in the way we report the most commonly used outcome measure for GA in interventional trials. I also found that eyes with SDD, junctional changes at transition zone on FAF, and multifocal lesions had higher progression rates by both area and linear based measures of growth rate. Therefore, I propose the measurement of GA expansion be modelled based on individual biomarkers present in that particular eye.

One of the key design characteristics of a clinical trial for GA is the eligibility criteria. For GA studies this would entail accurate identification of true atrophic lesions for inclusion in the trial. The cRORA definition includes presence of 3 main features i.e., zone if 250 microns hyper transmission, RPE attenuation and outer retinal layer subsidence. However, I found variability in detection of each of these features. The subjectivity of these parameters was evident with high intra-grader agreement as parameters assessed inaccurately across one set of images were assessed incorrectly across the second set. CAM report 6 also looked at intergrader agreement for grading these

parameters and their results were similar to my work with variations in agreement for each of these features (Wu, Pfau et al. 2022). This could be attributed to the microstructural phenotypic heterogeneity that exists in OCT features defining atrophy.

For example, a cRORA lesion overlying a drusen would have a different feature combination profile from a cRORA lesion that has developed over a collapsed drusen or a flat RPE. The highly refractile or fibrous contents of some drusen may block hyper transmission or, remnants of atrophied RPE as persistent laminar deposits in a cRORA lesion may attribute a different feature profile to it. These inconsistencies can also be explained by the differential prevalence of these individual features in a group of cRORA lesions indicating that atrophy on OCT has significant variations and each lesion may not have the entire deck of lesions as per definition. Heterogeneity would also impact eligibility criteria for trials and in-trial assessments. For instance, let's consider two cRORA lesions, example 1: a cRORA lesion overlying a drusen with patchy EZ/ELM disruption and example 2: a cRORA lesion with RPE remnants as persistent laminar deposit might meet the criteria for inclusion into the same trial. However, each of these might respond differentially to an intervention. This could be due to variation in target molecule of drug, i.e., a drug that preserves PR loss may show better outcome in case of the first cRORA lesion whereas a drug that targets RPE preservation may do well in the second situation. An additional factor could be the contents of the drusen influencing drug pharmacodynamics. My results exemplify the unmet need to further refine the definition for atrophy classification and make it inclusive of phenotypic heterogeneity and objective in nature.

I studied another element of heterogeneity in GA growth which is directionality of growth. This directionality of growth is highly relevant while recruiting patients with preserved fovea in a clinical trial. Ex-ante identification of aggressive GA border towards fovea would aid selection of high-risk patients into clinical trials. This is also important keeping in mind the regional therapeutic approaches (stem cell injection and subretinal therapies) which may be delivered to a specific quadrant. Thus, the practical question is how we identify these edges on the most commonly performed imaging modality i.e., OCT. To answer this question, I studied the edges of atrophic lesions and found that irrespective of whether the edge was a fast or slow progressing edge, at baseline they appeared similar. As these images were 12 months apart, I hypothesized that there are

interim events at shorter intervals that attributes the edge its progression rate and thereby directionality to the lesion itself. This event could be photoreceptor disruption or loss which could act as the precursor lesion.

Photoreceptor loss has been shown to be an early atrophic sign for high-risk iAMD (Wang, Sadda et al. 2023). In geographic atrophy where progression means irreversible RPE cell loss the objective identification of an early sign of progression would be valuable. It would function as an ideal early surrogate marker of progression and valuable clinical trial end point to study the efficacy of intervention. As it is a subtle and potentially subjective marker, I used an automated method to measure PR loss using the metric EZ:ELM ratio. I found that en-face maps of photoreceptor loss versus RPE loss showed significantly rapid progression as early as 3 months follow up period.

To summarize these structural markers may be indicators of disease progression preceding the final event of RPE cell death. Therefore, modelling of progression growth rates based on multi-modal imaging markers as an outcome measure for clinical trial might be the way forward. Collating all my findings from the work done on phenotypic heterogeneity in eyes with geographic atrophy, I propose a granular working classification of atrophy eyes to aid better patient selection in clinical trials and better design of clinical trial outcomes. (Table 6.3).

Table 6.3 Proposed imaging based classification for GA based on the results of this thesis.

	On OCT – mandatory to be present	**On OCT – other features**	**En-face OCT**	**On FAF**
Features	Continuous choroidal hypertransmission ≥ 250 µ Subsidence of inner retinal layers	SDD Thin choroid	Decreasing trend in EZ/ELM ratio within 500 µ transition zone	Patchy/diffuse changes in transition zone Multifocal lesions Extrafoveal location
Atrophy-Fast progressor	Presence of one or both mandatory features with 2 or more features on OCT and FAF inclusive of SDD/multifocality			
Atrophy – slow progressor	Presence of one or both mandatory features with 2 or more features on OCT and FAF exclusive of SDD/multifocality			

In conclusion, heterogeneity both at presentation and along the course of therapy is a significant determinant of final outcomes in eyes with varying severity of AMD. It is important to remember that this heterogeneity exists across patient demographic factors, imaging features and treatment regimens and each of these factors modulate the outcomes via a complex relationship. To be able to dissect the complex interplay among these features completely would certainly aid accurate prediction of response in these eyes. The results of my work in this thesis help to partly explain this conundrum by showing that variations in imaging features on OCT play a considerable part in defining an individuals' disease progression and/or final structural and functional outcomes.

6.2 Future work

The studies reported in this thesis provide a better understanding of the phenotypic heterogeneity in both non-neovascular and nAMD. Yet the completed studies raise multiple relevant questions which have the potential to be answered in future research. Here I discuss potential future projects stemming from the work done in this thesis.

A primary challenge for AMD drug discovery is the de facto standard endpoint in ophthalmic clinical trials, change in BCVA over time. Despite multiple activities of daily living affected by ocular disease (e.g., walking, reading, driving, grasping, and eye movements), BCVA only measures fine visual resolution which is not clinically meaningful in early AMD or extrafoveal GA given the variability in visual assessment. Therefore, for non-neovascular AMD and especially GA drug discovery, visual acuity endpoint is an insensitive endpoint and require impractical large or long clinical trials. Function endpoints other than visual acuity such as LLVA can also be considered for regulatory approval, but so far, no therapy has been approved by this means. Thus, to expedite intervention trials, it is paramount critical to explore the correlation of alternative functional measures such as LLVA and RIT to OCT markers.

Secondly, I have shown that several visual function tests may be affected in AMD independent of the current AMD classification based on CFP. These markers of disease progression on CFP are slowly progressive, which means that large and lengthy clinical trials are required to detect clinically meaningful treatment effects for preventative options or treatment of non-neovascular AMD. To shorten clinical trial duration, the OCT classification could be used. For this purpose, we need to validate the structural markers

identified in this thesis as surrogate for early disease progression that could also precede visual function deficits. Based on results of chapter 2 and 4 I propose a prospective observational study on eyes with high-risk iAMD and GA. The aim of the study will be to identify OCT imaging biomarkers of disease progression as early as 3 to 6 months.

I also found a correlation between thinner choroid and effects on visual cycle evidenced by a prolonged RIT in eyes with AMD, especially SDD. Nitric oxide (NO) is a known potent vasodilator and has a key role in regulating vascular tone in the choroid. Sildenafil acts by augmenting the effect of NO by inhibiting phosphodiesterase 5 (PDE5) and thereby preventing degradation of cyclic guanosine monophosphate (cGMP). Subject to autonomic control, choroid can undergo cGMP mediated smooth muscle relaxation that can lead to choroidal congestion. The importance of studying choroidal circulation lies in the fact that an elevated choroidal blood flow directly impacts retina and RPE (Arora, Surakiatchanukul et al. 2022). Therefore, drugs increasing choroidal blood flow like sildenafil could be used therapeutically in diseases where choroidal ischaemia is present.

With regards to its effect on the visual cycle, inhibition of PDE6 with sildenafil would lead to inhibition of cGMP hydrolysis thereby mimicking changes to photoreceptors in the dark. Thus, sildenafil simulates biochemical changes that occur in darkness and inhibits shedding of ROS. Additionally, sildenafil inhibits thickening of BrM by decreasing Warburg glycolysis and promotes recovery of EZ (Arora, Surakiatchanukul et al. 2022). My hypothesis is, if sildenafil is shown to improve choroidal perfusion in eyes with dry AMD, it can potentially be used as treatment in eye with AMD with choroidal ischaemia. Also, improvement in dark adaptation will mechanistically prove that there is a relation of rod dysfunction with impaired choroidal perfusion in AMD. Sildenafil is readily accessible, and the results will inform the need for larger trials on Sildenafil and other interventions to improve choroidal non-perfusion.

Another area of potential future work is in the treatment of fibrosis in nAMD. Development of therapies for prevention of fibrosis in nAMD remains an unmet need and evidence has shown that anti VEGF therapy does not prevent fibrosis. Drug development in this area requires adequate characterization of fibrosis with standardized terms for establishment of endpoint and biomarkers. My work in this thesis

has identified baseline features that increased the odds of development of fibrosis following anti VEGF therapy. The fibrotic process is a complex interplay of various factors involving multiple molecular mediators and pathways for example cytokine, chemokine and toll-like receptor (TLR) antagonists, angiogenesis inhibitors, TGFβ signalling modifiers, immune cell modulators, or stem/progenitor cell transplantation strategies. Combination of anti-platelet derived growth factor therapy and anti VEGF therapy has given encouraging results in pre-clinical data and might be promising in the future.

6.3 Outputs from this thesis

6.3.1 Peer reviewed manuscripts

1. **Chandra S**, Grewal MK, Gurudas S, et al. Quantitative Autofluorescence in Non-Neovascular Age Related Macular Degeneration. *Biomedicines*. 2023;11(2):560. Published 2023 Feb 15. doi:10.3390/biomedicines11020560

2. **Chandra S**, Gurudas S, Burton BJL, et al. Associations of presenting visual acuity with morphological changes on OCT in neovascular age-related macular degeneration: PRECISE Study Report 2 [published online ahead of print, 2023 Oct 18]. *Eye (Lond)*. 2023;10.1038/s41433-023-02769-5. doi:10.1038/s41433-023-02769-5

3. **Chandra S**, Gurudas S, Pearce I, et al. Baseline characteristics of eyes with early residual fluid post loading phase of aflibercept therapy in neovascular AMD: PRECISE Study Report 3 – Accepted for publication

4. Chorev M*, Haderlein J*, **Chandra S***, et al. A Multi-Modal AI-Driven Cohort Selection Tool to Predict Suboptimal Non-Responders to Aflibercept Loading-Phase for Neovascular Age-Related Macular Degeneration: PRECISE Study Report 1. *J Clin Med*. 2023;12(8):3013. Published 2023 Apr 20. doi:10.3390/jcm12083013 **Joint first author*

5. **Chandra S**, Arpa C, Menon D, et al. Ten-year outcomes of anti-vascular endothelial growth factor therapy in neovascular age-related macular degeneration. *Eye (Lond)*. 2020;34(10):1888-1896. doi:10.1038/s41433-020-0764-9

6. **Chandra S**, Rasheed R, Menon D, et al. Impact of injection frequency on 5-year real-world visual acuity outcomes of aflibercept therapy for neovascular age-related macular degeneration. *Eye (Lond)*. 2021;35(2):409-417. doi:10.1038/s41433-020-0851-y

7. Sivaprasad S, **Chandra S**, Kwon J, Khalid N, Chong V. Perspectives from clinical trials: is geographic atrophy one disease? *Eye (Lond)*. 2023;37(3):402-407. doi:10.1038/s41433-022-02115-1

8. **Chandra S**, Rasheed R, Sen P, Menon D, Sivaprasad S. Inter-rater reliability for diagnosis of geographic atrophy using spectral domain OCT in age-related macular degeneration. *Eye (Lond)*. 2022;36(2):392-397. doi:10.1038/s41433-021-01490-5

6.3.2 Conference abstracts

1. European Society of Retina Specialists- EURETINA 2019- Free paper Oral Presentation. *10-year outcome of antiVEGF therapy in neovascular AMD*. **Shruti Chandra**; Deepthy Menon; Sobha Sivaprasad.

2. Association for Research in Vision and Ophthalmology – ARVO 2020 – Virtual Poster Presentation. *Progression of geographic atrophy in Age related Macular degeneration: Comparative analysis of methods of measurement.* **Shruti Chandra**; Joan Nunez; Sarega Gurudas; Daniel Yim; Sobha Sivaprasad.

3. European Society of Retina Specialists- EURETINA 2020- Virtual Free paper Presentation. *Course of sub-retinal fluid over 10 years in patients with neovascular age related macular degeneration and impact on visual acuity.* **Shruti Chandra**; Deepthy Menon; Sobha Sivaprasad.

4. European Society of Retina Specialists- EURETINA 2021- Virtual Free paper Presentation. *Influence of fibrosis on visual outcomes in eyes with neovascular age related macular degeneration.* **Shruti Chandra**; Deepthy Menon, Eleni Karatsai, Sridevi Thottarath, Sobha Sivaprasad.

5. Association for Research in Vision and Ophthalmology – ARVO 2023 – Poster Presentation. *Rod Intercept Time in expanded classification of Non-neovascular Age related Macular Degeneration (AMD).* **Shruti Chandra**; Sarega Gurudas; Manjot K Grewal; Syed Ahmer Raza; Glen Jeffery; Sobha Sivaprasad.

6. Association for Research in Vision and Ophthalmology – ARVO 2024 – Abstract Submitted. *Quantifying photoreceptor health using automated normalised ellipsoid zone reflectivity in age related macular degeneration*. Edward Adams; **Shruti Chandra**; Sobha Sivaprasad.

7 References

(2001). "The Age-Related Eye Disease Study system for classifying age-related macular degeneration from stereoscopic color fundus photographs: the Age-Related Eye Disease Study Report Number 6." Am J Ophthalmol **132**(5): 668-681.

Abdelfattah, N. S., H. Zhang, D. S. Boyer, P. J. Rosenfeld, W. J. Feuer, G. Gregori and S. R. Sadda (2016). "Drusen Volume as a Predictor of Disease Progression in Patients With Late Age-Related Macular Degeneration in the Fellow Eye." Invest Ophthalmol Vis Sci **57**(4): 1839-1846.

Ach, T., C. Huisingh, G. McGwin, Jr., J. D. Messinger, T. Zhang, M. J. Bentley, D. B. Gutierrez, Z. Ablonczy, R. T. Smith, K. R. Sloan and C. A. Curcio (2014). "Quantitative autofluorescence and cell density maps of the human retinal pigment epithelium." Invest Ophthalmol Vis Sci **55**(8): 4832-4841.

Ach, T., E. Tolstik, J. D. Messinger, A. V. Zarubina, R. Heintzmann and C. A. Curcio (2015). "Lipofuscin redistribution and loss accompanied by cytoskeletal stress in retinal pigment epithelium of eyes with age-related macular degeneration." Invest Ophthalmol Vis Sci **56**(5): 3242-3252.

Alten, F., C. R. Clemens, P. Heiduschka and N. Eter (2013). "Localized reticular pseudodrusen and their topographic relation to choroidal watershed zones and changes in choroidal volumes." Invest Ophthalmol Vis Sci **54**(5): 3250-3257.

Amato, A., A. Arrigo, F. Borghesan, E. Aragona, C. Vigano, A. Saladino, F. Bandello and M. Battaglia Parodi (2022). "Baseline sattler layer-choriocapillaris complex thickness cutoffs associated with age-related macular degeneration progression." Retina **42**(9): 1683-1692.

Arepalli, S. and P. K. Kaiser (2021). "Pipeline therapies for neovascular age related macular degeneration." International Journal of Retina and Vitreous **7**(1): 55.

Arora, S., T. Surakiatchanukul, T. Arora, C. Cagini, M. Lupidi and J. Chhablani (2022). "Sildenafil in ophthalmology: An update." Survey of Ophthalmology 67(2): 463-487.

Beatty, S., I. J. Murray, D. B. Henson, D. Carden, H. Koh and M. E. Boulton (2001). "Macular pigment and risk for age-related macular degeneration in subjects from a Northern European population." Invest Ophthalmol Vis Sci **42**(2): 439-446.

Bhatt, A. (2021). "Artificial intelligence in managing clinical trial design and conduct: Man and machine still on the learning curve?" Perspect Clin Res **12**(1): 1-3.

Bhutto, I. A., K. Uno, C. Merges, L. Zhang, D. S. McLeod and G. A. Lutty (2008). "Reduction of endogenous angiogenesis inhibitors in Bruch's membrane of the submacular region in eyes with age-related macular degeneration." Arch Ophthalmol **126**(5): 670-678.

Bill, A., P. Törnquist and A. Alm (1980). "Permeability of the intraocular blood vessels." Trans Ophthalmol Soc U K (1962) **100**(3): 332-336.

Bindewald, A., A. C. Bird, S. S. Dandekar, J. Dolar-Szczasny, J. Dreyhaupt, F. W. Fitzke, W. Einbock, F. G. Holz, J. J. Jorzik, C. Keilhauer, N. Lois, J. Mlynski, D. Pauleikhoff, G. Staurenghi and S. Wolf (2005). "Classification of fundus autofluorescence patterns in early age-related macular disease." Invest Ophthalmol Vis Sci **46**(9): 3309-3314.

Bindewald, A., S. Schmitz-Valckenberg, J. J. Jorzik, J. Dolar-Szczasny, H. Sieber, C. Keilhauer, A. W. Weinberger, S. Dithmar, D. Pauleikhoff, U. Mansmann, S. Wolf and F. G. Holz (2005). "Classification of abnormal fundus autofluorescence patterns in the junctional zone of geographic atrophy in patients with age related macular degeneration." Br J Ophthalmol **89**(7): 874-878.

Bogunovic, H., S. M. Waldstein, T. Schlegl, G. Langs, A. Sadeghipour, X. Liu, B. S. Gerendas, A. Osborne and U. Schmidt-Erfurth (2017). "Prediction of Anti-VEGF Treatment Requirements in Neovascular AMD Using a Machine Learning Approach." Invest Ophthalmol Vis Sci **58**(7): 3240-3248.

Borrelli, E., A. Uji, D. Sarraf and S. R. Sadda (2017). "Alterations in the Choriocapillaris in Intermediate Age-Related Macular Degeneration." Invest Ophthalmol Vis Sci **58**(11): 4792-4798.

Brandl, C., M. E. Zimmermann, F. Günther, T. Barth, M. Olden, S. C. Schelter, F. Kronenberg, J. Loss, H. Küchenhoff, H. Helbig, B. H. F. Weber, K. J. Stark and I. M. Heid (2018). "On the impact of different approaches to classify age-related macular degeneration: Results from the German AugUR study." Sci Rep **8**(1): 8675.

Bressler, N. M., S. B. Bressler and E. S. Gragoudas (1987). "Clinical characteristics of choroidal neovascular membranes." Arch Ophthalmol **105**(2): 209-213.

Bui, P. T. A., G. S. Reiter, M. Fabianska, S. M. Waldstein, C. Grechenig, H. Bogunovic, M. Arikan and U. Schmidt-Erfurth (2022). "Fundus autofluorescence and optical coherence tomography biomarkers associated with the progression of geographic atrophy secondary to age-related macular degeneration." Eye (Lond) **36**(10): 2013-2019.

Burke, T. R., T. Duncker, R. L. Woods, J. P. Greenberg, J. Zernant, S. H. Tsang, R. T. Smith, R. Allikmets, J. R. Sparrow and F. C. Delori (2014). "Quantitative fundus autofluorescence in recessive Stargardt disease." Invest Ophthalmol Vis Sci **55**(5): 2841-2852.

Camino, A., Y. Guo, Q. You, J. Wang, D. Huang, S. T. Bailey and Y. Jia (2019). "Detecting and measuring areas of choriocapillaris low perfusion in intermediate, non-neovascular age-related macular degeneration." Neurophotonics **6**(4): 041108.

Capuano, V., E. H. Souied, A. Miere, C. Jung, E. Costanzo and G. Querques (2016). "Choroidal maps in non-exudative age-related macular degeneration." Br J Ophthalmol **100**(5): 677-682.

Cascella, R., C. Strafella, G. Longo, L. Manzo, M. Ragazzo, C. De Felici, S. Gambardella, L. T. Marsella, G. Novelli, P. Borgiani, F. Sangiuolo, A. Cusumano, F. Ricci and E. Giardina (2018). "Assessing individual risk for AMD with genetic counseling, family history, and genetic testing." Eye (Lond) **32**(2): 446-450.

Chaudhary, V., F. G. Holz, S. Wolf, E. Midena, E. H. Souied, H. Allmeier, G. Lambrou, T. Machewitz and P. Mitchell (2022). "Association Between Visual Acuity and Fluid Compartments with Treat-and-Extend Intravitreal Aflibercept in Neovascular Age-Related Macular Degeneration: An ARIES Post Hoc Analysis." Ophthalmol Ther **11**(3): 1119-1130.

Chaudhary, V., F. Matonti, J. Zarranz-Ventura and M. W. Stewart (2022). "Impact of fluid compartments on functional outcomes for patients with neovascular age-related macular degeneration: A Systematic Literature Review." Retina **42**(4): 589-606.

Chen, L., J. D. Messinger, Y. Zhang, R. F. Spaide, K. B. Freund and C. A. Curcio (2020). "Subretinal drusenoid deposit in age-related macular degeneration: Histologic Insights Into Initiation, Progression to Atrophy, and Imaging." Retina **40**(4): 618-631.

Cheng, H., P. A. Kaszubski, H. Hao, C. Saade, C. Cunningham, K. B. Freund and R. T. Smith (2016). "The Relationship Between Reticular Macular Disease and Choroidal Thickness." Curr Eye Res **41**(11): 1492-1497.

Cheng, Q. E., J. Gao, B. J. Kim and G. S. Ying (2018). "Design Characteristics of Geographic Atrophy Treatment Trials: Systematic Review of Registered Trials in ClinicalTrials.gov." Ophthalmol Retina **2**(6): 518-525.

Cheung, C. M. G., D. S. Grewal, K. Y. C. Teo, A. Gan, A. Mohla, U. Chakravarthy, T. Y. Wong and G. J. Jaffe (2019). "The Evolution of Fibrosis and Atrophy and Their Relationship with Visual Outcomes in Asian Persons with Neovascular Age-Related Macular Degeneration." Ophthalmol Retina **3**(12): 1045-1055.

Cheung CMG, R. H. G., Anna-Maria Demetriades, Philippe Margaron, Carlos Quezada Ruiz, David Silverman, Jane Ives, Karen Basu, Audrey Souverain, Ming Yang, Hugh Lin. (2022). Faricimab in Neovascular Age-Related Macular Degeneration (nAMD): Efficacy, Safety, and Durability Through Week 48 in the Phase 3 TENAYA and LUCERNE Trials. 22nd EURETINA Hamburg, Germany.

Christensen, D. R. G., F. E. Brown, A. J. Cree, J. A. Ratnayaka and A. J. Lotery (2017). "Sorsby fundus dystrophy - A review of pathology and disease mechanisms." Exp Eye Res **165**: 35-46.

Clemens, C. R., A. Wolf, F. Alten, C. Milojcic, P. Heiduschka and N. Eter (2017). "Response of vascular pigment epithelium detachment due to age-related macular degeneration to monthly treatment with ranibizumab: the prospective, multicentre RECOVER study." Acta Ophthalmol **95**(7): 683-689.

Colijn, J. M., M. Meester-Smoor, T. Verzijden, A. de Breuk, R. Silva, B. M. J. Merle, A. Cougnard-Grégoire, C. B. Hoyng, S. Fauser, A. Coolen, C. Creuzot-Garcher, H. W. Hense, M. Ueffing, C. Delcourt, A. I. den Hollander and C. C. W. Klaver (2021). "Genetic Risk, Lifestyle, and Age-Related Macular Degeneration in Europe: The EYE-RISK Consortium." Ophthalmology **128**(7): 1039-1049.

Corvi, F., L. Tiosano, G. Corradetti, M. G. Nittala, S. Lindenberg, A. R. Alagorie, J. A. McLaughlin, T. K. Lee and S. R. Sadda (2021). "Choriocapillaris flow deficits as a risk factor for progression of age-related macular degeneration." Retina **41**(4): 686-693.

Coscas, G., U. De Benedetto, F. Coscas, C. I. Li Calzi, S. Vismara, F. Roudot-Thoraval, F. Bandello and E. Souied (2013). "Hyperreflective dots: a new spectral-domain optical coherence tomography entity for follow-up and prognosis in exudative age-related macular degeneration." Ophthalmologica **229**(1): 32-37.

Csaky, K., F. Ferris, 3rd, E. Y. Chew, P. Nair, J. K. Cheetham and J. L. Duncan (2017). "Report From the NEI/FDA Endpoints Workshop on Age-Related Macular Degeneration and Inherited Retinal Diseases." Invest Ophthalmol Vis Sci **58**(9): 3456-3463.

Csincsik, L., K. A. Muldrew, A. Bettiol, D. M. Wright, P. J. Rosenfeld, N. K. Waheed, T. Empeslidis, E. De Cock, T. C. N. Yamaguchi, R. E. Hogg, T. Peto and U. Chakravarthy (2023). "The Double Layer Sign Is Highly Predictive of Progression to Exudation in Age-Related Macular Degeneration." Ophthalmol Retina.

Curcio, C. A. (2018). "Antecedents of Soft Drusen, the Specific Deposits of Age-Related Macular Degeneration, in the Biology of Human Macula." Invest Ophthalmol Vis Sci **59**(4): Amd182-amd194.

Curcio, C. A. (2018). "Soft Drusen in Age-Related Macular Degeneration: Biology and Targeting Via the Oil Spill Strategies." Invest Ophthalmol Vis Sci **59**(4): Amd160-amd181.

Curcio, C. A., M. Johnson, J. D. Huang and M. Rudolf (2009). "Aging, age-related macular degeneration, and the response-to-retention of apolipoprotein B-containing lipoproteins." Prog Retin Eye Res **28**(6): 393-422.

Curcio, C. A., J. D. Messinger, K. R. Sloan, G. McGwin, N. E. Medeiros and R. F. Spaide (2013). "Subretinal drusenoid deposits in non-neovascular age-related macular degeneration: morphology, prevalence, topography, and biogenesis model." Retina **33**(2): 265-276.

Curcio, C. A. and C. L. Millican (1999). "Basal linear deposit and large drusen are specific for early age-related maculopathy." Arch Ophthalmol **117**(3): 329-339.

Damian, I. and S. D. Nicoară (2022). "SD-OCT Biomarkers and the Current Status of Artificial Intelligence in Predicting Progression from Intermediate to Advanced AMD." Life (Basel) **12**(3).

Davis, M. D., R. E. Gangnon, L. Y. Lee, L. D. Hubbard, B. E. Klein, R. Klein, F. L. Ferris, S. B. Bressler and R. C. Milton (2005). "The Age-Related Eye Disease Study severity

scale for age-related macular degeneration: AREDS Report No. 17." Arch Ophthalmol **123**(11): 1484-1498.

de Oliveira Dias, J. R., Q. Zhang, J. M. B. Garcia, F. Zheng, E. H. Motulsky, L. Roisman, A. Miller, C. L. Chen, S. Kubach, L. de Sisternes, M. K. Durbin, W. Feuer, R. K. Wang, G. Gregori and P. J. Rosenfeld (2018). "Natural History of Subclinical Neovascularization in Nonexudative Age-Related Macular Degeneration Using Swept-Source OCT Angiography." Ophthalmology **125**(2): 255-266.

Delori, F. C., M. R. Fleckner, D. G. Goger, J. J. Weiter and C. K. Dorey (2000). "Autofluorescence distribution associated with drusen in age-related macular degeneration." Invest Ophthalmol Vis Sci **41**(2): 496-504.

Demirs, J. T., J. Yang, M. A. Crowley, M. Twarog, O. Delgado, Y. Qiu, S. Poor, D. S. Rice, T. P. Dryja, K. Anderson and S. M. Liao (2021). "Differential and Altered Spatial Distribution of Complement Expression in Age-Related Macular Degeneration." Invest Ophthalmol Vis Sci **62**(7): 26.

Detaram, H. D., N. Joachim, G. Liew, K. V. Vu, G. Burlutsky, P. Mitchell and B. Gopinath (2020). "Smoking and treatment outcomes of neovascular age-related macular degeneration over 12 months." Br J Ophthalmol **104**(7): 893-898.

Domalpally, A., R. Danis, E. Agrón, B. Blodi, T. Clemons and E. Chew (2016). "Evaluation of Geographic Atrophy from Color Photographs and Fundus Autofluorescence Images: Age-Related Eye Disease Study 2 Report Number 11." Ophthalmology **123**(11): 2401-2407.

Domalpally, A., R. P. Danis, J. White, A. Narkar, T. Clemons, F. Ferris and E. Chew (2013). "Circularity index as a risk factor for progression of geographic atrophy." Ophthalmology **120**(12): 2666-2671.

Dugel, P. U., A. Koh, Y. Ogura, G. J. Jaffe, U. Schmidt-Erfurth, D. M. Brown, A. V. Gomes, J. Warburton, A. Weichselberger and F. G. Holz (2020). "HAWK and HARRIER: Phase 3, Multicenter, Randomized, Double-Masked Trials of Brolucizumab for Neovascular Age-Related Macular Degeneration." Ophthalmology **127**(1): 72-84.

Duker, J. S., P. K. Kaiser, S. Binder, M. D. de Smet, A. Gaudric, E. Reichel, S. R. Sadda, J. Sebag, R. F. Spaide and P. Stalmans (2013). "The International Vitreomacular

Traction Study Group classification of vitreomacular adhesion, traction, and macular hole." Ophthalmology **120**(12): 2611-2619.

Eleftheriadou, M., M. Gemenetzi, M. Lukic, S. Sivaprasad, P. G. Hykin, R. D. Hamilton, R. Rajendram, A. Tufail and P. J. Patel (2018). "Three-Year Outcomes of Aflibercept Treatment for Neovascular Age-Related Macular Degeneration: Evidence from a Clinical Setting." Ophthalmol Ther **7**(2): 361-368.

Eleftheriadou, M., C. Vazquez-Alfageme, C. M. Citu, R. Crosby-Nwaobi, S. Sivaprasad, P. Hykin, R. D. Hamilton and P. J. Patel (2017). "Long-Term Outcomes of Aflibercept Treatment for Neovascular Age-Related Macular Degeneration in a Clinical Setting." Am J Ophthalmol **174**: 160-168.

Farazdaghi, M. K. and K. B. Ebrahimi (2019). "Role of the Choroid in Age-related Macular Degeneration: A Current Review." J Ophthalmic Vis Res **14**(1): 78-87.

Fernández, E. J., B. Hermann, B. Povazay, A. Unterhuber, H. Sattmann, B. Hofer, P. K. Ahnelt and W. Drexler (2008). "Ultrahigh resolution optical coherence tomography and pancorrection for cellular imaging of the living human retina." Opt Express **16**(15): 11083-11094.

Ferris, F. L., 3rd, C. P. Wilkinson, A. Bird, U. Chakravarthy, E. Chew, K. Csaky and S. R. Sadda (2013). "Clinical classification of age-related macular degeneration." Ophthalmology **120**(4): 844-851.

Ferris, F. L., M. D. Davis, T. E. Clemons, L. Y. Lee, E. Y. Chew, A. S. Lindblad, R. C. Milton, S. B. Bressler and R. Klein (2005). "A simplified severity scale for age-related macular degeneration: AREDS Report No. 18." Arch Ophthalmol **123**(11): 1570-1574.

Feuer, W. J., Z. Yehoshua, G. Gregori, F. M. Penha, E. Y. Chew, F. L. Ferris, T. E. Clemons, A. S. Lindblad and P. J. Rosenfeld (2013). "Square root transformation of geographic atrophy area measurements to eliminate dependence of growth rates on baseline lesion measurements: a reanalysis of age-related eye disease study report no. 26." JAMA Ophthalmol **131**(1): 110-111.

Fleckenstein, M., T. D. L. Keenan, R. H. Guymer, U. Chakravarthy, S. Schmitz-Valckenberg, C. C. Klaver, W. T. Wong and E. Y. Chew (2021). "Age-related macular degeneration." Nat Rev Dis Primers **7**(1): 31.

Fleckenstein, M., P. Mitchell, K. B. Freund, S. Sadda, F. G. Holz, C. Brittain, E. C. Henry and D. Ferrara (2018). "The Progression of Geographic Atrophy Secondary to Age-Related Macular Degeneration." Ophthalmology **125**(3): 369-390.

Fragiotta, S., S. Abdolrahimzadeh, R. Dolz-Marco, Y. Sakurada, O. Gal-Or and G. Scuderi (2021). "Significance of Hyperreflective Foci as an Optical Coherence Tomography Biomarker in Retinal Diseases: Characterization and Clinical Implications." J Ophthalmol **2021**: 6096017.

Friedman, E. and M. O. Ts'o (1968). "The retinal pigment epithelium. II. Histologic changes associated with age." Arch Ophthalmol **79**(3): 315-320.

Fujimoto, J. G., C. Pitris, S. A. Boppart and M. E. Brezinski (2000). "Optical coherence tomography: an emerging technology for biomedical imaging and optical biopsy." Neoplasia **2**(1-2): 9-25.

Fung, A. T., J. Galvin and T. Tran (2021). "Epiretinal membrane: A review." Clin Exp Ophthalmol **49**(3): 289-308.

Garcia-Garcia, J., R. Usategui-Martin, M. R. Sanabria, E. Fernandez-Perez, J. J. Telleria and R. M. Coco-Martin (2022). "Pathophysiology of Age-Related Macular Degeneration: Implications for Treatment." Ophthalmic Res **65**(6): 615-636.

Gehrs, K. M., D. H. Anderson, L. V. Johnson and G. S. Hageman (2006). "Age-related macular degeneration--emerging pathogenetic and therapeutic concepts." Ann Med **38**(7): 450-471.

Gelfand, B. D. and J. Ambati (2016). "A Revised Hemodynamic Theory of Age-Related Macular Degeneration." Trends Mol Med **22**(8): 656-670.

Gerardo, L.-G., O.-M. Oscar, A. Sharmina, T. Yuehong, T. Katy, L. Harriet, K. Micaela, S. Maria, P. Cinthi, Y. Catherine, G. Arun, B. Alauddin, S. D. Mandip, D. Avnish, L. Gareth, N. Jagat, B. R. Richard, A. Y. Lawrence, K. B. Freund and S. Roland Theodore (2022). "Subretinal drusenoid deposits are strongly associated with coexistent high-risk vascular diseases." BMJ Open Ophthalmology 7(1): e001154.

Gin, T. J., Z. Wu, S. K. Chew, R. H. Guymer and C. D. Luu (2017). "Quantitative Analysis of the Ellipsoid Zone Intensity in Phenotypic Variations of Intermediate Age-Related Macular Degeneration." Invest Ophthalmol Vis Sci **58**(4): 2079-2086.

Gliem, M., P. L. Müller, R. P. Finger, M. B. McGuinness, F. G. Holz and P. Charbel Issa (2016). "Quantitative Fundus Autofluorescence in Early and Intermediate Age-Related Macular Degeneration." JAMA Ophthalmol **134**(7): 817-824.

Goh, K. L., C. J. Abbott, X. Hadoux, M. Jannaud, L. A. B. Hodgson, P. van Wijngaarden, R. H. Guymer and Z. Wu (2022). "Hyporeflective Cores within Drusen: Association with Progression of Age-Related Macular Degeneration and Impact on Visual Sensitivity." Ophthalmol Retina **6**(4): 284-290.

Greenberg, J. P., T. Duncker, R. L. Woods, R. T. Smith, J. R. Sparrow and F. C. Delori (2013). "Quantitative fundus autofluorescence in healthy eyes." Invest Ophthalmol Vis Sci **54**(8): 5684-5693.

Grewal, M. K., S. Chandra, S. Gurudas, A. Bird, G. Jeffery and S. Sivaprasad (2020). "Exploratory Study on Visual Acuity and Patient-Perceived Visual Function in Patients with Subretinal Drusenoid Deposits." J Clin Med **9**(9).

Grewal, M. K., S. Chandra, S. Gurudas, R. Rasheed, P. Sen, D. Menon, A. Bird, G. Jeffery and S. Sivaprasad (2022). "Functional clinical endpoints and their correlations in eyes with AMD with and without subretinal drusenoid deposits-a pilot study." Eye (Lond) **36**(2): 398-406.

Group, A. R. E. D. S. (2001). "The Age-Related Eye Disease Study system for classifying age-related macular degeneration from stereoscopic color fundus photographs: the Age-Related Eye Disease Study Report Number 6." Am J Ophthalmol **132**(5): 668-681.

Guymer, R. H., F. K. Chen, L. A. B. Hodgson, E. Caruso, C. A. Harper, S. S. Wickremashinghe, A. C. Cohn, P. Sivarajah, N. Tindill, C. D. Luu and Z. Wu (2021). "Subthreshold Nanosecond Laser in Age-Related Macular Degeneration: Observational Extension Study of the LEAD Clinical Trial." Ophthalmol Retina 5(12): 1196-1203.

Guymer, R., P. Luthert and A. Bird (1999). "Changes in Bruch's membrane and related structures with age." Prog Retin Eye Res **18**(1): 59-90.

Guymer, R. H., C. M. Markey, I. L. McAllister, M. C. Gillies, A. P. Hunyor and J. J. Arnold (2019). "Tolerating Subretinal Fluid in Neovascular Age-Related Macular Degeneration Treated with Ranibizumab Using a Treat-and-Extend Regimen: FLUID Study 24-Month Results." Ophthalmology **126**(5): 723-734.

Guymer, R. H., P. J. Rosenfeld, C. A. Curcio, F. G. Holz, G. Staurenghi, K. B. Freund, S. Schmitz-Valckenberg, J. Sparrow, R. F. Spaide, A. Tufail, U. Chakravarthy, G. J. Jaffe, K. Csaky, D. Sarraf, J. M. Monés, R. Tadayoni, J. Grunwald, F. Bottoni, S. Liakopoulos, D. Pauleikhoff, S. Pagliarini, E. Y. Chew, F. Viola, M. Fleckenstein, B. A. Blodi, T. H. Lim, V. Chong, J. Lutty, A. C. Bird and S. R. Sadda (2020). "Incomplete Retinal Pigment Epithelial and Outer Retinal Atrophy in Age-Related Macular Degeneration: Classification of Atrophy Meeting Report 4." Ophthalmology **127**(3): 394-409.

Haensli, C., Y. Sugiura, K. B. Freund and S. A. Zweifel (2021). "Correlation of outer retinal tubulations and choriocapillaris flow signal deficits surrounding geographic atrophy." Retina **41**(9): 1940-1947.

Haines, J. L., M. A. Hauser, S. Schmidt, W. K. Scott, L. M. Olson, P. Gallins, K. L. Spencer, S. Y. Kwan, M. Noureddine, J. R. Gilbert, N. Schnetz-Boutaud, A. Agarwal, E. A. Postel and M. A. Pericak-Vance (2005). "Complement factor H variant increases the risk of age-related macular degeneration." Science **308**(5720): 419-421.

Haj Najeeb, B., G. Deak, U. Schmidt-Erfurth and B. S. Gerendas (2020). "The RAP study, report two: The Regional Distribution of Macular Neovascularization Type 3, a Novel Insight Into Its Etiology." Retina **40**(12): 2255-2262.

Haj Najeeb, B. and U. Schmidt-Erfurth (2023). "Do patients with unilateral macular neovascularization type 3 need AREDS supplements to slow the progression to advanced age-related macular degeneration?" Eye (Lond) **37**(9): 1751-1753.

Hammadi, S., N. Tzoumas, M. Ferrara, I. P. Meschede, K. Lo, C. Harris, M. Lako and D. H. Steel (2023). "Bruch's Membrane: A Key Consideration with Complement-Based Therapies for Age-Related Macular Degeneration." J Clin Med **12**(8).

Hanson, R. L. W., A. Airody, S. Sivaprasad and R. P. Gale (2023). "Optical coherence tomography imaging biomarkers associated with neovascular age-related macular degeneration: a systematic review." Eye (Lond) **37**(12): 2438-2453.

Harrer, S., P. Shah, B. Antony and J. Hu (2019). "Artificial Intelligence for Clinical Trial Design." Trends Pharmacol Sci **40**(8): 577-591.

Hayes, M. J., D. Tracey-White, J. H. Kam, M. B. Powner and G. Jeffery (2021). "The 3D organisation of mitochondria in primate photoreceptors." Sci Rep **11**(1): 18863.

Heier, J. S., A. M. Khanani, C. Quezada Ruiz, K. Basu, P. J. Ferrone, C. Brittain, M. S. Figueroa, H. Lin, F. G. Holz, V. Patel, T. Y. Y. Lai, D. Silverman, C. Regillo, B. Swaminathan, F. Viola, C. M. G. Cheung and T. Y. Wong (2022). "Efficacy, durability, and safety of intravitreal faricimab up to every 16 weeks for neovascular age-related macular degeneration (TENAYA and LUCERNE): two randomised, double-masked, phase 3, non-inferiority trials." Lancet **399**(10326): 729-740.

Helga Kolb, R. F. N., Peter K. Ahnelt, Isabel Ortuño-Lizarán, Nicolas Cuenca (2020 Feb 7 [Updated 2020 May 20]). The Architecture of the Human Fovea. Webvision: The Organization of the Retina and Visual System. Salt Lake City (UT).

Hirabayashi, K., H. J. Yu, Y. Wakatsuki, K. M. Marion, C. C. Wykoff and S. R. Sadda (2023). "OCT Risk Factors for Development of Atrophy in Eyes with Intermediate Age-Related Macular Degeneration." Ophthalmol Retina **7**(3): 253-260.

Hirano, M., Y. Muraoka, T. Kogo, M. Ishikura, N. Nishigori, N. Ueda-Arakawa, M. Miyata, M. Hata, A. Takahashi, M. Miyake and A. Tsujikawa (2023). "Analysis of widefield choroidal thickness maps of healthy eyes using swept source optical coherence tomography." Sci Rep **13**(1): 11904.

Ho, A. C., T. A. Albini, D. M. Brown, D. S. Boyer, C. D. Regillo and J. S. Heier (2017). "The Potential Importance of Detection of Neovascular Age-Related Macular Degeneration When Visual Acuity Is Relatively Good." JAMA Ophthalmol **135**(3): 268-273.

Hogg, R. E. and U. Chakravarthy (2006). "Visual function and dysfunction in early and late age-related maculopathy." Prog Retin Eye Res **25**(3): 249-276.

Holz, F. G., A. Bindewald-Wittich, M. Fleckenstein, J. Dreyhaupt, H. P. Scholl and S. Schmitz-Valckenberg (2007). "Progression of geographic atrophy and impact of fundus autofluorescence patterns in age-related macular degeneration." Am J Ophthalmol **143**(3): 463-472.

Holz, F. G., S. R. Sadda, G. Staurenghi, M. Lindner, A. C. Bird, B. A. Blodi, F. Bottoni, U. Chakravarthy, E. Y. Chew, K. Csaky, C. A. Curcio, R. Danis, M. Fleckenstein, K. B. Freund, J. Grunwald, R. Guymer, C. B. Hoyng, G. J. Jaffe, S. Liakopoulos, J. M. Monés, A. Oishi, D. Pauleikhoff, P. J. Rosenfeld, D. Sarraf, R. F. Spaide, R. Tadayoni, A. Tufail, S. Wolf and S. Schmitz-Valckenberg (2017). "Imaging Protocols in Clinical Studies in

Advanced Age-Related Macular Degeneration: Recommendations from Classification of Atrophy Consensus Meetings." Ophthalmology **124**(4): 464-478.

Holz, F. G., J. S. Steinberg, A. Göbel, M. Fleckenstein and S. Schmitz-Valckenberg (2015). "Fundus autofluorescence imaging in dry AMD: 2014 Jules Gonin lecture of the Retina Research Foundation." Graefes Arch Clin Exp Ophthalmol **253**(1): 7-16.

Huisingh, C., G. McGwin, Jr., D. Neely, A. Zarubina, M. Clark, Y. Zhang, C. A. Curcio and C. Owsley (2016). "The Association Between Subretinal Drusenoid Deposits in Older Adults in Normal Macular Health and Incident Age-Related Macular Degeneration." Invest Ophthalmol Vis Sci **57**(2): 739-745.

Hwang, C. K., E. Agrón, A. Domalpally, C. A. Cukras, W. T. Wong, E. Y. Chew and T. D. L. Keenan (2021). "Progression of Geographic Atrophy with Subsequent Exudative Neovascular Disease in Age-Related Macular Degeneration: AREDS2 Report 24." Ophthalmol Retina **5**(2): 108-117.

Iaculli, C., A. Barone, M. Scudieri, M. Giovanna Palumbo and N. Delle Noci (2015). "Outer retinal tubulation: Characteristics in Patients With Neovascular Age-Related Macular Degeneration." Retina **35**(10): 1979-1984.

Jabbarpoor Bonyadi, M. H., M. Yaseri, M. Bonyadi, M. Soheilian and H. Nikkhah (2017). "Association of combined cigarette smoking and ARMS2/LOC387715 A69S polymorphisms with age-related macular degeneration: A meta-analysis." Ophthalmic Genet **38**(4): 308-313.

Jackson, G. R. and J. G. Edwards (2008). "A short-duration dark adaptation protocol for assessment of age-related maculopathy." J Ocul Biol Dis Infor **1**(1): 7-11.

Jaffe, G. J., U. Chakravarthy, K. B. Freund, R. H. Guymer, F. G. Holz, S. Liakopoulos, J. M. Monés, P. J. Rosenfeld, S. R. Sadda, D. Sarraf, S. Schmitz-Valckenberg, R. F. Spaide, G. Staurenghi, A. Tufail and C. A. Curcio (2021). "Imaging Features Associated with Progression to Geographic Atrophy in Age-Related Macular Degeneration: Classification of Atrophy Meeting Report 5." Ophthalmol Retina **5**(9): 855-867.

Jaffe, G. J., D. F. Martin, C. A. Toth, E. Daniel, M. G. Maguire, G. S. Ying, J. E. Grunwald and J. Huang (2013). "Macular morphology and visual acuity in the comparison of age-related macular degeneration treatments trials." Ophthalmology **120**(9): 1860-1870.

Jaffe, G. J., G. S. Ying, C. A. Toth, E. Daniel, J. E. Grunwald, D. F. Martin and M. G. Maguire (2019). "Macular Morphology and Visual Acuity in Year Five of the Comparison of Age-related Macular Degeneration Treatments Trials." Ophthalmology **126**(2): 252-260.

Jaisankar, D., G. Swaminathan, R. Roy, V. Kulothungan, T. Sharma and R. Raman (2018). "Association of obesity and age-related macular degeneration in Indian population." Indian J Ophthalmol **66**(7): 976-983.

Kaarniranta, K., H. Uusitalo, J. Blasiak, S. Felszeghy, R. Kannan, A. Kauppinen, A. Salminen, D. Sinha and D. Ferrington (2020). "Mechanisms of mitochondrial dysfunction and their impact on age-related macular degeneration." Prog Retin Eye Res **79**: 100858.

Kar, D., M. E. Clark, T. A. Swain, G. McGwin, Jr., J. N. Crosson, C. Owsley, K. R. Sloan and C. A. Curcio (2020). "Local Abundance of Macular Xanthophyll Pigment Is Associated with Rod- and Cone-Mediated Vision in Aging and Age-Related Macular Degeneration." Invest Ophthalmol Vis Sci **61**(8): 46.

Keane, P. A., P. J. Patel, S. Liakopoulos, F. M. Heussen, S. R. Sadda and A. Tufail (2012). "Evaluation of age-related macular degeneration with optical coherence tomography." Surv Ophthalmol **57**(5): 389-414.

Keenan, T. D., E. Agrón, A. Domalpally, T. E. Clemons, F. van Asten, W. T. Wong, R. G. Danis, S. Sadda, P. J. Rosenfeld, M. L. Klein, R. Ratnapriya, A. Swaroop, F. L. Ferris, 3rd and E. Y. Chew (2018). "Progression of Geographic Atrophy in Age-related Macular Degeneration: AREDS2 Report Number 16." Ophthalmology **125**(12): 1913-1928.

Khan, K. N., O. A. Mahroo, R. S. Khan, M. D. Mohamed, M. McKibbin, A. Bird, M. Michaelides, A. Tufail and A. T. Moore (2016). "Differentiating drusen: Drusen and drusen-like appearances associated with ageing, age-related macular degeneration, inherited eye disease and other pathological processes." Prog Retin Eye Res **53**: 70-106.

Khandhadia, S., J. Cherry and A. J. Lotery (2012). "Age-related macular degeneration." Adv Exp Med Biol **724**: 15-36.

Khanifar, A. A., A. F. Koreishi, J. A. Izatt and C. A. Toth (2008). "Drusen ultrastructure imaging with spectral domain optical coherence tomography in age-related macular degeneration." Ophthalmology **115**(11): 1883-1890.

Kim, B. J., D. C. Mastellos, Y. Li, J. L. Dunaief and J. D. Lambris (2021). "Targeting complement components C3 and C5 for the retina: Key concepts and lingering questions." Prog Retin Eye Res **83**: 100936.

Kim, D. Y., J. Loo, S. Farsiu and G. J. Jaffe (2021). "Comparison of single drusen size on color fundus photography and spectral-domain optical coherence tomography." Retina **41**(8): 1715-1722.

Kim, K. T., H. Lee, J. Y. Kim, S. Lee, J. B. Chae and D. Y. Kim (2020). "Long-Term Visual/Anatomic Outcome in Patients with Fovea-Involving Fibrovascular Pigment Epithelium Detachment Presenting Choroidal Neovascularization on Optical Coherence Tomography Angiography." J Clin Med **9**(6).

Klein, R., B. E. Klein and S. E. Moss (1995). "Age-related eye disease and survival. The Beaver Dam Eye Study." Arch Ophthalmol **113**(3): 333-339.

Klein, R., S. M. Meuer, C. E. Myers, G. H. Buitendijk, E. Rochtchina, F. Choudhury, P. T. de Jong, R. McKean-Cowdin, S. K. Iyengar, X. Gao, K. E. Lee, J. R. Vingerling, P. Mitchell, C. C. Klaver, J. J. Wang and B. E. Klein (2014). "Harmonizing the classification of age-related macular degeneration in the three-continent AMD consortium." Ophthalmic Epidemiol **21**(1): 14-23.

Kodjikian, L., M. Parravano, A. Clemens, R. Dolz-Marco, F. G. Holz, M. R. Munk, M. Nicolò, F. Ricci, R. Silva, S. J. Talks, R. K. Verma, J. Zarranz-Ventura and S. A. Zweifel (2021). "Fluid as a critical biomarker in neovascular age-related macular degeneration management: literature review and consensus recommendations." Eye (Lond) **35**(8): 2119-2135.

Lad, E. M., R. P. Finger and R. Guymer (2023). "Biomarkers for the Progression of Intermediate Age-Related Macular Degeneration." Ophthalmol Ther.

Laiginhas, R., Y. Shi, M. Shen, X. Jiang, W. Feuer, G. Gregori and P. J. Rosenfeld (2022). "Persistent Hypertransmission Defects Detected on En Face Swept Source Optical Computed Tomography Images Predict the Formation of Geographic Atrophy in Age-Related Macular Degeneration." Am J Ophthalmol **237**: 58-70.

Laiginhas, R., J. Yang, P. J. Rosenfeld and M. Falcão (2020). "Nonexudative Macular Neovascularization - A Systematic Review of Prevalence, Natural History, and Recent Insights from OCT Angiography." Ophthalmol Retina **4**(7): 651-661.

Lamb, T. D. and E. N. Pugh, Jr. (2004). "Dark adaptation and the retinoid cycle of vision." Prog Retin Eye Res **23**(3): 307-380.

Lei, J., S. Balasubramanian, N. S. Abdelfattah, M. G. Nittala and S. R. Sadda (2017). "Proposal of a simple optical coherence tomography-based scoring system for progression of age-related macular degeneration." Graefes Arch Clin Exp Ophthalmol **255**(8): 1551-1558.

Linsenmeier, R. A. and R. D. Braun (1992). "Oxygen distribution and consumption in the cat retina during normoxia and hypoxemia." J Gen Physiol **99**(2): 177-197.

Liu, J., M. Shen, R. Laiginhas, G. Herrera, J. Li, Y. Shi, F. Hiya, O. Trivizki, N. K. Waheed, C. Y. Chung, E. M. Moult, J. G. Fujimoto, G. Gregori and P. J. Rosenfeld (2023). "Onset and Progression of Persistent Choroidal Hypertransmission Defects in Intermediate Age-Related Macular Degeneration: A Novel Clinical Trial Endpoint." Am J Ophthalmol **254**: 11-22.

Llorente-González, S., M. Hernandez, J. González-Zamora, V. Bilbao-Malavé, P. Fernández-Robredo, M. Saenz-de-Viteri, J. Barrio-Barrio, M. J. Rodríguez-Cid, J. Donate, F. J. Ascaso, A. M. Gómez-Ramírez, J. Araiz, F. Armadá, Ó. Ruiz-Moreno, S. Recalde and A. García-Layana (2022). "The role of retinal fluid location in atrophy and fibrosis evolution of patients with neovascular age-related macular degeneration long-term treated in real world." Acta Ophthalmol **100**(2): e521-e531.

Maguire, M. G., D. F. Martin, G. S. Ying, G. J. Jaffe, E. Daniel, J. E. Grunwald, C. A. Toth, F. L. Ferris, 3rd and S. L. Fine (2016). "Five-Year Outcomes with Anti-Vascular Endothelial Growth Factor Treatment of Neovascular Age-Related Macular Degeneration: The Comparison of Age-Related Macular Degeneration Treatments Trials." Ophthalmology **123**(8): 1751-1761.

Maguire, P. and A. K. Vine (1986). "Geographic atrophy of the retinal pigment epithelium." Am J Ophthalmol **102**(5): 621-625.

Maharjan, J., Y. Ektefaie, L. Ryan, S. Mataraso, G. Barnes, S. Shokouhi, A. Green-Saxena, J. Calvert, Q. Mao and R. Das (2021). "Enriching the Study Population for Ischemic Stroke Therapeutic Trials Using a Machine Learning Algorithm." Front Neurol **12**: 784250.

Margolis, R. and R. F. Spaide (2009). "A pilot study of enhanced depth imaging optical coherence tomography of the choroid in normal eyes." Am J Ophthalmol **147**(5): 811-815.

Mayer, M. J., B. Ward, R. Klein, J. B. Talcott, R. F. Dougherty and A. Glucs (1994). "Flicker sensitivity and fundus appearance in pre-exudative age-related maculopathy." Invest Ophthalmol Vis Sci **35**(3): 1138-1149.

Merle, B. M., R. E. Silver, B. Rosner and J. M. Seddon (2015). "Adherence to a Mediterranean diet, genetic susceptibility, and progression to advanced macular degeneration: a prospective cohort study." Am J Clin Nutr **102**(5): 1196-1206.

Merle, B. M. J., J. M. Colijn, A. Cougnard-Grégoire, A. P. M. de Koning-Backus, M. N. Delyfer, J. C. Kiefte-de Jong, M. Meester-Smoor, C. Féart, T. Verzijden, C. Samieri, O. H. Franco, J. F. Korobelnik, C. C. W. Klaver and C. Delcourt (2019). "Mediterranean Diet and Incidence of Advanced Age-Related Macular Degeneration: The EYE-RISK Consortium." Ophthalmology **126**(3): 381-390.

Mitter, S. K., C. Song, X. Qi, H. Mao, H. Rao, D. Akin, A. Lewin, M. Grant, W. Dunn, Jr., J. Ding, C. Bowes Rickman and M. Boulton (2014). "Dysregulated autophagy in the RPE is associated with increased susceptibility to oxidative stress and AMD." Autophagy **10**(11): 1989-2005.

Monés, J. and M. Biarnés (2018). "Geographic atrophy phenotype identification by cluster analysis." Br J Ophthalmol **102**(3): 388-392.

Monge, M., A. Araya and L. Wu (2022). "Subretinal drusenoid deposits: An update." Taiwan J Ophthalmol 12(2): 138-146.

Moreno-García, A., A. Kun, O. Calero, M. Medina and M. Calero (2018). "An Overview of the Role of Lipofuscin in Age-Related Neurodegeneration." Front Neurosci **12**: 464.

Moult, E. M., A. Y. Alibhai, B. Lee, Y. Yu, S. Ploner, S. Chen, A. Maier, J. S. Duker, N. K. Waheed and J. G. Fujimoto (2020). "A Framework for Multiscale Quantitation of Relationships Between Choriocapillaris Flow Impairment and Geographic Atrophy Growth." Am J Ophthalmol **214**: 172-187.

Müller, P. L., S. Wolf, R. Dolz-Marco, A. Tafreshi, S. Schmitz-Valckenberg and F. G. Holz (2019). Ophthalmic Diagnostic Imaging: Retina. High Resolution Imaging in Microscopy

and Ophthalmology: New Frontiers in Biomedical Optics. J. F. Bille. Cham (CH), Springer Copyright 2019, The Author(s). 87-106.

Mullins, R. F., M. N. Johnson, E. A. Faidley, J. M. Skeie and J. Huang (2011). "Choriocapillaris vascular dropout related to density of drusen in human eyes with early age-related macular degeneration." Invest Ophthalmol Vis Sci **52**(3): 1606-1612.

Muth, D. R., M. D. Toro, A. Bajka, K. Jonak, R. Rieder, M. M. Kohler, J. M. Gunzinger, E. H. Souied, M. Engelbert, K. B. Freund and S. A. Zweifel (2022). "Correlation between Macular Neovascularization (MNV) Type and Druse Type in Neovascular Age-Related Macular Degeneration (AMD) Based on the CONAN Classification." Biomedicines **10**(10).

Narayan, D. S., G. Chidlow, J. P. Wood and R. J. Casson (2017). "Glucose metabolism in mammalian photoreceptor inner and outer segments." Clin Exp Ophthalmol **45**(7): 730-741.

Narita, C., Z. Wu, P. J. Rosenfeld, J. Yang, C. Lyu, E. Caruso, M. McGuinness and R. H. Guymer (2020). "Structural OCT Signs Suggestive of Subclinical Nonexudative Macular Neovascularization in Eyes with Large Drusen." Ophthalmology **127**(5): 637-647.

Nassisi, M., E. Baghdasaryan, T. Tepelus, S. Asanad, E. Borrelli and S. R. Sadda (2018). "Topographic distribution of choriocapillaris flow deficits in healthy eyes." PLoS One **13**(11): e0207638.

Nassisi, M., J. Lei, N. S. Abdelfattah, A. Karamat, S. Balasubramanian, W. Fan, A. Uji, K. M. Marion, K. Baker, X. Huang, E. Morgenthien and S. R. Sadda (2019). "OCT Risk Factors for Development of Late Age-Related Macular Degeneration in the Fellow Eyes of Patients Enrolled in the HARBOR Study." Ophthalmology **126**(12): 1667-1674.

NICE (2018). Age-related macular degeneration NICE Guideline G82, National Institute for Health and Care Excellence.

Nickla, D. L. and J. Wallman (2010). "The multifunctional choroid." Prog Retin Eye Res **29**(2): 144-168.

Nigalye, A. K., K. Hess, S. J. Pundlik, B. G. Jeffrey, C. A. Cukras and D. Husain (2022). "Dark Adaptation and Its Role in Age-Related Macular Degeneration." J Clin Med **11**(5).

Ohji, M., A. A. Okada, K. Sasaki, S. C. Moon, T. Machewitz and K. Takahashi (2021). "Relationship between retinal fluid and visual acuity in patients with exudative age-

related macular degeneration treated with intravitreal aflibercept using a treat-and-extend regimen: subgroup and post-hoc analyses from the ALTAIR study." Graefes Arch Clin Exp Ophthalmol **259**(12): 3637-3647.

Olchawa, M. M., J. A. Furso, G. M. Szewczyk and T. J. Sarna (2017). "Lipofuscin-mediated photic stress inhibits phagocytic activity of ARPE-19 cells; effect of donors' age and antioxidants." Free Radic Res **51**(9-10): 799-811.

Oshima, Y., S. Oshima, H. Nambu, S. Kachi, S. F. Hackett, M. Melia, M. Kaleko, S. Connelly, N. Esumi, D. J. Zack and P. A. Campochiaro (2004). "Increased expression of VEGF in retinal pigmented epithelial cells is not sufficient to cause choroidal neovascularization." J Cell Physiol **201**(3): 393-400.

Owsley, C., M. E. Clark, C. E. Huisingh, C. A. Curcio and G. McGwin, Jr. (2016). "Visual Function in Older Eyes in Normal Macular Health: Association with Incident Early Age-Related Macular Degeneration 3 Years Later." Invest Ophthalmol Vis Sci **57**(4): 1782-1789.

Owsley, C., C. Huisingh, G. R. Jackson, C. A. Curcio, A. J. Szalai, N. Dashti, M. Clark, K. Rookard, M. A. McCrory, T. T. Wright, M. A. Callahan, L. B. Kline, C. D. Witherspoon and G. McGwin, Jr. (2014). "Associations between abnormal rod-mediated dark adaptation and health and functioning in older adults with normal macular health." Invest Ophthalmol Vis Sci **55**(8): 4776-4789.

Owsley, C., G. R. Jackson, A. V. Cideciyan, Y. Huang, S. L. Fine, A. C. Ho, M. G. Maguire, V. Lolley and S. G. Jacobson (2000). "Psychophysical evidence for rod vulnerability in age-related macular degeneration." Invest Ophthalmol Vis Sci **41**(1): 267-273.

Owsley, C., G. R. Jackson, M. White, R. Feist and D. Edwards (2001). "Delays in rod-mediated dark adaptation in early age-related maculopathy." Ophthalmology **108**(7): 1196-1202.

Owsley, C., G. McGwin, Jr., M. E. Clark, G. R. Jackson, M. A. Callahan, L. B. Kline, C. D. Witherspoon and C. A. Curcio (2016). "Delayed Rod-Mediated Dark Adaptation Is a Functional Biomarker for Incident Early Age-Related Macular Degeneration." Ophthalmology **123**(2): 344-351.

Pfau, M., M. Lindner, L. Goerdt, S. Thiele, J. Nadal, M. Schmid, S. Schmitz-Valckenberg, S. R. Sadda, F. G. Holz and M. Fleckenstein (2019). "Prognostic value of shape-descriptive factors for the progression of geographic atrophy secondary to age-related macular degeneration." Retina **39**(8): 1527-1540.

Pfau, M., L. von der Emde, L. de Sisternes, J. A. Hallak, T. Leng, S. Schmitz-Valckenberg, F. G. Holz, M. Fleckenstein and D. L. Rubin (2020). "Progression of Photoreceptor Degeneration in Geographic Atrophy Secondary to Age-related Macular Degeneration." JAMA Ophthalmol **138**(10): 1026-1034.

Qu, J., S. B. Velaga, A. H. Hariri, M. G. Nittala and S. Sadda (2018). "Classification and quantitative analysis of geographic atrophy junctional zone using spectral domain optical coherence tomography." Retina **38**(8): 1456-1463.

Querques, L., M. Parravano, E. Borrelli, A. Chiaravalloti, M. Tedeschi, R. Sacconi, I. Zucchiatti, F. Bandello and G. Querques (2020). "Anatomical and functional changes in neovascular AMD in remission: comparison of fibrocellular and fibrovascular phenotypes." Br J Ophthalmol **104**(1): 47-52.

Reiter, G. S., L. Schwarzenbacher, D. Schartmüller, V. Röggla, C. Leydolt, R. Menapace, U. Schmidt-Erfurth and S. Sacu (2021). "Influence of lens opacities and cataract severity on quantitative fundus autofluorescence as a secondary outcome of a randomized clinical trial." Sci Rep **11**(1): 12685.

Reiter, G. S., R. Told, M. Schranz, L. Baumann, G. Mylonas, S. Sacu, A. Pollreisz and U. Schmidt-Erfurth (2020). "Subretinal Drusenoid Deposits and Photoreceptor Loss Detecting Global and Local Progression of Geographic Atrophy by SD-OCT Imaging." Invest Ophthalmol Vis Sci **61**(6): 11.

Riedl, S., W. D. Vogl, J. Mai, G. S. Reiter, D. Lachinov, C. Grechenig, A. McKeown, L. Scheibler, H. Bogunović and U. Schmidt-Erfurth (2022). "The Effect of Pegcetacoplan Treatment on Photoreceptor Maintenance in Geographic Atrophy Monitored by Artificial Intelligence-Based OCT Analysis." Ophthalmol Retina **6**(11): 1009-1018.

Rim, T. H., A. Y. Lee, D. S. Ting, K. Teo, B. K. Betzler, Z. L. Teo, T. K. Yoo, G. Lee, Y. Kim, A. C. Lin, S. E. Kim, Y. C. Tham, S. S. Kim, C. Y. Cheng, T. Y. Wong and C. M. G. Cheung (2021). "Detection of features associated with neovascular age-related macular degeneration in ethnically distinct data sets by an optical coherence tomography: trained deep learning algorithm." Br J Ophthalmol **105**(8): 1133-1139.

Rofagha, S., R. B. Bhisitkul, D. S. Boyer, S. R. Sadda and K. Zhang (2013). "Seven-year outcomes in ranibizumab-treated patients in ANCHOR, MARINA, and HORIZON: a multicenter cohort study (SEVEN-UP)." Ophthalmology **120**(11): 2292-2299.

Ross, A. H., L. Downey, H. Devonport, R. P. Gale, A. Kotagiri, S. Mahmood, H. Mehta, N. Narendran, P. J. Patel, N. Parmar and N. Jain (2020). "Recommendations by a UK expert panel on an aflibercept treat-and-extend pathway for the treatment of neovascular age-related macular degeneration." Eye (Lond) **34**(10): 1825-1834.

Rudolf, M., S. D. Vogt, C. A. Curcio, C. Huisingh, G. McGwin, Jr., A. Wagner, S. Grisanti and R. W. Read (2013). "Histologic basis of variations in retinal pigment epithelium autofluorescence in eyes with geographic atrophy." Ophthalmology **120**(4): 821-828.

Sadda, S., N. M. Holekamp, D. Sarraf, A. Ebraheem, W. Fan, L. Hill, S. Blotner, G. Spicer and S. Gune (2022). "Relationship between retinal fluid characteristics and vision in neovascular age-related macular degeneration: HARBOR post hoc analysis." Graefes Arch Clin Exp Ophthalmol **260**(12): 3781-3789.

Sadda, S. R., R. Guymer, F. G. Holz, S. Schmitz-Valckenberg, C. A. Curcio, A. C. Bird, B. A. Blodi, F. Bottoni, U. Chakravarthy, E. Y. Chew, K. Csaky, R. P. Danis, M. Fleckenstein, K. B. Freund, J. Grunwald, C. B. Hoyng, G. J. Jaffe, S. Liakopoulos, J. M. Monés, D. Pauleikhoff, P. J. Rosenfeld, D. Sarraf, R. F. Spaide, R. Tadayoni, A. Tufail, S. Wolf and G. Staurenghi (2018). "Consensus Definition for Atrophy Associated with Age-Related Macular Degeneration on OCT: Classification of Atrophy Report 3." Ophthalmology **125**(4): 537-548.

Sadigh, S., A. V. Cideciyan, A. Sumaroka, W. C. Huang, X. Luo, M. Swider, J. D. Steinberg, D. Stambolian and S. G. Jacobson (2013). "Abnormal thickening as well as thinning of the photoreceptor layer in intermediate age-related macular degeneration." Invest Ophthalmol Vis Sci **54**(3): 1603-1612.

Sarks, S., S. Cherepanoff, M. Killingsworth and J. Sarks (2007). "Relationship of Basal laminar deposit and membranous debris to the clinical presentation of early age-related macular degeneration." Invest Ophthalmol Vis Sci **48**(3): 968-977.

Sarks, S. H. (1973). "New vessel formation beneath the retinal pigment epithelium in senile eyes." Br J Ophthalmol **57**(12): 951-965.

Sayegh, R. G., C. Simader, U. Scheschy, A. Montuoro, C. Kiss, S. Sacu, D. P. Kreil, C. Prünte and U. Schmidt-Erfurth (2011). "A systematic comparison of spectral-domain optical coherence tomography and fundus autofluorescence in patients with geographic atrophy." Ophthalmology **118**(9): 1844-1851.

Schmidt-Erfurth, U., H. Bogunovic, A. Sadeghipour, T. Schlegl, G. Langs, B. S. Gerendas, A. Osborne and S. M. Waldstein (2018). "Machine Learning to Analyze the Prognostic Value of Current Imaging Biomarkers in Neovascular Age-Related Macular Degeneration." Ophthalmol Retina **2**(1): 24-30.

Schmidt-Erfurth, U., S. M. Waldstein, G. G. Deak, M. Kundi and C. Simader (2015). "Pigment epithelial detachment followed by retinal cystoid degeneration leads to vision loss in treatment of neovascular age-related macular degeneration." Ophthalmology **122**(4): 822-832.

Schmitz-Valckenberg, S., J. A. Sahel, R. Danis, M. Fleckenstein, G. J. Jaffe, S. Wolf, C. Pruente and F. G. Holz (2016). "Natural History of Geographic Atrophy Progression Secondary to Age-Related Macular Degeneration (Geographic Atrophy Progression Study)." Ophthalmology **123**(2): 361-368.

Scholl, H. P., M. Fleckenstein, L. G. Fritsche, S. Schmitz-Valckenberg, A. Göbel, C. Adrion, C. Herold, C. N. Keilhauer, F. Mackensen, A. Mössner, D. Pauleikhoff, A. W. Weinberger, U. Mansmann, F. G. Holz, T. Becker and B. H. Weber (2009). "CFH, C3 and ARMS2 are significant risk loci for susceptibility but not for disease progression of geographic atrophy due to AMD." PLoS One **4**(10): e7418.

Schultz, H., Y. Song, B. H. Baumann, R. J. Kapphahn, S. R. Montezuma, D. A. Ferrington and J. L. Dunaief (2019). "Increased serum proteins in non-exudative AMD retinas." Exp Eye Res **186**: 107686.

Seddon, J. M., J. Cote, N. Davis and B. Rosner (2003). "Progression of age-related macular degeneration: association with body mass index, waist circumference, and waist-hip ratio." Arch Ophthalmol **121**(6): 785-792.

Seddon, J. M., P. J. Francis, S. George, D. W. Schultz, B. Rosner and M. L. Klein (2007). "Association of CFH Y402H and LOC387715 A69S with progression of age-related macular degeneration." Jama **297**(16): 1793-1800.

Seddon, J. M., D. S. McLeod, I. A. Bhutto, M. B. Villalonga, R. E. Silver, A. S. Wenick, M. M. Edwards and G. A. Lutty (2016). "Histopathological Insights Into Choroidal Vascular Loss in Clinically Documented Cases of Age-Related Macular Degeneration." JAMA Ophthalmol **134**(11): 1272-1280.

Sepah, Y. J., A. Akhtar, M. A. Sadiq, Y. Hafeez, H. Nasir, B. Perez, N. Mawji, D. J. Dean, D. Ferraz and Q. D. Nguyen (2014). "Fundus autofluorescence imaging: Fundamentals and clinical relevance." Saudi J Ophthalmol **28**(2): 111-116.

Sharma, S., C. A. Toth, E. Daniel, J. E. Grunwald, M. G. Maguire, G. S. Ying, J. Huang, D. F. Martin and G. J. Jaffe (2016). "Macular Morphology and Visual Acuity in the Second Year of the Comparison of Age-Related Macular Degeneration Treatments Trials." Ophthalmology **123**(4): 865-875.

Shen, L., F. Liu, H. Grossetta Nardini and L. V. Del Priore (2018). "Natural History of Geographic Atrophy in Untreated Eyes with Nonexudative Age-Related Macular Degeneration: A Systematic Review and Meta-analysis." Ophthalmol Retina **2**(9): 914-921.

Shen, L. L., M. Sun, A. Ahluwalia, M. M. Park, B. K. Young and L. V. Del Priore (2021). "Local Progression Kinetics of Geographic Atrophy Depends Upon the Border Location." Invest Ophthalmol Vis Sci **62**(13): 28.

Shen, L. L., M. Sun, A. Ahluwalia, B. K. Young, M. M. Park and L. V. Del Priore (2021). "Geographic Atrophy Growth Is Strongly Related to Lesion Perimeter: Unifying Effects of Lesion Area, Number, and Circularity on Growth." Ophthalmol Retina **5**(9): 868-878.

Shen, L. L., M. Sun, H. K. Grossetta Nardini and L. V. Del Priore (2020). "Progression of Unifocal versus Multifocal Geographic Atrophy in Age-Related Macular Degeneration: A Systematic Review and Meta-analysis." Ophthalmol Retina **4**(9): 899-910.

Shen, L. L., M. Sun, S. Khetpal, H. K. Grossetta Nardini and L. V. Del Priore (2020). "Topographic Variation of the Growth Rate of Geographic Atrophy in Nonexudative Age-Related Macular Degeneration: A Systematic Review and Meta-analysis." Invest Ophthalmol Vis Sci **61**(1): 2.

Sheth, J., G. Anantharaman, S. Chandra and S. Sivaprasad (2018). ""Double-layer sign" on spectral domain optical coherence tomography in pachychoroid spectrum disease." Indian J Ophthalmol **66**(12): 1796-1801.

Sivaprasad, S., T. A. Bailey and V. N. Chong (2005). "Bruch's membrane and the vascular intima: is there a common basis for age-related changes and disease?" Clin Exp Ophthalmol **33**(5): 518-523.

Sivaprasad, S., S. Chandra, J. Kwon, N. Khalid and V. Chong (2023). "Perspectives from clinical trials: is geographic atrophy one disease?" Eye (Lond) **37**(3): 402-407.

Spaide, R. F. (2013). "Outer retinal atrophy after regression of subretinal drusenoid deposits as a newly recognized form of late age-related macular degeneration." Retina **33**(9): 1800-1808.

Spaide, R. F. and C. A. Curcio (2011). "Anatomical correlates to the bands seen in the outer retina by optical coherence tomography: literature review and model." Retina **31**(8): 1609-1619.

Spaide, R. F., G. J. Jaffe, D. Sarraf, K. B. Freund, S. R. Sadda, G. Staurenghi, N. K. Waheed, U. Chakravarthy, P. J. Rosenfeld, F. G. Holz, E. H. Souied, S. Y. Cohen, G. Querques, K. Ohno-Matsui, D. Boyer, A. Gaudric, B. Blodi, C. R. Baumal, X. Li, G. J. Coscas, A. Brucker, L. Singerman, P. Luthert, S. Schmitz-Valckenberg, U. Schmidt-Erfurth, H. E. Grossniklaus, D. J. Wilson, R. Guymer, L. A. Yannuzzi, E. Y. Chew, K. Csaky, J. M. Monés, D. Pauleikhoff, R. Tadayoni and J. Fujimoto (2020). "Consensus Nomenclature for Reporting Neovascular Age-Related Macular Degeneration Data: Consensus on Neovascular Age-Related Macular Degeneration Nomenclature Study Group." Ophthalmology **127**(5): 616-636.

Spaide, R. F., S. Ooto and C. A. Curcio (2018). "Subretinal drusenoid deposits AKA pseudodrusen." Surv Ophthalmol **63**(6): 782-815.

Sparrow, J. R., T. Duncker, K. Schuerch, M. Paavo and J. R. L. de Carvalho, Jr. (2020). "Lessons learned from quantitative fundus autofluorescence." Prog Retin Eye Res **74**: 100774.

Sparrow, J. R., H. R. Vollmer-Snarr, J. Zhou, Y. P. Jang, S. Jockusch, Y. Itagaki and K. Nakanishi (2003). "A2E-epoxides damage DNA in retinal pigment epithelial cells. Vitamin E and other antioxidants inhibit A2E-epoxide formation." J Biol Chem **278**(20): 18207-18213.

Spencer, C., S. Abend, K. J. McHugh and M. Saint-Geniez (2017). "Identification of a synergistic interaction between endothelial cells and retinal pigment epithelium." J Cell Mol Med **21**(10): 2542-2552.

Spraul, C. W. and H. E. Grossniklaus (1997). "Characteristics of Drusen and Bruch's membrane in postmortem eyes with age-related macular degeneration." Arch Ophthalmol **115**(2): 267-273.

Staurenghi, G., S. Sadda, U. Chakravarthy and R. F. Spaide (2014). "Proposed lexicon for anatomic landmarks in normal posterior segment spectral-domain optical coherence tomography: the IN•OCT consensus." Ophthalmology **121**(8): 1572-1578.

Steinberg, J. S., M. Saßmannshausen, M. Fleckenstein, R. Fimmers, A. Oishi, F. G. Holz and S. Schmitz-Valckenberg (2016). "Correlation of Partial Outer Retinal Thickness With Scotopic and Mesopic Fundus-Controlled Perimetry in Patients With Reticular Drusen." Am J Ophthalmol **168**: 52-61.

Strauss, O. (1995). The Retinal Pigment Epithelium. Webvision: The Organization of the Retina and Visual System. H. Kolb, E. Fernandez and R. Nelson. Salt Lake City (UT), University of Utah Health Sciences Center. Copyright: © 2023 Webvision .

Sunness, J. S., J. Gonzalez-Baron, C. A. Applegate, N. M. Bressler, Y. Tian, B. Hawkins, Y. Barron and A. Bergman (1999). "Enlargement of atrophy and visual acuity loss in the geographic atrophy form of age-related macular degeneration." Ophthalmology **106**(9): 1768-1779.

Sunness, J. S., G. S. Rubin, A. Broman, C. A. Applegate, N. M. Bressler and B. S. Hawkins (2008). "Low luminance visual dysfunction as a predictor of subsequent visual acuity loss from geographic atrophy in age-related macular degeneration." Ophthalmology **115**(9): 1480-1488, 1488.e1481-1482.

Tadi., K. H. N. B. C. P. P. (2023 Jan [Updated 2023 Aug 8]). Anatomy, Head and Neck: Eye Retina. StatPearls [Internet]. Treasure Island (FL), StatPearls Publishing.

Talks, J. S., A. J. Lotery, F. Ghanchi, S. Sivaprasad, R. L. Johnston, N. Patel, M. McKibbin, C. Bailey and S. Mahmood (2016). "First-Year Visual Acuity Outcomes of Providing Aflibercept According to the VIEW Study Protocol for Age-Related Macular Degeneration." Ophthalmology **123**(2): 337-343.

Tan, A. C. S., P. Astroz, K. K. Dansingani, J. S. Slakter, L. A. Yannuzzi, C. A. Curcio and K. B. Freund (2017). "The Evolution of the Plateau, an Optical Coherence Tomography Signature Seen in Geographic Atrophy." Invest Ophthalmol Vis Sci **58**(4): 2349-2358.

Tan, J. S., P. Mitchell, A. Kifley, V. Flood, W. Smith and J. J. Wang (2007). "Smoking and the long-term incidence of age-related macular degeneration: the Blue Mountains Eye Study." Arch Ophthalmol **125**(8): 1089-1095.

Tao, L. W., Z. Wu, R. H. Guymer and C. D. Luu (2016). "Ellipsoid zone on optical coherence tomography: a review." Clin Exp Ophthalmol **44**(5): 422-430.

Thee, E. F., M. A. Meester-Smoor, D. T. Luttikhuizen, J. M. Colijn, C. A. Enthoven, A. E. G. Haarman, D. Rizopoulos and C. C. W. Klaver (2020). "Performance of Classification Systems for Age-Related Macular Degeneration in the Rotterdam Study." Transl Vis Sci Technol **9**(2): 26.

Thiele, S., Z. Wu, B. Isselmann, M. Pfau, R. H. Guymer and C. D. Luu (2022). "Natural History of the Relative Ellipsoid Zone Reflectivity in Age-Related Macular Degeneration." Ophthalmol Retina **6**(12): 1165-1172.

Thorell, M. R., R. Goldhardt, R. P. Nunes, C. A. de Amorim Garcia Filho, A. M. Abbey, A. E. Kuriyan, Y. S. Modi, G. Gregori, Z. Yehoshua, W. Feuer, S. Sadda and P. J. Rosenfeld (2015). "Association Between Subfoveal Choroidal Thickness, Reticular Pseudodrusen, and Geographic Atrophy in Age-Related Macular Degeneration." Ophthalmic Surg Lasers Imaging Retina **46**(5): 513-521.

Thottarath, S., S. Chandra, S. Gurudas, W. S. Tsai, A. Giani, E. De Cock, T. C. N. Yamaguchi and S. Sivaprasad (2023). "Study protocol on prevalence of non-exudative macular neovascularisation and its contribution to prediction of exudation in fellow eyes with unilateral exudative AMD (EYE-NEON)." Eye (Lond) **37**(14): 3004-3008.

Timothy Lai, S. M., Anna-Maria Demetriades, Carlos Quezada Ruiz, David Silverman, Jane Ives, Balakumar Swaminathan, Hugh Lin (2022). Faricimab in Neovascular Age-Related Macular Degeneration: 48-Week Results by Dosing Interval Cohort in the Phase 3 TENAYA and LUCERNE Trials. 22nd EURETINA Hamburg, Germany.

Ting, D. S. W., L. Peng, A. V. Varadarajan, P. A. Keane, P. M. Burlina, M. F. Chiang, L. Schmetterer, L. R. Pasquale, N. M. Bressler, D. R. Webster, M. Abramoff and T. Y. Wong

(2019). "Deep learning in ophthalmology: The technical and clinical considerations." Prog Retin Eye Res **72**: 100759.

Tiosano, L., G. Corradetti and S. R. Sadda (2021). "Progression of choriocapillaris flow deficits in clinically stable intermediate age-related macular degeneration." Eye (Lond) **35**(11): 2991-2998.

Toprak, I., V. Yaylalı and C. Yildirim (2017). "Early deterioration in ellipsoid zone in eyes with non-neovascular age-related macular degeneration." Int Ophthalmol **37**(4): 801-806.

Uji, A., M. G. Nittala, A. Hariri, S. B. Velaga and S. R. Sadda (2019). "Directional kinetics analysis of the progression of geographic atrophy." Graefes Arch Clin Exp Ophthalmol **257**(8): 1679-1685.

van de Kraats, J. and D. van Norren (2007). "Optical density of the aging human ocular media in the visible and the UV." J Opt Soc Am A Opt Image Sci Vis **24**(7): 1842-1857.

Veerappan, M., A. M. El-Hage-Sleiman, V. Tai, S. J. Chiu, K. P. Winter, S. S. Stinnett, T. S. Hwang, G. B. Hubbard, 3rd, M. Michelson, R. Gunther, W. T. Wong, E. Y. Chew and C. A. Toth (2016). "Optical Coherence Tomography Reflective Drusen Substructures Predict Progression to Geographic Atrophy in Age-related Macular Degeneration." Ophthalmology **123**(12): 2554-2570.

Velaga, S. B., M. G. Nittala, A. Hariri and S. R. Sadda (2022). "Correlation between Fundus Autofluorescence and En Face OCT Measurements of Geographic Atrophy." Ophthalmol Retina **6**(8): 676-683.

von der Emde, L., R. H. Guymer, M. Pfau, E. Caruso, P. Sivarajah, L. A. B. Hodgson, M. B. McGuinness, K. R. Sloan and Z. Wu (2021). "Natural history of quantitative autofluorescence in intermediate age-related macular degeneration." Retina **41**(4): 694-700.

Waldstein, S. M., C. Simader, G. Staurenghi, N. V. Chong, P. Mitchell, G. J. Jaffe, C. Lu, T. A. Katz and U. Schmidt-Erfurth (2016). "Morphology and Visual Acuity in Aflibercept and Ranibizumab Therapy for Neovascular Age-Related Macular Degeneration in the VIEW Trials." Ophthalmology **123**(7): 1521-1529.

Waldstein, S. M., W. D. Vogl, H. Bogunovic, A. Sadeghipour, S. Riedl and U. Schmidt-Erfurth (2020). "Characterization of Drusen and Hyperreflective Foci as Biomarkers for

Disease Progression in Age-Related Macular Degeneration Using Artificial Intelligence in Optical Coherence Tomography." JAMA Ophthalmol **138**(7): 740-747.

Waldstein, S. M., J. Wright, J. Warburton, P. Margaron, C. Simader and U. Schmidt-Erfurth (2016). "Predictive Value of Retinal Morphology for Visual Acuity Outcomes of Different Ranibizumab Treatment Regimens for Neovascular AMD." Ophthalmology **123**(1): 60-69.

Wang, X., S. R. Sadda, M. S. Ip, D. Sarraf and Y. Zhang (2023). "In Vivo Longitudinal Measurement of Cone Photoreceptor Density in Intermediate Age-Related Macular Degeneration." Am J Ophthalmol **248**: 60-75.

Willoughby, A. S., G. S. Ying, C. A. Toth, M. G. Maguire, R. E. Burns, J. E. Grunwald, E. Daniel and G. J. Jaffe (2015). "Subretinal Hyperreflective Material in the Comparison of Age-Related Macular Degeneration Treatments Trials." Ophthalmology **122**(9): 1846-1853.e1845.

Wong, J. H. C., J. Y. W. Ma, A. I. Jobling, A. Brandli, U. Greferath, E. L. Fletcher and K. A. Vessey (2022). "Exploring the pathogenesis of age-related macular degeneration: A review of the interplay between retinal pigment epithelium dysfunction and the innate immune system." Front Neurosci **16**: 1009599.

Wong, T. Y., U. Chakravarthy, R. Klein, P. Mitchell, G. Zlateva, R. Buggage, K. Fahrbach, C. Probst and I. Sledge (2008). "The natural history and prognosis of neovascular age-related macular degeneration: a systematic review of the literature and meta-analysis." Ophthalmology **115**(1): 116-126.

Wu, Z., L. N. Ayton, R. H. Guymer and C. D. Luu (2013). "Relationship between the second reflective band on optical coherence tomography and multifocal electroretinography in age-related macular degeneration." Invest Ophthalmol Vis Sci **54**(4): 2800-2806.

Wu, Z., L. N. Ayton, R. H. Guymer and C. D. Luu (2014). "Low-luminance visual acuity and microperimetry in age-related macular degeneration." Ophthalmology **121**(8): 1612-1619.

Wu, Z., K. L. Goh, L. A. B. Hodgson and R. H. Guymer (2023). "Incomplete Retinal Pigment Epithelial and Outer Retinal Atrophy: Longitudinal Evaluation in Age-Related Macular Degeneration." Ophthalmology **130**(2): 205-212.

Wu, Z., C. D. Luu, L. A. B. Hodgson, E. Caruso, N. Tindill, K. Z. Aung, M. B. McGuinness, G. Makeyeva, F. K. Chen, U. Chakravarthy, J. J. Arnold, W. J. Heriot, S. R. Durkin and R. H. Guymer (2020). "Prospective Longitudinal Evaluation of Nascent Geographic Atrophy in Age-Related Macular Degeneration." Ophthalmol Retina **4**(6): 568-575.

Wu, Z., M. Pfau, B. A. Blodi, F. G. Holz, G. J. Jaffe, S. Liakopoulos, S. R. Sadda, G. Staurenghi, E. Bjelopera, T. Brown, P. Chang, J. Choong, G. Corradetti, F. Corvi, A. Domalpally, C. Hurtenbach, M. G. Nittala, A. Olson, J. W. Pak, J. Pappe, M. Saßmannshausen, C. Skalak, S. Thiele, R. H. Guymer and S. Schmitz-Valckenberg (2022). "OCT Signs of Early Atrophy in Age-Related Macular Degeneration: Interreader Agreement: Classification of Atrophy Meetings Report 6." Ophthalmol Retina **6**(1): 4-14.

Yehoshua, Z., P. J. Rosenfeld, G. Gregori, W. J. Feuer, M. Falcão, B. J. Lujan and C. Puliafito (2011). "Progression of geographic atrophy in age-related macular degeneration imaged with spectral domain optical coherence tomography." Ophthalmology **118**(4): 679-686.

Yehoshua, Z., F. Wang, P. J. Rosenfeld, F. M. Penha, W. J. Feuer and G. Gregori (2011). "Natural history of drusen morphology in age-related macular degeneration using spectral domain optical coherence tomography." Ophthalmology **118**(12): 2434-2441.

Ying, G. S., J. Huang, M. G. Maguire, G. J. Jaffe, J. E. Grunwald, C. Toth, E. Daniel, M. Klein, D. Pieramici, J. Wells and D. F. Martin (2013). "Baseline predictors for one-year visual outcomes with ranibizumab or bevacizumab for neovascular age-related macular degeneration." Ophthalmology **120**(1): 122-129.

Ying, G. S., M. G. Maguire, E. Daniel, F. L. Ferris, G. J. Jaffe, J. E. Grunwald, C. A. Toth, J. Huang and D. F. Martin (2015). "Association of Baseline Characteristics and Early Vision Response with 2-Year Vision Outcomes in the Comparison of AMD Treatments Trials (CATT)." Ophthalmology **122**(12): 2523-2531.e2521.

Young, R. W. (1987). "Pathophysiology of age-related macular degeneration." Surv Ophthalmol **31**(5): 291-306.

Yu, D. Y. and S. J. Cringle (2001). "Oxygen distribution and consumption within the retina in vascularised and avascular retinas and in animal models of retinal disease." Prog Retin Eye Res **20**(2): 175-208.

Zarranz-Ventura, J., G. Liew, R. L. Johnston, W. Xing, T. Akerele, M. McKibbin, L. Downey, S. Natha, U. Chakravarthy, C. Bailey, R. Khan, R. Antcliff, S. Armstrong, A. Varma, V. Kumar, M. Tsaloumas, K. Mandal, C. Bunce and A. Tufail (2014). "The neovascular age-related macular degeneration database: report 2: incidence, management, and visual outcomes of second treated eyes." Ophthalmology **121**(10): 1966-1975.

Zayit-Soudry, S., I. Moroz and A. Loewenstein (2007). "Retinal pigment epithelial detachment." Surv Ophthalmol **52**(3): 227-243.

Zheng, F., Q. Zhang, Y. Shi, J. F. Russell, E. H. Motulsky, J. T. Banta, Z. Chu, H. Zhou, N. A. Patel, L. de Sisternes, M. K. Durbin, W. Feuer, G. Gregori, R. Wang and P. J. Rosenfeld (2019). "Age-dependent Changes in the Macular Choriocapillaris of Normal Eyes Imaged With Swept-Source Optical Coherence Tomography Angiography." Am J Ophthalmol **200**: 110-122.

Zhou, H., H. Zhang, A. Yu and J. Xie (2018). "Association between sunlight exposure and risk of age-related macular degeneration: a meta-analysis." BMC Ophthalmol **18**(1): 331.

Zhu, L., Y. Zheng, C. H. von Kerczek, L. D. Topoleski and R. W. Flower (2006). "Feasibility of extracting velocity distribution in choriocapillaris in human eyes from ICG dye angiograms." J Biomech Eng **128**(2): 203-209.

Zouache, M. A., I. Eames, C. A. Klettner and P. J. Luthert (2016). "Form, shape and function: segmented blood flow in the choriocapillaris." Sci Rep **6**: 35754.

Zweifel, S. A., Y. Imamura, T. C. Spaide, T. Fujiwara and R. F. Spaide (2010). "Prevalence and significance of subretinal drusenoid deposits (reticular pseudodrusen) in age-related macular degeneration." Ophthalmology **117**(9): 1775-1781.

Zweifel, S. A., R. F. Spaide, C. A. Curcio, G. Malek and Y. Imamura (2010). "Reticular pseudodrusen are subretinal drusenoid deposits." Ophthalmology **117**(2): 303-312.e301.

8 Appendices

8.1 Appendix 1

Table S1.1 summarizing ongoing clinical trial in intermediate AMD and the clinical end points for these trials (Lad, Finger et al. 2023).

Trial	Type	Indication	Key endpoints
LEAD (NCT01790802)	Interventional	High-risk iAMD	(*Primary*) multimodal imaging endpoint comprising nGA (*Secondary*) change in: Drusen volume LLVA Microperimetry
NCT02848313	Phase I, interventional	iAMD	(*Secondary*) change in drusen complex volume
NCT04778436	Pilot, interventional	iAMD	(*Primary*) change in drusen in the macula
DELPHI (NCT04735263)	Phase II, interventional	iAMD	(*Primary*) drusen volume
NCT05562219	Phase II, interventional	iAMD	(*Primary*) change in drusen area
REVERS (NCT05056025)	Interventional	iAMD	(*Primary*) microperimetry (*Secondary*) conversion from iRORA to cRORA (*Secondary*) area of cumulative cRORA conversion
NCT05230537	Phase II, interventional	iAMD	(*Primary*) development of new iRORA (*Secondary*) change in contrast sensitivity
NCT03178149	Phase Ib, interventional	iAMD/GA	(*Secondary*) Changes in ellipsoid zone
Duke FEATURE (NCT01822873)	Observational	iAMD	*Secondary*: Dark adaptation CCT red Microperimetry
MACUSTAR (NCT03349801)	Observational	iAMD	*Primary*: LLVA Microperimetry PROs

Trial	Type	Indication	Key endpoints
HONU (NCT05300724)	Observational	iAMD	*Primary*: Conversion to iAMD with nGA and iRORA Conversion to GA and cRORA
BIRC-01, BIRC-02 (NCT04469140, NCT03688243)	Observational	Dry AMD	(*Primary*) Choroidal perfusion (*Secondary*) Drusen volume
PINNACLE (NCT04269304)	Observational	iAMD	(*Secondary*) Machine learning to predict progression
ALSTAR2 (NCT04112667)	Observational	Early AMD	(*Primary*) Dark adaptation *Secondary*: Microperimetry Acuity Contrast sensitivity
Immuno AMD	Observational	AMD	Blood markers of immunosenescence

AMD age-related macular degeneration, CCT cone-specific contrast test, cRORA complete RPE and outer retinal atrophy, GA geographic atrophy, iAMD intermediate age-related macular degeneration, iRORA incomplete RPE and outer retinal atrophy, LLVA low-light visual acuity, nGA nascent geographic atrophy, PRO patient-reported outcome, RPE retinal pigment epithelium

8.2 Appendix 2

A. Manual of Operations

Primary Objective:

To analyse OCT images (n= at least 3000 patients) and OCT and OCT-A (n=1000 patients) imaging in a large group of treatment-naïve neovascular AMD patients from baseline to the end of three loading injections, in order to discover imaging predictors for treatment response to intravitreal aflibercept therapy.

This is a multi-centre study that will evaluate imaging biomarkers as predictors for response to intravitreal aflibercept therapy treatment. Consenting patients with a previous or current diagnosis of neovascular AMD will agree for collection of Heidelberg OCT imaging data at the time of diagnosis and during the loading phase of the first three injections. OCTA images at baseline will also be collected.

SD OCT and OCT-A Imaging

Fixation Guidelines:

Explain to your subject what he/she will see during the OCT examination. Looking directly into the camera lens, the subject will see a bright blue dot that represents the internal fixation target. In addition to the blue fixation target, a set of red lines will be visible. While the OCT images are taken, the red light will move. Tell the patient that the eye always reacts sensitively to movement and that this is normal that they will sometimes involuntarily look at the moving lights. In this case, the OCT measurement will stop (fixation loss) and start again as soon as the subject looks back at the fixation target. Encourage the patient to blink regularly during the examination.

Blinking corrects the tear film at the corneal surface, which is required for a good image quality. Fixation loss and blinking will only slightly prolong the acquisition time. Please allow for at least one minutes resting time between scan acquisitions.

When entering the patient's details at the baseline scan; last name:

a. Last Name: Enter study name "Precise"
b. First Name: Enter centre number and patient study number – (e.g. 01- 0001)
c. Date of Birth: Enter 01/01/1900
d. Gender: must be entered.
e. Patient ID: Enter Patient study number (e.g. 0001)

Align the cSLO fundus reference image for even fundus illumination edge to edge, adjust image for sharp focus Please ensure all baseline scans are centred on the fovea.

All images taken after the initial baseline scan must be acquired using the follow-up mode.

SD OCT Scan Protocol: **Mandatory at Baseline and Visit 4/Optional at visit 2 and 3**

1) Macula Volume Scan: 20°x20°, 49 Sections, High Speed, 15 Frames minimum (ART) (**Study eye only**):

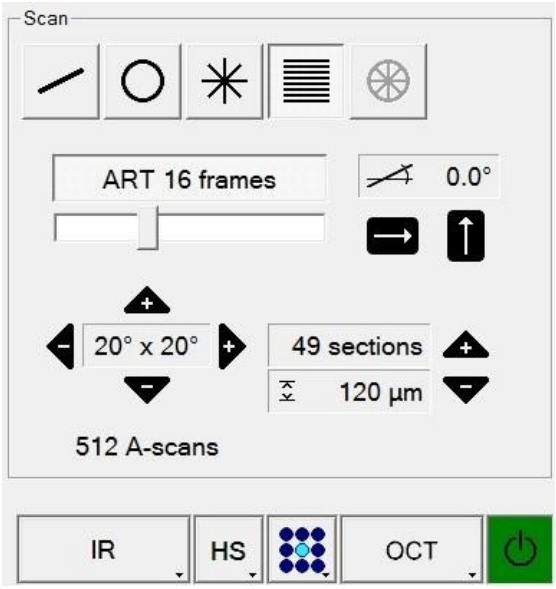

OCT-A Scan Protocols: **Mandatory at Baseline/Optional at Visits 2, 3 and 4**.

If the patient is not compliant with both OCT-A scans at baseline, only scan 1 will be performed at subsequent visits:

1) OCT-A Volume scan: 20°x 20°, 512 Sections, High Speed, 5 Frames (ART) (**Study eye only**):

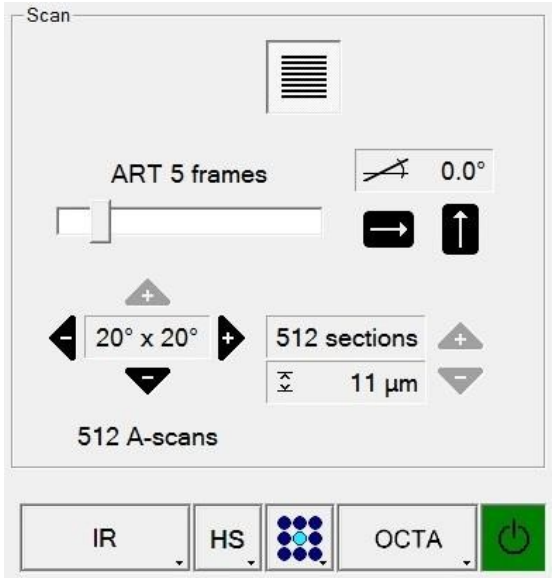

2) OCT-A Volume scan: 10°x 10°, 512 Sections, High Resolution, 5 Frames (ART) (**Study eye only**):

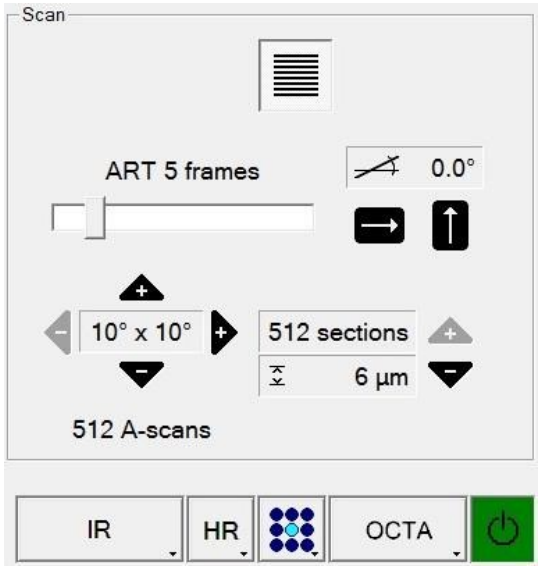

Quality Criteria:

Please inspect each scan after acquisition to check if all quality criteria were met.

The criteria include excellent signal strength; correct positioning of the scan pattern (centring of the fovea), a continuous tomogram map, and absence of motion artefacts. Fovelar / centre-point thickness on the macular thickness protocol should ideally have a standard deviation of less than 10% of the thickness value with the software able to map the inner and outer boundaries of the retina – if this is not the case please repeat until a satisfactory image set is acquired or save the best three scan sets and note reason for

poor scans. The retinal segmentation indicated by the red lines should not contain obvious errors at the centre. Select the Thickness Profile tab to check this.

The red, automatically determined segmentation lines should be steady and should follow the correct anatomical retinal layers. This ensures the correct computation of the numerical mean thickness and volume data. Repeat the scans if the criteria are not met.

Data Export

You will have received a 1 terabyte USB device branded **diskashur**. There will be a red light at the bottom of the device that is lit once the device is linked to a computer using the USB cable. You would have received a PIN number (via email) to unlock the USB.

To unlock the drive enter the user PIN provided and press the **UNLOCK** button. The device will be installed and a drive will appear on your screen. Take note of the drive as this is where the images will need to be saved.

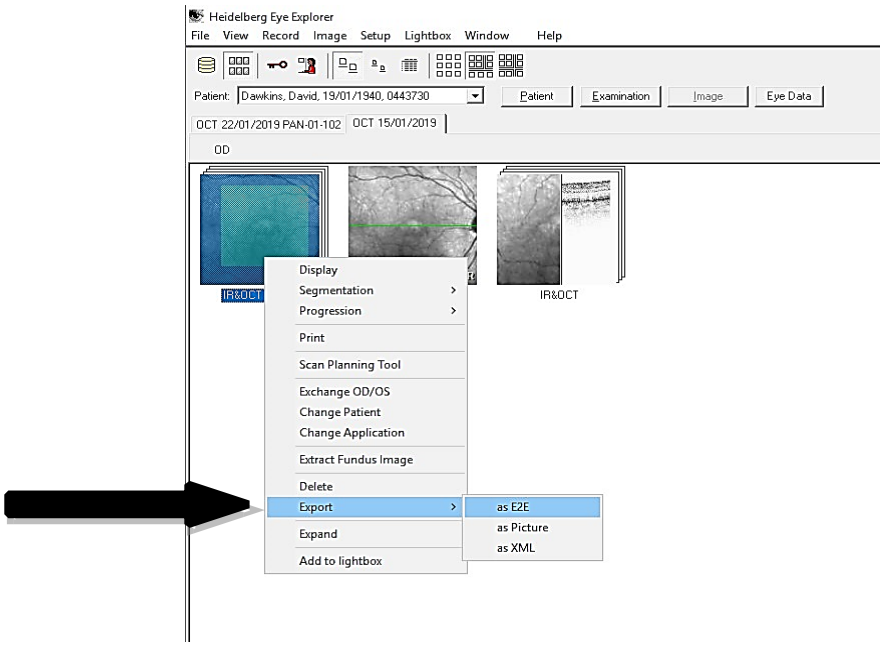

Right click on the image icon and from the drop down and select **EXPORT →E2E**.

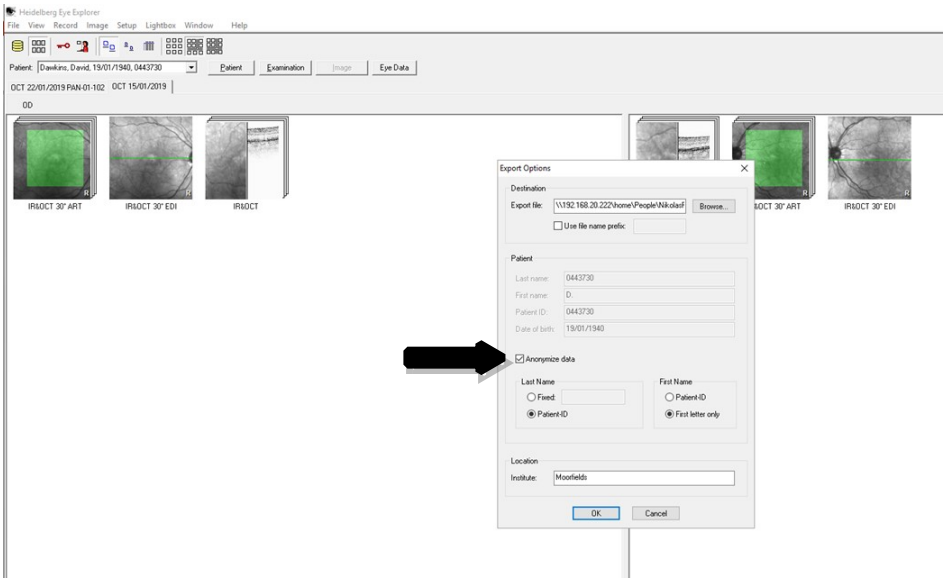

Another box will appear called Export Options. Please click on the anonymise data box.

Export the images to this drive using E2E files. Choose the destination file in the browse box and save all the E2E files to the USB

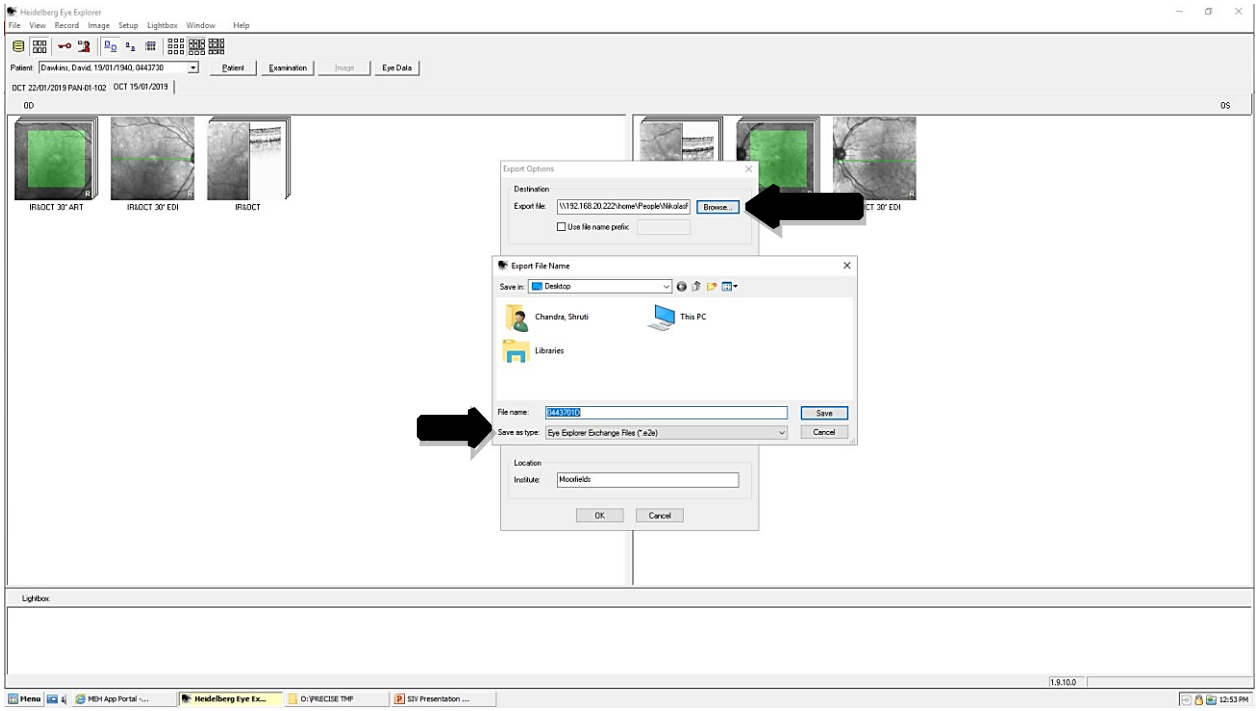

B. Grading sheet for PRECISE data – neovascular AMD

1. Study ID: PRECISE ID
2. Age: Age in years
3. Gender: 0- Male; 1- Female
4. Study Eye: 0- Right; 1- Left
5. Vol scan: Volume scan graded 0-19; 1- 25; 2- 31; 3- 49 line scan
6. Image Gr/UnGr: Image gradable or not 0 - Ungradable; 1 - Gradable
7. If UnGr: If image ungradable cause of ungradability 0- >50% haem; 1- >500um foveal atrophy; 2- central fibrotic scar size GLD 1000um; 3- no CNV; 4- poor quality <= 20dB
8. MNV: Presence of CNV 0- No; 1- Yes Foveal; 2- Yes Non Foveal; 3- Yes Foveal+Non foveal
9. MNV Type: 1- Type 1; 2-Type 2; 3- RAP; 4- PCV
10. Cmpnt 1mm: Presence of any component of MNV complex(fluid or contiguous blood or PED or fibrosis) at fovea i.e central 1mm 0- No; 1- Yes
11. SRF: Presence of Subretinal fluid 0- No; 1- Yes Foveal; 2- Yes Non Foveal; 3- Yes Foveal+Non foveal
12. IRF: Presence of Intraretinal fluid 0- No; 1- Yes Foveal; 2- Yes Non Foveal; 3- Yes Foveal+Non foveal
13. PED: Presence of Pigment Epithelial Detachment 0- No; 1- Yes Foveal; 2- Yes Non Foveal; 3- Yes Foveal+Non foveal
14. PED Type: Type of Pigment epithelial detachment 0- No PED; 1- Serous PED; 2- FVPED; 3- Hgheic PED
15. PED Ht: Highest vertical measurement of the PED (related to CNV) in microns, measured from tip of RPE to Bruch's membrane
16. Scan# PED: Scan number where PED height is measured
17. PED Feature: 0- No PED; 1- Lamellar; 2- Wrinkled; 3: obvious RPE rip with folding of RPE
18. OCT Phntyp: OCT phenotype 1- : IRF and SRF; 2- SRF only phenotype; 3- PED+SRF; 4- PED+IRF; 5- PED+SRF+IRF
19. Drusen: Presence of Drusen 0- No; 1- Yes
20. SDD: Presence of subretinal drusenoid deposit 0- No; 1- Yes
21. HDL: Hyporeflective Drusenoid Lesion 0- No; 1- Yes

22. HRF: Hyperreflective Foci 0- No; 1- Yes
23. EZ loss: Loss of Ellipsoid zone 0- No; 1- Yes Foveal; 2- Yes Non Foveal; 3- Yes Foveal+Non foveal
24. ELM loss: Loss of External limiting membrane 0- No; 1- Yes Foveal; 2- Yes Non Foveal; 3- Yes Foveal+Non foveal
25. SHRM: Presence of subretinal hyperreflective material 0- No; 1- Yes Foveal; 2- Yes Non Foveal; 3- Yes Foveal+Non foveal
26. SHRM Wd: Measure of MAXIMUM SHRM width in microns
27. SHRM Ht: Measure of Height of SHRM in microns where width was measured
28. Scan#SHRM: Scan number where SHRM width and height is measured
29. Atrophy: Presence of atrophy 0- No; 1- Yes Foveal; 2- Yes Non Foveal; 3- Yes Foveal+Non foveal
30. Fibrosis: Presence of Fibrosis 0- No; 1- Yes Foveal; 2- Yes Non Foveal; 3- Yes Foveal+Non foveal
31. ORT: Presence of outer retinal tubulation 0- No; 1- Yes Foveal; 2- Yes Non Foveal; 3- Yes Foveal+Non foveal
32. VMT: Presence of vitreomacular traction 0- No; 1- Yes Foveal; 2- Yes Non Foveal; 3- Yes Foveal+Non foveal
33. ERM: Presence of Epiretinal membrane 0- No; 1- Yes Foveal; 2- Yes Non Foveal; 3- Yes Foveal+Non foveal
34. PVD: Presence of PVD 0- No; 1- Yes Foveal; 2- Yes Non Foveal; 3- Yes Foveal+Non foveal; 4- Not seen on OCT
35. CST: Central subfield thickness in microns

8.3 Appendix 3

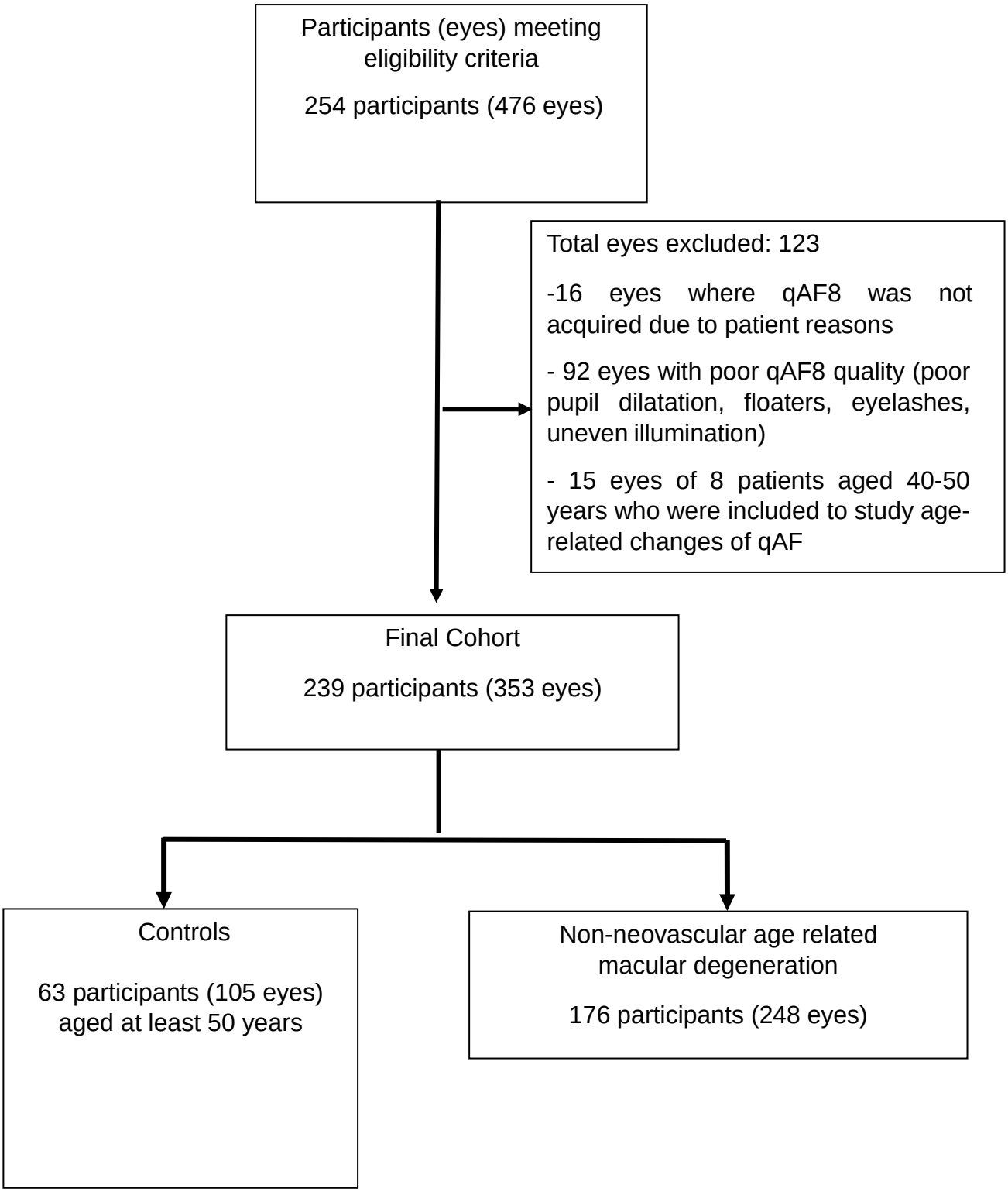

Figure S3.1 Flowchart showing patient flow in the PEONY study

8.4 Appendix 4

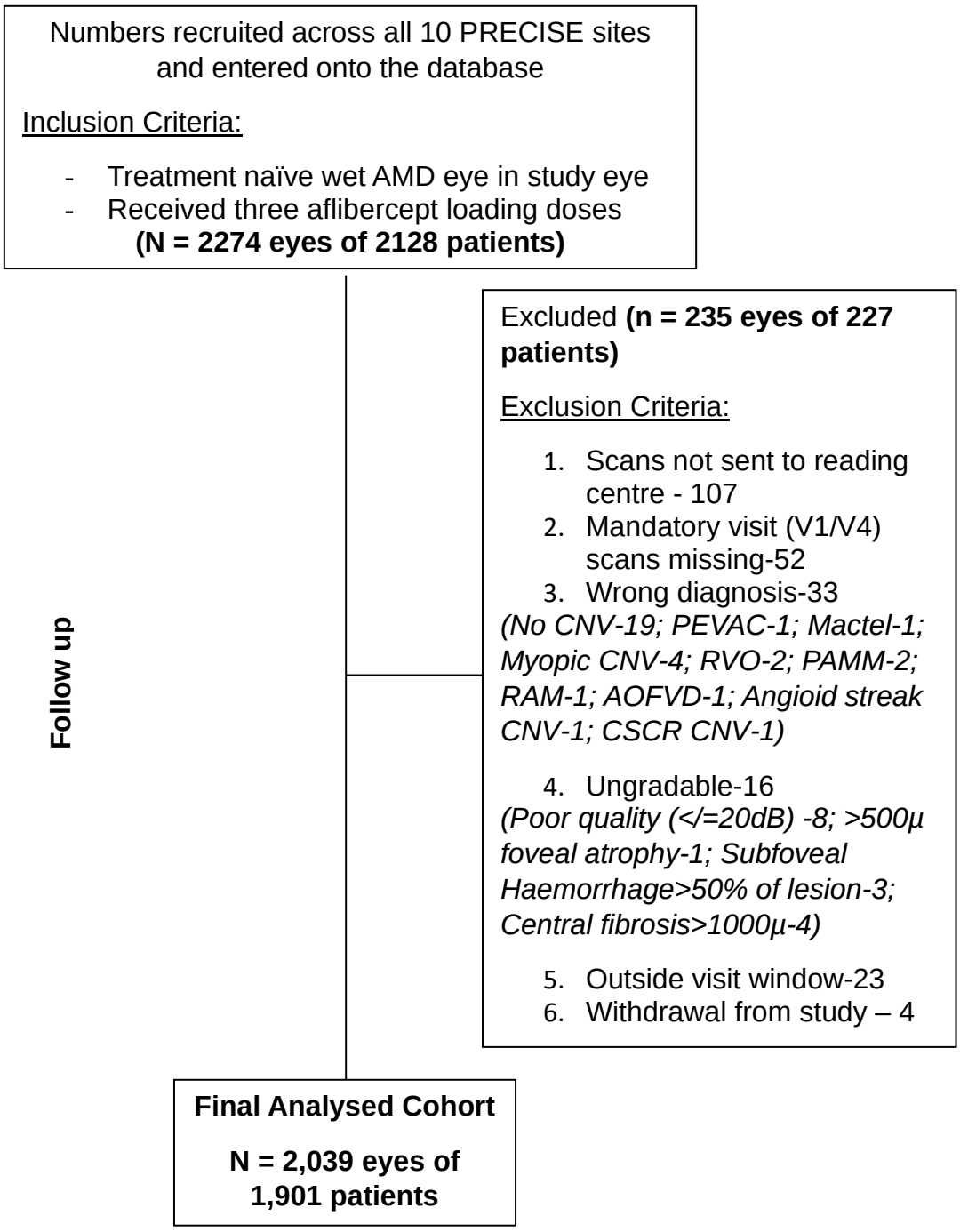

Figure S4.1: Participant Flow for Chapter 4, section 4.2

***Abbreviations**: AMD- Age related macular degeneration; Angioid streak CNV- Angioid streak related choroidal neovascularization; AOFVD- Adult onset foveomacular vitelliform dystrophy; CSCR CNV- Central serous chorioretinopathy related choroidal neovascularization; CNV-Choroidal neovascularization; dB- decibel; Mactel- Macular telangiectasia; Myopic CNV- Myopic choroidal neovascularization; PAMM- Paracentral acute middle maculopathy; PEVAC-Perifoveal exudative vascular anomalous complex; RAM- Retinal artery macroaneurysm; RVO- Retinal vein occlusion; V1- Visit 1; V4- Visit 4; µ-microns*

Table S4.1. Ocular and OCT characteristics associated with VA>=68 ETDRS letters and VA<54 ETDRS letters – univariate and multivariable analysis using Generalised Estimating Equations (GEE)

	VA>=68 N=2,039; Events=650				**VA<54 N=2,039; Events=660**			
	Univariate		**Multivariable**		**Univariate**		**Multivariable**	
Characteristic	**OR (95% CI)**	**p-value**	**OR (95% CI)**	**p-value**	**OR (95% CI)**	**p-value**	**OR (95% CI)**	**p-value**
Age, years								
< 60	—		—		—		—	
60-69	1.41 (0.60 - 3.30)	0.43	1.44 (0.56 - 3.73)	0.45	0.61 (0.26 - 1.46)	0.27	0.56 (0.17 - 1.83)	0.34
70-79	1.07 (0.47 - 2.42)	0.87	1.11 (0.45 - 2.73)	0.83	0.86 (0.38 - 1.96)	0.73	0.97 (0.31 - 2.96)	0.95
>=80	0.79 (0.35 - 1.77)	0.56	0.88 (0.35 - 2.16)	0.77	1.09 (0.49 - 2.45)	0.83	1.11 (0.36 - 3.39)	0.86
Gender								
Female	—		—		—		—	
Male	1.09 (0.90 - 1.32)	0.37	1.20 (0.96 - 1.50)	0.11	0.97 (0.80 - 1.18)	0.77	0.96 (0.75 - 1.23)	0.76
Ethnicity								
White	—		—		—		—	
Non-White (Black/South Asian/other Asian/other)	0.75 (0.47 - 1.19)	0.22	0.65 (0.39 - 1.08)	0.10	1.22 (0.79 - 1.88)	0.37	1.31 (0.76 - 2.24)	0.33
Location of MNV								
Foveal involving	—		—		—		—	
Non-Foveal location	3.64 (2.34 - 5.65)	**<0.001**	1.76 (0.93 - 3.32)	0.08	0.20 (0.09 - 0.41)	**<0.001**	0.53 (0.20 - 1.42)	0.21
MNV Type								
Type 1	—		—		—		—	

	VA>=68 N=2,039; Events=650				VA<54 N=2,039; Events=660			
	Univariate		Multivariable		Univariate		Multivariable	
Characteristic	**OR (95% CI)**	**p-value**	**OR (95% CI)**	**p-value**	**OR (95% CI)**	**p-value**	**OR (95% CI)**	**p-value**
Type 2+ mixed	0.49 (0.39 - 0.61)	**<0.001**	0.91 (0.67 - 1.24)	0.55	2.16 (1.72 - 2.71)	**<0.001**	1.12 (0.80 - 1.56)	0.52
RAP	0.49 (0.38 - 0.63)	**<0.001**	0.92 (0.62 - 1.37)	0.68	1.72 (1.33 - 2.22)	**<0.001**	0.76 (0.52 - 1.11)	0.16
PCV	0.33 (0.21 - 0.53)	**<0.001**	0.61 (0.36 - 1.05)	0.08	3.24 (2.21 - 4.76)	**<0.001**	1.66 (1.00 - 2.76)	**0.049**
Subfoveal presence of any component of MNV complex								
No	—		—		—		—	
Yes	0.26 (0.15 - 0.46)	**<0.001**	0.79 (0.35 - 1.77)	0.56	5.19 (2.00 - 13.5)	**<0.001**	1.33 (0.36 - 4.92)	0.67
CST per 100 microns increase	0.61 (0.56 - 0.67)	**<0.001**	0.71 (0.65 - 0.78)	**<0.001**	1.54 (1.44 - 1.65)	**<0.001**	1.40 (1.30 - 1.51)	**<0.001**
Presence of SRF								
No	—		—		—		—	
Yes, Foveal involving	1.49 (1.14 - 1.95)	**0.004**	1.27 (0.86 - 1.88)	0.22	0.73 (0.56 - 0.95)	**0.02**	0.75 (0.51 - 1.08)	0.12
Yes, Non-Fovea involving	0.99 (0.74 - 1.32)	0.92	1.17 (0.78 - 1.74)	0.45	1.28 (0.98 - 1.68)	0.07	0.94 (0.65 - 1.36)	0.74
Presence of IRF								
No	—		—		—		—	
Yes, Foveal involving	0.39 (0.31 - 0.48)	**<0.001**	0.60 (0.43 - 0.84)	**0.003**	2.65 (2.16 - 3.25)	**<0.001**	2.14 (1.55 - 2.94)	**<0.001**

	VA>=68 N=2,039; Events=650				VA<54 N=2,039; Events=660			
	Univariate		Multivariable		Univariate		Multivariable	
Characteristic	**OR (95% CI)**	**p-value**	**OR (95% CI)**	**p-value**	**OR (95% CI)**	**p-value**	**OR (95% CI)**	**p-value**
Yes, Non-Foveal involving	0.82 (0.62 - 1.09)	0.18	0.85 (0.60 - 1.22)	0.39	1.14 (0.83 - 1.55)	0.43	0.97 (0.63 - 1.50)	0.88
Presence of PED								
No	—		—		—		—	
Yes, Foveal involving	1.82 (1.11 - 3.01)	**0.02**	1.63 (0.92 - 2.89)	0.10	0.63 (0.42 - 0.94)	**0.02**	0.78 (0.46 - 1.32)	0.35
Yes, Non-Foveal involving	3.09 (1.81 - 5.27)	**<0.001**	1.83 (0.99 - 3.36)	0.05	0.37 (0.23 - 0.59)	**<0.001**	0.77 (0.43 - 1.38)	0.38
Presence of SHRM								
No	—		—		—		—	
Yes, Foveal involving	0.39 (0.31 - 0.47)	**<0.001**	0.63 (0.46 - 0.88)	**0.007**	2.62 (2.13 - 3.22)	**<0.001**	1.73 (1.21 - 2.46)	**0.002**
Yes, Non-Foveal involving	0.94 (0.70 - 1.27)	0.69	1.09 (0.72 - 1.64)	0.69	1.04 (0.73 - 1.48)	0.82	0.99 (0.60 - 1.61)	0.95
Presence of Atrophy								
No	—		—		—		—	
Yes, Foveal involving	0.11 (0.05 - 0.23)	**<0.001**	0.27 (0.09 - 0.85)	**0.03**	8.82 (5.76 - 13.5)	**<0.001**	5.54 (2.94 - 10.5)	**<0.001**
Yes, Non-Foveal involving	1.11 (0.85 - 1.45)	0.42	0.89 (0.63 - 1.25)	0.49	0.68 (0.51 - 0.91)	**0.01**	0.85 (0.57 - 1.26)	0.42
Presence of fibrosis								
No	—		—		—		—	
Yes, Foveal involving	0.05 (0.02 - 0.10)	**<0.001**	0.18 (0.07 - 0.48)	**<0.001**	11.7 (8.51 - 16.0)	**<0.001**	3.85 (2.34 - 6.34)	**<0.001**

	VA>=68 N=2,039; Events=650				VA<54 N=2,039; Events=660			
	Univariate		Multivariable		Univariate		Multivariable	
Characteristic	**OR (95% CI)**	**p-value**	**OR (95% CI)**	**p-value**	**OR (95% CI)**	**p-value**	**OR (95% CI)**	**p-value**
Yes, Non-Foveal involving	0.57 (0.26 - 1.25)	0.16	0.66 (0.25 - 1.75)	0.40	1.29 (0.61 - 2.74)	0.51	0.93 (0.39 - 2.22)	0.88
Presence of ORT								
No	—		—		—		—	
Yes, Foveal involving	0.62 (0.24 - 1.65)	0.34	1.21 (0.32 - 4.59)	0.78	2.74 (1.24 - 6.05)	**0.01**	1.49 (0.44 - 5.07)	0.52
Yes, Non-Foveal involving	0.82 (0.37 - 1.81)	0.63	2.00 (0.63 - 6.37)	0.24	1.28 (0.60 - 2.72)	0.53	0.46 (0.15 - 1.44)	0.18
Presence of SDD								
No	—		—		—		—	
Yes	1.18 (0.97 - 1.45)	0.10	1.23 (0.96 - 1.57)	0.10	0.70 (0.57 - 0.87)	**0.001**	0.75 (0.57 - 0.99)	**0.04**
HRF								
No	—		—		—		—	
Yes	0.87 (0.71 - 1.06)	0.16	1.13 (0.89 - 1.44)	0.30	1.09 (0.89 - 1.34)	0.41	0.81 (0.62 - 1.07)	0.13
Presence of ERM								
No	—		—		—		—	
Yes, Foveal involving	0.77 (0.46 - 1.30)	0.33	0.80 (0.47 - 1.38)	0.43	1.41 (0.87 - 2.29)	0.16	1.76 (0.98 - 3.17)	0.06
Yes, Non-Foveal involving	0.72 (0.49 - 1.06)	0.10	0.67 (0.42 - 1.05)	0.08	1.01 (0.71 - 1.44)	0.96	0.97 (0.64 - 1.47)	0.89
EZ/ELM loss								
Neither Foveal-involving	—		—				—	

	VA>=68 N=2,039; Events=650				VA<54 N=2,039; Events=660			
	Univariate		**Multivariable**		**Univariate**		**Multivariable**	
Characteristic	**OR (95% CI)**	**p-value**	**OR (95% CI)**	**p-value**	**OR (95% CI)**	**p-value**	**OR (95% CI)**	**p-value**
At least one Foveal-involving	0.04 (0.02 - 0.08)	**<0.001**	0.22 (0.09 - 0.57)	**0.002**	18.8 (14.0 – 25.1)	**<0.001**	3.83 (2.34 - 6.27)	**<0.001**
Both ungradable	0.44 (0.35 – 0.55)	**<0.001**	0.70 (0.52 - 0.96)	**0.03**	2.35 (1.84 – 2.98)	**<0.001**	1.28 (0.92 - 1.78)	0.14

Abbreviations: OCT- Optical coherence tomography; ETDRS- Early Treatment Diabetic Retinopathy Study; GEE -Generalised Estimating Equation; VA- Visual Acuity; OR- Odds Ratio; CI- Confidence interval; MNV – Macular neovascularisation; PCV- polypoidal vasculopathy; RAP-retinal angiomatous proliferation; EZ- Ellipsoid zone; ELM- External limiting membrane.

Table S4.2. Ocular and OCT characteristics associated with moderate VA comparing moderate (VA 54-67) vs good VA (VA>=68) and moderate (VA 54-67) vs poor VA (VA<54) – univariable and multivariable analysis using Generalised Estimating Equations (GEE)

	VA 54-67 vs VA>=68 N= 1379; Events=729				**VA 54-67 vs VA<54** N=1389; Events=729			
	Univariate		**Multivariable**		**Univariate**		**Multivariable**	
Characteristic	**OR (95% CI)**	**p-value**	**OR (95% CI)**	**p-value**	**OR (95% CI)**	**p-value**	**OR (95% CI)**	**p-value**
Age, years								
< 60	—		—		—		—	
60-69	0.86 (0.32 - 2.29)	0.76	0.78 (0.27 - 2.23)	0.64	1.50 (0.55 - 4.07)	0.43	1.48 (0.41 - 5.32)	0.54
70-79	1.00 (0.39 - 2.56)	>0.99	0.90 (0.33 - 2.47)	0.84	1.16 (0.45 - 2.97)	0.76	0.96 (0.29 - 3.22)	0.95
>=80	1.29 (0.51 - 3.30)	0.59	1.12 (0.41 - 3.07)	0.82	1.03 (0.41 - 2.63)	0.95	0.87 (0.26 - 2.93)	0.82
Gender								
Female	—		—		—		—	
Male	0.90 (0.72 - 1.12)	0.34	0.84 (0.66 - 1.06)	0.15	0.97 (0.78 - 1.21)	0.81	0.99 (0.76 - 1.29)	0.93
Ethnicity								
White	—		—		—		—	
black/south Asian/other	1.27 (0.75 - 2.15)	0.37	1.54 (0.90 - 2.64)	0.11	0.93 (0.57 - 1.51)	0.76	0.92 (0.51 - 1.66)	0.79
Location of MNV								
Yes, Foveal involving	—		—		—		—	
Yes, Non-Foveal	0.41 (0.25 - 0.66)	**<0.001**	0.62 (0.32 - 1.20)	0.16	3.04 (1.36 - 6.79)	**0.007**	1.94 (0.54 - 6.91)	0.31
MNV Type								
Type 1	—		—		—		—	
Type 2	1.58 (1.22 - 2.03)	**<0.001**	1.00 (0.71 - 1.40)	>0.99	0.58 (0.45 - 0.74)	**<0.001**	0.93 (0.65 - 1.32)	0.69
RAP	1.84 (1.38 - 2.45)	**<0.001**	1.18 (0.78 - 1.80)	0.44	0.77 (0.58 - 1.03)	**0.08**	1.51 (1.00 - 2.27)	**0.049**
PCV	1.92 (1.14 - 3.25)	**0.01**	1.38 (0.77 - 2.49)	0.28	0.42 (0.27 - 0.64)	**<0.001**	0.65 (0.38 - 1.12)	0.12

	VA 54-67 vs VA>=68 N= 1379; Events=729				**VA 54-67 vs VA<54** N=1389; Events=729			
	Univariate		**Multivariable**		**Univariate**		**Multivariable**	
Characteristic	**OR (95% CI)**	**p-value**	**OR (95% CI)**	**p-value**	**OR (95% CI)**	**p-value**	**OR (95% CI)**	**p-value**
Subfoveal presence of any component of MNV complex								
No	—		—		—		—	
Yes	2.55 (1.38 - 4.68)	**0.003**	1.20 (0.52 - 2.78)	0.67	0.34 (0.12 - 0.93)	**0.04**	0.90 (0.18 - 4.45)	0.90
CST per 100 microns increase	1.36 (1.23 - 1.49)	**<0.001**	1.29 (1.17 - 1.43)	**<0.001**	0.72 (0.67 - 0.78)	**<0.001**	0.77 (0.71 - 0.84)	**<0.001**
Presence of SRF								
No	—		—		—		—	
Yes, Foveal involving	0.72 (0.53 - 0.97)	**0.03**	0.78 (0.52 - 1.19)	0.25	1.18 (0.88 - 1.59)	0.27	1.26 (0.84 - 1.91)	0.26
Yes, Non-Foveal	0.85 (0.62 - 1.18)	0.34	0.78 (0.51 - 1.20)	0.27	0.73 (0.54 - 0.99)	**0.04**	1.05 (0.71 - 1.57)	0.81
Presence of IRF								
No	—		—		—		—	
Yes, Foveal involving	1.81 (1.41 - 2.31)	**<0.001**	1.40 (0.98 - 2.01)	0.07	0.49 (0.39 - 0.62)	**<0.001**	0.52 (0.37 - 0.74)	**<0.001**
Yes, Non-Foveal	1.21 (0.88 - 1.66)	0.25	1.14 (0.78 - 1.66)	0.50	0.97 (0.68 - 1.37)	0.84	1.08 (0.69 - 1.71)	0.73
Presence of PED								
No	—		—		—		—	
Yes, Foveal involving	0.64 (0.37 - 1.11)	0.11	0.60 (0.32 - 1.10)	0.10	1.33 (0.85 - 2.07)	0.21	1.13 (0.65 - 1.96)	0.66
Yes, Non-Foveal	0.44 (0.24 - 0.80)	**0.007**	0.55 (0.29 - 1.04)	0.07	1.87 (1.12 - 3.13)	**0.02**	1.07 (0.58 - 1.97)	0.84
Presence of SHRM								
No	—		—		—		—	
Yes, Foveal involving	1.90 (1.51 - 2.39)	**<0.001**	1.53 (1.06 - 2.20)	**0.02**	0.51 (0.40 - 0.64)	**<0.001**	0.64 (0.44 - 0.93)	**0.02**
Yes, Non-Foveal	1.06 (0.75 - 1.48)	0.75	0.95 (0.61 - 1.47)	0.80	0.98 (0.66 - 1.46)	0.94	1.02 (0.60 - 1.74)	0.93
Presence of Atrophy								

	VA 54-67 vs VA>=68 N= 1379; Events=729				**VA 54-67 vs VA<54** N=1389; Events=729			
	Univariate		**Multivariable**		**Univariate**		**Multivariable**	
Characteristic	**OR (95% CI)**	**p-value**	**OR (95% CI)**	**p-value**	**OR (95% CI)**	**p-value**	**OR (95% CI)**	**p-value**
No	—		—		—		—	
Yes, Foveal involving	2.87 (1.19 - 6.91)	**0.02**	1.93 (0.65 - 5.74)	0.24	0.17 (0.10 - 0.27)	**<0.001**	0.22 (0.11 - 0.44)	**<0.001**
Yes, Non-Foveal	1.06 (0.80 - 1.42)	0.68	1.18 (0.82 - 1.70)	0.36	1.51 (1.09 - 2.09)	**0.01**	1.24 (0.83 - 1.87)	0.30
Presence of fibrosis								
No	—		—		—		—	
Yes, Foveal involving	6.26 (2.86 - 13.7)	**<0.001**	4.08 (1.58 - 10.5)	**0.004**	0.15 (0.10 - 0.20)	**<0.001**	0.33 (0.20 - 0.56)	**<0.001**
Yes, Non-Foveal	1.83 (0.76 - 4.40)	0.18	1.71 (0.61 - 4.80)	0.31	0.98 (0.44 - 2.18)	0.95	1.25 (0.49 - 3.19)	0.64
Presence of ORT								
No	—		—		—		—	
Yes, Foveal involving	0.89 (0.26 - 3.09)	0.85	0.48 (0.12 - 1.97)	0.31	0.34 (0.13 - 0.91)	**0.032**	0.47 (0.11 - 1.95)	0.30
Yes, Non-Foveal	1.14 (0.45 - 2.86)	0.79	0.50 (0.15 - 1.70)	0.27	0.81 (0.34 - 1.92)	0.63	1.73 (0.56 - 5.38)	0.34
Presence of SDD								
No	—		—		—		—	
Yes	0.98 (0.78 - 1.23)	0.88	0.87 (0.67 - 1.12)	0.28	1.42 (1.12 - 1.79)	**0.004**	1.28 (0.95 - 1.73)	0.10
HRF								
No	—		—		—		—	
Yes	1.14 (0.90 - 1.43)	0.27	0.89 (0.69 - 1.16)	0.40	0.98 (0.77 - 1.24)	0.85	1.20 (0.90 - 1.60)	0.22
Presence of ERM								
No	—		—		—		—	
Yes, Foveal involving	1.12 (0.61 - 2.07)	0.72	1.07 (0.59 - 1.93)	0.83	0.74 (0.42 - 1.31)	0.31	0.59 (0.30 - 1.14)	0.12
Yes, Non-Foveal	1.53 (1.01 - 2.32)	**0.047**	1.69 (1.06 - 2.69)	**0.03**	1.17 (0.79 - 1.73)	0.42	1.18 (0.76 - 1.82)	0.46
EZ/ELM								
Neither Foveal involving	—		—		—		—	

	VA 54-67 vs VA>=68 N= 1379; Events=729				**VA 54-67 vs VA<54** N=1389; Events=729			
	Univariate		**Multivariable**		**Univariate**		**Multivariable**	
Characteristic	**OR (95% CI)**	**p-value**	**OR (95% CI)**	**p-value**	**OR (95% CI)**	**p-value**	**OR (95% CI)**	**p-value**
Foveal-involving EZ/ELM	6.20 (3.36 - 11.4)	**<0.001**	2.52 (1.05 - 6.08)	**0.04**	0.10 (0.07 - 0.13)	**<0.001**	0.36 (0.21 - 0.61)	**<0.001**
Both ungradable	1.87 (1.47 - 2.38)	**<0.001**	1.37 (0.98 - 1.92)	0.06	0.57 (0.44 - 0.74)	**<0.001**	0.92 (0.65 - 1.30)	0.63

Abbreviations: OCT- Optical coherence tomography; ETDRS- Early Treatment Diabetic Retinopathy Study; GEE -Generalised Estimating Equation; VA- Visual Acuity; OR- Odds Ratio; CI- Confidence interval; MNV – Macular neovascularisation; PCV- polypoidal vasculopathy; RAP-retinal angiomatous proliferation; EZ- Ellipsoid zone; ELM- External limiting membrane.

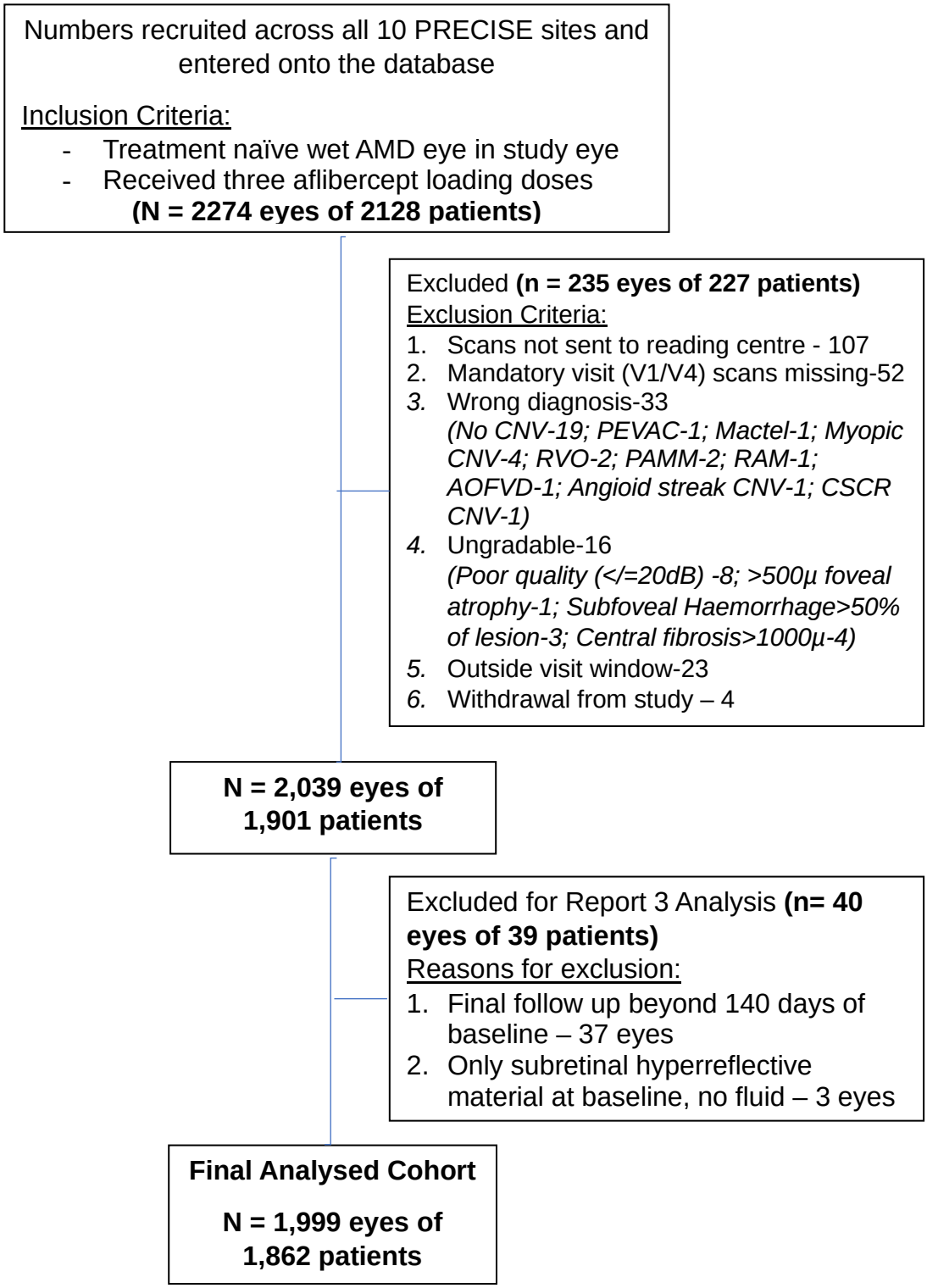

Figure S4.2: Participant Flow for Chapter 4, section 4.3

***Abbreviations**: AMD- Age related macular degeneration; Angioid streak CNV- Angioid streak related choroidal neovascularization; AOFVD- Adult onset foveomacular vitelliform dystrophy; CSCR CNV- Central serous chorioretinopathy related choroidal neovascularization; CNV- Choroidal neovascularization; dB- decibel; Mactel- Macular telangiectasia; Myopic CNV- Myopic choroidal neovascularization; PAMM- Paracentral acute middle maculopathy; PEVAC-Perifoveal exudative vascular anomalous complex; RAM- Retinal artery macroaneurysm; RVO- Retinal vein occlusion; V1- Visit 1; V4- Visit 4; µ-microns*

Table S4.3. Demographic and OCT features associated with early residual fluid at visit 4 - univariate and multivariable analysis using Generalised Estimating Equations (GEE) for early residual fluid, presence of eSRF and presence of eIRF

	ERF				**SRF**				**IRF**			
	Univariate		**Multivariable**		**Univariate**		**Multivariable**		**Univariate**		**Multivariable**	
Characteristic	OR (95% CI)	p-value	OR (95% CI)	p-value	OR (95% CI)	p-value	OR (95% CI)	p-value	OR (95% CI)	p-value	OR (95% CI)	p-value
Age, per 5 year increase	0.83 (0.78 - 0.88)	<0.001			0.79 (0.74 - 0.84)	<0.001			1.04 (0.97 - 1.11)	0.27		
Age, years												
< 70	—		—		—		—		—		—	
70-79	1.02 (0.75 - 1.39)	0.91	1.12 (0.81 - 1.55)	0.50	0.95 (0.70 - 1.30)	0.74	1.14 (0.81 - 1.60)	0.45	1.29 (0.86 - 1.93)	0.22	1.21 (0.77 - 1.90)	0.40
>=80	0.58 (0.43 - 0.78)	<0.001	0.73 (0.53 - 1.00)	0.049	0.48 (0.35 - 0.65)	<0.001	0.75 (0.54 - 1.05)	0.09	1.32 (0.90 - 1.95)	0.16	0.96 (0.62 - 1.50)	0.86
Gender												
Female	—		—		—		—		—		—	
Male	1.33 (1.11 - 1.60)	0.002	1.21 (1.00 - 1.46)	0.06	1.34 (1.11 - 1.61)	0.002	1.19 (0.96 - 1.47)	0.10	1.13 (0.90 - 1.40)	0.28	1.16 (0.91 - 1.48)	0.23
Ethnicity												
White	—		—		—		—		—		—	
black/south Asian/other	1.41 (0.93 - 2.14)	0.11	1.53 (0.99 - 2.36)	0.06	1.46 (0.97 - 2.22)	0.07	1.62 (1.03 - 2.56)	0.04	1.08 (0.66 - 1.77)	0.77	1.24 (0.69 - 2.24)	0.47
Visit 1 visual acuity categories, ETDRS												
>=68	—		—		—		—		—		—	

	ERF				SRF				IRF			
	Univariate		**Multivariable**		**Univariate**		**Multivariable**		**Univariate**		**Multivariable**	
Characteristic	OR (95% CI)	p-value	OR (95% CI)	p-value	OR (95% CI)	p-value	OR (95% CI)	p-value	OR (95% CI)	p-value	OR (95% CI)	p-value
54-67	0.86 (0.70 - 1.07)	0.17	0.88 (0.70 - 1.12)	0.30	0.73 (0.58 - 0.91)	0.004	0.81 (0.63 - 1.04)	0.10	1.58 (1.18 - 2.12)	0.002	1.20 (0.87 - 1.65)	0.28
<54	0.97 (0.78 - 1.21)	0.82	0.84 (0.63 - 1.12)	0.24	0.65 (0.52 - 0.82)	<0.001	0.70 (0.51 - 0.96)	0.03	2.78 (2.10 - 3.70)	<0.001	1.34 (0.93 - 1.93)	0.11
Visit 1 visual acuity, per 5 letter increase	1.01 (0.98 - 1.04)	0.71			1.06 (1.03 - 1.10)	<0.001			0.88 (0.85 - 0.92)	<0.001		
Visit 1 visual acuity, per 5 letter decrease	0.99 (0.96 - 1.02)	0.71			0.94 (0.91 - 0.98)	<0.001			1.13 (1.09 - 1.17)	<0.001		
CST per 100 microns increase	1.26 (1.18 - 1.33)	<0.001	1.31 (1.22 - 1.41)	<0.001	1.20 (1.13 - 1.27)	<0.001	1.29 (1.20 - 1.39)	<0.001	1.23 (1.16 - 1.31)	<0.001	1.19 (1.10 - 1.30)	<0.001
Central subfield thickness quartiles												
<=340	—				—				—			
(340,415]	1.50 (1.17 - 1.92)	0.001			1.63 (1.25 - 2.13)	<0.001			1.16 (0.83 - 1.62)	0.39		
(415,525]	1.88 (1.46 - 2.41)	<0.001			1.92 (1.48 - 2.50)	<0.001			1.55 (1.13 - 2.13)	0.007		
>525	2.66 (2.06 - 3.42)	<0.001			2.29 (1.76 - 2.98)	<0.001			2.55 (1.88 - 3.46)	<0.001		
CNV Type												

	ERF				SRF				IRF			
	Univariate		**Multivariable**		**Univariate**		**Multivariable**		**Univariate**		**Multivariable**	
Characteristic	OR (95% CI)	p-value	OR (95% CI)	p-value	OR (95% CI)	p-value	OR (95% CI)	p-value	OR (95% CI)	p-value	OR (95% CI)	p-value
Type 1	—		—		—		—		—		—	
Type 2	0.86 (0.69 - 1.06)	0.15	0.95 (0.72 - 1.24)	0.69	0.69 (0.56 - 0.85)	<0.001	0.87 (0.65 - 1.15)	0.33	1.86 (1.42 - 2.44)	<0.001	1.27 (0.89 - 1.81)	0.20
RAP	0.41 (0.32 - 0.52)	<0.001	0.70 (0.51 - 0.97)	0.03	0.14 (0.10 - 0.19)	<0.001	0.58 (0.38 - 0.88)	0.01	2.66 (1.99 - 3.56)	<0.001	1.01 (0.71 - 1.45)	0.95
PCV	1.29 (0.87 - 1.90)	0.21	0.98 (0.61 - 1.56)	0.92	1.03 (0.70 - 1.51)	0.88	0.91 (0.56 - 1.47)	0.69	2.27 (1.46 - 3.53)	<0.001	1.28 (0.71 - 2.28)	0.41
Presence of any component of CNV complex												
No	—		—		—		—		—		—	
Yes	1.09 (0.63 - 1.87)	0.77	0.94 (0.42 - 2.09)	0.87	1.13 (0.64 - 1.99)	0.68	0.70 (0.28 - 1.77)	0.45	0.83 (0.44 - 1.55)	0.55	0.84 (0.36 - 2.01)	0.70
Presence of CNV												
Yes, Foveal involving	—		—		—		—		—		—	
Yes, Non-Foveal	0.93 (0.60 - 1.43)	0.73	1.35 (0.70 - 2.60)	0.37	0.81 (0.51 - 1.28)	0.36	1.04 (0.51 - 2.13)	0.92	1.16 (0.70 - 1.93)	0.56	1.64 (0.80 - 3.39)	0.18
Combination of SRF and/or IRF												
IRF only	—		—		—		—		—		—	
IRF and SRF	2.33 (1.76 - 3.08)	<0.001	1.62 (1.17 - 2.22)	0.003	10.3 (5.65 - 18.6)	<0.001	6.79 (3.61 - 12.8)	<0.001	1.71 (1.28 -	<0.001	1.31 (0.94 - 1.83)	0.11

	ERF				SRF				IRF			
	Univariate		**Multivariable**		**Univariate**		**Multivariable**		**Univariate**		**Multivariable**	
Characteristic	OR (95% CI)	p-value	OR (95% CI)	p-value	OR (95% CI)	p-value	OR (95% CI)	p-value	OR (95% CI)	p-value	OR (95% CI)	p-value
									2.28)			
SRF only	3.57 (2.73 - 4.67)	<0.001	2.26 (1.59 - 3.20)	<0.001	35.1 (19.5 - 63.0)	<0.001	19.9 (10.4 - 37.9)	<0.001	0.24 (0.17 - 0.34)	<0.001	0.22 (0.14 - 0.33)	<0.001
Presence of PED												
No	—		—		—		—		—		—	
Yes, Foveal involving	1.13 (0.76 - 1.68)	0.55	1.02 (0.66 - 1.56)	0.94	1.42 (0.93 - 2.19)	0.11	1.14 (0.71 - 1.85)	0.58	0.81 (0.51 - 1.30)	0.38	1.13 (0.68 - 1.87)	0.64
Yes, Non-Foveal	1.08 (0.69 - 1.68)	0.74	1.38 (0.86 - 2.21)	0.19	1.16 (0.72 - 1.86)	0.54	1.47 (0.86 - 2.52)	0.16	0.92 (0.54 - 1.55)	0.75	1.31 (0.74 - 2.31)	0.36
Presence of Atrophy or ORT	0.54 (0.43 - 0.66)	<0.001	0.70 (0.50 - 0.99)	0.04	0.34 (0.26 - 0.44)	<0.001	0.63 (0.42 - 0.93)	0.02	1.41 (1.11 - 1.80)	0.006	0.78 (0.53 - 1.15)	0.20
Presence of fibrosis												
No	—		—		—		—		—		—	
Yes	1.33 (1.04 - 1.71)	0.02	1.33 (0.92 - 1.92)	0.13	0.90 (0.70 - 1.17)	0.43	1.31 (0.85 - 2.01)	0.22	2.55 (1.95 - 3.33)	<0.001	1.23 (0.82 - 1.84)	0.33
Presence of SHRM												
No	—		—		—		—		—		—	
Yes	1.04 (0.87 - 1.25)	0.65	0.93 (0.71 - 1.22)	0.60	1.06 (0.88 - 1.28)	0.52	0.93 (0.70 - 1.24)	0.63	1.25 (1.00 - 1.55)	0.05	0.92 (0.64 - 1.30)	0.62
Presence of												

	ERF				**SRF**				**IRF**			
	Univariate		**Multivariable**		**Univariate**		**Multivariable**		**Univariate**		**Multivariable**	
Characteristic	OR (95% CI)	p-value	OR (95% CI)	p-value	OR (95% CI)	p-value	OR (95% CI)	p-value	OR (95% CI)	p-value	OR (95% CI)	p-value
Drusen												
No	—		—		—		—		—		—	
Yes	0.90 (0.65 - 1.24)	0.52	1.13 (0.76 - 1.66)	0.55	1.02 (0.73 - 1.43)	0.89	1.30 (0.84 - 2.00)	0.24	0.76 (0.53 - 1.09)	0.14	0.99 (0.62 - 1.58)	0.96
Presence of SDD												
No	—		—		—		—		—		—	
Yes	0.70 (0.58 - 0.85)	<0.001	1.04 (0.83 - 1.29)	0.75	0.57 (0.46 - 0.70)	<0.001	1.00 (0.78 - 1.29)	0.99	1.06 (0.84 - 1.35)	0.60	1.01 (0.77 - 1.33)	0.96
Presence of HRF												
No	—		—		—		—		—		—	
Yes	1.03 (0.85 - 1.25)	0.74	1.16 (0.94 - 1.43)	0.17	0.95 (0.78 - 1.16)	0.63	1.19 (0.94 - 1.51)	0.14	1.31 (1.03 - 1.67)	0.03	1.03 (0.78 - 1.35)	0.85
Presence of VMT or ERM												
No	—		—		—		—		—		—	
Yes	1.00 (0.77 - 1.31)	0.99	1.19 (0.89 - 1.59)	0.25	0.64 (0.48 - 0.86)	0.003	0.78 (0.56 - 1.10)	0.15	1.65 (1.22 - 2.22)	0.001	1.61 (1.14 - 2.26)	0.006
EZ/ELM												
Neither EZ/ELM loss	—		—		—		—		—		—	
EZ/ELM loss	0.69 (0.56 - 0.86)	<0.001	0.92 (0.62 - 1.35)	0.66	0.42 (0.33 - 0.52)	<0.001	0.84 (0.54 - 1.31)	0.45	2.99 (2.28 - 3.90)	<0.001	1.54 (0.96 - 2.45)	0.07

	ERF				SRF				IRF			
	Univariate		**Multivariable**		**Univariate**		**Multivariable**		**Univariate**		**Multivariable**	
Characteristic	OR (95% CI)	p-value	OR (95% CI)	p-value	OR (95% CI)	p-value	OR (95% CI)	p-value	OR (95% CI)	p-value	OR (95% CI)	p-value
Both ungradable	0.68 (0.55 - 0.84)	<0.001	0.70 (0.53 - 0.92)	0.01	0.58 (0.47 - 0.73)	<0.001	0.79 (0.59 - 1.07)	0.13	2.03 (1.53 - 2.68)	<0.001	1.12 (0.77 - 1.65)	0.56

Abbreviations: OCT- Optical coherence tomography; ETDRS- Early Treatment Diabetic Retinopathy Study; GEE -Generalised Estimating Equation; VA- Visual Acuity; OR- Odds Ratio; CI- Confidence interval

[a] *Not included in multivariable analysis.*

A. AI system development and Methodology for Chapter 4, Section 4.4.2

Data splitting

To develop an AI-based treatment response selection, we divided all OCT scans into train, validation and test sets. First, from the overall number of patients, 20% were randomly selected for test; 20% of the remaining patents were then selected for validation.

Splits were generated at the patient level to avoid having the same patient in the train and test sets. We stratified by protocol (standard or short), binary treatment outcome and scan size. Due to the short protocol sub-cohort size, we subsequently merged all non-training samples of the short protocol to a single hold-out test set. All algorithms were thus only tuned to perform well on the validation set of the standard protocol, or the training set of the short protocol (see the transfer learning step in the Supplementary Material). Both sub-cohorts' training sets were further split into five folds, again by randomly sampling patients, stratified by clinic and outcome.

Pre-processing

All OCT scans were first subject to a standardised pre-processing algorithm. This consisted of three individual steps. First, the raw images were loaded scan-by-scan by their order in the volume and resized by linear interpolation to a unified height of 200 pixels and width of 300 pixels. Subsequently, we subsampled all individual OCT scans to yield a total of 20 scans per eye. This was done by selecting 20 scans from the total number of scans in regular intervals, for eyes with more than 20 scans, and evenly duplicating scans, for eyes with less than 20 scans. Lastly, we normalised each resulting $20 \times 200 \times 300$ data matrix by mapping its individual 1% and 99% percentile to -1 and 1, respectively. We did not normalise by common reference due to the large variability in intensity between studies.

Clinical features were normalised as follows. For numerical features (e.g., age) we extracted the mean and standard deviation (SD) from the training set only to scale all values (including validation and test sets) to have a mean of 0 and SD of 1 by subtracting the mean and dividing by the SD of all training samples. After normalising, missing values were imputed by the mean (i.e., 0). CST was the only strictly positive variable that was strongly skewed, and we first transformed the natural scale of the

variable by applying the natural logarithm followed by normalisation. Binary (sex) and multi-class variables (clinic) were one-hot encoded.

Augmentation

Images were further pre-processed by implementing a two-dimensional (2D) wavelet decomposition via a Daubechies order 1 wavelet, to subsequently only use ‘edges’ as image input, again individually standardised to a mean of 0 and SD of 1 [1]. The size of the input matrix was not changed by the wavelet transformation. A simple on-off Boolean hyperparameter controlled whether models were trained purely on the original OCT scans or on their wavelet transformations.

We also introduced a simple foreground detection algorithm. We aimed at finding both the upper and lower background of the relevant retinal layers by reviewing the OCT scans by image column, marking the start of tissue by the following criteria. Since there appeared to be a salient ‘edge’ between the retinal layers and the upper background, we based the detection on a composite criterion: seen from the top of the image, tissue detection by finding a significant ‘edge’ (based on the wavelet transformation) of at least two SDs above wavelet mean, logical-OR-connected with the surpassing of a baseline luminosity value, calculated by image column, regressed towards the luminosity of the whole image by 50%. For the lower background, as in general no distinct ‘edge’ was present, we introduced only a simple threshold value, calculated, again, based on the column-wise luminosity, regressed towards the luminosity of the whole image by 50%.

OCT image backgrounds were then set to 0 for all further training steps. Both upper and lower luminosity threshold values were controlled (multiplied) by hyperparameters pertaining to a respective luminosity percentile value, to enable coarser to finer background detection.

In addition to these image transformations, we applied image augmentations in every training epoch. These affine transformations were applied to each 2D scan, consistently for each OCT volume. The augmentations consisted of a rotation from −20° to +20°, translation of up to 10 pixels, flipping the image left to right, and scaling of the image, either zooming in, by 0 to 50%, or out, by 0 to 20%.

Model pipeline

The fuse-med-ml (version 0.1.10, open-source python) library was used throughout the image classification process [2]. Given the binary labels, the ensuing classification task was attempted by three different model types, using the pre-processed OCT images or the clinical features as input.

First, we employed two different artificial neural network architectures: a) a three-dimensional (3D) class activation maps network, and b) a 2.5D Resnet50 network [3, 4].

The former was a pure 3D convolutional neural network (i.e., 3D kernels) with six convolutional layers [5].The latter consisted of a single 2D Resnet50 network that was applied individually for every 2D scan (i.e., 2D kernels), followed by an averaging of output features from over all scans, which resulted in a total volume output (thus '2.5D') [6,7].

Both networks were adapted with an input layer to adjust for the size of OCT images (20 dimensional with only one channel each), as well as a classification layer based on the cross-entropy loss.

Hyperparameters included CNN type, batch size, learning rate, dropout rate, weight decay, background detection level and wavelet transformation, as well as the training folds (1 out of 5 for cross-validation). Models were trained for up to 100 epochs using the Adam optimizer, after which we selected the best epoch on the cross-validation held-out set (1 out of 5). We ran hyperparameter tuning, randomly sampling parameters and choosing the best model based on its performance on the validation dataset [8]. The final model was a 2.5D Resnet50 with input wavelet transformation, a batch size of 4, learning rate of 3.4×10^{-6}, weight decay of 0.036 and dropout rate of 0.24.

Secondly, we trained a simple image classification model based on a 2D Fast Fourier Transformation (FFT) of every OCT scan. Given the sparsity of natural images in the Fourier domain, we first reduced the overall number of features by approximately 85% to the most dominant frequencies. The transformed one-dimensional vectors, representing the 2D frequency maps, were used as direct input to a l_1-norm regularised logistic regression (Lasso), with the volume labels applied to each scan [9]. The strength of regularisation was tuned in 5-fold cross-validation. The final model reached in general

a similar level of performance as the final CNN (see Results) but was dropped consecutively by the ensemble feature selection (see below).

Thirdly, a logistic regression with l_2-norm regularisation based on all clinical features (i.e., age, sex, (log.) CST, visual acuity and TRV) was standardised as described above. The strength of regularisation was again tuned in 5-fold cross-validation, after which the model was applied to the validation and test sets.

All models were either trained on standard or short protocol data, never on both simultaneously. However, since the performance of applying the CNN image classifier of the standard protocol sub-cohort on the short protocol sub-cohort was poor, we used the final CNN trained on standard protocol sub-cohort data to retrain on the short protocol sub-cohort tuning set, in order to employ the benefits of transfer learning [10,11]. Thus, we report three different kinds of model performances: models trained and tested on the standard protocol sub-cohort data, trained on standard data and tested on short protocol data (in general the least promising), and trained on short protocol data (CNN also pretrained on standard protocol sub-cohort data) and tested on short protocol data.

Finally, we trained an ensemble of all three model types to reach a single classifier. To this end, we used the outcome scores of all models [0-1] on the training data to also train an ensemble in the form of a logistic regression classifier with l_2-norm regularisation, again tuned in 5-fold cross-validation. We ran a forward feature selection algorithm for the standard protocol data, selecting the CNN as well as the clinical feature classifier based on the prediction performance on the validation data [12]. Adding the FFT-based classifier did not further improve the performance on validation. This procedure was not repeated for the short protocol dataset.

References

1. Daubechies I. Ten lectures on wavelets. USA: Society for Industrial and Applied Mathematics. 1992.

2. Golts A, Raboh M, Itaijj, *et al.* IBM/fuse-med-ml: 0.1.12. Zenodo, 2022 DOI:10.5281/ZENODO.5146491.

3. Zhou B, Khosla A, Lapedriza A, Oliva A, Torralba A. Learning deep features for discriminative localization. 2015. http://arxiv.org/abs/1512.04150 (accessed 11 August 2022).

4. Rabinovici-Cohen S, Abutbul A, Fernández XM, Hijano Cubelos O, Perek S, Tlusty T. Multimodal prediction of breast cancer relapse prior to neoadjuvant chemotherapy treatment. In: Rekik I, Adeli E, Park SH, Valdés Hernández M del C, eds. Predictive intelligence in medicine. Cham: Springer International Publishing, 2020: 188–99.

5. Maetschke S, Antony B, Ishikawa H, Wollstein G, Schuman J, Garnavi R. A feature agnostic approach for glaucoma detection in OCT volumes. *PLoS ONE* 2019; 14: e0219126.

6. He K, Zhang X, Ren S, Sun J. Deep residual learning for image recognition. *2016 IEEE Conference on Computer Vision and Pattern Recognition (CVPR)* 2016: 770–8.

7. Raboh M, Levanony D, Dufort P, Sitek A. Context in medical imaging: The case of focal liver lesion classification. In: Colliot O, Išgum I, eds. Medical imaging 2022: Image processing. SPIE, 2022: 165–72.

8. Kinga D, Adam JB. A method for stochastic optimization. International Conference on Learning Representations (ICLR). 2015.

9. Tibshirani R. Regression shrinkage and selection via the Lasso. *J R Statist Soc B* 1996; 58: 267–88.

10. Zhuang F, Qi Z, Duan K, *et al.* A comprehensive survey on transfer learning. 2020. http://arxiv.org/abs/1911.02685 (accessed 11 August 2022).

11. Antony BJ, Maetschke S, Garnavi R. Automated summarisation of SDOCT volumes using deep learning: Transfer learning vs de novo trained networks. *PLoS ONE* 2019; 14: e0203726.

12. Raschka S. MLxtend: Providing machine learning and data science utilities and extensions to Python’s scientific computing stack. *J Open Source Softw* 2018; 3: 638.

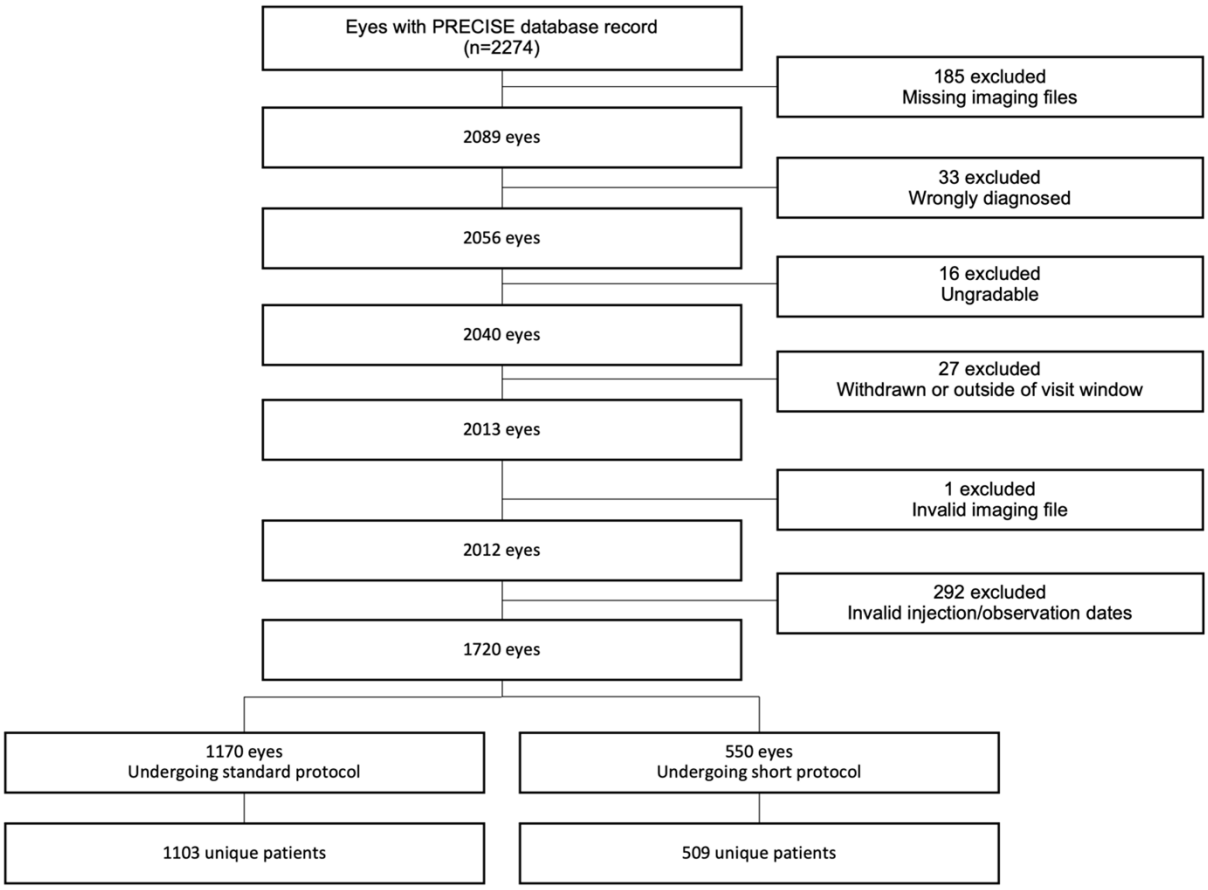

Figure S4.3 Participant flow for Chapter 4, section 4.4

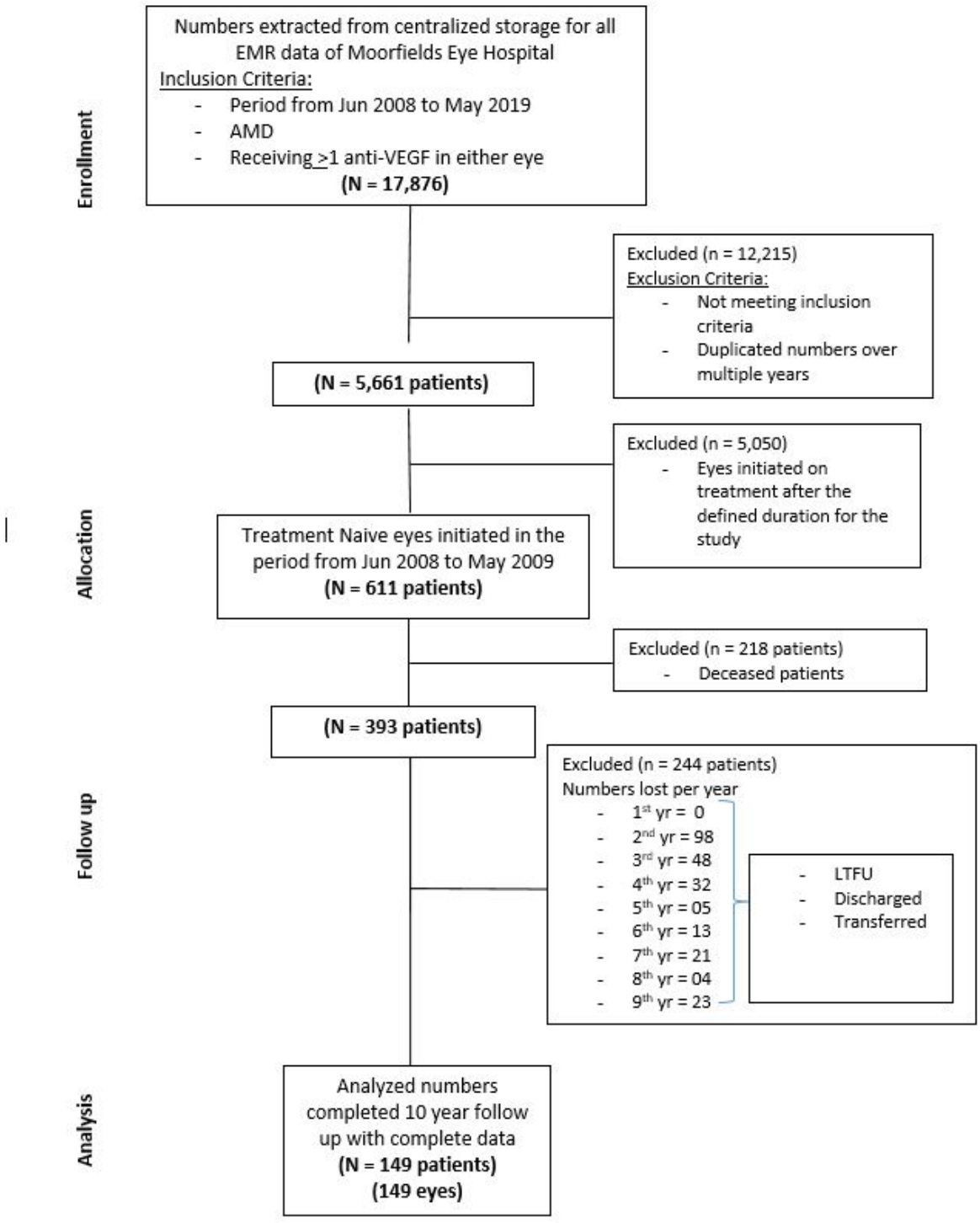

Figure S4.4: Participant Flow for Chapter 4, section 4.5

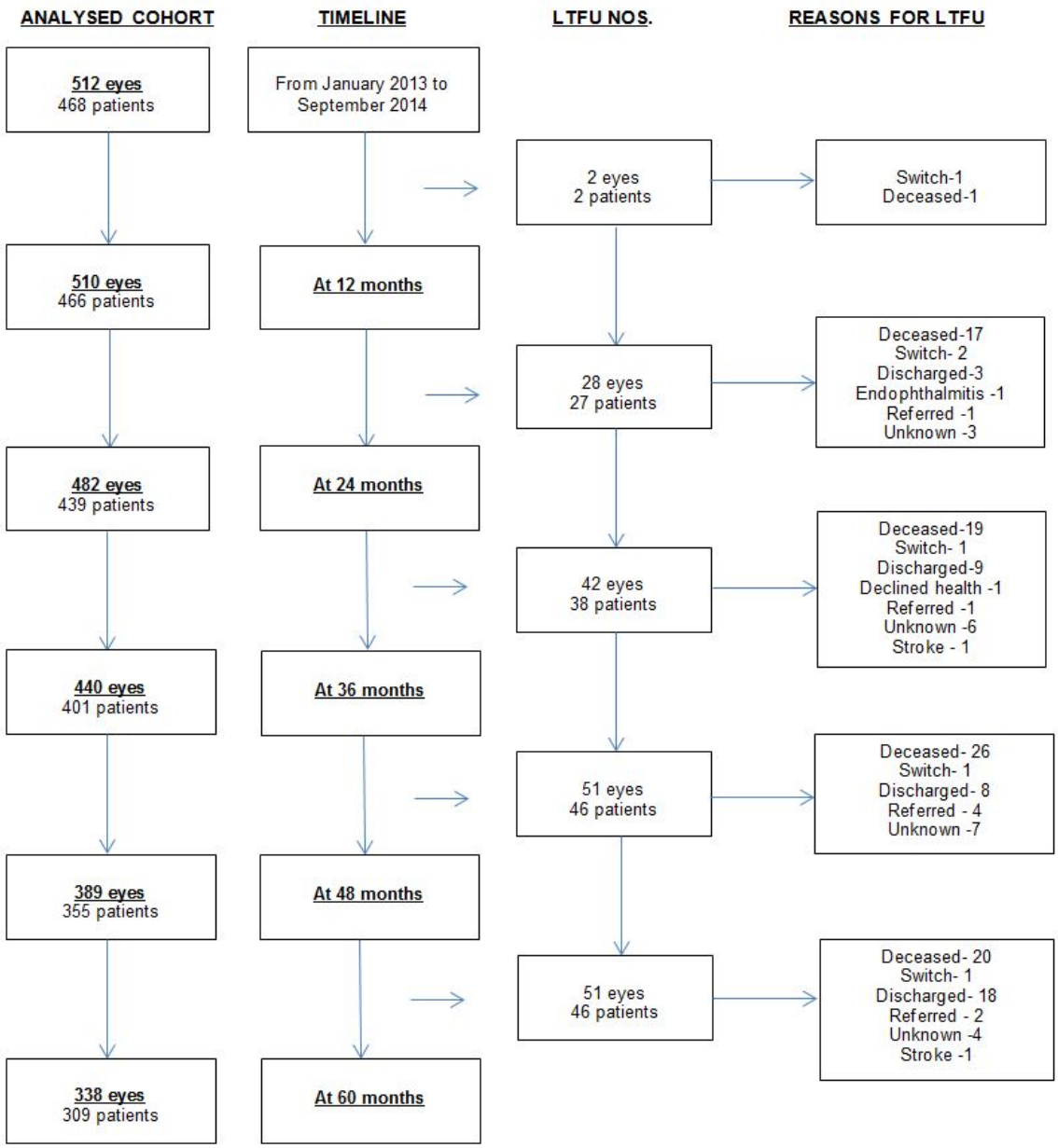

Figure S4.5: Participant Flow for Chapter 4, section 4.6